Theoretical investigation of CH,HC contacts and other intramolecular interactions in 2,2′-Bipyridine and its complexes with metal ions

by

Jurgens Hendrik de Lange[a]

Supervisor: Professor Ignacy Cukrowski[b]
Department of Chemistry,
University of Pretoria

Submitted in partial fulfilment of the requirements of the degree
Masters of Science
in the Faculty of Natural and Agricultural Sciences
University of Pretoria
Pretoria, South Africa
September, 2013

E-mails: [a] jurgensdl@tuks.co.za

[b] ignacy.cukrowski@up.ac.za

Declaration

I hereby declare that the work contained within this Dissertation is my own. It is being submitted for the degree Masters of Science at the University of Pretoria, and has not been submitted before for any degree or examination at any other institution.

_____

(Signature of Candidate)

____ day of _____ 2013

Outputs from this work

Jurgens de Lange and Ignacy Cukrowski. Stable CH•••HC interactions in Zn^{II}(Bipiridyl) complexes: A theoretical investigation, *Proceedings of the South African Chemical Institute Young Chemists' Symposium,* University of Pretoria, November 2012. (*oral, received 1st prize for best presentation)*

Jurgens de Lange and Ignacy Cukrowski. Stabiele CH•••HC verbindings in metaalbiridielkomplekse: 'n Teoretiese ondersoek, *Proceedings of the Suid-Afrikaanse Akademie vir Wetenskap en Kuns, Studentesimposium in die Natuurwetenskappe,* North-West University, October 2012. (*oral, received 1st prize for best presentation)*

Jurgens de Lange and Ignacy Cukrowski. H--H clashes in 2,2′-Bipyridine does not exist − a theoretical comparison of intramolecular interactions, *Proceedings of the South African Chemical Institute Inorganic Chemistry Conference*¸ University of KwaZulu-Natal, June 2013. (*poster).*

Jurgens de Lange and Ignacy Cukrowski. Computational investigation of bonding CH•••HC and other intramolecular interactions in 2,2′-Bipyridine, *Proceedings of the 12th International Chemistry Conference Africa 2013*, University of South Africa, July 2013. *(oral).*

Ignacy Cukrowski, Jurgens de Lange and Mariusz Mitoraj. Bonding and Non-bonding Interactions in Zn^{II} Complexes with 2,2′-Bipyridyl: DFT, QTAIM, IQA, NCI and ETS-NOCV Comparative Studies, *Chemistry– a European Journal.* (Submitted for publication).

Ignacy Cukrowski, Jurgens de Lange. Bonding Interactions in Ni^{II} Complexes with 2,2′-Bipyridyl: DFT and QTAIM Comparative Studies. (In preparation)

Jurgens de Lange, Ignacy Cukrowski. A rigorous theoretical investigation of the physical natures of close H--H contacts and other intramoleulcar interactions in 2,2′-Bipyridine: A QTAIM, NCI, ETS-NOCV and IQA study. (In preparation)

Abstract

2,2′-Bipyridine (BPy), one of the most widely used ligands in coordination chemistry, exists naturally in the *s*-trans conformation but must preorganize to the *s*-cis conformer in order to form chelating complexes. Lower stability of the *s*-cis conformer was mainly attributed to steric 3,3′-hydrogen clashes and nitrogen lone pair-lone pair interactions, but recent trends in the literature suggest that these clashes might be bonding interactions in similar molecules. These close contacts are also present in metal complexes with BPy and are often used as "steric repulsions" in order to explain trends in formation constants.

In the present work we investigate the CH•••HC interaction in the free ligand as well as in $Zn^{II}(BPy)_n(OH_2)_{6-2n}$ and $Ni^{II}(BPy)_n(OH_2)_{6-2n}$ complexes. We use multiple distinct advances in theoretical chemistry in order to arrive at a consistent and coherent model describing these interactions. The Quantum Theory of Atoms in Molecules (QTAIM) reveals the presence of an atomic interaction line (a bond path) for the CH•••HC interaction. Using the Interacting Quantum Atoms (IQA) energy decomposition scheme we show that the CH•••HC interaction is attractive and quantum mechanical in nature. The Extended Transition State coupled with Natural Orbitals for Chemical Valence (ETS-NOCV) energy decomposition scheme show favorable orbital mixing, and Non-Covalent Interaction (NCI) analysis reveals that no steric (Pauli) strain exists in the valence (overlap) regions of the interaction - electron density is concentrated rather than depleted in the bonding region.

We also studied various other interactions, ranging from purely repulsive (N--N interaction in the *s*-cis conformer of BPy), purely electrostatic (CH•••N interaction in *s*-trans conformer of BPy), H-bonding (CH–N and CH–O bonds in complexes) to coordination bonds and covalent bonds. Using a comparative approach, we show the similarities and differences among the interactions, and conclude that the CH•••HC interaction cannot be classified as a "steric repulsion" - the interaction is similar in properties to every studied known bonding interaction and opposite in nature to the studied known repulsions.

Finally, we suggest novel interpretations and understanding of the nature of intramolecular interactions and the field of theoretical chemistry, as well as representing the first work to combine and corroborate QTAIM, IQA, NCI and ETS-NOCV findings.

Keywords: Theoretical Chemistry, 2,2′-Bipyridine, H-clash, QTAIM, IQA, NCI, ETS-NOCV, coordination chemistry

Acknowledgements

My deepest gratitude goes out to my father, who offered moral and financial support continuously, lovingly and without question, my grandfather, for many fruitful discussions on the nature of the publication business and the peer-review system, as well as the rest of my family, for their continued understanding. My mother, who encouraged me to start this journey but could not be here to see it finished. My peers - students, colleagues and professors - who provided encouragement along the way.

My complete appreciation and respect goes out to my supervisor and mentor, Prof. Ignacy Cukrowski, for dedication, encouragement, intellectual stimulation, financial and moral support, friendship, and, most of all, belief in my abilities. Finally, to my wife Laetitia and the bond we share - a bond stronger and infinitely more complex than any other interaction described in this work.

Table of Contents

Page

List of Figures Page

Chapter 3

Chapter 4

Chapter 5

Appendix A

Appendix B

Appendix C

Appendix E

List of Tables Page

Chapter 3

Chapter 4

Chapter 5

Appendix A

Appendix B

Appendix C

Appendix D

Appendix E

List of abbreviations

BPy – 2,2′-Bipyridine

ZnL_n – $Zn^{II}(BPy)_n(OH_2)_{6-2n}$

NiL_n – $Ni^{II}(BPy)_n(OH_2)_{6-2n}$

DFT – Density Functional Theory

MO – Molecular Orbital

NBO – Natural Bond Orbital

QTAIM – Quantum Theory of Atoms in Molecules

IQA – Interacting Quantum Atoms

NCI – Non-Covalent Interactions

ETS – Extended Transition State

NOCV – Natural Orbitals for Chemical Valence

AIL – Atomic Interaction Line

BCP – Bond Critical Point

RCP – Ring Critical Point

ZFS – Zero flux surface

ADF – Amsterdam Density Functional

HF – Hartree-Fock

X3LYP – Extended 3-parameter hybrid exchange potential with Lee-Yang-Parr's correlation functional

PCM – Polarizable Continuum Model

UFF – United Force Field

Φ(1) – The dihedral angle given by N1, C12, C11 and N2 (Chapter 2)

Φ(2) – The dihedral angle given by H13, C3, C10, H20 (Chapter 2)

BL – Bond length

DA – Dihedral Angle

EIR – Energy Interaction Ratio

PEI – Privileged Exchange Index

Chapter 1

Introduction

The chemical bond is the most central concept in the study of chemistry, and understanding it is one of the most important goals of all chemists. Fundamental knowledge of the chemical bond also leads to improved research output of all fields dependent on chemistry, such as biology, geology, medicine and engineering. With the advent and development of modern powerful computing, chemistry has begun its evolution from a predominantly experimental and industry-driven science to a field rooted in physics and mathematics, an upward change which allow us to critically and theoretically investigate the building blocks of chemistry. One of these building blocks is the concept of bonding - how it is defined, the physical models which can describe it most accurately, the underlying mechanisms through which it occurs and the causal effects resulting from it which produces the wide variety of phenomena that we see in labs, reactors and common reality every day.

From a theoretical and computational chemistry perspective, it is useful to understand chemical bonding mathematically, so that the concepts arising from the theoretical study of bonds can be transferred epistemologically to other branches of chemistry and physical science. A good example of this transfer of knowledge is in force-field methods: a force-field (whether it is based on experimental or structural data[1–2], or based on rigorous quantum mechanical calculations[3–6]) can be used by non-theoretical scientists without the deeper mathematical and physical knowledge of the equations governing the force-field to understand and predict phenomena in their own fields, usually in a manner that is relatively cheap to calculate. Recently, sophisticated force fields[1–6] have been developed which the non-theoretical scientist can easily use. In addition, computationally cheaper theories such as Density Functional Theory (DFT) are rising in popularity among non-theoreticians, and it falls to the theoretical chemist to test, develop and show the proper use of these types of theories.

A major problem in this line of study is the concept of intramolecular binding, and how to define it. Typically, the bond dissociation energy is defined as $E(A\text{–}B) = E(AB) - E(A) - E(B)$ - or the difference between the molecular energy and the energy of the isolated atoms or fragments. While this definition holds for diatomics or bimolecular complexes, it fails to define intramolecular bonds. Specifically, it is impossible to dissociate an intramolecular interaction in fully separated fragments without breaking some other bond, too. Alternatively, the dissociation of an intramolecular interaction

might be incorrectly approximated by comparing two different conformers of a molecule, one with the intramolecular interaction present and one without. Unfortunately, formation or dissociation of an *intramolecular* interaction will be caused by or be the cause of a change in the geometry of the entire molecule. Consequently, such a change will incur differences in the chemical environments of each atom, leading to changed energies and charge distributions which will obfuscate the nature of the intramolecular interaction.

The problem of intramolecular binding is also quite related to the concept of strain - an intramolecular interaction (such as a hydrogen bond in i.e. glycine) will only form when the interacting atoms are geometrically in a favourable position towards each other. While such an interaction is most obviously stabilizing, it is plausible that the formation of an interaction will cause the weakening of another bond in another part of the molecule. Such an interaction is locally stabilizing, but molecularly destabilizing. Alternatively, formation of interaction might cause the dissociation of another, affecting the molecular energy in a non-trivial manner. These hypothetical situations highlight our lack of conceptual knowledge with regards to intramolecular bonding. While it is easy to proclaim that if a classical bond, such as an H-bond, is locally stabilizing even when a molecular destabilization is seen because of *a priori* knowledge, what happens when we are faced with a potentially locally stabilizing/molecularly destabilizing intramolecular interaction but with an unknown nature?

Such a case was recently found in the form of close H-clashes in the planar form of biphenyl. These clashes, present in hundreds of molecules, are usually interpreted as destabilizing "steric repulsions"[7–10], but recent theoretical[11–15] and experimental[16–18] evidence suggests that CH•••HC interactions in biphenyl and other molecules are, in fact, stabilizing bonding interactions. Since the planar form of biphenyl is higher in energy than the twisted form, the CH•••HC interaction is a perfect example of a potentially locally stabilizing but molecularly destabilizing interaction, and it is therefore important to discover the nature of this interaction, as a locally stabilizing interaction might be molecularly stabilizing in other molecules.

2,2′-Bipyridine (BPy), named one of the most commonly used and important ligands[19], is a molecule similar to biphenyl but with the ability to form strong complexes with transition metals in a bidentate fashion. In order to do so, BPy must deform from its lowest energy structure, *s*-trans, to the higher in energy structure with N-atoms cis to each

other, *s*-cis. In *s*-cis, hydrogens in the bay region (3,3′-hydrogens) are involved in a close contact, and have been used (together with the lone-pair-lone-pair repulsions of the N--N interaction) to explain the increased energy of *s*-cis and certain trends in formation constants of BPy with metal ions[7–10]. However, in light of the recent discovery of potentially stabilizing CH•••HC interactions, we decided to investigate these claims regarding BPy and investigate the nature of the CH,HC contact in free BPy as well as BPy-metal complexes.

Our investigation is theoretical in nature, but unlike some other works on the subject of CH•••HC interactions[11–15], we will explore the CH•••HC interaction using multiple but different theoretical tools and approaches in order to arrive at a consistent and exhaustive model for these interactions. In addition, we will investigate other intramolecular interactions in BPy and BPy-complexes in a comparative fashion, providing new insights to the general field of intramolecular interactions. Finally, using multiple theories in any study inherently reveals more applications and deeper understanding of each method.

This work is presented as a collection of mostly independent manuscripts, some ready and some in preparation for publication. Chapter 2 gives a brief overview of general quantum Chemistry and the methods used in this work. Chapter 3 performs an in-depth study of the intramolecular interactions present in the free BPy ligand and its various conformers. The Quantum Theory of Atoms in Molecules (QTAIM), the Interacting Quantum Atoms (IQA) energy decomposition scheme, the Non-Covalent Interactions (NCI) real space method and the Extended Transition State coupled with Natural Orbitals for Chemical Valence (ETS-NOCV) energy decomposition scheme are all used in the analysis. While Chapter 3 mostly describes the interaction between atoms of interest (in terms of energetics and charge distributions), Appendix A shows preliminary results related to the changes in atomic and bond properties of other regions of the molecule in order to detect where the strain is localized. Chapter 4 performs an in-depth study of the intramolecular interactions present in complexes of BPy with aqueous Zn^{II}, using Density Functional Theory (DFT), QTAIM, IQA, NCI and ETS-NOCV. The interactions present in $Zn^{2+}(BPy)_n(OH_2)_{6-2n}$ complexes are analysed in a comparative fashion in an effort to study the trends in unknown (controversial) interactions in comparison to the trends in known (classical) bonds. Finally, Chapter 5 shows a predominantly DFT and in-depth QTAIM study of the intramolecular interactions present in complexes of BPy with aqueous Ni^{II}. Intramolecular interactions are compared to the geometric and topological

trends of all other interactions and bonds, including coordination and covalent bonds. Appendix D gives preliminary results with regards to the atomic energy changes when *s*-trans BPy is deformed into the higher energy *s*-cis conformers and conformers present in $Ni^{2+}(BPy)_n(OH_2)_{6-2n}$, as well as the changes in atomic properties when the ligand undergoes coordination to Ni^{II}. Major conclusions and suggestions for future research are summarized in the final chapter, Chapter 6. Supplementary information, data and graphs are provided for Chapters 3 through 5 in Appendices B, C and E.

Previous studies of BPy. Bipyridine have been studied extensively before, both experimentally and computationally. Hancock and Martell reported in 1989[7] that BPy shows lowered complex stability than 1,10-phenanthroline because of steric clashes between 3,3′ H-atoms, using measured formation constants and molecular mechanics to support their statements. At this time, the conformational preference of BPy in solution was not yet known. Further molecular mechanics[21] and semi-empirical[22] calculations suggested that BPy exists mostly in the *s*-trans conformation, with two rotation barriers corresponding to the perpendicular and *s*-cis conformations. These studies were soon supplemented with various *ab initio* and DFT calculations, ranging from STO-3G[23–25], BP86[26], B3LYP[27] and various MP2 and high-level[28–31] calculations. The results from these works, including experimentally determined rotation barriers[32–33] confirm the preferential existence of BPy in the *s*-trans confirmation. H--H and N--N clashes were consistently given throughout all BPy literature as the reason for the increased energy of *s*-cis.

Interestingly, BPy has also been studied using QTAIM. Alkorta *et al* [27] studied BPy and various derivatives and protonated forms. However, although they report the molecular graphs of many of the studied compounds, they do not show nor discuss the molecular graphs for free BPy or any derivative containing an H--H clash. Very recently, Hancock and Nikolayenko revisited the question of the effect of H-clashes on the conformational preference of BPy and concluded again that no stabilization can arise from the CH•••HC interaction in BPy, based on the observation that *s*-trans is lower in energy than *s*-cis and the non-planarity of BPy when coordinated to very large metal ions. While these observations (and the others surrounding BPy, as discussed above) are accurate with regards to the potential surface of BPy, the claim that the increased energy of *s*-cis is a result of clashing H-atoms remains unsupported, and the nature of CH•••HC interactions in BPy is still unknown.

Mechanisms of a bonding interaction. The terms "bonding interaction" and "chemical bond" are separate concepts, with the focus of this work on the former. A generally accepted mechanism of chemical bonding is the accumulation or concentration of electronic charge density in the inter-nuclear (or bonding) regions of an interaction. Density concentration in this region increases the only attractive term of the general Hamiltonian - V_{ne}, the attraction between nuclei and electrons - thereby creating a bonding interaction between atoms.

However, any concentration or pressurized region of density comes at a price[20] - an increase in the repulsion between electrons, V_{ee}. V_{ee} gives rise to the Coulomb-hole - regions of decreased probability of finding an electron because of electrostatic repulsion. In addition, because of the antisymmetric nature of fermions, electrons of the same spin cannot exist in the same region of space, an effect independent of the charge of electrons or the electrostatic repulsion between them. This effect of correlation between same-spin electrons results in the Fermi-hole - regions of decreased density of same-spin electrons. The Fermi-hole results in a stabilizing electron exchange contribution to the Hamiltonian, V_{ee}^{X} - decreased density of same-spin electrons allows naturally for increased density of electrons of opposite spin.

In order for the concentration in the inter-nuclear region to be necessary and sufficient to form a bonding interaction, spin-coherence (or electron sharing) must occur between atoms, resulting in the quantum-mechanical or covalent part of any bond. Due to the non-locality of the exchange stabilization, the electron clouds of any two atoms (whether bonded or non-bonded) will show some degree of delocalization between them. A major effort of this work will be to show when the quantum-mechanical part of any interaction is marginal or arbitrary - the result of two close but effectively non-interacting atoms - or when it is an indication of a significant degree of covalency. In addition, we also show examples of interactions with electron depletion in the inter-nuclear region - interactions where a large V_{ee} but comparatively small V_{ee}^{X} are seen and where removal of electron density is more beneficial than its accumulation. Such interactions are classical representations of the concept of "steric hindrance".

Finally, we must mention that the presence of concentration in the bonding region of interactions does not signify a bond - it only indicates a degree of a quantum-mechanical bonding interaction. For a bonding interaction to be classified as a bond, the total

electrostatic interactions must also be considered (as it is possible that a repulsive electrostatic interaction can override the quantum-mechanical stabilization of an interaction), as well as the effects of formation or dissociation of the interaction on the atoms, fragments and molecules involved. Such considerations are mentioned in the various chapters throughout this work, where applicable.

Contributions to the understanding of theoretical chemical tools. Although the focus of this work is on the study of intramolecular interactions, a few novel contributions is made which contributes to the understanding and interpretation of existing methods and theories. It is the first work of its kind to combine QTAIM, IQA, NCI and ETS-NOCV results, as well as one of few works to truly consider phenomenon from multiple perspectives given by each theory. In Chapter 3, the concepts of net Pauli-Orbital and net Pauli-NOCV deformation densities, used to study the dominating electron deformation effect in any interaction, and the Privileged Exchange Index (PEI) as a NCI-based diagnostic to study the degree of covalency and predict the existence of bond paths, is introduced. Chapter 3 also provides additional interpretation and understanding regarding the bond path. Chapter 4 introduces the Energy Interaction Ratio (EIR) as a quick diagnostic for understanding the attractive/repulsive nature of interactions, as well as electrostatic/covalent nature. 1D topology maps (cross-sections of the electron density distributions of interactions) are explored as a potential aid for understanding electron densities. Finally, the work represents a step forward in the understanding of various intramolecular interactions, as well as the mechanisms guiding them.

References

[1] E. M. Engler, J. D. Andose, P. V. R. Schleyer, *J. Am. Chem. Soc.*, **1973**, *95*, 8005–8025.

[2] S. L. Mayo, B. D. Olafson, W. A. Goddard, *J. Phys. Chem.*, **1990**, *94*, 8897–8909.

[3] T. A. Pascal, N. Karasawa, W. A. Goddard, *J. Chem. Phys.*, **2010**, *133*, 134114–134131.

[4] A. Monari, J. Rivail, X. Assfeld, *Acc. Chem. Res.*, **2013**, *46*, 596–603.

[5] Y. Duan, C. Wu, S. Chowdhury, M. C. Lee, G. Xiong, W. Zhang, R. Yang, P. Cieplak, R. Luo, T. Lee, J. Caldwell, J. Wang, P. Kollman, *J. Comp. Chem.*, **2003**, *24*, 1999–2012.

[6] P. L. A. Popelier, A generic force field based on Quantum Chemical Topology *in Modern Charge Density Analysis*, 2012, Springer Netherlands

[7] R. D. Hancock, A. E. Martell, *Chem. Rev.* **1989**, *89*, 1875–1914.

[8] D. Buist, N. J. Williams, J. H. Reibenspies, R. D. Hancock, *Inorg. Chem.* **2010**, *49*, 5033–5039.

[9] G. M. Cockrell, G. Zhang, D. G. VanDerveer, R. P. Thummel, R. D. Hancock, *J. Am. Chem. Soc*. **2008**, *130*, 1420–1430.

[10] S. Del Piero, P. Di Bernardo, R. Fedele, A. Melchior, P. Polese, M. Tolazzi, *Eur. J. Inorg. Chem.* **2006**, 3738–3745.

[11] E. A. Zhurova, C. F. Matta, N. Wu, V. V. Zhurov, A. A. Pinkerton, *J. Am. Chem. Soc.* **2006**, *128*, 8849–8861.

[12] C. F. Matta, J. Hernández-Trujillo, T. H. Tang, R. F. W. Bader, *Chem. Eur. J.* **2003**, *9*, 1940–1951.

[13] R. F. W. Bader, *J. Phys. Chem. A* **2009**, *113*, 10391–10396.

[14] A. M. Pendás, E. Francisco, M. A. Blanco, C. Gatti, *Chem. Eur. J.* **2007**, *13*, 9362–9371.

[15] F. Cortés-Guzmán, J. Hernández-Trujillo, G. Cuevas, *J. Phys. Chem. A* **2003**, *107*, 9253–9256.

[16] K. N. Robertson, O. Knop, T. S. Cameron, *Can. J. Chem.* **2003**, *81*, 727–743.

[17] K. N. Robertson, *in Intermolecular Interactions in a Series of Organoammonium Tetraphenyl-borates*; Ph.D. Thesis, Dalhousie University, Halifax, Canada, **2001.**

[18] E. A. Zhurova, V. G. Tsirelson, V. V Zhurov, A. I. Stash, A. A. Pinkerton, *Acta Cryst. B* **2006**, *62*, 513–520.

[19] C. Kaes, A. Katz, M. Hosseini, *Chem. Rev.*, **2000**, *100*, 3553–3590

[20] J. Tao, G. Vignale, I. V. Tokatlys, *Phys. Rev. Lett.*, **2008**, *100*, 206405–206409

[21] C. Jaime, J. Font, *J. Org. Chem.*, **1990**, *55*, 2637–2644

[22] R. Benedix, P. Bimer, H. Hennig, *J. Mol. Struct. Theochem.*, **1982**, *90*, 65–69

[23] V. Barone, F. Lelj, N. Russo, *Int. J. Quantum Chem.*, **1986**, *29*, 541–551

[24] E. von Nagy-Felsobuki, *Chem. Phys. Lett.*, **1996**, *127*, 245–247

[25] H. J. Hofmann, R. Cimiraglia, J. Tomasi, *J. Mol. Struc. Theochem.*, **1986**, *139*, 213–219

[26] S. Zahn, W. Reckien, B. Kirchner, H. Staats, J. Matthey, A. Lützen, *Chem. Eur. J.*, **2009**, *15*, 2572–2580

[27] I. Alkorta, J. Elguero, C. Roussel, *Comp. Theor. Chem.*, **2011**, *966*, 334–339

[28] A. Göller, U. W. Grummt, *Chem. Phys. Lett.*, **2000**, *321*, 399–405

[29] A. Göller, U. W. Grummt, *Chem. Phys. Lett.*, **2002**, *354*, 233–242

[30] S. T. Howard, *J. Am. Chem. Soc.*, **1996**, *118*, 10269–10274

[31] L. Oresmaa, M. Haukka, P. Vainiotalo, T. A. Pakkanen, *J. Org. Chem.*, **2002**, *67*, 8216–8219

[32] H. Uchimura, A. Tajiri, M. Hatano, *Bull. Chem. Soc. Jpn.*, **1984**, *57*, 341–348

[33] D. J. Barker, L. A. Summers, R. P. Cooney, *J. Mol. Struct.*, **1987**, *159*, 249–254

[34] R. D. Hancock, I. V. Nikolayenko, *J. Phys. Chem. A*, **2012**, *116*, 8572–8583

Chapter 2

Theoretical Background

Introduction

The ideal model chemistry – the ultimate goal of computational and theoretical chemistry – should contain extensive predictive power, aid fundamental understanding and insight, be accurate to the point of no reasonable doubt, inherent in its statements and should be pragmatically applicable to systems studied by chemists. In this regard, some existing models used by both experimentalists and theoreticians alike only approach the ideal model chemistry in a very small subset of chemical problems. These models include classical molecular mechanics (MM) and semi-empirical methods, both of which are very attractive for larger chemical systems due to their low costs, but are wholly inaccurate except for the molecular systems upon which force field or empirical parameters were fitted.[1] On the other hand, advanced quantum mechanical theories such as the Lagrangian approach to chemistry[2], Bohmian mechanics and non-linear quantum chemistry[3] and relativistic quantum mechanics[4] are showing great promise with regards to accuracy, predictive power and insight, but due to underdevelopment with regards to the mathematical and physical implementation these methods remain non-applicable to the study of chemical systems.

The offset between practicality and power is a common theme in computational chemistry, and possibly the reason why wavefunction-based quantum mechanics (and the implicit physical interpretations thereof, such as the wave-particle duality) became so popular and developed in quantum chemistry today. Wavefunction mechanics, intrinsically exact, is scalable and modular and allows for varying degrees of accuracy with corresponding changes in computational cost. In addition, wavefunction mechanics is in principle *ab initio* (Latin, "from the ground up"), therefore reducing the probability of biased interpretations – distortion of the results by "moulding the model to fit the interpretation". In addition, through the use of the variational principle and its application in quantum chemistry, *ab initio* methods allow novel insights and new understandings of some fundamental concepts in chemistry. It is for these reasons that we, like so many other computational chemists, use and depend on wavefunction-based quantum mechanics to model complex chemical systems.

This chapter gives a brief theoretical background for the methods used in this work. It is organised as follows: a short discussion on quantum chemistry, including the various methods which can be used to study it and some comments regarding implementation is

presented first. Then Hartree-Fock theory is discussed, as well as its implementation and followed by the same for Density Functional Theory. The next section details advanced modern density and wavefunction analyses – the physical background of these methods, their implementation and interpretation and the advantages and pitfalls of each method. Finally, the last section introduces an algorithm used for calculating cross-sections of the electron density – a simple but newly introduced method which is implemented in this work.

The first section will focus mainly on the basic concepts, approximations, computational machinery and analysis of wavefunction-based quantum chemical methods (henceforth referred to just as quantum mechanics or quantum chemistry). The fundamental postulate of quantum mechanics and the action of operators on the wavefunction are discussed first, followed by discussions of the Born-Oppenheimer approximation and the variational principle. The mathematical construction of a trail wavefunction through basis sets, calculation of the energy of a wavefunction using the Hartree-Fock method and the effects of electron-electron correlation are then briefed.

The work presented in this chapter follow principally two comprehensive and well-written textbooks on Quantum Chemistry, *A Chemist's Guide to Density Functional Theory* by Koch and Holthausen[5] and *Essentials of Computational Chemistry, Theories and Models (2nd Edition)* by Cramer[6]. Minor contributions were also taken from the textbooks by McWeeny, 1992[7], Atkins and Friedman, 1997[8] and Szabo and Ostlund, 1982[9].

Quantum Chemistry

The fundamental postulate of quantum chemistry states that some function Ψ exists for any chemical system and, upon action of some appropriate operator Ô, returns observable properties. In mathematical terms:

$$\hat{O}\Psi = A\Psi \tag{2.1}$$

which, in analogy to matrix algebra, is an eigenvalue equation with eigenfunction Ψ and (usually scalar) eigenvalue A. Formally, Ψ has the dimensions of the square root of a probability density, and therefore the product of Ψ with its complex conjugate Ψ*

generates a probability density - the probability of finding a particle (proton or electron) at a specific coordinate in multi-dimensional space. For the sake of simplicity the complex conjugate, Ψ^*, will be omitted, giving $|\Psi^*\Psi| = |\Psi|^2$.

The ultimate goal of most quantum chemical theories is to find the solutions to the time-independent, non-relativistic Schrödinger equation:

$$\hat{H}\Psi_i(\vec{x}_1, \vec{x}_2, \ldots, \vec{x}_N, \vec{R}_1, \vec{R}_2, \ldots, \vec{R}_M) = E_i\Psi_i(\vec{x}_1, \vec{x}_2, \ldots, \vec{x}_N, \vec{R}_1, \vec{R}_2, \ldots, \vec{R}_M) \tag{2.2}$$

where Ψ_i is a function of N electrons and M nuclei, as well as the coordinates in multi-dimensional space of each. E_i is the energy associated with a specific Ψ_i and $\hat{H}$ the general Hamiltonian operator,

$$\hat{H} = -\frac{1}{2}\sum_{i=1}^{N}\nabla_i^2 - \frac{1}{2}\sum_{A=1}^{M}\frac{1}{M_A}\nabla_i^2 - \sum_{i=1}^{N}\sum_{A=1}^{M}\frac{Z_A}{r_{iA}} + \sum_{i=1}^{N}\sum_{j>i}^{N}\frac{1}{r_{ij}} + \sum_{A=1}^{M}\sum_{B>A}^{M}\frac{Z_A Z_B}{R_{AB}} \tag{2.3}$$

or,

$$\hat{H} = \hat{T}_e + \hat{T}_N + \hat{V}_{eN} + \hat{V}_{ee} + \hat{V}_{NN} \tag{2.4}$$

where $\hat{T}_e$ and $\hat{T}_N$ represent the electronic and nuclear kinetic energy operators, respectively, and $\hat{V}_{eN}$, $\hat{V}_{ee}$ and $\hat{V}_{NN}$ are the electron-nuclear, electron-electron and nuclear-nuclear potential energy operators, respectively. r_{iA}, r_{ij} and R_{AB} are the distance between a specific electronic coordinate and nuclear coordinate, the distance between two electronic coordinates and the distance between two nuclear coordinates, respectively. Z_A gives the nuclear charge for nucleus A whilst M_A gives the mass of nucleus A. Finally, ∇^2 refers to the Laplacian operator in Cartesian coordinates - the trace of the Hessian matrix of partial second derivatives.

There are, in fact, a multitude of acceptable eigenfunctions Ψ with corresponding and different eigenvalue E in the general form of Eq. 2.2. This set of wavefunctions is defined in such a manner to be orthonormal,

$$\int \Psi_i \Psi_j d\mathbf{r} = \delta_{ij} \tag{2.5}$$

where δ_{ij} is the Kronecker delta, which is equal to one if $i = j$ and zero otherwise. Eq. 2.5 shows that all wavefunctions are both orthogonal (their integrated product is zero) and normalized (the probability density when $i = j$ is equal to one).

Nuclear Correlation. Each potential energy term in Eq 2.3 is generated by pairwise interaction between two particles. If each particle were moving independently of all other particles, then all the terms in Eq. 2.3 would've been easy to calculate. However, particle movement is said to be *correlated* - interdependent movement of each particle with every other particle causes fluctuations in the kinetic energy of each particle as well as in the attractions and repulsions between particles. Unfortunately, to account for all types of particle correlation is a very daunting task numerically, and no exact solutions exist to calculate correlation analytically.

Luckily, nuclear correlation (correlated nuclear-nuclear movement as well as nuclear-electron movement) can be discarded in a relatively mild adjustment known as the Born-Oppenheimer approximation. Because of the very large difference in mass between protons and electrons, electrons have much higher velocities and momenta than protons. The interdependency between electron and nuclei movements can thus be safely removed, and for most systems it is enough to calculate the electronic energy for fixed nuclear coordinates. The so-called electronic Hamiltonian can now be constructed:

$$\hat{H}_{elec} = \hat{T}_e + \hat{V}_{ee} + \hat{V}_{eN} + \hat{V}_{NN} \qquad (2.6)$$

Note that the nuclear kinetic energy does not contribute to the electronic energy since the nuclei are fixed (corresponding to a kinetic energy of zero) and the potential energy due to nuclear-nuclear repulsions is merely a constant for the given nuclei coordinates. The problem of correlated nuclear-electron computation is also fixed. However, electron correlation is still present and can contribute significantly to the final energy of the system. Electron correlation will be discussed later.

For the rest of this work, we will assume the Born-Oppenheimer approximation to hold and all wavefunctions and operators, unless otherwise noted, will be only for the electronic case.

The Variational Principle. In order to solve the Schrodinger equation (Eq. 2.2), we must first set up the *specific* Hamiltonian for that system. It is clear from Eq. 2.6 and Eq. 2.4. that the specific Hamiltonian for a system depends only on the i) number of electrons in the system, N, and ii) the position and charges of all nuclei in the system. However, the problem now comes in in finding all the eigenfunctions Ψ_i and corresponding eigenvalues E_i in order to solve Eq. 2.2. Unfortunately, no such strategy to solve the Schrödinger equation exactly exists yet.

Using the variational principle, the ground state can be approached through variational calculus. The observable expectation value of any operator acting on the square modulus of any arbitrary trail wavefunction, Ψ_{trail}, is given by

$$\langle \hat{O} \rangle = \int \Psi_{trail}^{*} \hat{O} \Psi_{trail} d\mathbf{r} = \langle \Psi_{trail}^{*} | \hat{O} | \Psi_{trail} \rangle \tag{2.7}$$

In other words, the expectation value of an operator acting on a wavefunction is given by the integrand over all coordinates of the operator acting on the wavefunction and the product with its complex conjugate (note that since Ψ is Hermitian, the order of the wavefunction or complex conjugate does not matter). Dirac's *bracket* notation is illustrated through the identity on the RHS of Eq. 2.7.

Ψ_{trail} will be an upper bound to the ground state energy, E_0, because of the variational principle:

$$\langle \Psi_{trail} | \hat{H} | \Psi_{trail} \rangle = E_{trail} \geq E_0 = \langle \Psi_0 | \hat{H} \quad | \Psi_0 \rangle \tag{2.8}$$

A minimization then takes place until $E_{trail} = E_0$.

The variational principle therefore allow us to calculate the ground state energy and associated wavefunction, without the need to calculate all the (possibly infinite) eigenvectors of eq. 2.2.

Basis sets. The preceding text has discussed the operations surrounding the wavefunction, but has not made any mention with regards to the shape of the wavefunction itself. In principle, any mathematical function adhering to certain rules can be used in order to construct a trail wavefunction. For this reason it is often practical to describe a wavefunction in such a manner that is i) easy and relatively fast to compute, ii) encompassing of a wide range of Hilbert (function) space and iii) have some degree of physical and chemical sense. The latter is by no means a requirement, yet most modern quantum chemical software mathematically constructs wavefunctions with some semblance of chemical concepts. The following section will describe the manner in which the trail wavefunctions computed in this work have been constructed.

The basis set is a linear combination of a set of *N* functions,

$$\phi = \sum_{i=1}^{N} a_i \varphi_i \tag{2.9}$$

where N is the number of electrons, φ_i are one-electron "orbitals", each of which generally consists of a set of Gaussian primitives, and a_i are scalar coefficients. Computationally, the use of such a basis set greatly aids the computational process as the functions themselves (the one-electron orbitals) can be pre-optimized or fitted to certain experimental data and only the coefficients a_i need to be optimized during the variational minimization of the wavefunction.

The Gaussian primitives are constructed analogous to one-electron orbitals of the hydrogen atom, generating mathematical distributions which resemble 1*s*, 2*p*, 2*s*, 3*s*, 3*d* etc. functions for each atom in the molecule. In order to describe the general trends and show the correct asymptotic behaviour as the real electron density of a hydrogen atom, multiple Gaussian primitives are grouped (contracted) together and scaled linearly, with a general increase in the number of primitives giving a more accurate description. However, each additional Gaussian primitive results in an additional set of equations which must be solved simultaneously, increasing computational costs exponentially. Therefore, basis sets can be tweaked in order to provide the best possible description for the chemical problem at hand with the lowest necessary computational cost. It must be stressed, however, that expressing the wavefunction in terms of Gaussian type orbitals (GTO) does not *determine* the final ground state wavefunction - rather, the choice of basis set determines the possible space and forms a trail wavefunction can populate.

Many different basis sets are relatively freely available, with many reviews of commonly used basis sets[10] as well as some on-line providers[11]. In this work we have exclusively used the 6-311++G(d,p) basis set by Pople and co-workers[10], and only this basis set will be discussed here in any detail. 6-311++G(d,p) is, first of all, known as a split-valence basis set, where all the core electrons are described by six Gaussian primitives per atomic orbital and all valence electrons are treated as three (valence-triple-ζ) different atomic orbitals. The first of these valence atomic orbitals is constructed by three Gaussian primitives, and the remaining two orbitals are treated by a single Gaussian only. Furthermore, *p*- and s-orbitals are "polarized" in 6-311++G(d,p) with orbitals with higher angular momentum, slightly changing the character of each type of orbital. Lastly, very diffuse functions (functions with very small coefficients) are included for both H-atoms as well as for heavy atoms in order to better describe regions of very little electron density, particularly important for modelling anions and van der Waals interactions. Similar basis

sets have been used to study H--H interactions in biphenyl[12] - a molecule very similar to bipyridine which is studied in this work.

The Hartree-Fock Approximation

While the variational principle provides a wonderful tool to find the exact wavefunction, searching over all possible (and potentially infinite) wavefunctions is practically impossible. However, the variational principle can also be applied to a subset of wavefunctions, which, under mild yet physically sound approximations, can include wavefunctions very close to the exact wavefunction. The simplest yet still powerful subset of wavefunctions are those falling under the umbrella of the Hartree-Fock (HF) approximation.

In the HF approximation, rather than treating the N-electron wavefunction *as is*, a product of N one-electron wavefunctions is used. The product of these one-electron wavefunctions is referred to as a Slater determinant:

$$\Phi_{\mathrm{SD}} = \frac{1}{\sqrt{\mathrm{N!}}}\det\{\psi_1\ \psi_2 \ldots \psi_{\mathrm{N}}\} \tag{2.10}$$

Each one-electron wavefunction ψ_i is called a spin orbital and is a function of three spatial coordinates and one spin function, $\alpha(s)$ or $\beta(s)$. Similar to Eq. 2.5, spin orbitals are also orthonormal:

$$\int \psi_i \psi_j d\mathbf{r} = \langle \psi_i | \psi_j \rangle = \delta_{ij} \tag{2.11}$$

Again, the Kronecker delta is used (which is equal to 1 if $i = j$, and zero otherwise). The Slater determinant is antisymmetric, as any determinant changes sign if two columns or rows are interchanged, thereby accounting for the antisymmetric nature of the exact wavefunction.

The lowest energy Slater determinant can now be found using the variational principle under the constraint that the spin orbitals remain orthonormal. It can be shown that the purely electronic (without nucleus-nucleus repulsion) Hamiltonian operator for the N-electron wavefunction is similar to a Hamiltonian for a 1-electron spin orbital,

$$\hat{h}_i = -\frac{1}{2}\nabla_i^2 \quad -\sum_A^M \frac{Z_A}{r_{iA}} + \sum_{j\neq i}^{N-1} \int \frac{|\psi_j|^2}{r_{ij}} d\mathbf{r} \tag{2.12}$$

The last term in Eq. 2.12 is the electron-electron repulsion felt by the i^{th} spin-orbital by the electron density in every other j^{th} spin-orbital. However, evaluating the operation of $\hat{h}_i$ on a spin-orbital requires integration of ψ_i, which is what we are trying to calculate in the first place! The Hartree-Fock scheme solves this problem by calculating the wavefunction and subsequently minimizing the energy expectation value iteratively, through a procedure known as the Self-Consistent Field (SCF). During the SCF procedure, a set of 'guess' spin-orbitals are generated and a one-electron Hamiltonian is constructed, evaluated (which generates a new set of spin-orbitals) and repeated until the difference between the energies of two subsequent sets are within some arbitrary threshold value.

Note that the expectation values of multiple $\hat{h}_i$ acting on every spin orbitals, when combined to give the molecular E, is actually double-counting the electron-electron repulsion. This can be (and usually is) easily corrected by subtracting half the total electron-electron repulsion from the final energy.

HF therefore allows a surprisingly cheap calculation of the approximate wavefunction and provides relatively accurate results for most systems, but as we shall see, fails to account for a major part of chemical interactions.

Electron correlation. The major pitfall of the Hartree-Fock method is that, in using one-electron spin-orbitals instead of the N-electron wavefunction, an essentially non-interacting system is created. This non-interacting system is relatively far removed from a truly fully-interacting system, as each electron, in its own spin-orbital, only experiences the *average* repulsion from all other electrons. The effect is lessened through the SCF procedure, which minimizes the energy, and the antisymmetric property of Slater determinants, but still does not account for the fluctuations in electron-electron repulsion due to the actual position and momentum of an electron relative to every other electron in real time. Correcting for these effects is known under the heading of electron correlation and is highly dependent on the spin-state of each spin-orbital.

Electron correlation comes in two flavours: Coulomb and Fermi correlation (also called correlation and exchange, respectively). As we shall see below, HF already accounts for Fermi correlation exactly, but totally disregards Coulomb correlation.

Electron correlation is most easily understood with the *pair density* $\rho_2(x_1, x_2)$:

$$\rho_2(x_1, x_2) = \mathrm{N}(\mathrm{N}-1)\int\cdots\int|\Psi(x_1, x_2, \ldots, x_N)|^2 dx_3, dx_4, \ldots, dx_N, \tag{2.13}$$

The pair density gives the probability of finding an electron at x_2, given an electron is already present at x_1. The pair density is equal to zero if $x_1 = x_2$ (two electrons with the same spin cannot be found at the same place), resulting in an effect which is known as the Pauli Exclusion Principle. However, for electrons with opposite spin functions, the pair density does not equal zero even if the electrons are in the same space.

If we analyse the HF pair density for a two-electron system with two spatial orbitals ϕ_1 and ϕ_2 and spin functions σ_1 and σ_2:

$$\rho_2^{HF}(x_1, x_2) = [\det\{\phi_1(r_1)\sigma_1(s_1)\phi_2(r_2)\sigma_2(s_2)\}]^2 \tag{2.14}$$

which becomes, after expanding the determinant and squaring:

$$\begin{aligned}\rho_2^{HF}(x_1, x_2) = {} & \phi_1(r_1)^2\phi_2(r_2)^2\sigma_1(s_1)^2\sigma_2(s_2)^2 \\ & +\phi_1(r_2)^2\phi_2(r_1)^2\sigma_1(s_2)^2\sigma_2(s_1)^2 \\ & -2\phi_1(r_1)\phi_2(r_1)\phi_1(r_2)\phi_2(r_2)\sigma_1(s_1)\sigma_2(s_1)\sigma_1(s_2)\sigma_2(s_2)\end{aligned} \tag{2.15}$$

In order to get the spin-independent pair density, Eq. 2.15 can be integrated over both spins s_1 and s_2. Doing so results in simply 1 for the spin-integral of the first two terms. If the spins of the two electrons are antiparallel - that is, $\sigma_1 \neq \sigma_2$, the last term in Eq. 2.15 will vanish, and the overall HF-pair density for two electrons with opposite spin then becomes $\rho_2^{HF,\sigma_1\neq\sigma_2}(r_1, r_2) = \rho_1(r_1)\rho_2(r_2)$ which is exactly the same as for the entirely uncorrelated non-interacting system. If, however, the spins are parallel ($\sigma_1 = \sigma_2$), the last term in Eq. 2.15 will not vanish, and $\rho_2^{HF,\sigma_1=\sigma_2}(r_1, r_2)$ becomes much more than the simple uncorrelated situation. Therefore, the HF scheme covers the electron correlation arising from the antisymmetry of the wavefunction exactly, but does not include the correlation due to spin-independent Coulomb repulsions in an exact quantum mechanical wavefunction. In other words, the movement of electrons with like spin are mostly correlated in HF theory, but electrons of opposite spin are entirely uncorrelated.

The energy resulting from Fermi-correlation (exchange) can be calculated by considering the interaction of the electron density with a hole function - a spatial and spin distribution relating the region where an electron will *not* be found, given another electron already at a specific coordinate. Since the exchange stabilization energy results from

electrons having the same spin, Fermi-correlation reduces the electron density relative to a non-interacting reference density and therefore always decreases the overall electron-electron repulsion - in that sense it can be said that the quantum mechanical exchange energy is always stabilizing. The exchange hole can also be quite delocalized - for instance, the exchange hole for a reference electron in a benzene molecule is delocalized equally on every carbon atom. This suggests a reduced probability of finding another electron of the same spin all over the aromatic system, and, since electrons are indistinguishable, means that the *reference* electron can be found equally on every carbon atom. In other words, an electron is delocalized along the exchange-hole.

In general, the electron correlation resulting from Fermi-correlation is much greater than the correlation resulting from Coulomb-correlation, which is why HF theory still produces relatively accurate results. However, in systems where electron dispersion (an aspect of Coulomb-correlation) is very important, HF have been known to produce quite large errors. This is particularly true in the case of Van der Waal's bonded interactions. Coulomb-correlation can be included, in varying degrees, through a number of methods which include perturbation theory, configuration interaction theory or Density Functional Theory (DFT). In this work, only HF and DFT methods are used, so higher-order *ab initio* electron-correlation will not be discussed.

Density Functional Theory

Ab initio quantum chemical methods - where the wavefunction is the central quantity - were discussed in the previous section. These methods are in principle exact, and any inaccuracies present are a result of certain approximations made in order to be able to solve the relevant equations, or to speed up computations. However, there are a number of problems associated with the *ab initio* approach: i) scaling - the wavefunction depends on 4N variables, and becomes unmanageable when all but the simplest molecules are concerned; ii) unobservable - the wavefunction itself cannot be measured experimentally, only through appropriate operators can the wavefunction be related to experimental data; iii) non-intuitive - the multidimensional complex wavefunction is difficult to interpret and understand, and once again one must turn to the use of appropriate operators to interpret the subtle effects of the wavefunction, and iv) high computational cost (in both memory

storage as well as processing speeds) for all but the most severe approximations (such as HF). There is therefore sufficient reason to explore central quantities other than the wavefunction in order to predict chemical phenomena.

One of the most avenues which were explored historically is the electron density. The reasons for this is obvious: i) the electron density is the most direct observable relating to the wavefunction itself, ii) the electron density can be accurately measured, iii) the electron density is more intuitive (especially for chemists) than the wavefunction, and iv) all of the information required to construct the Hamiltonian can be extracted from the electron density. Specifically, integrating the electron density gives the total number of electrons, N, and the electron density has maxima (specifically, cusps) at the nuclear coordinates. The local behaviour of the electron density at the cusps can even be evaluated to give the total nuclear charge for a specific atom. Therefore, with the electron density as the primary, quantitative and qualitative measure, one can establish all the necessary information in order to set up a Hamiltonian, and, consequently, a wavefunction.

Hohenberg and Kohn, in 1964, provided proof for this statement, showing that all the required information for quantum chemistry is available through analysis of the electron density (the first Hohenberg-Kohn theorem). The proof is based on the logical philosophical method, known as *reductio ad absurdum.* Assume two wavefunctions, with two possibly distinct Hamiltonians, but still generating the exact, ground state electron density. Given now as axiom that the external potential ($V_{ext} = V_{Ne} + V_{NN}$) generating the Hamiltonians must differ by *more* than a constant, it is easy to show that the axiom must be incorrect - that there cannot be two different external potentials which result in the same ground state electron density. Or, in other words, the ground state density uniquely specifies the terms resulting in the Hamiltonian and the wavefunction:

$$\rho_0 \Rightarrow \{N, Z_A, R_A, \} \Rightarrow \hat{H} \Rightarrow \Psi_0 \Rightarrow E_0$$

Thus the ground state energy, E_0, is a functional of the ground state electron density:

$$E_0 = \int \rho_0(\mathbf{r}) V_{Ne}\, d\mathbf{r} + T[\rho_0] + E_{ee}[\rho_0] \qquad (2.16)$$

The last two terms are universally valid; their forms are independent of the number of electrons, N, the coordinates of the nuclei, R_A, and the nuclear charges, Z_A. This gives rise to the combination of the last two terms of Eq. 2.16 into a separate functional, known as the Hohenberg-Kohn functional, $F_{HK}[\rho_0] = T[\rho_0] + E_{ee}[\rho_0]$. Therefore, any arbitrary

density fed into $F_{HK}[\rho_0]$ will give the expectation value for the sum of the electronic kinetic energies and the electron-electron repulsion, with the shape of $F_{HK}[\rho_0]$ independent of the system at hand. If $F_{HK}[\rho_0]$ were known exactly, the Schrodinger equation could be solved, also exactly. Unfortunately, the precise form of $F_{HK}[\rho_0]$ is not known, and neither are the two components of $F_{HK}[\rho_0]$ - $T[\rho_0]$ and $E_{ee}[\rho_0]$. However, the electron-electron repulsion functional does contains a classical and quantum mechanical contribution, $J[\rho]$ and $E_{QM}[\rho]$:

$$E_{ee}[\rho] = \frac{1}{2}\iint \frac{\rho(\mathbf{r}_1)\rho(\mathbf{r}_2)}{r_{12}} + E_{QM}[\rho] = J[\rho] + E_{QM}[\rho] \qquad (2.17)$$

Finding increasingly accurate forms for $E_{QM}[\rho]$ and $T[\rho]$ is one of the major challenges for DFT (since $J[\rho]$ is already known from classical mechanics).

Whereas the first Hohenberg-Kohn theorem shows that the ground state electron density is sufficient to obtain all properties related to the system, the second Hohenberg-Kohn theorem deals with the problem of *how* to determine the ground state density. The theorem, presented here without proof, states that $F_{HK}[\rho]$ delivers the lowest energy if and only if the input density, ρ, equals the true ground state density, ρ_0. As with HF theory, the lowest energy of $F_{HK}[\rho]$ can be found via the variational principle.

The Kohn-Sham approach. In order to approximate $F_{HK}[\rho]$, Kohn and Sham reported in 1965 an approach similar to the HF orbital approach but in a DFT context, by assuming a non-interacting reference system constructed from a set of one-electron functions. In this manner, the non-interacting kinetic energy can be calculated fairly accurately, with the remaining portion of the kinetic energy (arising through the real, dynamical interactions between electrons) contributing a minor part. Arising from this approach is then also a correlation contribution to the non-interacting electron-electron repulsion. $F_{HK}[\rho]$, in the Kohn-Sham context, is now composed of the following terms:

$$F_{KS}[\rho] = T_S[\rho] + J[\rho] + E_{XC}[\rho] \qquad (2.18)$$

where $T_s[\rho]$ is the kinetic energy of the non-interacting system, $J[\rho]$ the classical (Coulombic) electron-electron repulsion and $E_{XC}[\rho]$ - the so-called exchange-correlation functional which includes all the quantum-mechanical effects arising from a dynamical particle-wave electron model, such as the electron-electron correlation, antisymmetry

effects (exchange) and also the remaining contribution of the true kinetic energy, $T_c[\rho] = T[\rho] - T_s[\rho]$.

The one-electron functions of the Kohn-Sham approach are constructed in a very similar fashion as the one-electron orbitals in HF theory - through a Slater determinant and with a Hamiltonian operator for the non-interacting system,

$$\hat{H}_S = -\frac{1}{2}\sum_{i}^{N}\nabla_i^2 + \sum_{i}^{N} V_S(\mathbf{r}) \tag{2.19}$$

where $V_S(\mathbf{r})$ is the effective, local potential of the non-interacting system and does not include any electron-electron interactions. Connecting the non-interacting system to the true system is done by choosing $V_S(\mathbf{r})$ in such a manner so that the electron density of the non-interacting system is equal to the true ground state density,

$$\rho_S(\mathbf{r}) = \sum_{i}^{N}\sum_{s}|\varphi_i(\mathbf{r},s)|^2 = \rho_0(\mathbf{r}) \tag{2.20}$$

where the electron density is constructed in the usual and same manner as in the HF-scheme - through summation of the squared moduli of each one-electron function.

The final energy, which is then minimized (and under the usual constraints of orthonormality for the one-electron coefficients), has the following form:

$$E[\rho] = T_S[\rho] + J[\rho] + E_{XC}[\rho] + E_{Ne}[\rho] \tag{2.21}$$

Each term in Eq. 2.21 can be calculated explicitly, with equations very similar to the ones used in HF theory, except for $E_{XC}[\rho]$.

Very interesting is the difference in the formalism with regards to the use of one-electron functions in HF and Kohn-Sham-DFT (KS-DFT) models. In HF theory, the wavefunction is approximated by using a Slater determinant with one-electron orbitals (with some severe consequences); in KS-DFT theory, the use of a Slater determinant is in principle exact.

Exchange-Correlation functionals. The hunt for exchange-correlation functionals of increasing accuracy (or better fit-for-purpose) lies at the crux of DFT development, with schemes ranging from simple functionals based on a uniform electron gas, with local approximations for the exchange energy to very sophisticated and complicated functionals

with multiple empirical parameters. Interestingly, some of the most successful functionals are those whose success cannot be inherently explained. One class of functionals which has received tremendous success, due mostly to relatively cheap computational cost and high accuracy for generalized purposes, are the so-called hybrid functionals. These class of functionals combine HF exchange with one or more exchange and correlation functionals in a weighted fashion. For instance, Becke's three parameter hybrid functional combined with Lee-Yang-Parr correlation, or B3LYP,

$$\mathrm{E}_{\mathrm{XC}}^{\mathrm{B3}} = \mathrm{E}_{\mathrm{XC}}^{\mathrm{LSD}} + a(E_{XC}^{HF} - E_{X}^{LSD}) + bE_{X}^{B} + cE_{C}^{PW91} \qquad (2.22)$$

which contains fractions of *exact* exchange energy (from the HF scheme), the exchange and correlation functional resulting from the local spin density model (where the exchange is modelled locally and uniformly in a spherical fashion), the exchange from Becke's 1988 exchange functional and the correlation contribution from Perdew and Wang's 1991 functional. The coefficients a, b and c are chosen in order to optimize certain chemical properties on a test series of molecules.

The combination of HF and DFT in the manner of hybrid functionals allows some cancellation of the errors introduced by the lack of correlation in HF and the inaccuracies inherent in exchange-correlation (XC) functionals. In addition, combining different XC contributions from different approaches in a fitted manner allows XC functionals to be constructed for specific purposes. For instance, one can take B3LYP and optimize the parameters to perform better geometry optimizations, or to improve calculated vibrational spectra.

In this work we are mainly working with the extended hybrid functional combined with the Lee-Yang-Parr correlation functional, or X3LYP[34]. Similar to B3LYP, X3LYP was optimized in order to significantly improve the accuracy for hydrogen-bonded complexes and Van der Waals interactions.

Modern charge density and wavefunction analyses

The discussions in the previous sections detailed the theory involved for calculating the quantum mechanical system. However, many modern methods exist which can be used to extract chemically relevant information from the state function for additional

interpretation. In this work two different flavours of analyses are used - analyses based on the electron density distribution and analyses based on the wavefunction. Using the charge density is a very chemically intuitive approach, as the charge density is a real everywhere, and it is an observable (and experimentally measurable) property. In addition, charge density analyses are generally more invariant to the level of theory used (HF, DFT etc.) than analyses based on the wavefunction. However, one loses information regarding the phase of the wavefunction, which includes the exchange and correlation properties of electron dynamics, as well as the lack of information regarding excited states, which can have large implications regarding the reactivity of molecules. On the other hand, wavefunction analyses provides one with all the system information at hand, but becomes more difficult to interpret because of the complex nature of the wavefunction. One of the features of this work is the inclusion of both types of analyses and interpreting the informational collage that is subsequently generated. However, more emphasis is placed on charge-density analyses for a purely pragmatic reason - it is chemically more intuitive to interpret than in-depth studies on the wavefunction.

QTAIM. Bader's Quantum Theory of Atoms in Molecules[13] (QTAIM) is an extension of the physics of an open system to the study of atoms as they exist in molecules. An atom as an open system (Ω) is bounded by a surface $S(\Omega;\mathbf{r})$ of zero-flux in the gradient vector field of the electron density $\rho(\mathbf{r})$,

$$\nabla\rho(\mathbf{r}) \bullet \mathbf{n}(\mathbf{r}) = 0 \qquad (2.23)$$

for all $\mathbf{r}$ on the surface. The result is an exhaustive and physically sound partitioning of a molecule into real-space atomic contributions. The properties of an atom can be calculated in the same fashion as molecular properties, by evaluating Heisenberg's equation of motion for a given operator on the atom and its boundaries. These atomic properties are additive to give the molecular property. In fact, it has been shown that since QTAIM can be derived from Schwinger's principle of least action, the physics of the entire molecule is a special limiting case to the physics of an open system.[2,14–16] The gradient vector field of the electron density is also used to define molecular structure, by finding lines of maximum density connecting atom pairs. Such lines are called atomic interaction lines (AIL) or bond paths. On each AIL exists a special critical point of rank three called a bond critical point (BCP), which is a local minimum on the vector defined by the AIL and local maxima in the axes perpendicular to the AIL (a (3,-1) critical point). In addition, each interacting atom pair connected by an AIL shares a zero-flux interatomic surface (ZFS),

centred on the BCP and extending to infinity. ZFSs shows various properties associated with the interaction between two atoms[13,17–19] and integration of specific values related to the surface has been correlated with bond strength[19]. Lastly, in this work the atomic net charge is often used,

$$q(\boldsymbol{\Omega}) = \int_{\Omega} \rho(\boldsymbol{r}) d\boldsymbol{r} + Z(\boldsymbol{\Omega}) \tag{2.24}$$

where the first term of the RHS is the integrated electron density (or electron population) of the basin and the second term is the effective nuclear charge. It is important to note that many different definitions of atomic charges exist, such as Hirshfield atomic charges[28], Mulliken population analysis[29] and Natural Atomic Orbitals[30]. The expectation values of these very different atomic charges also differ significantly, and there is no golden standard of atomic charge calculations as of yet. However, QTAIM atomic charges (despite being called 'exaggerated'[31] or 'not as expected from chemical intuition'[32]) are, in the same manner as the entire theory of QTAIM, rooted in quantum mechanics and show great correlation with experimental results. [33]

IQA. The Interacting Quantum Atoms (IQA) approach of Pendás, Blanco and Francisco[20,21] is an energy decomposition scheme which calculates the interactions of particles (protons and electrons) within atomic basins (defined by QTAIM, although the scheme can be applied to any atoms-in-molecules approach[20]). IQA can effectively split the terms of the general multi-electron Hamiltonian into intra- and interatomic terms, which it calculates (especially the very expensive V_{ee}-based calculations) through the use of an efficient algorithm for calculating the second-order density matrix[21]. The various terms resulting from such decomposition can then be combined into chemically relevant values, resulting in an intra-atomic (or atomic self-energy),

$$E_{Self}^{A} = T^{A} + V_{en}^{AA} + V_{ee}^{AA} \tag{2.25}$$

and an interatomic interaction energy,

$$E_{Int}^{AB} = V_{en}^{AB} + V_{ne}^{AB} + V_{nn}^{AB} + V_{ee}^{AB} \tag{2.26}$$

where T^{A} indicates the integrated kinetic electron energy, V_{en} and V_{ne} the attraction between electrons and nuclei, V_{nn} the repulsion between nuclei and V_{ee} the electron-electron repulsion. These terms typically attain very large but opposite values, resulting in large cancellations. The electron-electron term, V_{ee}^{AB}, can be decomposed further into a classical (Coulomb) component and an exchange-correlation stabilization. The total

diatomic interaction energy (E_{Int}^{AB}) can now be partitioned into a classical or electrostatic component,

$$V_{Cl}^{AB} = V_{en}^{AB} + V_{ne}^{AB} + V_{nn}^{AB} + V_{eeC}^{AB} \tag{2.27}$$

and a quantum-mechanical (exchange-correlation) component,

$$V_{XC}^{AB} = V_{eeX}^{AB} + V_{eeCorr}^{AB} \tag{2.28}$$

V_{XC}^{AB} is usually negative, due to the stabilizing nature of the dominant exchange term, V_{eeX}^{AB}, whereas the sign of V_{Cl}^{AB} is dependent on the nature of the interaction. Finally, V_{XC}^{AB} and V_{Cl}^{AB} are combined to give the total interaction energy,

$$E_{Int}^{AB} = V_{XC}^{AB} + V_{Cl}^{AB} \tag{2.29}$$

which is a measure of the strength of an interaction as well as providing valuable information regarding the nature of the interaction. The overall energy of an atom in a molecule is then given by the combination of intra- and interatomic terms,

$$E_{Total}^{A} = E_{Intra}^{AA} + \frac{1}{2}\sum_{B\neq A}^{N} E_{Inter}^{AB} \tag{2.30}$$

Note that E_{Intra}^{AA}will change significantly when the charge within the atom is reorganized (because of a changing chemical and physical environment) and when charge transfer occurs [20]. Since the formation of an intramolecular interaction induces both charge transfer and charge reorganization, a significant change in E_{Intra}^{AA} will be seen, corresponding to the atomic deformation (or promotion) as a local effect of the interaction. Therefore, it is important to realize that the interaction energy for a specific interaction is not equal to the binding or dissociation energy of that interaction, as a change in E_{Int}^{AB} might have an equal or even greater but opposite effect on the corresponding E_{Self}^{A} and E_{Self}^{B}.

ETS-NOCV. The Extended Transition State coupled with Natural Orbitals for Chemical Valence (ETS-NOCV) is formulated and described by Mitoraj *et al*[22–24] and briefly described here following the original derivation. ETS, an energy decomposition scheme, is a fragment based approach which decomposes the heat of formation, $\Delta E_{Bind} = E_{AB} - E_A - E_B$, into a number of chemical meaningful components, calculated in a series of different steps:

$$\Delta E_{Bind} = \Delta E_{Prep} + \Delta E_{Elstat} + \Delta E_{Pauli} + \Delta E_{Orb} \tag{2.31}$$

ΔE_{Prep} is calculated in the first step by distorting the two fragments A^0 and B^0 from their respective equilibrium geometries to A and B, the final geometries as they exist in the combined molecule. In the second step, the distorted fragments A and B are brought together from infinite separation to the distances they occupy in the final molecule but without changing the densities of each fragment. The energy change calculated by this step is given by ΔE_{Elstat}, or the electrostatic ETS energy. The irregular wavefunction for the combined system at this state is given by $\Psi^A\Psi^B$. However, this wavefunction is not antisymmetric and does not comply with the Pauli Exclusion Principle. In the third step, ΔE_{Pauli} is calculated by performing a Löwdin orthogonalization and thereby constructing the normalized, antisymmetric wavefunction:

$$\Psi^0 = N\hat{A}\{\Psi^A\Psi^B\} \tag{2.32}$$

The proper wavefunction Ψ^0 can be seen as an excited state, as it adheres to the Pauli Exclusion Principle but is far away from the minimized, ground state wavefunction, as fragment orbitals are not interacting in a stabilized manner yet. The final wavefunction is then constructed by minimizing the orbitals of Ψ^0, the fourth and final step which produces ΔE_{Orb}. Occupied and virtual fragment orbitals of A and B now mix with each other (in both intra- and interfragment fashion), allowing for spin-pairing and favourable occupation of all electrons.

The density change of the final step, $\Delta\rho_{Orb}$, can be further decomposed and localized through the NOCV procedure:

$$\Delta\rho_{Orb} = \rho - \rho^0 = \sum_{k=1}^{N/2} \nu_k\left[-\Psi_{-k}^2(\mathbf{r}) + \Psi_k^2(\mathbf{r})\right] = \sum_{k=1}^{N/2} \Delta\rho_k \tag{2.33}$$

where the orbital deformation density, $\Delta\rho_{\mathrm{Orb}}$, is expressed as a sum of pairs of complementary orbitals corresponding to eigenvalues (υ_k) equal in absolute value but opposite in sign. A complementary NOCV pair gives a deformation density, $\Delta\rho_{\mathrm{Orb}}(k)$, defining separate channels for charge transfer. Visual inspection of each deformation density can provide chemically meaningful information related to orbital mixing (and the consequences of inter-fragment spin-pairing) when the final wavefunction, Ψ, is compared with the non-interacting excited state, Ψ^0. ΔE_{Orb} can be decomposed into contributions relating to each NOCV in a procedure described in Ref. 19.

The concepts of deformation densities are used extensively throughout this work, with the general term deformation density implying the difference in electron density between a final and initial state. Four different densities are present in the ETS–NOCV scheme: the isolated fragment densities, ρ^A and ρ^B, the Pauli density (non-interacting, orthogonalized combination of fragment densities), ρ^0, the Orbital density (or final, SCF-minimized density), ρ, and the Orbital density decomposed in the kth NOCV contribution, ρ^k. From these various densities, five different *deformation* densities can be constructed: the Pauli deformation density ($\Delta\rho_{Pauli} = \rho^0 - (\rho^A + \rho^B)$), the Orbital deformation density ($\Delta\rho_{Orb} = \rho - \rho^0$), the kth NOCV deformation density ($\Delta\rho_{Orb}{}^k = \Delta\rho^k$, see Eq. 2.33), the Net Pauli-Orbital deformation density ($\Delta\rho_{Net} = \Delta\rho_{Pauli} + \Delta\rho_{Orb} = \rho - (\rho^A + \rho^B)$) and the Net Pauli-NOCV deformation density ($\Delta\rho_{Net}{}^k = \Delta\rho_{Pauli} + (\Delta\rho_{Orb}{}^k)$. The Net Pauli-Orbital deformation density is usually just known as the total deformation density, or sometimes just the deformation density, and refers to the change in density of the isolated fragments with regards to the final ground-state density. It is a very useful quantity, as it can be used to gauge whether the Pauli deformation density or the Orbital deformation density is the dominant effect in a specific region of space. It can be localized to some extent by using the Net Pauli-NOCV deformation density, which combines the total Pauli deformation density with a localized portion of the Orbital deformation density. It is used throughout this work to determine how the Pauli Exclusion Principle interferes (constructively or destructively) with a specific NOCV-localized orbital mixing, and which effect (Pauli or Orbital) is dominant.

NCI. The Non-Covalent Interactions (NCI) method[25–26] is, like QTAIM and IQA, a real-space method with focus on the electron density. NCI is able to identify all interactions which are stabilizing or destabilizing in the inter-nuclear regions through 3-D surfaces smeared between close contacts. NCI identifies areas where the electron density deviates with respect to the distribution of a homogenous electron gas, as described by the reduced density gradient (RDG):

$$s(\rho) = \frac{1}{C_F}\frac{|\nabla\rho|}{\rho^{4/3}} \tag{2.34}$$

where $C_F = 2(3\pi^2)^{1/3}$ is a constant and the 4/3 exponent of the density ensures that s(ρ) is a dimensionless quantity. The RDG has very large positive values in density tails (at distances far away from nuclei), but approaches zero in regions where an interatomic interaction is present. This feature can be exploited by plotting the RDG against $\rho(\mathbf{r})$. In

such plots, interactions appear as sudden troughs against an exponentially increasing RDG with decreasing $\rho(\mathbf{r})$. These troughs can also be visualized through isosurfaces of the RDG, allowing meaningful chemical interpretation.

In order to classify regions of NCI-defined interaction as either stabilizing or destabilizing, the second derivative of the electron density can be used. The eigenvalues of the Hessian-matrix are, by convention, defined in the order of $\lambda_1 \leq \lambda_2 \leq \lambda_3$. Topologically, the density *along an interaction* will always be less than the density at the nuclei and therefore at least one λ eigenvalue will be positive (giving $\lambda_3 > 0$, by the above-mentioned convention). λ_2 then gives a useful indication of whether electron density is locally concentrated ($\lambda_2 < 0$) or depleted ($\lambda_2 > 0$) in an axis perpendicular to the interaction. Any interaction which is destabilizing in the inter-nuclear region (steric interactions) will therefore show a depletion of electron density, whereas stabilizing interactions (such as hydrogen-bonds) will show a region of electron concentration. Colouring isosurfaces of RDG with the sign of λ_2 times $\rho(\mathbf{r})$ can give an indication of the local depletion or concentration of each NCI-defined interaction region. In addition, plots of RDG against $\text{sign}(\lambda_2)\rho(\mathbf{r})$, henceforth known as NCI-plots, show interactions as troughs in either the concentration or depletion regions.

It is important not to confuse "destabilizing in the internuclear region" as used above with an overall destabilizing interaction. While NCI is able to identify interactions in the internuclear (bonding) regions of interactions, it does not provide any information with regards to the overall inter-basin interaction energies. Therefore, it is possible for NCI to show a region of concentration between two highly positively charged atoms, relating the possibility of a concentration of electron density which functions to partially screen large V_{nn} repulsions.

Development of an algorithm for interaction cross-sections

Quantum chemical topology is a very useful field, as it allows a close-up view of the point-by-point distribution of charge throughout a molecule. However, these analyses are usually carried out in 3D space, resulting in a minor loss of information with regards to the topology of charge and derived fields in 1D or 2D space. A good example is the Laplacian operator, for which the expectation value is usually reported as the trace of the Hessian

matrix at a point but the individual eigenvalues and eigenvectors of the Hessian matrix contain very useful information (as is clear from the NCI method). We have found that 1D topology maps lend some additional information, useful for interpreting the results reported by QTAIM and NCI analyses. To this end we have developed a small utility application which can calculate 1D cross-sections of the electron density and its 1D partial derivatives. Even though the algorithm for these calculations is simple and easily coded, we have included it here for the sake of clarity with regards to the results presented in the following chapters. The application was written using Microsoft Visual C# 2010 and is not yet available for use outside of our own labs.

The purpose of the application is to calculate the cross-section of electron density along the eigenvector specified by the λ_2 eigenvalue of the Hessian matrix (henceforth referred to as just the λ_2 eigenvector), given a specific starting coordinate (usually the point of minimum electron density between two nuclei). The application accepts as input the nuclear coordinates of two close atoms, and finds the coordinate of minimum electron density between the atoms. Alternatively, one can specify any coordinate as starting point. The electron density at this coordinate is recorded, and the λ_2 eigenvector *direction* is then calculated. A new coordinate is found at a user-specified interval distance away from the input coordinate, and the electron density is recorded. This step is repeated until the length of the entire cross-section path is the same as a user-specified input length. The first and second partial derivatives are then calculated.

The user must also specify a wavefunction file (with extension .wfn), which can be generated in most quantum chemical software. The wavefunction file contains all of the molecular orbital and primitive coefficients, and the electron density at a Cartesian coordinate **r** is recorded in the following manner:

$$\rho(\mathbf{r}) = \left(\frac{1}{\sqrt{\mathrm{N!}}} \sum_{i}^{M} \varphi_i(\mathbf{r}) O_i \right)^2 \tag{2.35}$$

where φ_i is the i^{th} molecular orbital, O_i its occupation, N the total number of electrons and M the number of occupied molecular orbitals. Each molecular orbital is expressed in terms of a weighted sum of primitives,

$$\varphi_i(\mathbf{r}) = \sum_{j}^{L} \phi_j(\mathbf{r}) c_j \tag{2.36}$$

where ϕ_j is a Gaussian function and c_j a molecular orbital coefficient (which is read from the wavefunction file). Each Gaussian function is of a specific type and dependent on an exponential factor and the distance **r** from the primitive centre (the coordinates of a specific nucleus). All of this information is also read from the wavefunction file, and the formula of each type of primitive was included in the code from the suitable basis set descriptions.

Once $\rho(\mathbf{r})$ has been determined, the Hessian matrix can be calculated:

$$\mathbf{H}(\mathbf{r}) = \begin{pmatrix} \frac{\partial^2\rho}{\partial x^2} & \frac{\partial^2\rho}{\partial x\partial y} & \frac{\partial^2\rho}{\partial x\partial z} \\ \frac{\partial^2\rho}{\partial y\partial x} & \frac{\partial^2\rho}{\partial y^2} & \frac{\partial^2\rho}{\partial y\partial z} \\ \frac{\partial^2\rho}{\partial z\partial x} & \frac{\partial^2\rho}{\partial z\partial y} & \frac{\partial^2\rho}{\partial z^2} \end{pmatrix} \tag{2.37}$$

Partial second derivatives are calculated through the finite difference method[35], with sufficiently small perturbations of 0.001 bohr. The λ_2 eigenvector can be calculated by diagonalizing **H**(**r**), which is accomplished through a unitary transformation, $\mathbf{r'} = \mathbf{rU}$, where **U** is a unitary matrix constructed from a set of three eigenvalue equations,

$$\mathbf{H}\mathbf{u}_i = \lambda_i \mathbf{u}_i \tag{2.38}$$

The new coordinate system given by $\mathbf{r'}$ contains the unit vector $\mathbf{y'}$, which, when expressed in the original coordinate system, gives the direction of the λ_2 eigenvector.

Following the λ_2 eigenvector in this manner gives a very good description of the electron density as it curves throughout the interaction, proceeding exactly through any critical points in the region. However, for distances further away from the interaction of interest (and closer to other interaction regions), the λ_2 eigenvector is not applicable anymore for the cross-section of the interaction of interest. Therefore, the user can specify which part of the cross-section should be treated according to analysis of the λ_2 eigenvector and which part should be linear, i.e. continuing along the last calculated direction without recalculating the λ_2 eigenvector.

The output of this code then produces a set of coordinates and distances away from the input coordinate (or, if two nuclei coordinates were given as input, the point of minimum density between the nuclei) as well as the electron density and its partial first and second derivatives with respect to the cross-section path. This data can be plotted to give a graph

which clearly shows the behaviour of the electron density and its derivatives when the cross-section of the interaction between two atoms is considered. In addition, we have included automatic script generation for visualization of the actual cross-section path in VMD[27].

We plan to extend the code to include 1D topology maps of other functions, such as the potential and kinetic energy distributions and the electron localization function. In addition, we want to include 2D and 3D radial distribution plots, which can give an indication of the electron concentration with respect to a nuclei as opposed to a Cartesian system.

Conclusions

In order to investigate the possibility of CH•••HC interactions in bipyridine and bipyridyl-containing metal complexes, we need to be able to calculate the properties and electronic charge distribution of the studied molecules. Using quantum wavefunction mechanics, we approach the quantum chemical solutions via two major models: Hartree-Fock theory and Density Functional Theory.

HF theory is fast, wavefunction-based theory which assumes that the wavefunction is composed of N 1-electron orbitals. Constructing these orbitals to be orthogonal to each other introduces the effects of antisymmetry on the combined wavefunction, resulting in an exact description of quantum mechanical exchange (or electron correlation for electrons of like spin). However, spin-independent electron-electron correlation is absolutely disregarded, leading to major deviations of the calculated wavefunction with regards to reality. This is particularly true for Van der Waals interactions. That said, HF theory is still a robust and very useful method, and, being an *ab initio* method, allows the calculation of certain post-SCF analysis.

DFT, unlike HF, is a totally different approach based on the electron density as a primary quantity. All other chemical properties can be derived from the density, including

the wavefunction itself. In DFT, all classical energetic contributions are calculated by constructing a non-interacting reference system (but with the exact ground state density). All quantum mechanical effects, resulting from the kinetic energy and potential energy of a dynamical interacting system, are then included in a separate functional. Unfortunately, the form of this functional is unknown and must be approximated, a process which can change the computational cost and accuracy of DFT quite significantly. However, compared to HF, DFT methods contain significant electron-electron correlation, resulting in much more accurate geometries, energies and chemical properties. Unfortunately, due to the manner in which DFT is calculated, certain advanced analyses cannot be performed - most notably IQA. The primary reason for this problem is the fact that the kinetic energy in DFT is contained partially in $J[\rho]$ and partially in $E_{XC}[\rho]$ - therefore, separating different components of the Hamiltonian into meaningful contributions (such as E_{Intra} or E_{Inter}) is impossible with regards to DFT formalism.

Three advanced density analyses were discussed (QTAIM, NCI and IQA) and one wavefunction-based analysis (ETS-NOCV). Whereas QTAIM gives a robust description of an atom in a molecule, and consequently recovers typical line-structures through a collection of atomic interaction lines called a molecular graph, NCI is able to detect many more intramolecular interactions through the deviations of the expected behaviour of the electron density in comparison to a uniform electron gas. Combining the two methods already gives a comprehensive description of interactions throughout a system, as not all NCI-defined interactions shows the presence of an AIL. The question as to why this is so is very important, and will be addressed to a certain extent throughout this work. IQA provides a strong energetic connection to a typical QTAIM analysis through partitioning of the Hamiltonian into separate intra-atomic and interatomic components, as well as grouping certain terms together to give the classical (electrostatic) and quantum-mechanical (exchange-correlation) contributions of an interaction. However, IQA is limited to *ab initio* methods, which, in this work, is only HF theory. Finally, ETS-NOCV takes a completely different approach to energy decomposition by separating the steps in wavefunction calculations and assigning energy and charge deformations to each step, allowing the calculation of so-called electrostatic energy, Pauli-deformation energy and orbital deformation energy. The recently developed NOCV contribution towards the ETS scheme allows the orbital deformation density and energy to be partitioned into separate

contributions, a very useful method to study the weaker interactions in a specific fragmentation scheme.

Finally, we present here for the first time 1D topology maps of the cross-sections of interactions. The algorithm for our in-house code is presented, and is based on following the density and density derivatives along the λ_2 eigenvector in between two nuclei.

References

[1] A. R. Leach, D. Schomburg, *in Molecular modelling: principles and applications.* Longman, London, 1996

[2] R. F. W. Bader, "*The Lagrangian Approach to Chemisty"* in The Quantum Theory of Atoms in Molecules: From Solid State to DNA and Drug Design, Wiley-VCH, Weinheim, 2007.

[3] D. Durr, S. Goldstein, R. Rumulka, N. Zanghi, *Phys. Rev. Lett.*, **2004**, *93*, 090402

[4] E. Lehmann, R. K. Puri, A. Faessler, T. Maruyama, G. Q. Li, N. Ohtsuka, S. W. Huang, D. T. Khoa, M. A. Matin, *Prog. Part. Nucl. Phys.*, **1993**, *30*, 219–228

[5] W. Koch, M. C. Holthausen, *in A Chemist's Guide to Density Functional Theory*. Second Edition, Wiley-VCH, Weinheim, 2001.

[6] C. J. Cramer, *in Essentials of Computational Chemistry: Theories and Models*. Second Edition, John Wiley & Sons, Ltd, West-Sussex, 2004.

[7] R. McWeeny, *in Methods of Molecular Quantum Mechanics*. Second Edition, Academic Press, London, 1992.

[8] P. W. Atkins, R. S. Friedman, *in Molecular Quantum Mechanics.* Third Edition, Oxford University Press, Oxford, 1997.

[9] A. Szabo, N. S. Ostlund, *in Modern Quantum Chemistry: Introduction to Advanced Electronic Structure Theory*, MacMillan Publishing Co., New York, 1982

[10] E. R. Davidson, D. Feller, *Chem. Rev.*, **1986**, *4*, 681–696

[11] K. L. Schuchardt, B. T. Didier, T. Elsethagen, L. Sun, V. Gurumoorthi, J. Chase, J. Li, T. L. Windus, *J. Chem. Inf. Mod.*, **2007**, *47*, 1045–1052

[12] C. F. Matta, J. Hernández-Trujillo, T. H. Tang, R. F. W. Bader, *Chem. Eur. J.* **2003**, *9*, 1940–1951

[13] R. F. W. Bader, *in Atoms in Molecules: A Quantum Theory*; Oxford University Press: Oxford, U.K. 1990

[14] R. F. W. Bader, *J. Mol. Struct: Theochem*, **2010**, *943*, 2–18

[15] R. F. W. Bader, *J. Phys. Chem. A.*, **2007**, *111*, 7966–7972

[16] S. Srebrenik, R. F. W. Bader, *J. Chem. Phys.*, **1975**, *63*, 3945

[17] R. F. W. Bader, "Confined Atoms Treated as Open Quantum Systems" *in "Advances in Quantum Chemistry, Vol. 57"*, Elsevier Inc., 2009

[18] R. F. W. Bader, D. Fang, *J. Chem. Theory Comput.*, **2005**, *1*, 403–414

[19] J. A. Platts, *Phys. Chem. Chem. Phys.*, **2005**, *7*, 3805–3810

[20] M. A. Blanco, A. M. Pendás, E. Francisco, *J. Chem. Theory Comput.*, **2005**, *1*, 1096–1109.

[21] A.M Pendás, M. A. Blanco, E. Francisco, *J. Comp. Chem.*, **2006**, *28*, 161–184

[22] M. Mitoraj, A. Michalak, T. Ziegler, *J. Chem. Theory Comput.*, **2009**, *5*, 962–975

[23] A. Michalak, M. Mitoraj, T. Ziegler, *J. Phys. Chem. A.*, **2008**, *112*, 1933–1939

[24] T. Ziegler, A. Rauk, *Inorg. Chem.*, **1979**, *18*, 1755–1759

[25] E. R. Johnson, S. Keinan, P. Mori-Sánchez, J. Contreras-García, A. J. Cohen, W. Yang, *J. Am. Chem. Soc.*, **2010**, *132*, 6498–6506

[26] A. Otero-de-la-roza, R. Johnson, J. Contreras-garcia, *Phys. Chem. Chem. Phys.*, **2012**, *14*, 12165–12172.

[27] W. Humphrey, A. Dalke, K. Schulten, *J. Molec. Graphics*, **1996**, *14.1*, 33-38.

[28] F. L. Hirshfield, *Theoret. Chim. Acta. (Berl.)*, **1977**, *44*, 129–138

[29] R. S. Mulliken, *J. Chem. Phys.*, **1955**, *23*, 1833–1840

[30] A. E. Reed, L. A. Curtiss, F. Weinhold, *Chem. Rev.*, **1988**, *88*, 899–926

[31] A. Haaland,T. U. Helgaker, K. Ruud, D. J. Shorokhov, *J. Chem. Educ.*, **2000**, *77*, 1076–1076

[32] F. Jensen, *in Introduction to Computational Chemistry*; John Wiley and Sons: New York, 1999.

[33] R. F. W. Bader, C. F. Matta, *J. Phys. Chem. A*, **2004**, *108*, 8385–8394

[34] X. Xu, Q. Zhang, R. P. Muller, W. A. Goddard, *J. Chem. Phys.*, **2005**, *112*, 014105–014118

[35] K. Mattsson, J. Nordström, *J. Comp. Phys.*, **2004**, *119*, 503–540.

Chapter 3

A rigorous theoretical investigation of the physical natures of close H--H contacts and other intramoleulcar interactions in 2,2′-Bipyridine.

Abstract:

Intramolecular interactions present in various conformers of 2,2′-bypiridine (BPy) have been investigated using multiple theoretical tools in a comparative fashion, with specific focus on elucidating the chemical nature of the supposedly steric clash in the close contact between hydrogen atoms in the 3 and 3′ positions. It was found that the CH•••HC interaction in the *s*-cis conformer shows an attractive interaction energy using the Interacting Quantum Atoms (IQA) energy decomposition scheme. Using the newly-developed Non-Covalent Interactions (NCI) technique, it was found that electron density is concentrated within the bonding region of the CH•••HC interaction. The Extended Transition State coupled with Natural Orbitals for Chemical Valence (ETS-NOCV) energy decomposition scheme showed that: i) significant and stabilizing orbital mixing occurs and ii) that the accumulated density resulting from orbital mixing is greater than the removal of density resulting from enforcing the Pauli Exclusion Principle. Lastly, it is shown that electron density is accumulated in the H3,H3′ atomic basins upon formation of the CH•••HC interaction using the Quantum Theory of Atoms in Molecules (QTAIM) and an atomic interaction line or bond path is seen. In comparison, the N--N interaction in *s*-cis shows directly opposite observations, and is clearly repulsive. The attractive CH•••N interaction in *s*-trans is similar to the CH•••HC interaction, but whereas the latter is predominantly quantum mechanical in nature, the former is fully electrostatic. This result is confirmed through a novel interpretation of the bond path, using an NCI-based indicator. Using four different theoretical tools we produce a consistent model which describes all intramolecular interactions present in BPy, and confirm the stabilizing nature of CH•••HC interaction in this molecule.

Introduction

Two chemical concepts are commonly used to explain the energy of one conformer relative to another: the strain of the backbone of the molecule, and the presence or absence of intramolecular interactions. These concepts are sometimes related in a molecule – the formation of a stabilizing interaction might only occur in the presence of significant backbone strain, leading to the formation of new bonds and interactions which are locally stabilizing but molecularly destabilizing. Both strain and the strength of intramolecular interactions are difficult to quantify by examining the change in molecular energy alone - a specific interaction might be wrongly interpreted as repulsive or stabilizing because of an increase or decrease in molecular energy, respectively, when the dominant change in energy might be caused by the increase or release of backbone strain. Understanding the nature of specific intramolecular interactions, especially those which have been heuristically (and sometimes arbitrarily) assigned to be either stabilizing or destabilizing, is thus of key importance in the development of chemistry as a locally stabilizing interaction which is overall destabilizing in one molecule might be overall stabilizing in another.

The binding energy of a chemical bond can be calculated in diatomics by evaluating the energy of the molecule with the energy of the atoms *in vacuo*, $E(A\text{–}B) = E(AB) - E(A) - E(B)$. This definition of the energy of a chemical bond, while well-defined and useful for the study of diatomic molecules or supramolecular dimers, is less clear when applied to intramolecular interactions in polyatomic molecules. Since the formation of an intramolecular interaction will occur simultaneously with a structural and therefore chemical change within the molecule (which will by itself also change the energy of the molecule), can we truly localize, quantify and describe an intramolecular interaction with the same conceptual precision with which we can analyse an intermolecular bond? Specifically, can we isolate an interaction theoretically and describe the effects of its formation on the interacting atoms, fragments and molecule? In addition, intramolecular interactions usually do not have the freedom to dissociate because of the presence of external constraints (such as a strong bond forcing the geometry in a preferred conformation), which further clouds the concept of the binding energy for an intramolecular interaction - rather, the question arises whether a specific forced interaction is stabilizing or destabilizing to the molecule as a whole. Such energetics are difficult to

quantify as an ideal reference state (a state identical in every way to the conformer of interest except for the presence of the interaction in question) is usually not available.

The concept of intramolecular binding and how to define it is similar to the question of whether atoms exist within molecules, since both are vague elements of the whole where a change in one element will cause a change in all others. The existence of atoms in molecules has been the subject of many theoretical developments of the last four decades, and to date at least ten novel atom-in-molecule partitioning theories have evolved[1–11]. Some of these theories are robust and well developed, and using the Quantum Theory of Atoms in Molecules (QTAIM) as an example, has very strong roots in physics[1,12–15] and correlations with experimental data[16]. A large body of proof exists[1,12–16] which give weight to the existence of an atom in a molecule. Many attempts have been made for partitioning, localizing and analysing bonds in molecules, ranging from bond energy decomposition schemes[17–20] to schemes which analyse charge density, rearrangements and transfers[21-24]. That said, the study of bonding and interactions has been very active recently with new interactions being discovered or reinterpreted, such as the halide-halide inter- and intramolecular bonds[25–29], charge-shift bonds[30–32], dihydrogen bonds[33–38] and ion-ion interactions[39–42]. One such interaction is the controversial CH•••HC interaction, present in many molecules such as biphenyl, 1,10-phenantrene and natural estrogen (3-hydroxy-1,3,5-(10)-estratrien-17-one) among others[43]. The nature of these CH•••HC interactions has been the source of an on-going debate, creating a large division in the principle theories of both sides - Bader's Quantum Theory of Atoms in Molecules (among others) supporting a stabilizing interaction model[43–48] and various Energy Decomposition Analysis techniques for the repulsive viewpoint[49–50].

A close H--H contact is present in the *s*-cis conformer of 2,2′-Bipyridine (BPy), as shown in Figure 3.1, and is usually used, together with lone-pair lone-pair repulsions on N atoms and the absence of a stabilizing CH•••N interaction in *s*-trans, to explain the increased energy of *s*-cis relative to *s*-trans[51–56]. In this model, the interaction between close H--H contacts has been called "steric hindrance" or "Pauli repulsion" even recently despite the similarity between H--H contacts in BPy with the CH•••HC interaction in biphenyl. These interpretations were mostly assumed in the literature, although Hancock and Nikolayenko[55] have recently studied the H--H contact in BPy and concluded that there exists no evidence from molecular orbital theory nor from NBO theory to support the presence of increased electron density in the bonding region of these atoms. However,

both MO and NBO theory, though useful to calculate electronic structure and analyse classical bonds, respectively, make the unproven implicit assumption that electrons exist only in maximally occupied finite partitions in Hilbert-space.[57–59] In contrast, real-space methods (such as QTAIM, NCI or IQA) or orbital-methods which do not make the same assumption (such as NOCV) can detect interactions in an unbiased fashion.

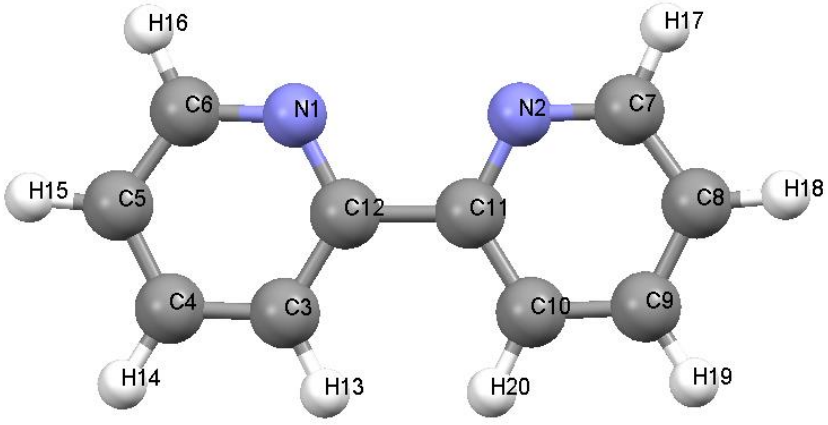

Figure 3.1. Ball-and-stick representation of the *s*-cis conformer of 2,2′-Bipyridine

Members of our group recently reported[60–61] that CH•••HC interactions in Ni^{II} and Zn^{II} complexes with NTPA (nitrilotri-3-propanoic acid) are in fact bonding interactions, based on a real-space QTAIM analysis as well as a natural orbital based approach, the Extended Transition State combined with Natural Orbitals for Chemical Valence (ETS-NOCV)[22]. Our analysis clearly showed that electron density is accumulated in a preferential manner in the bonding region of these interactions. Our results for the CH•••HC interactions in metal complexes with NTPA, as well as the finding by others of a bond path between the H--H contacts of biphenyl have led us to suspect that such a bonding interaction might be found in the supposedly clashing 3,3′ H-atoms of *s*-cis BPy.

For the purposes of further understanding the nature of intramolecular interactions and towards the eventual goal of estimating the stabilization or destabilization that intramolecular interactions contribute to the molecular energy, we present here a study of the various interactions in all forms of the free BPy ligand using a multi-theoretical approach. Using QTAIM[1], the Interacting Quantum Atoms (IQA) energy decomposition scheme in real-space[23], ETS-NOCV[22] and the recently developed Non-Covalent Interactions (NCI) technique[24], the aim of this chapter is to arrive at a consistent model for all the intramolecular interactions in BPy and to add to the understanding of each

interaction's chemical nature. We are specifically interested in the controversial H--H contact in BPy, and will compare the physical properties of the interaction with those of other interactions present in BPy, CH•••N and N--N interactions. The rest of the chapter is organized as follows: After a brief theoretical background and discussion of the computational methods used, Section 3.1 will discuss the molecular energy and geometrical changes which occur in BPy as *s*-trans is rotated along the junction C–C bond, Section 3.2 will show the results from each theoretical tool applied to the CH•••HC interaction, Section 3.3 will discuss and compare the physical properties of the N--N and CH•••N interactions with those of the CH•••HC interaction and Section 3.4 will explore the differences between the interactions by a) analysing the effects of including the Pauli deformation density from the ETS scheme, $\Delta\rho_{\text{Pauli}}$, with the results obtained from ETS-NOCV analysis and b) expanding on the interpretation of bond paths and the presence or absence of strain in the bonding region of each interaction.

Finally, it is important to state that the goal of this work is not to quantify or even recover the relative energies between conformers of BPy in terms of bond- and interaction energies, but rather to qualitatively understand the chemical nature of the interactions present in BPy. However, since any arbitrary decomposition scheme (whether it be decomposition of the molecular energy, electron density or molecular structure) must be related to some relevant experimental observation[62], the potential energy surface and the rotational barrier of BPy will be used throughout as an observational benchmark which our qualitative model should meet.

Appendix A discusses some preliminary results related to studying the causal effects that the formation of each interaction induces in the involved atoms' atomic properties, as well as the nature of each interaction with regards to the overall relative molecular energy. Appendix A uses QTAIM- and IQA-defined atomic energies, as well as looking at the changes in surface virials (QTAIM) and interaction energies (IQA) when *s*-trans is changed to *s*-cis. However, it should be noted that the results (including their interpretation) in Appendix A are still in infancy and are only included because these preliminary results show remarkable corroboration with the rest of the results shown in this chapter. Appendix B provides supplementary figures and tables not included in Chapter 3.

Computational Methods

All conformers of BPy were optimized in Gaussian 09c[63] using the Hartree-Fock approximation and 6-311++g(d,p) as a basis set. The effect of aqueous solvent was approximated with the Polarizable Continuum Model (PCM-UFF). QTAIM and IQA analyses were performed using AIMAll software[64]. All integrations were of sufficient accuracy (L(**Ω**) ≤ 1.0E-05 for all atoms). NCI analysis was carried out with NCIPlot 2.0[24] and visualized in VMD 1.9.1[65]. Frequency calculations were carried out first numerically and then analytically, and any reported molecular energy is the free energy (corrected with the zero-point vibrational energies and enthalpic and entropic contributions).

In order to perform ETS-NOCV analysis, all structures were re-optimized in ADF 2010[66–67], with the X3LYP functional, an augmented triple-ζ with polarization basis set and the COSMO model to approximate solvation. ETS-NOCV analysis was performed on the optimized geometries in ADF. The fragmentation scheme that was used is shown in Figure 3.2. The central C11–C12 bond was broken, and the N--N, CH•••HC and CH•••N interactions with it, in order to create two radical pyridine fragments.

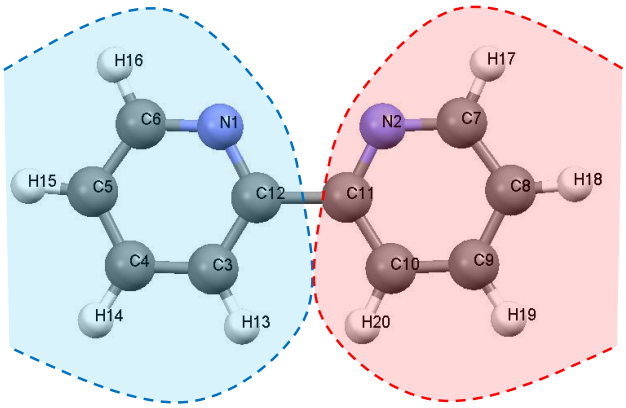

Figure 3.2. Fragmentation scheme used for ETS-NOCV analysis

Results and Discussion

Geometric analysis and free energy surface. Full Cartesian coordinates and thermochemical data for selected conformers of BPy are shown in Tables B1-B4 in Appendix B.

The potential energy surface of BPy with the dihedral angle DA(N1,C12,C11,N2) (henceforth referred to as Φ(1)) as the reaction coordinate is shown in Figure 3.3. Four stationary points are observed: the global minimum at *s*-trans (Φ(1) = 180°), a local maximum for the perpendicular structure (Φ(1) = 90°) at +3.87 kcal·mol^{-1} higher in energy than s-trans, a local minimum (Φ(1) = ~37°) at +2.56 kcal·mol^{-1} and the global maximum at *s*-cis (Φ(1) = 00°), +4.06 kcal·mol^{-1} higher in energy than *s*-trans, which is also the value of the calculated rotational barrier. The higher energy of Φ(1) = 90° is usually explained using conjugation - that the central C–C bond is weakened because of lack of effective π-bonding in the perpendicular Φ(1) = 90° conformer[51–56,68–70]. As Φ(1) is changed from 90° to 00°, increasing conjugation effects along the central C11–C12 bond decrease the molecular energy until it reaches the local minimum of Φ(1) = ~37°. Thereafter, in the region of 0° < Φ(1) < 37°, the molecular energy rises again. This increase in energy is usually attributed to the formation of N--N and CH•••HC interactions[51,69]. Our energetic results are identical to what has been observed in the literature.[55–56]

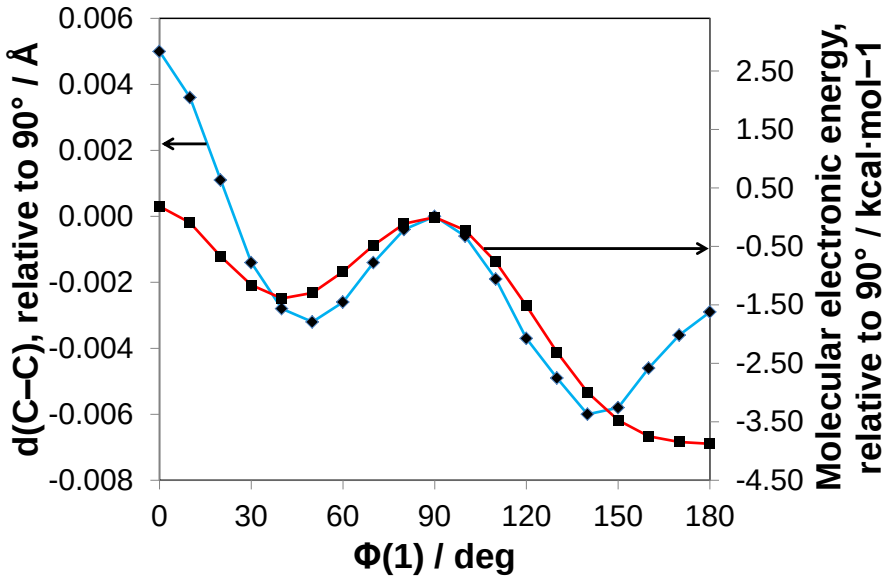

Figure 3.3. Variation in the junction C11–C12 bond length (diamonds with blue line) and variation in electronic energy (squares with red line) with Φ(1) of the free ligand BPy. All values are relative to Φ(1) = 90°

From geometrical analysis, when interatomic distances are compared with the van der Waals radii, three types of intramolecular close contacts can be identified in different conformers of BPy. In *s*-cis, two interactions, N--N with d(N--N) = 2.711 Å and a

CH•••HC with d(CH•••HC) = 2.009 Å are present. In *s*-trans, two CH•••N interactions exist with d(CH•••N) = 2.487 Å each. These intramolecular contacts are significantly shorter than the sum of Van der Waal's radii of atoms involved, 3.10 Å, 2.40 Å and 2.75 Å for the N--N, CH•••HC and CH•••N, respectively[71].

Distances between central carbon atoms, d(C11–C12) are shown in Table 3.1 and they are plotted in Figure 3.3 as a function of Φ(1).

Table 3.1. Selected geometrical data for the various conformers of 2,2′-Bipyridine

Φ(1) deg	d(C11–C12) Å	Δd(C11–C12)[a] Å	Φ(2) deg	δΦ(2 – 1)[b] deg
0	1.506	0.005	0.0	0.0
10	1.504	0.004	18.2	8.2
20	1.502	0.001	33.4	13.4
30	1.499	-0.001	45.6	15.6
40	1.498	-0.003	56.3	16.3
50	1.498	-0.003	66.1	16.1
60	1.498	-0.003	75.5	15.5
70	1.499	-0.001	84.9	14.9
80	1.500	0.000	94.0	14.0
90	1.501	0.000	102.9	12.9
100	1.500	-0.001	111.7	11.7
110	1.499	-0.002	120.4	10.4
120	1.497	-0.004	128.8	8.8
130	1.496	-0.005	137.1	7.1
140	1.495	-0.006	145.3	5.3
150	1.495	-0.006	153.6	3.6
160	1.496	-0.005	162.2	2.2
170	1.497	-0.004	171.0	1.0
180	1.498	-0.003	180.0	0.0

[a]Relative to Φ(1) = 90°. [b]Deviation of DA(**H13**,C3,C10,**H20**) (Φ(2)) from Φ(1).

The change in d(C–C) shows a few similarities to the change of the molecular energy (Figure 3.3): a local maximum is seen at Φ(1) = 90°, consistent with a weakening C–C bond because of conjugation effects and d(C–C) decreases as Φ(1) is changed towards 0° or 180°. However, conjugation cannot solely explain the changes in d(C–C) as local maxima are seen for both *s*-cis and *s*-trans. Clearly, the interactions present in these planar conformers cause a lengthening of the C11–C12 bond, a change only reflected by the increase in molecular energy in *s*-cis. In *s*-trans, the energy reaches a global minimum, indicating that the increase seen in d(C–C) is due to strain caused by the presence of potentially stabilizing CH•••N interactions (discussed later). The origin of this strain can

either be geometric (in order to accommodate the CH•••N interactions at favourable distances) or electronic (removal of charge from C11 and C12 in order to strengthen the CH•••N interaction). This is a very important observation, as it shows that the strain caused by the presence of an intramolecular interaction need not be localized to that specific interaction. In terms of *s*-cis, a relatively large increase in d(C–C) of +0.005 Å (relative to Φ(1) = 90°) is seen, resulting in the global maximum. The strain in d(C–C) is now caused by the presence of the repulsive N--N interaction or the potentially stabilizing CH•••HC interaction. The only way to rationalize the changes in d(C–C) as well as the changes in the molecular energy is therefore to understand the nature of the intramolecular interactions.

The dihedral angle formed by the CH•••HC interaction - DA(**H13**,C3,C10,**H20**) (henceforth referred to as Φ(2)) - should reflect the constrained Φ(1). However, large variations are seen, and the differences between Φ(2) and Φ(1) (δΦ(2–1)) are shown in the last column of Table 3.1 and plotted in Figure 3.4. At *s*-cis and *s*-trans, Φ(2) is indeed equal to Φ(1), indicating that the H-atoms are perfectly planar with regards to the pyridine rings. This is unexpected for *s*-cis if H13 and H20 were truly involved in a repulsive clash. What is remarkable about Figure 3.4 is the asymmetric distribution of δ(Φ(2–1)) – the deviation is the largest in Φ(1) = 40°, decreasing slowly in the region of 40° ≤ Φ(1) ≤ 180° but decreasing sharply in the region of 0° ≤ Φ(1) ≤ 40° (the region where the CH•••HC interaction is present). This observation seems to indicate that in the region where we expect the largest deviation of Φ(2) from Φ(1) (if the H-atoms were clashing), the opposite is seen – H13 and H20 are interacting in a manner which reduces the deviation from planarity for these atoms, implying that the interaction between these atoms are significantly strengthened in the *s*-cis conformer.

Interpretation of these geometrical observations, as well as the changes in the molecular energy, is highly dependent on our understanding of the nature of the intramolecular interactions in BPy - a topic which will concern the rest of this work. The next section will discuss the theoretical description of the CH•••HC interactions in *s*-cis BPy.

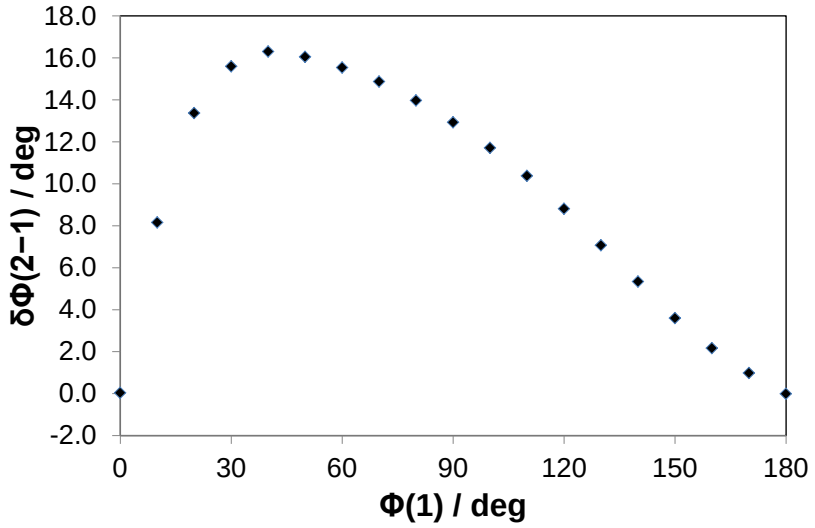

Figure 3.4. Deviation of the dihedral angle for H13,C3,C10 and H20 (Φ(2)) from the constrained dihedral angle for N1,C12,C11 and N2 (Φ(1)) for each conformer.

Theoretical description of CH•••HC interactions

Table 3.2 shows various theoretical descriptors from different methods describing the CH•••HC interaction. The following text will describe each descriptor in more detail.

QTAIM. Figure 3.5 shows the molecular graph for the cis conformer, as generated by QTAIM. Bond critical points (BCPs) are shown by green dots, whereas ring critical points (RCPs) are shown by red dots. Atomic interaction lines (AILs) are indicated by solid lines and ring paths from BCPs to RCPs are indicated by dots. As the central dihedral angle is changed, an AIL appears between **H13** and **H20** at $\Phi(1) \leq 20°$. The formation of the AIL (which necessitates the existence of a BCP[1]) connects the two pyridine fragments, forming a 6-membered ring by C12, C3, **H13**, **H20**, C10 and C11 and a RCP is present. The electron density at the BCP and RCP formed by the CH•••HC interaction is shown in Table 3.2. ρ_{BCP}**(H13,H20)** as well as the associated ρ_{RCP} reaches a maximum in the cis conformer.

Topologically, the electron density along an AIL is at a maximum at each of the two nuclei and at a minimum at the BCP. With regards to the axes perpendicular to an AIL, each point on the AIL is a local maximum. Furthermore, according to the eigenvalues of the Hessian matrix, each point of an AIL also shows a local concentration of electron density with regards to the axes perpendicular to the AIL[1]. Therefore, the AIL appearing

between **H13** and **H20** at $\Phi(1) \leq 20°$ describes a *line of maximum, concentrated density* between these two atoms, which is absent when the atoms are separated enough. Local electron density accumulates and is attracted towards the inter-nuclear region of interacting **H**-atoms – a phenomenon which would not occur if the associated atoms were indeed clashing.

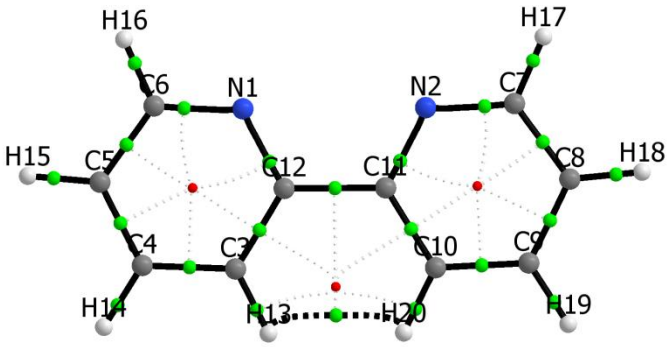

Figure 3.5. Molecular graph of the *s*-cis conformer of BPy**.**

Another consequence of the formation of an AIL between **H13** and **H20** is the presence of a zero-flux surface (ZFS) at the union of the atomic surfaces. We are interested in the virial of the force **H13** and **H20** exert on each other, V_s(**H13**‖**H20**), giving an indication of the energy released when the interatomic surface is formed. This inter-atomic potential energy is shown in Table 3.2, and is highly stabilizing by –22.76 kcal·mol^{-1}. V_s(**H13**‖**H20**), as well as similar analyses of other intramolecular interactions are shown in Figure A4 in Appendix A.

Lastly we consider the atomic net charge, *q*(**H13**). The charge shown in Table 3.2 is relative to the perpendicular non-interacting conformer, $\Phi(1) = 90°$. The net charge of **H13** in this conformer is +0.0295 *e* and decreases by –0.0092 *e* to +0.0203 *e* in the *s*-cis conformer. Figure 3.6a shows the relative changes of all hydrogens on one pyridine ring, indicating that the only **H13** undergoes any significant change in charge. **H13** (and **H20**) gains significant electron density as the CH•••HC interaction is formed. In addition, Figure 3.6b shows that for regions of d(**H13•••H20**) ≤ 2.500 Å electron density is deposited significantly in **H13** and **H20**.

Table 3.2. Theoretical descriptors of the CH•••HC interaction in BPy

		QTAIM				IQA			ETS-NOCV	NCI	
Φ(1)	**d(H,H)**	***ρ*(BCP)**	***ρ*(RCP)**	**V_s(H13‖H20)**	**Δ*q*(H13)**[a]	$E_{Int}^{CH\bullet\bullet\bullet HC}$	$V_{Cl}^{CH\bullet\bullet\bullet HC}$	$V_{X}^{CH\bullet\bullet\bullet HC}$	**ΔE_{Orb}**	$(-)\rho_{ICP}^{CH\bullet\bullet\bullet HC}$	$(+)\rho_{ICP}^{CH\bullet\bullet\bullet HC}$
Deg.	*Å*	*au*	*au*	*kcal·mol^{-1}*	*e*	*kcal·mol^{-1}*	*kcal·mol^{-1}*	*kcal·mol^{-1}*	*kcal·mol^{-1}*	*au*	*au*
0 (Cis)	2.009	0.01229	0.01119	-22.76	-0.00916	-3.03	-0.05	-2.97	-1.45	-0.01228	0.01120
10	2.041	0.01190	0.01113	-22.06	-0.00803	-2.81	-0.08	-2.74	-1.34	-0.01189	0.01114
20	2.130	0.01089	0.01074	-19.06	-0.00611	-2.30	-0.11	-2.18	-1.16	-0.01089	0.01074
30	2.257				-0.00403	-1.67	-0.11	-1.55	-1.01	-0.00968	0.00976
40	2.410				-0.00233	-1.13	-0.12	-1.01	-0.85	-0.00834	0.00854
50	2.593				-0.00130	-0.70	-0.13	-0.58	-0.74	-0.00658	0.00714
60	2.805		No Bond Path		-0.00071	-0.43	-0.15	-0.28			
70	3.046				-0.00043	-0.29	-0.17	-0.12			
80	3.302				-0.00021	-0.24	-0.19	-0.05			
90	3.555					-0.23	-0.21	-0.02			

[a] Relative to Φ(1) = 90°

These observations are again unexpected if the hydrogens were indeed clashing – electron density would've been removed from these atoms in order to (i) lessen the deformation caused by a decrease in atomic volume (as shown in Table B5 and Figure B1 of Appendix B) and (ii) lessen the effect of close electron-electron repulsions. The changes in q(**H13**) from Φ(1) = 90° to Φ(1) = 180° is related to the formation of a CH•••N interaction and will be discussed in Section 3.3, but already it is clear that the nature of these two interactions with regards to the electron population of the involved H-atoms is very different.

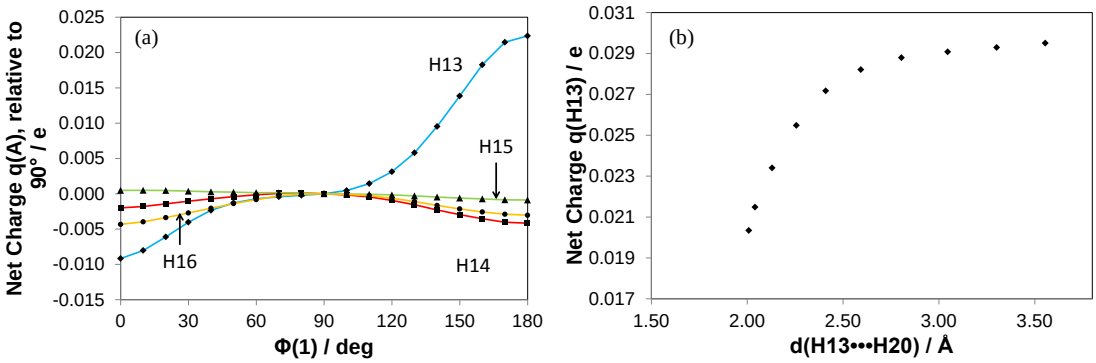

Figure 3.6. Atomic net charges of hydrogen atoms, (a) relative to the Φ(1) = 90° conformer and (b) as a function of the interaction distance.

IQA. Table 3.2 shows the CH•••HC interaction energy, $E_{Int}^{CH\bullet\bullet\bullet HC}$, as well as the partitioning of the interaction energy into the inter-atomic electrostatic (or classical) potential, $V_{Cl}^{CH\bullet\bullet\bullet HC}$, and the inter-atomic quantum exchange potential, $V_{X}^{CH\bullet\bullet\bullet HC}$. The exchange energy is always negative, as expected, but increases in value from almost 0 kcal·mol^{-1} in *s*-trans to –2.97 kcal·mol^{-1} in *s*-cis, showing the quantum mechanical stabilization resulting from electron delocalization when the CH•••HC interaction forms. Interestingly, the electrostatic potential is also close to zero, and even a little bit stabilizing (–0.05 kcal·mol^{-1}) in *s*-cis. Lastly, the summation of the classical and exchange terms gives $E_{Int}^{CH\bullet\bullet\bullet HC}$ with a value of –3.03 kcal·mol^{-1} in the *s*-cis conformer. Clearly, the interaction between particles of **H13** with particles in **H20** is stabilizing, and is quantum mechanical in origin.

ETS-NOCV. The relevant NOCV-based deformation density for the CH•••HC interaction is shown in Figure 3.7. The deformation density is stabilizing by $\Delta E_{\text{Orb}}(8)$ = –1.45 kcal·mol^{-1}. Electron density is accumulated preferentially in the inter-nuclear region, depleted in the non-bonding regions (the areas in **H13** and **H20** *outside* of the inter-nuclear

region) and in C3–C4 and C9–C10 bonds. Therefore, charge originating from neighbouring carbon atoms is transferred into the CH•••HC bonding region, forming a stabilized channel between the interacting atoms. This picture is concurrent with the QTAIM results (with the electron accumulation mimicking an AIL) as well as IQA results (stabilizing interaction energy and stabilizing orbital interaction energy).

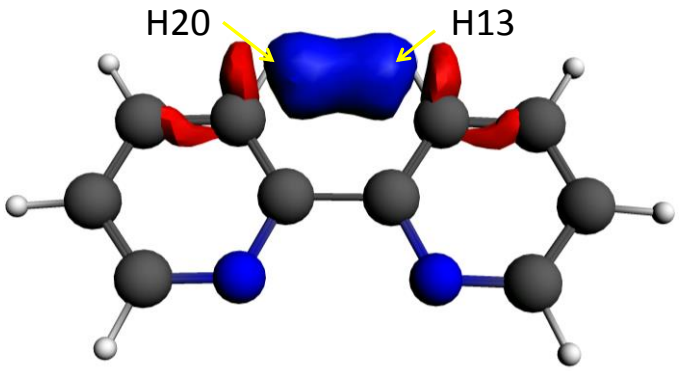

Figure 3.7. NOCV deformation density describing the CH•••HC interaction in the *s*-cis conformer of BPy. $\Delta\rho_8$, $\Delta E_{orb}(8)$ = –1.45 kcal·mol^{-1}, isovalue = 0.0007 au. Red-coloured regions show electron depletion, and blue-coloured regions show electron accumulation.

NCI. Figure 3.8a shows isosurfaces of the reduced density gradient (RDG), coloured with the value of sign(λ_2)ρ(**r**), for the region describing the CH•••HC interaction. The interatomic region (between **H13** and **H20)** is characterised by a local density concentration (coloured blue). In addition, there is a region of density depletion (coloured red) adjacent to the region of concentration, but it is located within the ring formed by C12, C3, **H13**, **H20**, C10 and C11. The regions of concentration and depletion corroborate with the positions of the QTAIM-defined BCP and a RCP, respectively. This is not surprising - a RCP is defined by two positive eigenvalues of the Hessian matrix, λ_2 and λ_3, and will thus appear as a region of depletion in the λ_2-centric NCI analysis. There is no NCI-based evidence of the inter-atomic region between these two H-atoms being strained due to high electron-electron or "Pauli-" repulsions (a depletion in electron density would have had to be observed).

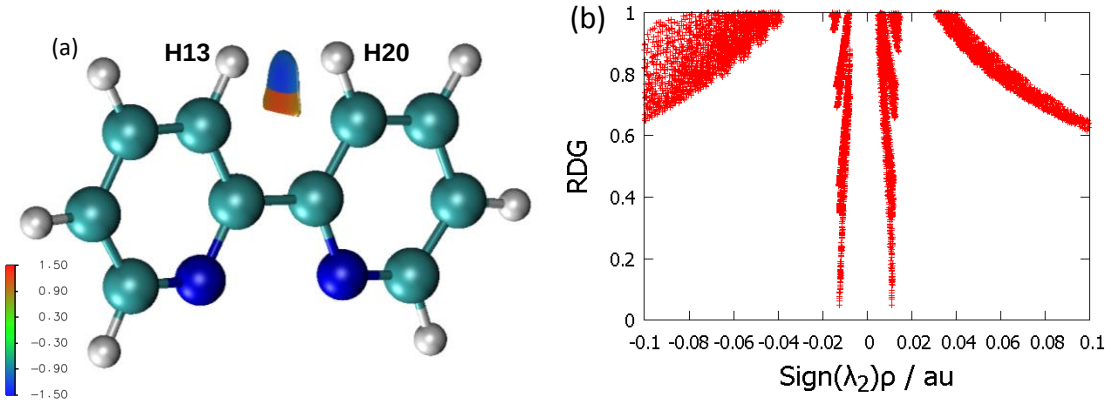

Figure 3.8. (a) NCI isosurface of RDG coloured with the value of sign(λ_2)ρ(**r**). Isosurface = 0.5. (b) NCI-Plot of RDG against sign(λ_2)ρ(**r**).

An NCI-plot of the RDG as a function of sign(λ_2)ρ(**r**) for the CH•••HC interaction is shown in Figure 3.8b. Two troughs are visible, corresponding to the concentration region between the diatomic interaction and the depletion region related to the polyatomic ring, as discussed above. The value of sign(λ_2)ρ(**r**) where the RDG in each trough approaches zero is known as NCI Interaction Critical Points (ICPs)[72]. The values of both ICPs, $(-)\rho_{ICP}^{CH\bullet\bullet\bullet HC}$ and $(+)\rho_{ICP}^{CH\bullet\bullet\bullet HC}$, are shown in Table 3.2. For $\Phi(1) \leq 20$, the values of $|(-)\rho_{ICP}^{CH\bullet\bullet\bullet HC}|$ correspond almost perfectly to the values of ρ_{BCP}(CH•••HC) – 0.01228 and 0.01229 au at $\Phi(1) = 0°$, respectively. Similarly so for the values of $(+)\rho_{ICP}^{CH\bullet\bullet\bullet HC}$ and the values of ρ_{RCP}(C12,C3,**H13**,**H20**,C10,C11). An interesting observation relates the values of both ICPs to the presence of an AIL. For an AIL to exist topologically, the density at a BCP must be larger than the density at an RCP. In NCI terms, $|(-)\rho_{ICP}^{AB}|$ must be larger than $(+)\rho_{ICP}^{AB}$. For $\Phi(1) \geq 30°$, no AIL is present and therefore no BCP or RCP. However, NCI still show regions of concentration and depletion - now corresponding to a pseudo-BCP and pseudo-RCP, respectively. As expected, for these regions $(+)\rho_{ICP}^{CH\bullet\bullet\bullet HC}$ is larger than $|(-)\rho_{ICP}^{CH\bullet\bullet\bullet HC}|$ - hence the disappearance of the topologically-defined AIL. This topic will be fully explored in Section 3.4. Lastly, it should be shown that the strength of the ring (as measured by $(+)\rho_{ICP}^{CH\bullet\bullet\bullet HC}$) increases with the strength of the intramolecular interaction (as measured by $(-)\rho_{ICP}^{CH\bullet\bullet\bullet HC}$) - an observation made before[73–75].

In conclusion, we have shown in this section that the electron density between supposedly clashing H--H contacts in BPy is in fact significantly concentrated in the bonding region and results in a stabilizing interaction which is quantum mechanical in nature.

The next section will perform similar analyses on the N--N interaction in *s*-cis, as well as the CH•••N interactions in *s*-trans.

Comparison with other close contacts in BPy

N--N Interaction. Figure 3.5 shows the molecular graph for the *s*-cis conformer. Clearly, no AIL between N1 and N2 is seen - no bridge of concentrated maximum density links these two atoms. The net charge of N1 in *s*-cis relative to Φ(1) = 90°, Δ*q*(N1), is shown in Table 3.3 and plotted as a function of the inter-nuclear separation in Figure 3.9. The net charge increases (becomes less negative) from –1.5276 *e* in Φ(1) = 90°, to –1.5143 *e* in Φ(1) = 00°. N1 therefore loses electrons as it comes into close-contact with N2. This is the opposite trend than what is seen in the CH•••HC interaction (Figure 3.6b), and is what is expected for a truly repulsive interaction - electron density is withdrawn from the interacting same atoms in order to reduce unfavourable electron-electron repulsion.

IQA data for the N--N interaction is collected in Table 3.3. Although there is a significant exchange stabilization (–8.51 kcal·mol^{-1} in *s*-cis), the interaction is overall highly repulsive (+255.60 kcal·mol^{-1}) because of very large electrostatic repulsion term (+264.11 kcal·mol^{-1}). More enlightening though, is the relative interaction energy as the interaction is still very repulsive even at large separations - E_{Int}^{N--N} increases by +20.59 kcal·mol^{-1} from 235.01 kcal·mol^{-1} in Φ(1) = 90° going to *s*-cis.

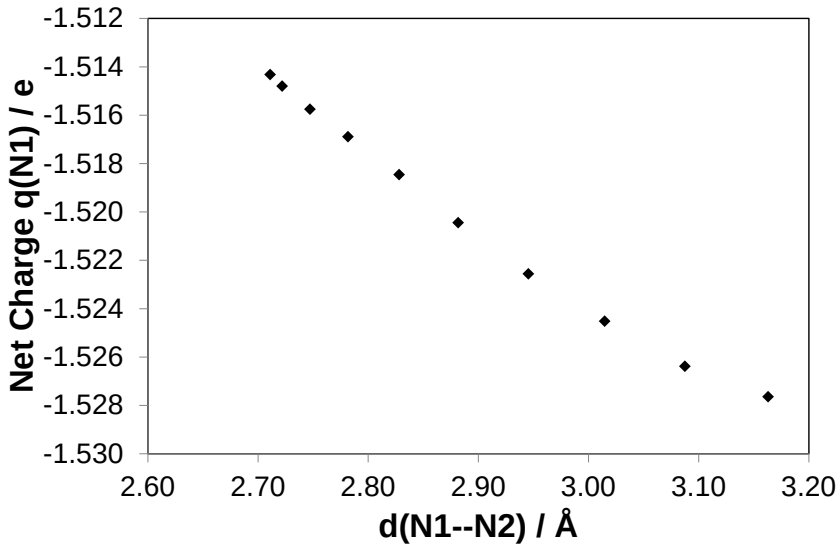

Figure 3.9. The net charge of N1 as a function of the inter-nuclear distance. d(N1--N2) decreases as Φ(1) = 90° is changed to Φ(1) = 00° (cis).

Table 3.3. Theoretical descriptors for N--N interaction in BPy

		QTAIM				IQA			ETS-NOCV	NCI	
Φ(1)	**d(N1,N2)**	ρ_{BCP}	ρ_{RCP}	V_s(N1‖N2)	q(N1)[a]	E_{int}^{N--N}	V_{Cl}^{N--N}	V_X^{N--N}	ΔE_{Orb}	$(-)\rho_{ICP}^{N--N}$	$(+)\rho_{ICP}^{N--N}$
Deg.	*Å*	*au*	*au*	*kcal·mol⁻¹*	*e*	*kcal·mol⁻¹*	*kcal·mol⁻¹*	*kcal·mol⁻¹*	*kcal·mol⁻¹*	*au*	*au*
0 (Cis)	2.711				0.01332	255.60	264.11	-8.51	-2.27	-0.01407	0.01447
10	2.722				0.01285	255.21	263.49	-8.28	-2.00	-0.01384	0.01425
20	2.747				0.01189	254.28	262.03	-7.76	-2.19	-0.01297	0.01340
30	2.782				0.01075	252.91	259.98	-7.07	-2.37	-0.01148	0.01217
40	2.828				0.00919	251.08	257.30	-6.22	-2.47	-0.00990	0.01087
50	2.882				0.00720	248.87	254.19	-5.32	-2.46	-0.00792	0.00935
60	2.946				0.00508	246.06	250.43	-4.36	-2.36		
70	3.015				0.00312	242.81	246.27	-3.47	-1.94		
80	3.088				0.00126	239.16	241.85	-2.69			
90	3.163	No Bond Path			0.00000	235.01	237.07	-2.06			
100	3.238				-0.00074	230.67	232.28	-1.61			
110	3.310				-0.00065	226.16	227.47	-1.31			
120	3.377				-0.00057	222.01	223.14	-1.13			
130	3.437				-0.00034	218.22	219.26	-1.04			
140	3.488				-0.00082	215.26	216.25	-0.99			
150	3.530				-0.00122	212.85	213.82	-0.97			
160	3.561				-0.00199	211.16	212.11	-0.95			
170	3.580				-0.00257	210.22	211.16	-0.94			
180 (Trans)	3.587				-0.00295	209.78	210.72	-0.94			

[a] Relative to Φ(1) = 90°

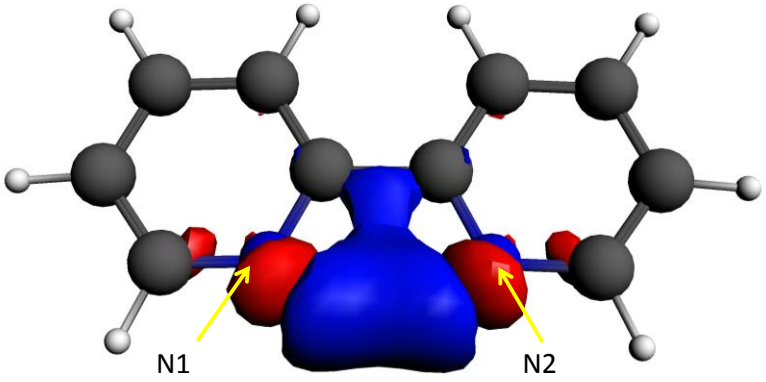

Figure 3.10. NOCV deformation density describing N--N interaction. $\Delta\rho(7)$, $\Delta E_{Orb}(7)$ = –2.27 kcal·mol^{-1}, Isosurface = 0.0003 au.

Finally, Figure 3.11a shows the RDG isosurface coloured with sign(λ_2)ρ(**r**) describing the N--N region in *s*-cis, and the corresponding NCI-plot in Figure 3.11b. Superficially, NCI shows similar results as CH•••HC in Figure 3.8 - a region of concentration is neighboured by a region of depletion (Figure 3.11a) and the NCI-plot shows two almost identical troughs (Figure 3.11b.). However, closer inspection reveals that, unlike for the CH•••HC interaction, the region of depletion is located in the inter-nuclear region and the region of concentration is located outside the inter-nuclear region. NCI thus show a clear region of steric strain in the valence region for the N--N interaction, consistent with the observation that charge is removed from N1 and N2 when the N--N interaction is formed. The region of concentration is either a topological consequence of the inter-atomic depletion, or it is a concentration as a result of quantum exchange between the two lone-pairs. Table 3.3 shows the sign(λ_2)ρ(**r**) value for each ICP trough. Since the values of each ICP for CH•••HC corresponded perfectly with the values of ρ_{BCP} and ρ_{RCP}, we assume here that the concentration ICP (–)ρ_{ICP}^{N--N} represents a pseudo-BCP, and the depletion peak (+)ρ_{ICP}^{N--N} a pseudo-RCP. Since in this case the (+)ρ_{ICP}^{N--N} is related to interatomic strain rather than a pure polyatomic ring effect, it is unlikely that an AIL will ever form as it will be very highly strained. It is then unsurprising that, unlike for the CH•••HC interaction in *s*-cis, the depletion ICP is larger in absolute value than the concentration ICP. This observation holds throughout conformers of all values of $\Phi(1)$ and is the reason why no topologically-defined BCP and RCP for the N--N interaction are present in any of the conformers.

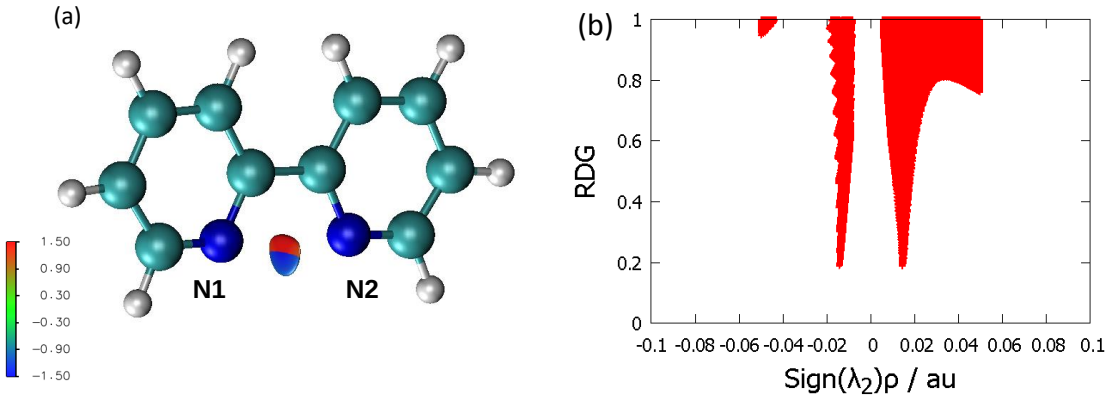

Figure 3.11. (a) NCI isosurface of RDG coloured with the value of sign(λ_2)ρ(r) for the N--N interaction. Isosurface = 0.5. (b) NCI-Plot of RDG against sign(λ_2)ρ(r) for the N--N interaction.

CH•••N Interaction. Figure 3.12 shows the molecular graph for the *s*-trans conformer. Like N--N, no AIL is seen between N1 and **H20** or N2 and **H13**, even though the inter-nuclear distance for each of these interactions is 2.487 Å, well within the sum of the interacting atoms' van der Waals radii (2.75 Å)[71]. The atomic net charges (relative to $\Phi(1) = 90°$) for both N1 and **H20** are displayed in Table 3.4. N1 has an atomic net charge of –1.52764 *e* at $\Phi(1) = 90°$, and becomes more negative by –0.00295 *e* to –1.53059 *e* in *s*-trans. **H20**, on the other hand, becomes more positive by +0.02236 *e* from +0.02951 *e* in $\Phi(1) = 90°$ to +0.05187 *e* in *s*-trans. The change in net charge for these atoms, relative to $\Phi(1) = 90°$, is displayed in Figure 3.13. Therefore, electron density is accumulated in the N1 and N2 atomic basins, whilst being depleted from the **H13** and **H20** basins. This observation can be explained by electrostatics - the interacting H- and N-atoms are positively and negatively charged, respectively. Therefore, we expect (and find - see IQA results below) an electrostatic interaction between these two atoms, which will be facilitated if the H-atom becomes more positive and the N-atom more negative. This observation is also in line with Popelier and Koch's criteria for hydrogen bonding[76], but since no AIL is present between these atoms, we cannot state (at least according to Popelier and Koch's criteria) that the CH•••N interaction is a true H-bond.

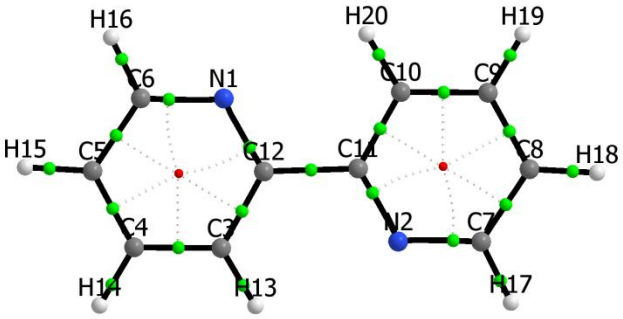

Figure 3.12. Molecular graph for the *s*-trans conformer.

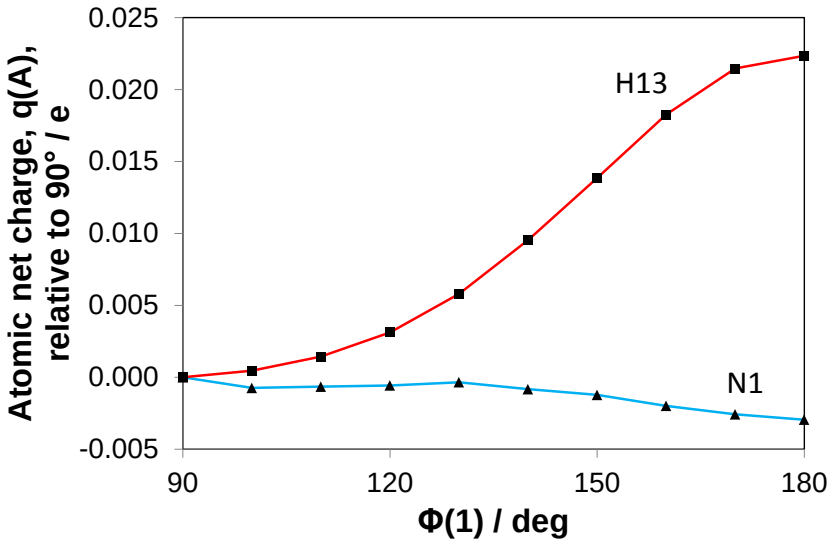

Figure 3.13. Change in atomic net charge, relative to Φ(1) = 90°. The blue line shows Δ*q*(N1), whilst the red line shows Δ*q*(**H20**).

The IQA results for the CH•••N interaction is shown in Table 3.4. $E_{Int}^{CH\bullet\bullet\bullet N}$ is negative and equal to –7.42 kcal·mol^{-1} in *s*-trans. The largest contributor is the electrostatic interaction, $V_{Cl}^{CH\bullet\bullet\bullet N}$ with a stabilization of –5.29 kcal·mol^{-1}. However, the exchange energy, $V_{X}^{CH\bullet\bullet\bullet N}$, is also contributing significantly, with a value of –2.13 kcal·mol^{-1}. The electrostatic portion of this interaction is even present in *s*-cis, with a value of –1.78 kcal·mol^{-1} and therefore becomes more stable from *s*-cis to *s*-trans by –3.51 kcal·mol^{-1}. CH•••N, like CH•••HC, is thus an attractive interaction, but whereas CH•••HC is quantum mechanical in nature, CH•••N is predominantly an electrostatic interaction.

Table 3.4. Theoretical descriptors for CH•••N interaction in BPy

		QTAIM				IQA[b]			ETS-NOCV	NCI	
Φ(1)	**d(N1,H20)**	ρ_{BCP}	ρ_{RCP}	**Δq(N1)[a]**	**Δq(H20)[a]**	E_{Int}^{CH--N}	V_{Cl}^{CH--N}	V_{X}^{CH--N}	**ΔE$_{Orb}$**	$(-)\rho_{ICP}^{N--N}$	$(+)\rho_{ICP}^{N--N}$
Deg.	*Å*	*au*	*au*	*kcal·mol^{-1}*	*e*	*kcal·mol^{-1}*	*kcal·mol^{-1}*	*kcal·mol^{-1}*	*kcal·mol^{-1}*	*au*	*au*
0 (Cis)	4.075			0.01332	-0.00916	-1.80	-1.78	-0.02			
10	4.056			0.01285	-0.00803						
20	4.009			0.01189	-0.00611						
30	3.950			0.01075	-0.00403						
40	3.878			0.00919	-0.00233	-2.27	-2.24	-0.03			
50	3.798			0.00720	-0.00130						
60	3.704			0.00508	-0.00071						
70	3.595			0.00312	-0.00043						
80	3.471			0.00126	-0.00021						
90	3.336	No Bond Path		0.00000	0.00000						
100	3.194			-0.00074	0.00046						
110	3.052			-0.00065	0.00144				-2.52		
120	2.918			-0.00057	0.00312				-3.36		
130	2.797			-0.00034	0.00580				-3.77	-0.00751	0.00821
140	2.690			-0.00082	0.00954				-4.03	-0.00962	0.01008
150	2.604			-0.00122	0.01385				-4.31	-0.01113	0.01137
160	2.540			-0.00199	0.01827				-4.60	-0.01238	0.01251
170	2.500			-0.00257	0.02147				-4.80	-0.01326	0.01333
180 (Trans)	2.487			-0.00295	0.02236	-7.42	-5.29	-2.13	-4.86	-0.01350	0.01360

[a] Relative to Φ(1) = 90°. [b] Only conformers for Φ(1) = 0°, Φ(1) = 40° and Φ(1) = 180° were calculated due to the high cost of IQA calculations.

Relevant NOCVs for the CH•••N interaction is displayed in Figure 3.14. The interaction is generally described by two different deformation densities - one pertaining to an induced electrostatic interaction, where density is depleted on H but accumulated on N ($\Delta\rho(6)$, Figure 3.14a), and one deformation density showing electron sharing, similar to what was seen for N--N and CH•••HC ($\Delta\rho(8)$, Figure 3.14b). $\Delta\rho(6)$, the electrostatic NOCV-pair, is always more stabilizing with $\Delta E_{Orb}(6) = -1.95$ kcal·mol^{-1} per interaction in *s*-trans. The second NOCV-pair, $\Delta\rho(8)$, shows an orbital stabilization of $\Delta E_{Orb}(8) = -0.48$ kcal·mol^{-1} per interaction. Together they give the overall stabilization from orbital mixing, ΔE_{Orb}(CH•••N) = –2.43 kcal·mol^{-1} per interaction. The electrostatic deformation density reflects the same results that the atomic net charges showed - electron density is withdrawn from **H13** and **H20**, but accumulated in N1 and N2. The accumulation of density is also shared across the C11–C12 bond, similar to the NOCVs describing N--N. The electron-sharing deformation density shows a more defined path, with electron density coming mostly from the nitrogen atom. The situation is the most defined in Figure 3.14c, for $\Phi(1) = 140°$. Here we see a clear exchange channel, with electron density being depleted from outside the inter-nuclear region and accumulated within it.

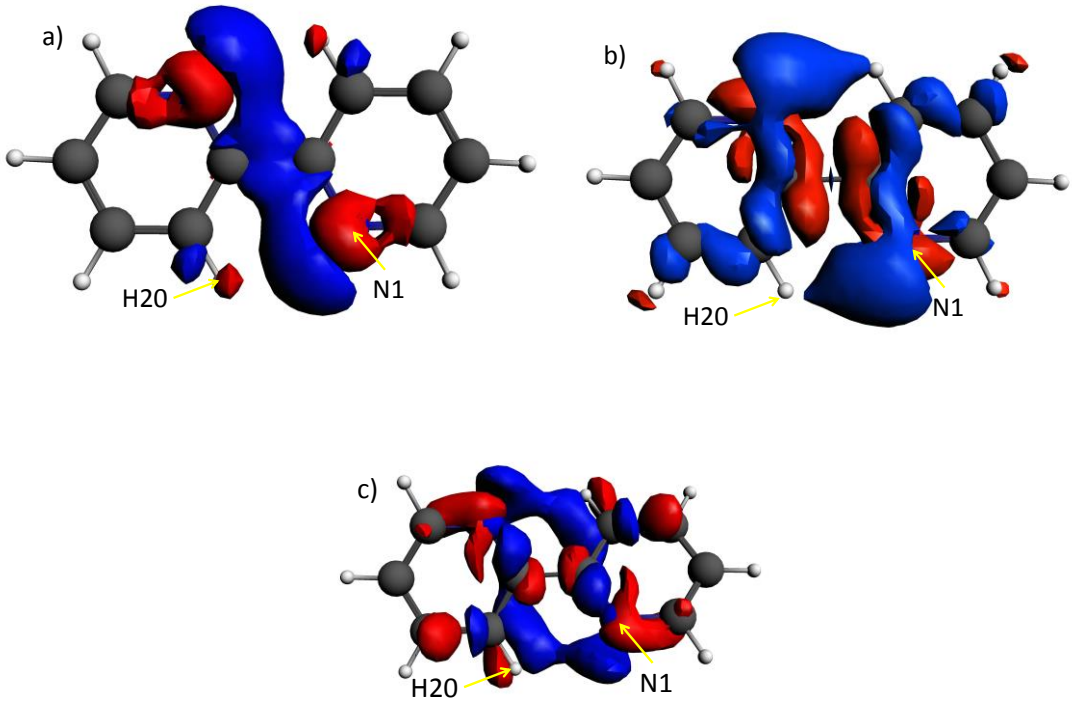

Figure 3.14. NOCV deformation densities for CH•••N interaction. (a) $\Delta\rho(6)$, $\Delta E_{Orb}(6) = -3.90$ kcal·mol^{-1}, Isosurface = 0.0002 au, s-trans. (b) $\Delta\rho(8)$, $\Delta E_{Orb}(8) = -0.96$ kcal·mol^{-1}, Isosurface = 0.00004 au, *s*-trans. (c) $\Delta\rho(9)$, $\Delta E_{Orb}(9) = -0.68$ kcal·mol^{-1}, Isosurface = 0.0001 au, $\Phi(1) = 140°$.

Finally, NCI plots and RDG isosurfaces for the CH•••N region in *s*-trans are shown in Figure 3.15. As for the CH•••HC interaction, no steric hindrance is seen. Instead, a concentrating pseudo-BCP and a depleting pseudo-RCP is seen, with $(-)\rho_{ICP}^{CH\bullet\bullet\bullet N}$ = -0.01350 au and $(+)\rho_{ICP}^{CH\bullet\bullet\bullet N}$ = 0.01360 au. Like N--N, $(+)\rho_{ICP}^{CH\bullet\bullet\bullet N}$ is slightly larger in value than $(+)\rho_{ICP}^{CH\bullet\bullet\bullet N}$. This supports our hypothesis that an AIL is only formed when $|(-)\rho_{ICP}^{AB}| > (+)\rho_{ICP}^{AB}$. Again, these observations will be discussed fully in Section 3.4.

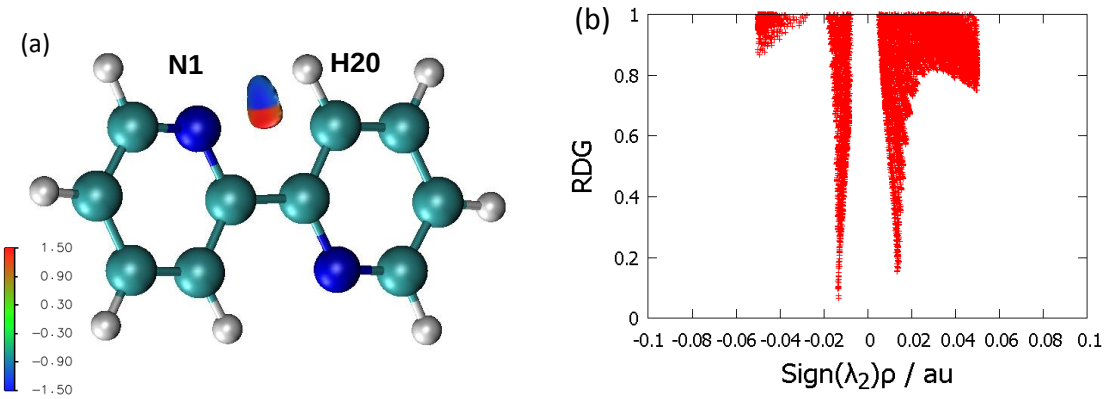

Figure 3.15. (a) NCI plots of RDG and $\lambda_2\rho$ for CH•••N interactions in trans. (b) Corresponding isosurfaces of the RDG coloured with $\lambda_2\rho$, with an isovalue of 0.5 au.

In conclusion, we have shown in this section that the CH•••N and N--N interactions in BPy are indeed attractive and repulsive, respectively, as what has been expected from the literature[51–56]. Both interactions are electrostatic in nature, but show some degree of orbital mixing/electron exchange stabilization. However, no AIL is seen for either of the interactions. In addition, electron density is concentrated in the bonding region of CH•••N but depleted in the inter-nuclear region of N--N.

Clearly, three similar but different in nature intra-molecular interactions are present in the different conformers of BPy. The next section will focus on the interpretation of the AIL, and how NCI, IQA and inclusion of the Pauli deformation density in ETS-NOCV analysis can be used to fully distinguish these interactions on a physical and chemical meaningful basis.

Classification of intramolecular interactions in BPy

Inclusion of Pauli deformation density in ETS-NOCV analysis. The Pauli deformation density – the difference between orthogonalized Pauli density, $\rho^o(AB)$, and the combined fragment density, $\rho(A) + \rho(B)$, gives an indication of the density rearrangements associated with enforcing the Pauli Exclusion Principle. Therefore, the Pauli deformation density for any close interaction will usually show depletion in the inter-nuclear region, due to the proximity of overlapping orbitals in the separate fragments. Figure 3.16a shows the total Pauli deformation density for *s*-cis. Clearly, the three points of close contact resulting from the fragmentation scheme used (Figure 3.2) - C12--C11, N1--N2 and H13--H20 - resulted in very large density depletion in the internuclear regions due to enforcing the Pauli Exclusion Principle on overlapping promolecular densities.

Whereas the Pauli-step in the ETS-scheme removes electron density from the internuclear region, performing a minimization on ρ^o generates the orbital deformation density ($\Delta\rho_{Orb} = \rho(AB) - \rho^o(AB)$ or the difference from the final SCF-minimized density and the Pauli-density, details are given in Chapter 2, section 2.4) and results in the final, lowest energy density, ρ. The orbital-mixing step usually accumulates significant density in the internuclear regions of bonds and interactions which can accommodate orbital mixing - mixing occupied and virtual as well as occupied with occupied orbitals to produce the final wavefunction. The total $\Delta\rho_{\mathrm{Orb}}$ for *s*-cis is shown in Figure 3.16b. Electron density is now donated into the bonding or internuclear regions of each interaction.

Combining $\Delta\rho_{\mathrm{Orb}}$ and $\Delta\rho_{\mathrm{Pauli}}$ gives the net Pauli and Orbital deformation density, $\Delta\rho_{Net} = \Delta\rho_{Pauli} + \Delta\rho_{Orb}$, and can be used to show whether the local removal of density in the Pauli-step is greater than the local accumulation of density in the Orbital-step for any given interaction. Alternatively, $\Delta\rho_{\mathrm{Net}}$ can be interpreted as the comparison of the density in the final wavefunction to the minimum densities of the non-interacting promolecular fragments. To aid interpretation, the localized NOCV deformation densities can be used for a given interaction instead of the total orbital deformation density, yielding the net Pauli and NOCV deformation densities, $\Delta\rho_{Net}(\mathrm{Y\text{--}X}) = \Delta\rho_{Pauli} + \Delta\rho_{Orb}(\mathrm{Y\text{--}X})$ (unfortunately no localization scheme exists yet for the decomposition of $\Delta\rho_{\mathrm{Pauli}}$). $\Delta\rho_{Net}(\mathrm{C\text{–}C})$ for the junction C11–12 bond is shown in Figure 3.16c, illustrating that

formation of the covalent C–C bond results in electron density accumulated in the inter-atomic bonding region while density is removed in the non-bonding regions within the rings, as expected. $\Delta\rho_{Net}$(CH•••HC) for the CH•••HC interaction is shown in Figure 3.16d. When compared to $\Delta\rho_{\text{Pauli}}$ in Figure 3.16a or to $\Delta\rho_{\text{Orb}}$(CH•••HC) in Figure 3.7, it is very clear that, while the Pauli-step removes density from the CH•••HC bonding region (indicated by a yellow dashed line in Figure 3.16d), the Orbital-step (localized via NOCVs) accumulates significantly more density in the same region. The net result is that orbital mixing for the CH•••HC interaction is dominant to the removal of density due to satisfying the Pauli Exclusion Principle, and the final electron density shows accumulation in the bonding region. Lastly, Figure 3.16e shows $\Delta\rho_{Net}$(N--N). Again, orbital mixing reduces the density depletion occurring from the Pauli step. However, unlike the CH•••HC interaction, in the inter-nuclear region of N--N (indicated by a green dashed line in Figure 3.16e), more density is removed because of the Pauli-step than density accumulated because of orbital mixing. The only region where orbital mixing is the dominant effect for N--N is outside the inter-nuclear region, in the lone-pairs of each N. Clearly, the N--N interaction shows significant steric strain, a result of the Pauli Exclusion Principle and two close electron-rich N-atoms.

Figure 3.17 shows the total Pauli, total Orbital and total net Pauli-Orbital deformation for *s*-trans. The electrostatic nature of this interaction is now perfectly visible - density is depleted in the **H20** and **H13** basins (because of orbital deformations) and accumulated in N1 and N2. Orbital effects play the dominant role for this interaction and thus no strain or "Pauli repulsion" is visible in the density distributions. Yet unlike the net Pauli-NOCV deformation for the CH•••HC interaction in Figure 16c, no channel of electron flow is seen for the CH•••N interaction.

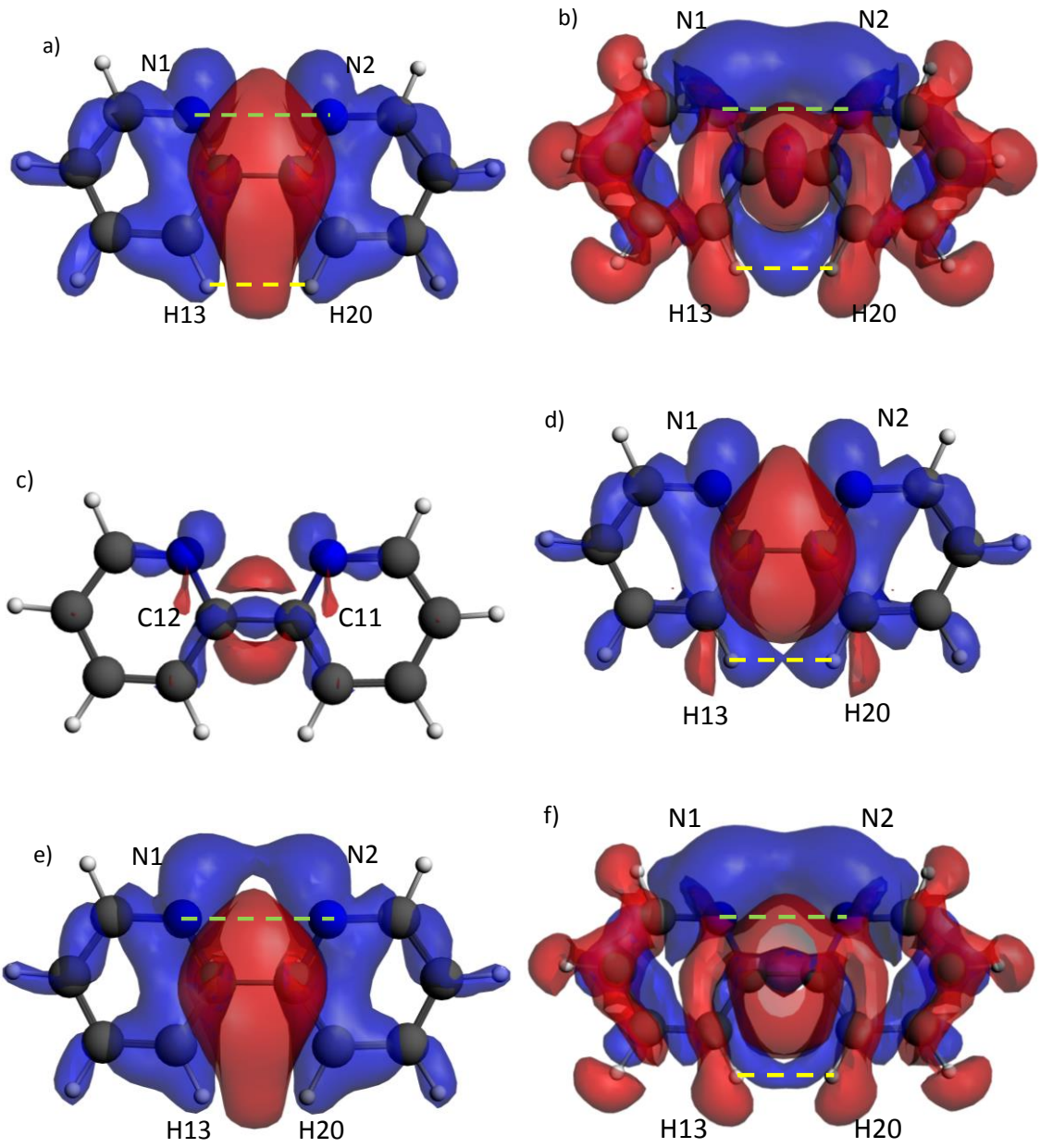

Figure 3.16. Pauli, Orbital and net deformation densities in *s*-cis BPy. Green and yellow dashed lines indicate the N1,N2 and H13,H20 geometric interatomic vectors, respectively. All isosurfaces at 0.00025 au.. (a) Total Pauli deformation, $\Delta\rho_{Pauli}$. (b) Total Orbital deformation, $\Delta\rho_{Orb}$. (c) Net Pauli-NOCV deformation for the C11–C12 bond, $\Delta\rho_{Net}$(C11–C12). (d) Net Pauli-NOCV deformation for the H13•••H20 interaction, $\Delta\rho_{Net}$(H13•••H20). (e) Net Pauli-NOCV deformation for the N1--N2 interaction, $\Delta\rho_{Net}$(N1--N2). (f) Total net Pauli-Orbital deformation , $\Delta\rho_{Net}$.

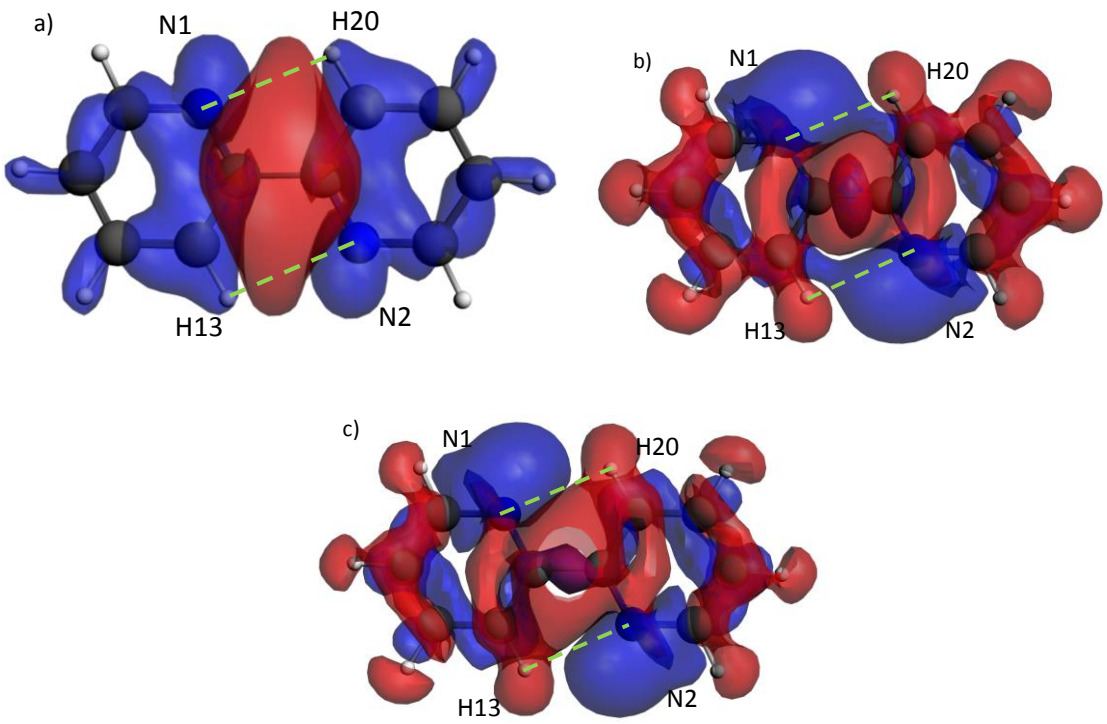

Figure 3.17. Pauli, Orbital and net deformation densities in *s*-trans BPy. Green dashed lines indicate the N1,H20 and N2,H13 interactions.. All isosurfaces at 0.00025 au. (a) Total Pauli deformation, $\Delta\rho_{\text{Pauli}}$. (b) Total Orbital deformation, $\Delta\rho_{\text{Orb}}$. (c) Net Pauli-NOCV deformation for the CH•••N interaction.

Bond Paths as privileged exchange channels. The three different intramolecular interactions present in s-cis and s-trans forms of BPy are similar in only one account: electrons are shared quantum mechanically across the interacting atomic basins. However, since the exchange interaction energy will always be negative, it is difficult to gauge whether V_X^{AB} for a given interaction is the result of significant spin coherence (as in the case of a classical covalent bond) or just the result of two atoms in a non-interacting close contact showing marginal exchange stabilization.

The differences between the CH•••HC, CH•••N and N--N interactions are illuminating: i) the inter-atomic interaction energy is attractive for the CH•••HC and CH•••N interactions, but repulsive for the N--N interaction, ii) CH•••N and N--N interactions are electrostatic in nature (either electrostatically attractive or repulsive, respectively) whereas the CH•••HC interaction is quantum mechanical in nature, iii) NCI shows no steric strain for the CH•••HC and CH•••N interaction, but depletion in the inter-nuclear region for the N--N interaction, iv) the net Pauli and orbital deformation density shows that only for the CH•••HC and CH•••N interactions is the charge accumulation in the bonding region

greater than the charge depletion due to the Pauli Exclusion Principle (although for the CH•••N interaction, no electron flow channel is seen in the net Pauli-NOCV deformation density), and v) an AIL is present only for the CH•••HC interaction. The last point is of particular importance - AILs are present for all classical chemical bonds, whether they are covalent organic bonds (usually with repulsive E_{Cl}^{AB}), coordination and hydrogen-bonds (usually $|V_{Cl}^{AB}| > |V_{X}^{AB}|$) or any other, recognized bond. In fact, Bader suggested that the presence of a bond path (AIL) indicates that atoms are bonded[45]. Why then does a bridge of maximum density only appear for the CH•••HC interaction when fairly large exchange stabilization is seen (for all three interactions), and in the case of CH•••N and CH•••HC interactions, no steric strain in the bonding region is apparent and attractive interaction energies are seen? In order to understand the nature of the AIL better, Pendás et al showed that AILs can be interpreted as privileged exchange channels - quantum-mechanical exchange channels which signal *preferred* interactions (in relation to neighbouring, competing interactions) [46]. They showed that such channels always stabilize the interaction, but are not dependent on the nature of the interaction (whether quantum mechanical or electrostatic) nor are they an indication of the overall *binding* energy between two atoms (which takes into account the induced changes within atomic basins as well, E_{Self}^{IQA}). Tognetti and Joubert[77] added further proof that AILs indeed signal privileged exchange channels by showing that the exchange energy or delocalization indices of a primary interaction of interest (with an AIL present) is greater than the delocalization of competing secondary interactions (without any AILs). We decided to follow their approach to further understand the fundamental differences between the CH•••HC, CH•••N and N--N interactions in BPy.

Following Tognetti and Joubert[77], the primary and secondary exchange channels for the interactions of interest are shown in Figure 3.18. The delocalization indices for each possible exchange channel, as well as the ratio of primary and greatest secondary exchange channels ($\beta = \frac{DI_p}{DI_s}$) are shown in Table 3.5.

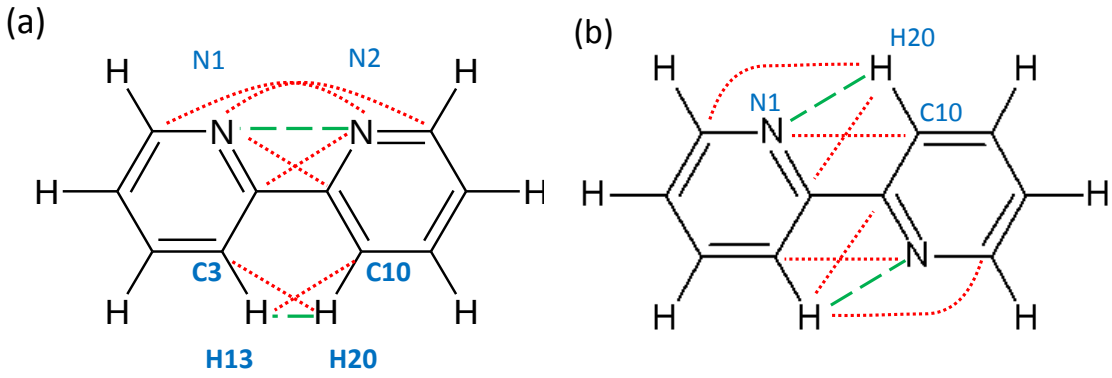

Figure 3.18. Possible competing exchange channels for CH•••HC and N--N in a) *s*-cis, and CH•••N in b) s-*trans*. Green dashes and red dots indicate primary and secondary exchange channels, respectively.

The primary and greatest secondary exchange channels for each intramolecular interaction are plotted as a function of Φ(1) in Figure 3.19. It can be clearly seen from Figure 3.19a that when the DI for the primary exchange channel is significantly greater than for its competing neighbours, such as for the CH•••HC interaction, an AIL is seen ($\beta \geq 1.20$). For the N--N interaction, in the region close to the *s*-cis conformer, the delocalization for the primary channel exceeds that of the greatest secondary channel, but only marginally ($\beta = 1.04$). This is in accordance with the results by Tognetti and Joubert[77], where they have observed a region of indeterminacy for competing exchange paths where an AIL might or might not form. Finally, the primary channel of the CH•••N interaction approaches but never exceeds the delocalization of the greatest secondary channel, and consequently no AIL is seen. Therefore, we can conclude that only the CH•••HC interaction can form *privileged* exchange channels. In light of our results from Sections 3.2 and 3.3, we can interpret this observation as follows: despite the presence of concentrated electron density in the bonding region of the CH•••N interaction (From NCI and ETS-NOCV results, Figures 3.15 and 3.14), electron exchange stabilization is still greater for other competing interactions (such as N1--C11, or N1--C10) than for the interaction of interest. For the N--N interaction, electron density is depleted in the inter-nuclear region (Figures 3.11 and 3.10) and it is thus expected that electron exchange stabilization is greater for competing interactions. On the other hand, CH,HC groups in BPy preferentially delocalize electrons across the CH•••HC interaction than in between other neighbouring interactions, consequently forming a bridge of maximal electron density between these atoms - a bond path.

Table 3.5. Primary and secondary exchange channels for intramolecular interactions in BPy

Interaction	Φ(1)	DI Primary[a]	DI Secondary[a]			$\beta = DI_p/DI_s$[b]
CH•••HC		***H13,H20***	*C10,H13*			
	0	0.0224	0.0146			**1.54**
	10	0.0208	0.0146			**1.43**
	20	0.0171	0.0142			**1.20**
	30	0.0127	0.0133			0.95
	40	0.0086	0.0120			0.72
	50	0.0053	0.0103			0.51
N--N		*N1,N2*	*N1,C11*	*N1,C7*		
	0	0.0792	0.0763	0.0025		1.04
	10	0.0776	0.0764	0.0025		1.02
	20	0.0738	0.0770	0.0025		0.96
	30	0.0687	0.0780	0.0025		0.88
	40	0.0623	0.0795	0.0025		0.78
	50	0.0552	0.0812	0.0024		0.68
CH•••N		*N1--**H20***	*N1-C10*	*C12-**H20***	*C6--**H20***	
	180	0.0369	0.0408	0.0040	0.0010	0.90
	170	0.0357	0.0406	0.0040	0.0010	0.88
	160	0.0325	0.0395	0.0044	0.0009	0.82
	150	0.0280	0.0380	0.0049	0.0008	0.74
	140	0.0227	0.0357	0.0055	0.0007	0.64
	130	0.0173	0.0328	0.0062	0.0005	0.53

[a] DI refers to the delocalization index, within the theory of QTAIM, in atomic units. Identical secondary exchange channels (due to symmetry) were omitted.

[b] The ratio of the primary DI and the greatest secondary DI, in this case always given by the first column of secondary DI. The region of Φ(1) ($0° \leq \Phi(1) \leq 20°$) where an AIL is seen for the CH•••HC interaction is in bold.

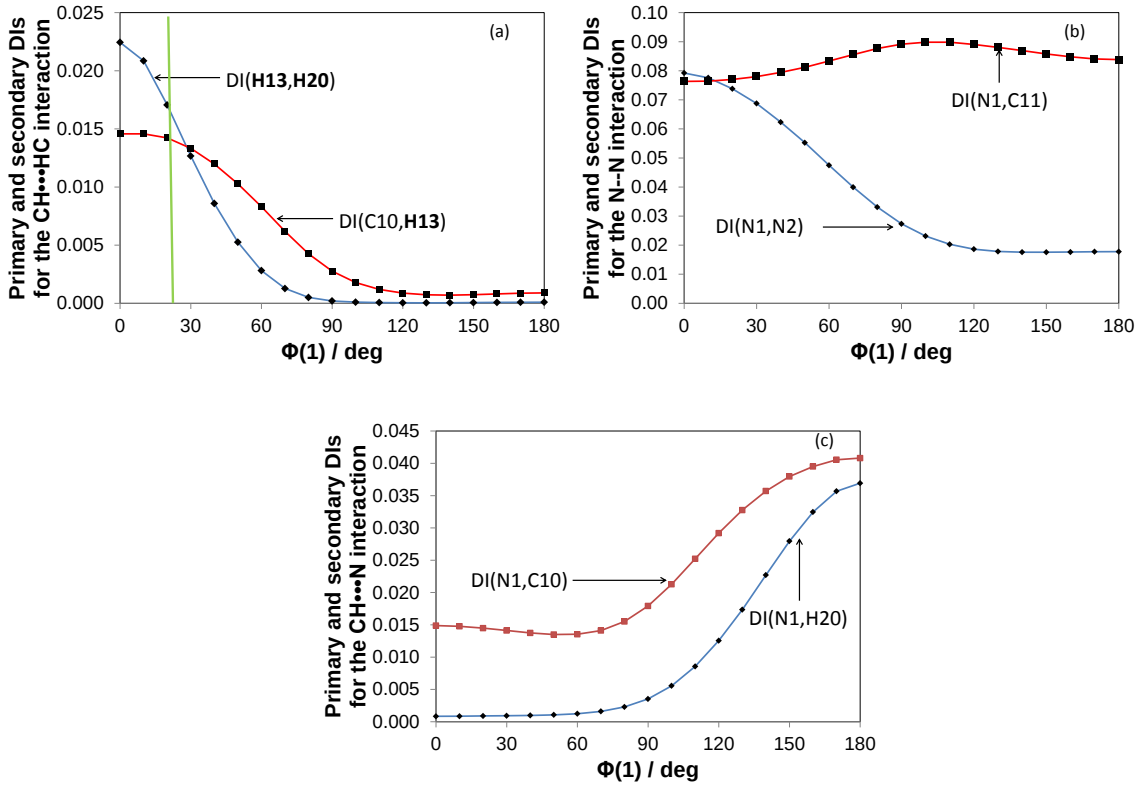

Figure 3.19. Delocalization indices for primary and greatest secondary exchange channels in a) CH•••HC, b) N--N and c) CH•••N. Blue graphs indicate the primary exchange channels, whereas red graphs show the secondary exchange channels. The value for Φ(1) (Φ(1) = 20°) where a CH•••HC AIL first appears is indicated as a green vertical line on a).

In order to better understand and explain this phenomenon, we suggest a new diagnostic based on the ICP values from an NCI-plot. For each intramolecular interaction in BPy we observe two troughs on a corresponding NCI-plot - one with a negative value of λ_2, indicating a region of concentrated density, and one with a positive value of λ_2, indicating a region of depleted density. In Sections 3.2 and 3.3 we showed that the values at the bottom of each trough, $(-)\rho_{ICP}^{AB}$ and $(+)\rho_{ICP}^{AB}$, correspond to a BCP (or pseudo-BCP) and a RCP (or pseudo-RCP), respectively. We also observed that an AIL only appears when $|(-)\rho_{ICP}^{AB}| > (+)\rho_{ICP}^{AB}$, which only occurs for the CH•••HC interaction in conformers with Φ(1) ≤ 20°. In other words, when the density at the point of greatest concentration (BCP or pseudo-BCP) is greater than the density at the point of greatest depletion (RCP or pseudo-RCP), an AIL is seen. This purely phenomological statement is in line with the topology of the electron density if the Poincaré-Hopf relationship (which relates the number of RCPs to the number of BCPs) is satisfied[1]. However, since an AIL can also be

interpreted as a privileged exchange channel, the topological criteria ($|(-)\rho_{ICP}^{AB}| > (+)\rho_{ICP}^{AB}$) and relative values of the density at BCPs and RCPs can be viewed in a new light: the density that is concentrated at a $(-)\rho_{ICP}^{AB}$ must be significant enough to overcome the effects of nearby density (including electron-electron effects such as the Pauli Exclusion Principle) resulting from every other atom in the ring at the exact same point. The following discussion provides evidence for this hypothesis.

Figure 3.20b-d shows the electron density as it changes along the vector defined by the junction BCP(C11,C12) and the NCI-defined ICP's, $(-)\rho_{ICP}^{AB}$ and $(+)\rho_{ICP}^{AB}$, for each interaction. Such a vector is shown graphically for the CH•••HC interaction in Figure 3.20a. This analysis illustrates perfectly the local density changes which lead to the presence of density concentrations and depletions defined by the eigenvector λ_2 in the NCI-analyses. In addition, the partial second derivative of the density with the change in **r** (in λ_2), shown in Figure B2 in Appendix B, can be used to pinpoint where the regions of depletion end and the regions of concentration begin. Figure 3.20b shows the density changes for the CH•••HC interaction. Two clear peaks can be seen, a local minimum corresponding to $(+)\rho_{ICP}^{CH\bullet\bullet\bullet HC}$ and local maximum corresponding to $(-)\rho_{ICP}^{CH\bullet\bullet\bullet HC}$. In this case the density at $(-)\rho_{ICP}^{CH\bullet\bullet\bullet HC}$ is strong enough to overcome the density resulting from the other bonds of the enclosed ring, thus $|(-)\rho_{ICP}^{CH\bullet\bullet\bullet HC}| > (+)\rho_{ICP}^{CH\bullet\bullet\bullet HC}$ and an AIL is formed. The region of depletion is a topological effect caused by the increased density at $(-)\rho_{ICP}^{CH\bullet\bullet\bullet HC}$. The atomic interaction line (dashed green line in Figure 3.20a) crosses the λ_2 eigenvector within a region of concentration, showing that there is no steric strain for this interaction. Figure 3.20c shows the density changes for the CH•••N interaction. Here the region of concentration is not strong enough to overcome the natural density falloff resulting from neighbouring atoms, and electrons will rather delocalize among other atoms of the ring than in the CH•••N interaction. In this case, $|(-)\rho_{ICP}^{CH\bullet\bullet\bullet N}| < (+)\rho_{ICP}^{CH\bullet\bullet\bullet N}$, resulting in no critical points and no AIL. As for the CH•••HC interaction, the depletion is a topological effect from the increased density at $(-)\rho_{ICP}^{CH\bullet\bullet\bullet N}$. The atomic interaction line lies within a region of concentration, indicating no steric strain. Lastly, Figure 3.20d shows the density changes for the N--N interaction. Unlike the CH•••HC and CH•••N interactions, the atomic interaction line now lies within a region of depletion, indicating a degree of steric strain in the bonding region. Here the density falloff resulting from neighbouring atoms and bonds is almost unperturbed, resembling the typical exponential decay of the electron density. $|(-)\rho_{ICP}^{N--N}|$ is significantly smaller than $(+)\rho_{ICP}^{N--N}$.

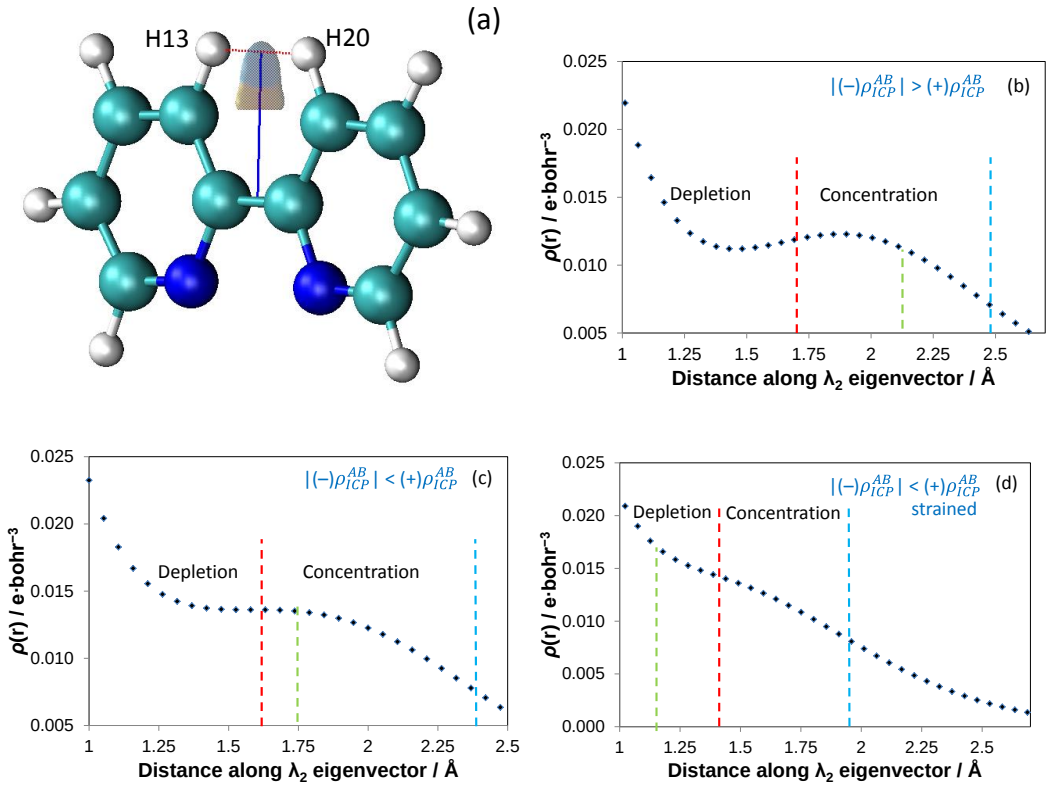

Figure 3.20. (a) NCI isosurface of CH•••HC interaction, with the blue line showing the λ_2 eigenvector from BCP(C11,C12) through $(+)\boldsymbol{\rho}_{ICP}^{CH\bullet\bullet\bullet HC}$ and $(-)\boldsymbol{\rho}_{ICP}^{CH\bullet\bullet\bullet HC}$ and the red line showing the interatomic vector for **H13** and **H20**. (b)-(d) The electron density as it changes along the λ_2 eigenvector for (b) CH•••HC, (c) CH•••N and (d) N--N interactions. The red line shows the end of the region of depletion, the blue line the end of the region of concentration and the dashed green line shows where the interatomic vectors crosses the λ_2 eigenvector.

We propose a new indicator, the ratio of $|(-)\rho_{ICP}^{AB}|$ / $(+)\rho_{ICP}^{AB}$ and called henceforth the privileged exchange index (PEI), which is a degree of the significance of the exchange stabilization of an intramolecular interaction. When PEI > 1, an AIL will be present, the interaction will be privileged, and the quantum mechanical component of the interaction will be significant with regards to the interacting atoms and the local chemical environment. When PEI < 1, no AIL will be present, the interaction will not be privileged and the exchange stabilization of the interaction will be comparable to the exchange between neighbouring (non-bonding) interactions.

The PEI is able to differentiate the three intramolecular interactions more completely. Table 3.6 shows the PEI for the three intramolecular interactions in BPy. As expected, the PEI is larger than 1 for the CH•••HC interaction when $\Phi(1) \leq 20°$ - when an AIL is present. In this region, electrons in **H13** are more likely to delocalize in **H20** and C3 than in other atoms of the ring and the exchange energy of the interaction is significant for the involved atoms. For both CH•••N and N--N interactions, the PEI approaches but never

reaches 1. Electrons in N1, for instance, will prefer to delocalize among other atoms of the rings (such as C11 or C10) than N2 or **H20** - hence larger density at the pseudo-RCP than the pseudo-BCP. The CH•••N and N--N interactions are thus truly only electrostatic (attractive and repulsive, respectively) in nature, with a non-interacting quantum component (the exchange energy of these interactions are the result of atoms in close contact as opposed to the preferential accumulation of electron density in classical bonds). On the other hand, the CH•••HC interaction is truly a quantum mechanical interaction - the concentration of electron density in the inter-nuclear region resulting from exchange stabilization (spin-pairing) is a significant and effect and a product of a bonding interaction.

Table 3.6. NCI comparison for intramolecular interactions in BPy

Interaction	Φ(1) deg	$(-)\rho_{ICP}^{AB}$ au	$(+)\rho_{ICP}^{AB}$ au	***PEI***[a]
CH•••HC	0	–0.01228	0.01120	**1.10**
	10	–0.01189	0.01114	**1.07**
	20	–0.01089	0.01074	**1.01**
	30	–0.00968	0.00976	0.99
	40	–0.00834	0.00854	0.98
	50	–0.00658	0.00714	0.92
N--N	0	–0.01407	0.01447	0.97
	10	–0.01384	0.01425	0.97
	20	–0.01297	0.01340	0.97
	30	–0.01148	0.01217	0.94
	40	–0.00990	0.01087	0.91
	50	–0.00792	0.00935	0.85
CH•••N	180	–0.01350	0.01360	0.99
	170	–0.01326	0.01333	0.99
	160	–0.01238	0.01251	0.99
	150	–0.01113	0.01137	0.98
	140	–0.00962	0.01008	0.95
	130	–0.00751	0.00821	0.91

[a]PEI = $\frac{|(-)\rho_{ICP}^{AB}|}{(+)\rho_{ICP}^{AB}}$, the privileged exchange index. Values larger than 1, and where an AIL is present is shown in bold.

This section has added weight to the importance of an AIL or bond path. According to our interpretation, the quantum mechanical exchange is only significant and indicative of a

bonding quantum interaction if i) the interaction is privileged - the delocalization for the primary interaction is greater than the delocalization of secondary competing interactions, and ii) the accumulation and concentration of density in the inter-nuclear region resulting from the exchange in the intramolecular interaction is greater than the residual density resulting from the other atoms of the ring. These criteria can be assumed if an AIL is present. Note that the inter-atomic electrostatic energy can still change the overall nature of the interaction, regardless of the presence of an AIL. It is also useful to remember that all classical bonds - such as covalent, coordination or hydrogen-bonds - are linked by QTAIM-defined bond paths. Therefore, these bonds are all privileged, and will have a PEI > 1 as well as $\beta > 1$. This observation strengthens our hypothesis that the CH•••HC interaction is a bonding interaction, despite the absence of significant electrostatic attraction.

In addition, this section has also shown the competing Pauli and Orbital-mixing effects as defined within the ETS framework. The Pauli Exclusion Principle keeps electron density from concentrating in the inter-nuclear region of the N--N interaction despite orbital mixing and results in a net depletion in that region. For the CH•••N and CH•••HC interactions on the other hand, orbital mixing causes electron density to be concentrated in the bonding regions of these interactions, despite the withdrawal effect of the Pauli Exclusion Principle. These results correlate perfectly with NCI findings.

Conclusions

This chapter has investigated 3 different intramolecular interactions in BPy using 4 unique theoretical tools; CH•••HC and N--N (present in the *s*-cis conformer) and CH•••N (present in the *s*-trans conformer) interactions were studied. A comparison of the three interactions is shown in Table 3.7.

The N--N interaction is an example of a typical repulsive interaction: the IQA-defined interaction energy is highly repulsive (+255.60 kcal·mol^{-1}) and increases by +20.59 kcal·mol^{-1} from $\Phi(1) = 90°$ to *s*-cis, corroborating with an increase of the atomic net charges (an outflow of electrons) by 0.0133 *e* in order to reduce the lone-pair lone-pair repulsion. Furthermore, the N--N interaction also shows strain in the inter-nuclear region - density is depleted in the region between N atoms (NCI) and despite the presence of orbital

mixing deformation densities from ETS-NOCV, $\Delta\rho_{Net}$(N--N) shows a depletion of density in the inter-nuclear region because of dominant Pauli Exclusion effects. Finally, electron delocalization across the N--N interaction is marginal and should be seen as non-bonded exchange as competing secondary exchange channels show similar or greater delocalization, and the PEI < 1.

We have shown that CH•••N interactions in BPy can indeed be classified as stabilizing interactions, as was classically suggested: the interaction energy is attractive (–7.42 kcal·mol^{-1} per interaction in *s*-trans) and dominantly electrostatic. Changes in the net charges of the atoms reflect this electrostatic nature, withdrawing electron density from the already positively charged H-atoms and accumulating density within the negatively charged N-atoms by +0.02236 *e* and –0.00295 *e*, respectively, relative to Φ(1) = 90°. In addition, neither NCI nor ETS-NOCV identifies any electronic strain in the bonding region - both methods show a concentration of electron density between the atoms, despite density removal due to the Pauli Exclusion Principle. However, like the N--N interaction the quantum mechanical exchange stabilization for the CH•••N interaction is marginal - competing exchange channels dominate leading to β < 1 and the PEI < 1. This interaction is thus an example of a purely electrostatic interaction.

Table 3.7. Comparison of the properties of intramolecular interactions in BPy

	N--N	**CH•••N**	**CH•••HC**
IQA	Repulsive	Attractive	Attractive
Δq(A)	Withdrawal of electrons	Accumulation on N, withdrawal on H	Accumulation of electrons
NCI	Density depleted	Density concentrated	Density concentrated
ETS-NOCV	Density depleted	Density concentrated	Density concentrated
PEI	0.97	0.99	**1.1**
β	1.04	0.9	**1.54**
AIL	No AIL present	No AIL present	**AIL present**

Lastly, we have shown that the supposedly clashing CH•••HC interaction shows none of the same physical properties as the repulsive N--N interaction: a stabilizing interaction energy of –3.03 kcal·mol^{-1} composed of mainly quantum mechanical terms (with the

electrostatic interaction energy also attractive but essentially zero). In addition, whereas electron density was withdrawn from the N-atoms, electron density is accumulated in the interacting H-atoms - the net charges of the interacting H-atoms decreases by –0.00916 *e* per H-atom in *s*-cis, relative to Φ(1) = 90°. Like the CH•••N interaction, no electronic strain can be seen in the bonding region of CH•••HC - rather, density accumulation resulting from orbital interactions dominates electron depletion due to the Pauli Exclusion Effect and leads to a region of NCI-defined electron concentration in the bonding region. Lastly, unlike the CH•••N and N--N interactions (but like every covalent, coordination or H-bond), the CH•••HC interaction is privileged - the PEI > 1 as well as β > 1 indicating that electrons in the H-atoms will preferentially delocalize across the CH•••HC interaction than with any other, neighbouring. Consequently, a bridge of maximum density (an AIL) is formed between the atoms and results in the formation of a zero-flux interaction surface.

In conclusion, no evidence was found to support the hypothesis that CH•••HC interactions are steric clashes, as the properties of the CH•••HC interaction is fully consistent with stabilizing, bonding interactions. We suggest that the relative increase in energy of *s*-cis to *s*-trans is mostly because of the highly repulsive N--N interaction despite the attractive CH•••HC interaction in *s*-cis, and the attractive CH•••N interactions in *s*-trans. However, our analysis is neither exhaustive with regards to the rest of the atoms and bonds, nor exhaustive with regards to the natures of the interactions. The preliminary results regarding changes in the atomic energies and other properties are collected in Appendix A.

References

[1] R. F. W. Bader, *in Atoms in Molecules: A Quantum Theory*; Oxford University Press: Oxford, U.K. 1990.

[2] L. Li, R. Parr,. *J Chem Phys*, **1986**, *84*, 1704

[3] F. L. Hirshfield, *Theor. Chim. Acta.*, **1977**, *44*, 129

[4] J. F. Rico, R. López, G. J. Ramírez, *J. Chem. Phys.*, **1999**, *110*, 4213

[5] A. D. J. Becke, *J. Chem. Phys.*, **1988**, *88*, 2547

[6] E. Francisco, A. M. Pendás, M. A. Blanco, *J. Chem. Theory Comput.*, **2006**, *2*, 90

[7] C. F. Guerra, J. W. Handgraaf, E. J. Baerends, F. M. Bickelhaupt, *J. Comput. Chem.*, **2003**, *25*, 189

[8] I. Mayer, *Chem. Phys. Lett.*, **2000**, *332*, 381

[9] S. F. Vyboishchikov, P. Salvador, M. J. Duran, *J. Chem. Phys.*, **2005**, *122*, 244110

[10] P. Salvador, I. Mayer, *J. Chem. Phys.*, **2004**, *120*, 5046

[11] D. R. Alcoba, A. Torre, L. Lain, R. C. Bochicchio, *J. Chem. Phys.*, **2005**, *122*, 074102

[12] R. F. W. Bader, "*The Lagrangian Approach to Chemisty"* in The Quantum Theory of Atoms in Molecules: From Solid State to DNA and Drug Design, Wiley-VCH, Weinheim, 2007

[13] R. F. W. Bader, *J. Mol. Struct: Theochem*, **2010**, *943*, 2–18

[14] R. F. W. Bader, *J. Phys. Chem. A.*, **2007**, *111*, 7966–7972

[15] S. Srebrenik, R. F. W. Bader, *J. Chem. Phys.*, **1975**, *63*, 3945

[16] C. F. Matta, R. F. W. Bader, *J. Phys. Chem A.*, **2006**, *110*, 6365–6371

[17] J. P. Foster, F. J. Wienhold, *J. Am. Chem. Soc.*, **1980**, *102*, 7211

[18] A. Becke, K. E. J. Edgecombe, *J. Chem. Phys.*, **1990**, *92*, 5397

[19] P. Coppens, *in "Electron Distribution and the Chemical Bond"*, Plenum Press, New York, 1982

[20] S. Dapprich, G. J. Frenking, *J. Phys. Chem.*, **1995**, *99*, 9352

[21] K. Kitaura, K. Morokuma, *Int. J. Quantum Chem.*, **1976**, *10*, 325

[22] M. Mitoraj, A. Michalak, T. Ziegler, *J. Chem. Theory Comput.*, **2009**, *5*, 962–975

[23] M. A. Blanco, A. M. Pendás, E. Francisco, *J. Chem. Theory Comput.*, **2005**, *1*, 1096–1109

[24] E. R. Johnson, S. Keinan, P. Mori-Sánchez, J. Contreras-García, A. J. Cohen, W. Yang, *J. Am. Chem. Soc.*, **2010**, *132*, 6498–6506.

[25] Y. V. Nelyubina, M. Y. Antipin, K. A. Lyssenko, *J. Phys. Chem. A.*, **2007**, *111*, 1091–1095

[26] F. F. Awwadi, R. D. Willett, K. A. Peterson, B. Twamley, *J. Phys. Chem. A.*, **2007**, *111*, 2319–2328

[27] F.Awwadi, S. F. Haddad, R. D. Willett, B. Twamley, *Cryst. Growth. Des.*, **2010**, *10*, 158–164

[28] M. E. Brezgunova, E. Aubert, S. Dahaoui, P. Fertey, S. Lebègue, C. Jelsch, J. G. Angyán, E. Espinosa, *Cryst. Growth Des.*, **2012**, *12*, 5373–5386

[29] H. R. Khavasi, A. A. Tehrani, *Inorg. Chem.*, **2013**, *52*, 2891–2905

[30] S. Shaik, D. Danovich, W. Wu, P. C. Hiberty, *Nat. Chem.*, **2009**, *1*, 443–449

[31] S. Shaik, D. Danovich, B. silvi, D. L. Lauvergnat, P. C. Hiberty, *Chem.–Eur. J.*, **2005**, *11*, 6358–6371

[32] S. Shaik, P. Maitre, G. Sini, P. C. Hiberty, *J. Am. Chem. Soc.*, **1992**, *114*, 7861–7866

[33] P. L. A. Popelier, *J. Phys. Chem. A.*, **1998**, *102*, 1873–1878

[34] W. T. Klooster, T. F. Koetzle, P. E. M. Siegbahn, T. B. Richardson, R. H. Crabtree, *J. Am. Chem. Soc.*, **1999**, *121*, 6337–6343

[35] I. Alkorta, J. Elguero, O. Mó, M. Yáñez, J. E. Del Bene, *J. Phys. Chem. A.*, **2002**, *106*, 9325–9330

[36] T. Richardson, S. de Gala, R. H. Crabtree, P. E. M. Siegbahn, *J. Am. Chem. Soc.*, **1995**, *117*, 12875–12876

[37] S. J. Grabowski, *Chem. Phys. Lett.*, **1999,** *312*, 542–547

[38] S. J. Grabowski, T. L. Robinson, J. Leszcynski, *Chem. Phys. Lett.*, **2004**, *386*, 44–48

[39] Y. V. Nelyubina, K. A. Lyssenko, V. Y. Kotov, M. Y. Antipin, *J. Phys. Chem. A.*, **2008**, *112*, 8790–8796

[40] E. J. Juárez-Pérez, R. Núñez, C. Viñas, R. Sillanpää, F. Texidor, *Eur. J. Inorg. Chem.*, **2010**, *2010*, 2385–2392

[41] P. Demyanov, P. Polestshuk, *Chem.–Eur. J.*, **2012**, *18*, 4982–4993

[42] G. V. Gibbs, R. T. Downs, D. F. Cox, N. L. Ross, M. B. Boisen, Jr., K. M. Rosso, *J. Phys. Chem. A.*, **2008**, *112*, 3693–3699

[43] E. A. Zhurova, C. F. Matta, N. Wu, V. V. Zhurov, A. A. Pinkerton, *J. Am. Chem. Soc.* **2006**, *128*, 8849–8861

[44] C. F. Matta, J. Hernández-Trujillo, T. H. Tang, R. F. W. Bader, *Chem. Eur. J.* **2003**, *9*, 1940–1951

[45] R. F. W. Bader, *J. Phys. Chem. A* **2009**, *113*, 10391–10396

[46] A. M. Pendás, E. Francisco, M. A. Blanco, C. Gatti, *Chem. Eur. J.* **2007**, *13*, 9362–9371

[47] F. Cortés-Guzmán, J. Hernández-Trujillo, G. Cuevas, *J. Phys. Chem. A* **2003**, *107*, 9253–9256

[48] J. Echeverría, G. Aullón, D. Danovich, S. Shaik, S. Alvarez, *Nat. Chem.* **2011,** *3*, 323-330;

[49] J. Poater, M. Solà, F. M. Bickelhaupt, *Chem. Eur. J.* **2006**, *12*, 2889–2895

[50] J. Poater, M. Solà, F. M. Bickelhaupt, *Chem. Eur. J.* **2006**, *12*, 2902–2905.

[51] R. D. Hancock, A. E. Martell, *Chem. Rev.* **1989**, *89*, 1875–1914

[52] D. Buist, N. J. Williams, J. H. Reibenspies, R. D. Hancock, *Inorg. Chem.* **2010**, *49*, 5033–5039

[53] G. M. Cockrell, G. Zhang, D. G. VanDerveer, R. P. Thummel, R. D. Hancock, *J. Am. Chem. Soc.* **2008**, *130*, 1420–1430

[54] S. Del Piero, P. Di Bernardo, R. Fedele, A. Melchior, P. Polese, M. Tolazzi, *Eur. J. Inorg. Chem.* **2006**, 3738–3745

[55] R. D. Hancock, I. V. Nikolayenko, *J. Phys. Chem. A* **2012**, *116*, 8572−8583

[56] I. Alkorta, J. Elguero, C. Roussel, *Comp. Theo. Chem.*, **2011**, *996*, 334–339

[57] R. F. W. Bader, *Int. J. Quantum Chem.*, **2003**, *94*, 173–177

[58] M. Labarca, O. Lombardi, *Found. Chem.*, **2010**, *12*, 149–157

[59] F. Cortés-Guzmán, R. F. W. Bader, *Coord. Chem. Rev.*, **2005**, *633–662*

[60] I. Cukrowski, K. K. Govender, *Inorg. Chem.* **2010**, *49*, 6931–6941

[61] I. Cukrowski, C. F. Matta, *Chem. Phys Lett.* **2010**, *499*, 66–69.

[62] J. Poater, M. Sol, F. M. Bickelhaupt, *Chem.–Eur. J.*, **2006**, *12*, 2902–2905

[63] Gaussian 09, Revision A.1, M. J. Frisch, G. W. Trucks, H. B. Schlegel, G. E. Scuseria, M. A. Robb, J. R. Cheeseman, G. Scalmani, V. Barone, B. Mennucci, G. A. Petersson, H. Nakatsuji, M. Caricato, X. Li, H. P. Hratchian, A. F. Izmaylov, J. Bloino, G. Zheng, J. L. Sonnenberg, M. Hada, M. Ehara, K. Toyota, R. Fukuda, J. Hasegawa, M. Ishida, T. Nakajima, Y. Honda, O. Kitao, H. Nakai, T. Vreven, J. A. Montgomery, Jr., J. E. Peralta, F. Ogliaro, M. Bearpark, J. J. Heyd, E. Brothers, K. N. Kudin, V. N. Staroverov, R. Kobayashi, J. Normand, K. Raghavachari, A. Rendell, J. C. Burant, S. S. Iyengar, J. Tomasi, M. Cossi, N. Rega, J. M. Millam, M. Klene, J. E. Knox, J. B. Cross, V. Bakken, C. Adamo, J. Jaramillo, R. Gomperts, R. E. Stratmann, O. Yazyev, A. J. Austin, R. Cammi, C. Pomelli, J. W. Ochterski, R. L. Martin, K. Morokuma, V. G. Zakrzewski, G. A. Voth, P. Salvador, J. J. Dannenberg, S. Dapprich, A. D. Daniels, Ö. Farkas, J. B. Foresman, J. V. Ortiz, J. Cioslowski, and D. J. Fox, Gaussian, Inc., Wallingford CT, 2009.

[64] AIMAll (Version 12.08.21), T. A. Keith, TK Gristmill Software, Overland Parks KS, USA, 2012 (aim.tkgristmill.com)

[65] W. Humphrey, A. Dalke, K. Schulten, *J. Molec. Graphics*, **1996**, *14.1*, 33-38.

[66] G. te Velde, F. M. Bickelhaupt, S. J. A. van Gisbergen, C. Fonseca Guerra, E. J. Baerends, J. G. Snijders, T. Ziegler, *J. Comp. Chem.* **2001**, *22*, 931

[67] C. Fonseca Guerra, J. G. Snijders, G. te Velde, E. J. Baerends, *Theoretical Chemistry Accounts* **1998**, *99*, 391. c) E. J. Baerends, T. Ziegler, J. Autschbach, D. Bashford, A. Bérces, F. M. Bickelhaupt, C. Bo, P. M. Boerrigter, L. Cavallo, D. P. Chong, L. Deng, R. M. Dickson, D. E. Ellis, M. van Faassen, L. Fan, T. H. Fischer, C. Fonseca Guerra, A. Ghysels, A. Giammona, S. J. A. van Gisbergen, A. W. Götz, J. A. Groeneveld, O. V. Gritsenko, M. Grüning, S. Gusarov, F. E. Harris, P. van den Hoek, C. R. Jacob, H. Jacobsen, L. Jensen, J. W. Kaminski, G. van Kessel, F. Kootstra, A. Kovalenko, M. V. Krykunov, E. van Lenthe, D. A. McCormack, A. Michalak, M. Mitoraj, J. Neugebauer, V. P. Nicu, L. Noodleman, V. P. Osinga, S. Patchkovskii, P. H. T. Philipsen, D. Post, C. C. Pye, W. Ravenek, J. I. Rodríguez, P. Ros, P. R. T. Schipper, G. Schreckenbach, J. S. Seldenthuis, M. Seth, J. G. Snijders, M. Solà, M. Swart, D. Swerhone, G. te Velde, P. Vernooijs, L. Versluis, L. Visscher, O. Visser, F. Wang, T. A. Wesolowski, E. M. van Wezenbeek, G. Wiesenekker, S. K. Wolff, T. K. Woo, A. L. Yakovlev, ADF2012, SCM, Theoretical Chemistry, Vrije Universiteit, Amsterdam, The Netherlands, http://www.scm.com

[68] S. T. Howard, *J. Am. Chem. Soc.*, **1996**, *118*, 10269–10274

[69] L. Oresmaa, M. Haukka, P. Vainiotale, T. A. Pakkanen, *J. Org. Chem.*, **2002**, *67*, 8216–8219

[70] S. Zahn, W. Reckien, B. Kirchner, H. Staats, J. Matthey, A. Lützen, *Chem. Eur. J.*, **2009**, *15*, 2572–2580

[71] A. Bondi, *J. Phys. Chem.*, **1964**, *3*, 441–451

[72] N. Gillet, R. Chaudret, J. Contreras-García, W. Yang, B. Silvi, J-P. Piquemal *J. Chem. Theory Comput.* **2012**, *8*, 3993−3997

[73] S. J. Grabowski, *Monatshefte für Chemie*, **2002**, *113*, 1373–1380

[74] M. Palusiak, T. M. Krygowski, *Chem.–Eur. J.*, **2007**, *13*, 7996–8006

[75] S. T. Howard, T. M. Krygowski, *Can. J. Chem.*, **1997**, *75*, 1174–1181.

[76] U. Koch, P. L. A. Popelier, *J. Phys. Chem.*, **1995**, *99*, 9747–9754

[77] V. Tognetti, L. Joubert, *J. Chem. Phys.* **2013**, *138*, 024102–024109

Chapter 4

Bonding and Non-bonding Interactions in Zn^{II} Complexes with 2,2′-Bipyridyl

Abstract:

Close hydrogens in the 3,3′ position of 2,2′-bipyridyl (BPy) complexes with Zn^{II}, classically labelled as steric clashes, have been found to be locally stabilizing. A rigorous theoretical analysis employing multiple techniques, including the Quantum Theory of Atoms in Molecules (QTAIM), the Interacting Quantum Atoms (IQA) energy decomposition scheme, the Noncovalent Interactions (NCI) method and the Extended Transition State coupled with Natural Orbitals for Chemical Valence (ETS-NOCV) energy decomposition scheme, was used to study CH•••HC as well as various other intramolecular interactions, coordination and covalent bonds in $Zn^{II}(BPy)_n(OH_2)_{6-2n}$ complexes. It was found that the CH•••HC interaction is electrostatically and quantum mechanically locally stabilizing, with the quantum mechanical contribution in excess. Electron density is concentrated within the bonding region in a channel-like fashion, resulting in the formation of a bridge of maximal density. No steric strain is seen for the CH•••HC interaction, nor for the entire BPy ligand - the only significant steric strain is located in the Zn^{II} coordination sphere. It is also shown that the physical properties of this interaction changes in a very similar fashion as the properties of all other intramolecular interactions and coordination bonds when successive ligands are coordinated. Finally, the results of the different techniques are shown to correlate near-perfectly, making this work the first of its kind to unite these four unique theoretical tools.

Introduction

The ligand 2,2′-bipyridyl (L) is an important representative of α-diimines and it has excellent ability to form complexes, hence its chemistry with tenths of metal ions has been investigated experimentally for years resulting in hundreds of formation constants reported.[1] Knowledge of the conformational structure of α-diimine ligands and information about the rotational energy barrier are important and useful for a better understanding of the complex formation process and trends in stability of complexes. Hence not surprisingly, these ligands have also been extensively studied computationally[2–14] and for over 40 years it is known that the most stable conformer of 2,2′-bipyridyl has two N-atoms *trans* to each other (s-*trans* conformer).[6–12] Lower stability of the conformer with nitrogens *cis* to each other (s-*cis* conformer) was attributed mainly to the steric hindrance of the 3,3′-hydrogen atoms and destabilizing nitrogen lone pair-lone pair interactions[8–14] in 2,2′-bipyridyl. To act as a chelate, this ligand must, however, attain the s-*cis* conformation resulting in the 3,3′-hydrogen atoms being in the close contact, CH•••HC (Figure 4.1).

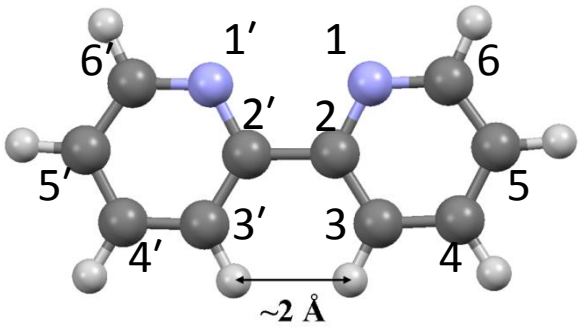

Figure 4.1. Higher energy conformer of the free ligand 2,2′-bipyridyl, as found in metal complexes, with N-atoms *cis* to each other (s-*cis* conformer) showing steric clash between 3,3′-hydrogen atoms.

It is a well-known fact that many, if not majority, of metal complexes with this ligand in crystals show nearly-planar structure of 2,2′-bipyridyl with geometric H-clashes present. These H-clashes are assumed to be also present in a solution and were often used to explain trends in experimental formation constants.[15–23] For instance, the unusual trend in the formation constants of Cu^{II} was attributed to steric repulsion between the 3,3′-hydrogens already fifty years ago.[15] More recently, the observed difference of about 1.4 log units for a set of metal ions with 1,10-phenanthroline and 2,2′-bipyridyl (the latter

ligand forms weaker complexes) was attributed to highly strained ligand in the s-*cis* conformer (as it is required for coordination to metal ions) because of the steric hindrance between the hydrogen atoms.[20] In very recent report, where H-clashes in phenanthrene and 2,2′-bipyridyl were investigated, Hancock and Nikolayenko[24] concluded that these contacts should be seen as unfavourable H--H nonbonded interactions of the H atoms, in principle, in all known cases where they are in a steric clash because "…the concept of energetically unfavorable nonbonded H--H interactions at short H--H separations has been very productive in explaining organic stereochemistry, and so the idea[25] that such interactions are energetically favorable would, if correct, overturn much chemical thinking built up over many decades". This statement clearly indicates how important to all branches of chemistry and how controversial the debate on the physical nature (stabilising or destabilizing) of the CH•••HC close contacts is. Clearly, regardless of the final output of the scientific debate, it is of paramount importance to fully uncover and understand the nature of this type of interactions and their role in chemistry. For instance, taking into the account the following two statements, "a traditional way of analysing the role of nonbonded repulsive forces in molecules has been that of molecular mechanics (MM)"[24] and "The MM approach is based on traditional views of nonbonded H--H interactions, which regard close proximity of nonbonded H atoms as a source of destabilization of molecules"[24] but assuming that CH•••HC close contacts were proved to be of a stabilizing nature, would have a huge implications because the force field parameters used in MM-based software would most likely have to be re-developed. To further stress the significance of this kind of interactions, one might also add to this a simple fact that in case of larger molecules (commonly studied by e.g. pharmaceutical companies or biochemists, medicinal chemists, etc.) MM is commonly used; hence changing force field parameters in MM-based packages would or might have quite an implication on the development of, e.g. new pharmaceutical drugs.

Close contacts between H-atoms are present in many molecules, e.g. in a natural estrogen, Estrone (3-hydroxy-1,3,5-(10)-estratrien-17-one)[26] and became, as already pointed out above, a subject of controversy. This is because many examples of intra- and intermolecular CH•••HC close contacts were interpreted as the H–H bonding interactions, either from the calculated[26–33] or experimental[26,34–36] electron density distributions, using the quantum theory of atoms in molecules (QTAIM)[25] of Bader. The formation of H–H bonds in some molecules was challenged in the literature[37–38] and rebutted.[39–40]

Criticism of the QTAIM-based interpretation of bonding interactions between clashing hydrogen atoms is based mainly on the "Pauli or exchange repulsions" (the destabilizing energy contribution acting on the clashing atoms) obtained from the energy decomposition analysis, such as the Extended Transition State (ETS) method[41–43] used in the study of *ortho*-hydrogens in planar biphenyl.[37]

Recently, members of our group have reported[32–33] the QTAIM-based study of Ni^{II} and Zn^{II} complexes with NTPA (nitrilotri-3-propanoic acid) and NTA (nitrilotriacetic acid) which form three 6-membered and 5-membered coordination rings, respectively. Our analysis revealed that (i) the CH•••HC contacts in the Ni^{II} and Zn^{II} complexes with NTPA cannot be used to explain the experimental trend in the formation constants in aqueous medium (NTPA complexes are significantly weaker when compared with NTA) and (ii) there are bonding interactions between H-atoms involved in the CH•••HC contacts. The ETS-NOCV charge and energy decomposition method[44–45] (ETS combined with the Natural Orbitals for Chemical Valence (NOCV) theory) as well as QTAIM were used recently[46] to study H-clashes in the ZnNTPA complex. This first implementation of QTAIM and ETS-NOCV in the study of non-bonding interactions in metal complexes has conclusively demonstrated[46] that the CH•••HC contacts are characterized by (i) the electron flow channel between the H-atoms involved as discovered by the ETS-NOCV analysis (on average, $\Delta E_{orb} = -1.35$ kcal mol^{-1}) and (ii) QTAIM defined a bond path which indicates the presence of a preferred quantum-mechanical exchange channel;[29] hence the presence of bonding interactions between the H-atoms of the CH•••HC contacts was confirmed by these two very different methods (theories).

The CH•••HC close contacts are ubiquitous[27] and, since our special interest is in understanding factors controlling metal complex stability and ligands' selectivity, we investigate here the CH•••HC close contacts made by the 3,3′-hydrogen atoms of the ligand 2,2′-bipyridyl (L) in metal complexes. To address in this work the main and fundamental question "Does the classical interpretation of the H--H close contacts holds as a nonbonded and molecular destabilization interaction resulting in highly strained ligand?" we decided to investigate specific physical components of this intramolecular interaction (between the 3,3′-hydrogen atoms) with hope to answer the following: (i) is the interatomic region strained?; (ii) what is the nature of the electrostatic interaction between these H-atoms, is it repulsive ($E_{elst} > 0$) or attractive?; (iii) is there any evidence of spin-pairing? (this is indicative of stabilizing contribution to this interaction); (iv) what is the

overall interaction energy between the 3,3′-hydrogen atoms, is it locally stabilizing (E_{int} < 0) or destabilizing?; and (v) are the CH•••HC, CH•••O or CH•••N intramolecular interactions in ZnL_n complexes fundamentally different, or is their underlying physical nature the same?

We must make it absolutely clear here that our aim is to investigate physical properties of intramolecular interactions and the different energy contributions of these interactions in order to establish whether they are locally of stabilizing or destabilizing nature (as we will discuss later, it is rather difficult, if not impossible, to rigorously quantify the effect of *any intramolecular interaction* on the final gain or loss of a molecular energy). To achieve our goals and to aid understanding of the nature of the H--H close contacts we (i) employed a number of very different energy partitioning methods, some of them developed very recently and (ii) decided to perform a comparative study which involves not only intramolecular interactions (such as CH•••HC, CH•••O or CH•••N) but also coordination and covalent bonds in the $[ZnL(H_2O)_4]^{2+}$, $[ZnL_2(H_2O)_2]^{2+}$ and $[ZnL_3]^{2+}$ complexes where all these interactions are present simultaneously (for simplicity, these complexes will be shown throughout the text as ZnL, ZnL_2 and ZnL_3).

Computational details

Suitable for energy optimization crystal structures for all forms of octahedral $Zn^{II}L(1)_nL(2)_m$ complexes (L(1) = 2,2′-bipyridyl, L(2) = H_2O (shown further as ZnL_n, $1 \leq n \leq 3$) were obtained from the Cambridge Crystal Structure Database.[47] These structures were optimized using DFT in Amsterdam Density Functional (ADF) 2010 software,[48–50] with X3LYP as the exchange-correlation functional and an augmented triple-ζ basis set with valence-shell polarization; the COSMO model was used to approximate an aqueous environment implicitly. ETS-NOCV analysis was computed within ADF on the energy-optimized structures (no imaginary frequencies were present). Wavefunctions for use in QTAIM, IQA and NCI analyses were generated from single point calculations using Gaussian 09, Revision B[51] with the X3LYP functional and 6-311++G(d,p) basis set. For the Gaussian calculations, PCM/UFF was used to model the solvent. Topological analysis, including molecular graph generation and calculation of interaction energies within the IQA approach, was carried out using AIMAll software.[52] NCI analysis was carried out using NCIPlot 2.0[53], and visualization of the resulting densities was done using VMD 1.9.1.[54]

To perform an IQA analysis, which needs a well-defined second-order density matrix (therefore ruling out DFT-densities), we re-optimized our structures at HF/6-311++G(d,p) with the PCM/UFF solvation model, using Gaussian09c. IQA analysis was performed for selected atoms and interactions on the resulting wavefunctions using AIMAll. All atomic integrations were of accurate integration - the atomic Lagrangian, $L(\Omega)$, deviated from zero only on the fifth decimal place for each atom.

Fragmentation Schemes. Several fragmentation schemes (for the purposes of ETS-NOCV analyses), needed to extract different types of the interatomic interactions (Zn–O, Zn–N, C–C, CH•••N, CH•••O and CH•••HC), have been considered and some of them (used for the general ML_2 case) are shown in Figure 4.2.

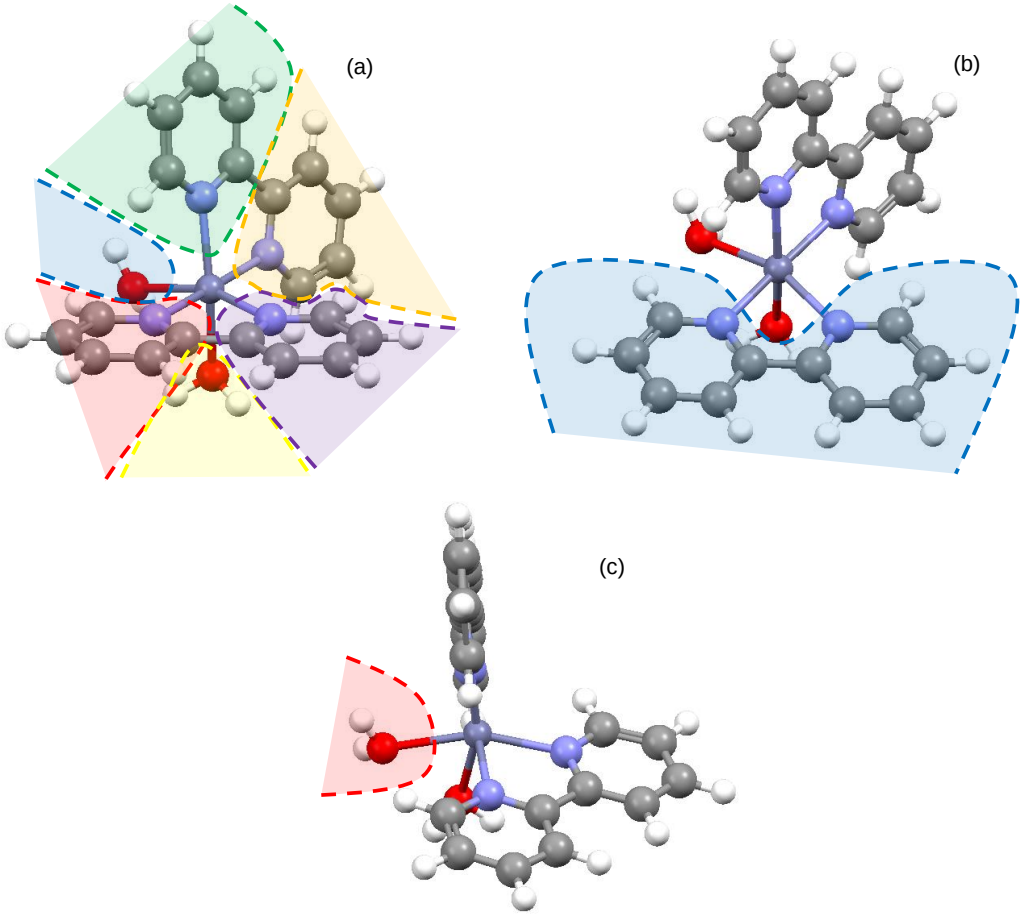

Figure 4.2. Fragmentation schemes used for ETS-NOCV analysis. (a) (*7*)-*pyr*, (b) (*2*)-*BPy*, and (c) (*2*)-*OH*$_2$.

The first scheme is labelled (*7*)-*pyr* and it refers to the use of seven different fragments which include radical pyridine promolecules. The seven-fragment scheme results in (i) four different H_2O molecules, a free Zn^{2+} cation and two pyridine radicals when

$Zn(BPy)(H_2O)_4^{2+}$ is analysed, (ii) two H_2O molecules, four pyridine radicals and a free Zn^{2+} cation in case of ML_2 analysis, and (iii) six pyridine radicals and a free Zn^{2+} cation in case of ML_3. We found that such partitioning was most suitable (*i.e.* it provided the most localized NOCVs) for description of the intramolecular C–C and CH•••HC interactions. Most informative NOCVs describing the Zn–N and Zn–O coordination bonds and CH•••O intramolecular interactions were generated from two-fragment schemes, (*2*)-*BPy* and (*2*)-*OH_2*, where a single BPy ligand or water molecule was separated from a complex, respectively, as shown in Figures 2(b-c) for ML_2. It should finally be added that all of our results are qualitatively reproducible across different fragmentation schemes – for example, the interactions seen in (*2*)-*BPy* (or even alternative schemes not included in this work) are seen in (*7*)-*pyr* as well. Similar is true for the remaining interactions.

Results and Discussion

Molecular geometries. We studied the successive coordination of BPy ligands to a Zn^{II} metal ion in aqueous solution and selected structural data obtained for the equilibrium structures of ZnL_n complexes are included in Table 1; Cartesian coordinates are given in Tables S1-S3 of the Supplementary Information (SI). Ball and stick representations, which also show numbering of atoms in complexes, are shown in Figure 4.3A.

Certain trends are observed for the change in geometry with successive ligand coordination. The average Zn–N bond length (BL) increases by a significant distance of ~0.1 Å, from 2.107 Å in ZnL to 2.218 Å in ZnL_3 and is coupled to a decrease in the N–Zn–N bite angle, from 79.13° in ZnL to on average 74.77° in ZnL_3. Opposite to the trend observed for BL(Zn–N), the distances between atoms involved in the intramolecular interactions become shorter when going from ZnL to ZnL_3; (i) d(CH•••HC) decreases from 2.048 Å in ZnL to an average of 2.034 and 2.010 Å in ZnL_2 and ZnL_3, respectively, d(CH•••O) decreases from an average of 2.544 Å in ZnL to an average of 2.453 Å in ZnL_2 and (iii) d(CH•••N) also decreases from an average of 2.815 Å in ZnL_2 to an average of 2.678 Å in ZnL_3. It is important to stress that the bipyridyl ligand molecules remain virtually planar in all equilibrium geometries of the ZnL_n complexes; as an example, the absolute maximum and minimum values of N_1-C_2-$C_{2'}$-$N_{1'}$ dihedral angle of 1.89 and 0.31°, respectively, were found in ZnL_2.

Table 4.1. Selected structural data for equilibrium geometries of the ZnL_n complexes

Complex	Bond length (Å)		Bite angle (deg)		Torsion (deg)		Close contacts (Å)	
ZnL	Zn–O1	2.162	N5-Zn-N6	79.13	N5-C15-C16-N6	-1.44	C**H14•••H18**C	2.048
	Zn–O2	2.194			**H14**-C13-C15-C16	0.05	CH8•••O1	2.544
	Zn–O3	2.162			**H18**-C17-C16-C15	0.05	CH24•••O3	2.544
	Zn–O4	2.194						
	average:	*2.178*						
	std dev:	*0.018*						
	Zn–N5	2.107						
	Zn–N6	2.107						
ZnL_2	Zn–N1	2.153	N1-Zn-N2	77.40	N1-C13-C14-N2	0.31	C**H16•••H18**C	2.031
	Zn–N2	2.143	N3-Zn-N4	77.48	**H16**-C15-C13-C14	-0.45	C**H32•••H36**C	2.036
	Zn–N3	2.149			**H18**-C17-C14-C13	0.52	CH24•••O6	2.451
	Zn–N4	2.143			N3-C33-C34-N4	1.89	CH42•••O5	2.455
	average:	*2.147*			**H32**-C31-C33-C34	0.18	CH26•••N2	2.810
	std dev:	*0.005*			**H36**-C35-C34-C33	0.79	CH8•••N4	2.819
	Zn–O5	2.273						
	Zn–O6	2.276						
ZnL_3	Zn–N55	2.217	N55-Zn-N56	74.76	N55-C9-C10-N56	0.76	C**H8•••H12**C	2.013
	Zn–N56	2.216	N57-Zn-N58	74.77	**H8**-C7-C9-C10	0.07	C**H26•••H30**C	2.007
	Zn–N57	2.215	N59-Zn-N60	74.78	**H12**-C11-C10-C9	-0.35	C**H44•••H48**C	2.011
	Zn–N58	2.220			N57-C27-C28-N58	0.38	CH20•••N55	2.668
	Zn–N59	2.218			**H26**-C25-C27-C28	0.10	CH54•••N56	2.671
	Zn–N60	2.217			**H30**-C29-C28-C27	0.00	CH38•••N57	2.684
	average:	*2.217*			N59-C45-C46-N60	1.61	CH18•••N58	2.685
	std dev:	*0.002*			**H44**-C43-C45-C46	0.15	CH2•••N59	2.685
					H48-C47-C46-C45	-0.34	CH36•••N60	2.672

QTAIM-based interpretation of the electron density topology. Figure 4.3B shows the molecular graphs of the ZnL_n complexes. Since AIL represents a 'bridge of density' or just a line of maximum density that links two atoms (a topological property of electron density which can be defined, in the form of operator, as a Dirac observable, making the AIL the measurable expectation value of a quantum mechanical operator[28]) it is undistinguishable for a single or triple bond, classical covalent or coordination bond, or closed-shell intra- or intermolecular interaction on a molecular graph. As one would expect, AILs exist between atoms involved in all 'classical' bonds, such as Zn–N and Zn–O coordination bonds as well as C–C covalent bonds; hence these AILs

(showed as solid lines in Figure 4.3B) one can safely call bond paths. This means that these molecular graphs not only reproduced molecular structures of bonded atoms in the ZnL_n complexes fully (as any chemist would build them using a ball-and-stick representation, such as seen in Figure 4.3A) but, in addition, revealed the formation of intra-molecular interactions shown as dashed lines in Figure 4.3B. In ML and ML_2, dashed AILs point at the presence of CH•••O interactions whereas the CH•••N interactions are indicated only in ML_2 and ML_3. Finally, in all ZnL_n complexes, AILs are always seen for the CH•••HC interactions between the 3,3′-H atoms.

Coordination bonds. Topological properties at BCPs for all coordination bonds (Zn–N and Zn–OH_2) in ZnL_n are collected in Table 4.2. It is seen that ρ_{BCP} is small (0.0405 a.u. < $\rho(r)$ < 0.0705 a.u.) and $\nabla^2\rho_{BCP}$ is positive (0.1519 a.u. < $\nabla^2\rho(r)$ < 0.2522 a.u.) indicating a "closed shell" character of the coordination bonds.[55] In addition, the sign and magnitude of the total energy density at the BCPs, $H(r) = G(r) + V(r)$, can also been used to characterize the nature of the bonding.[56–57] For a covalent interaction, the local electron potential energy density $V(r)$ dominates, hence $H(r) < 0$, whereas for a predominantly ionic interaction, the local electron kinetic energy density $G(r)$ dominates resulting in $H(r) > 0$.[58–61] It is seen in Table 4.2 that the local electron potential energy density $V(r)$ dominates in these two coordination bonds and results in the overall negative (although small) value of $H(r)$. This strongly points out at a significant covalent contribution, hence also recovers a 'classical' notion of a coordination bond where a donor atom (here N and O) shares a pair of electrons with the central metal ion. Besides the values of potential and kinetic energies at BCPs, one can also use their ratio, $|V(r)|/G(r)$, as another useful description;[61–62] $|V(r)|/G(r) < 1$ is characteristic of a typical ionic interaction and $|V(r)|/G(r) > 2$ is diagnostic of a 'classical' covalent interaction; hence an intermediate values, $1 < |V(r)|/G(r) < 2$, indicate an interactions of an intermediate character.

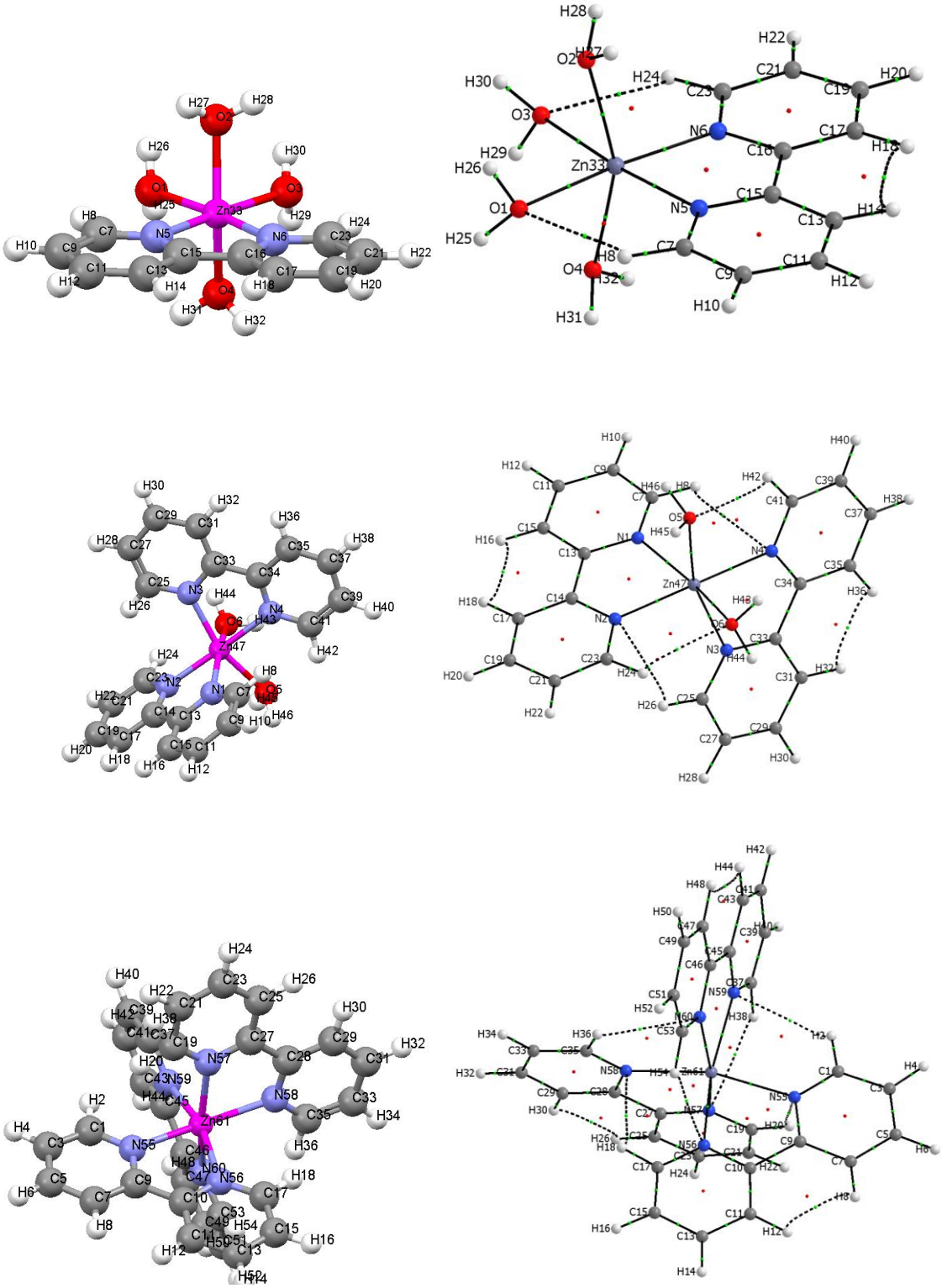

(A) (B)

Figure 4.3. Ball and stick representations (A) and QTAIM molecular graphs (B) of ZnL_n complexes.

Table 4.2. Topological data at the BCP for all coordination bonds in Zn^{II} complexes with 2,2´-bipyridyl (L) optimized at X3LYP[a]

Complex	Atoms	$\rho(r)$	$\nabla^2\rho(r)$	$V(r)$	$G(r)$	$H(r)$	$\lvert V(r)\rvert/G(r)$
ZnL	Zn–N5	0.07049	0.25214	-0.09374	0.07839	-0.01535	1.19583
	Zn–N6	0.07050	0.25216	-0.09374	0.07839	-0.01535	1.19583
	Average	*0.07049*	*0.25215*	*-0.09374*	*0.07839*	*-0.01535*	*1.19583*
	Zn–O1	0.05179	0.21854	-0.06855	0.06159	-0.00696	1.11298
	Zn–O2	0.04798	0.19761	-0.06256	0.05598	-0.00658	1.11750
	Zn–O3	0.05179	0.21860	-0.06857	0.06161	-0.00696	1.11295
	Zn–O4	0.04799	0.19768	-0.06258	0.05600	-0.00658	1.11747
	Average	*0.04989*	*0.20811*	*-0.06556*	*0.05880*	*-0.00677*	*1.11523*
ZnL_2	Zn–N1	0.06353	0.21913	-0.08205	0.06841	-0.01363	1.19928
	Zn–N2	0.06512	0.22452	-0.08426	0.07019	-0.01406	1.20036
	Zn–N3	0.06408	0.22207	-0.08303	0.06928	-0.01376	1.19860
	Zn–N4	0.06513	0.22464	-0.08430	0.07023	-0.01407	1.20032
	Average	*0.06446*	*0.22259*	*-0.08341*	*0.06953*	*-0.01388*	*1.19964*
	Zn-O5	0.04081	0.15334	-0.05033	0.04433	-0.00600	1.13533
	Zn–O6	0.04048	0.15193	-0.04985	0.04392	-0.00593	1.13508
	Average	*0.04065*	*0.15264*	*-0.05009*	*0.04412*	*-0.00597*	*1.13520*
ZnL_3	Zn–N55	0.05560	0.18015	-0.06872	0.05688	-0.01184	1.20819
	Zn–N56	0.05568	0.18055	-0.06885	0.05699	-0.01186	1.20802
	Zn–N57	0.05586	0.18139	-0.06914	0.05724	-0.01190	1.20783
	Zn–N58	0.05521	0.17832	-0.06807	0.05633	-0.01175	1.20855
	Zn–N59	0.05542	0.17931	-0.06841	0.05662	-0.01179	1.20828
	Zn–N60	0.05558	0.18008	-0.06869	0.05685	-0.01183	1.20816
	Average	*0.05556*	*0.17996*	*-0.06865*	*0.05682*	*-0.01183*	*1.20817*

[a] $\rho(r)$, $\nabla^2\rho(r)$, $V(r)$, $G(r)$, and $H(r)$ - all in atomic units.

Taking all these criteria into consideration, the QTAIM-defined topological properties at BCPs indicate a mixed (largely ionic with significant covalent component) character of these coordination bonds also because $H(r)$ is near zero and $1< |V(r)|/G(r) < 1.1$.

To facilitate our comparative studies and aid interpretation of changes observed in the ZnL_n complexes when the atomic crowding increases significantly from ZnL to ZnL_3, we have decided to investigate variation in a number of topological properties at BCPs with a change in the interatomic distances, d(A–B), for selected bonds and all intra-molecular interactions. Data obtained for the Zn–N coordination bonds are shown in Figure 4.4, where good linear relationships

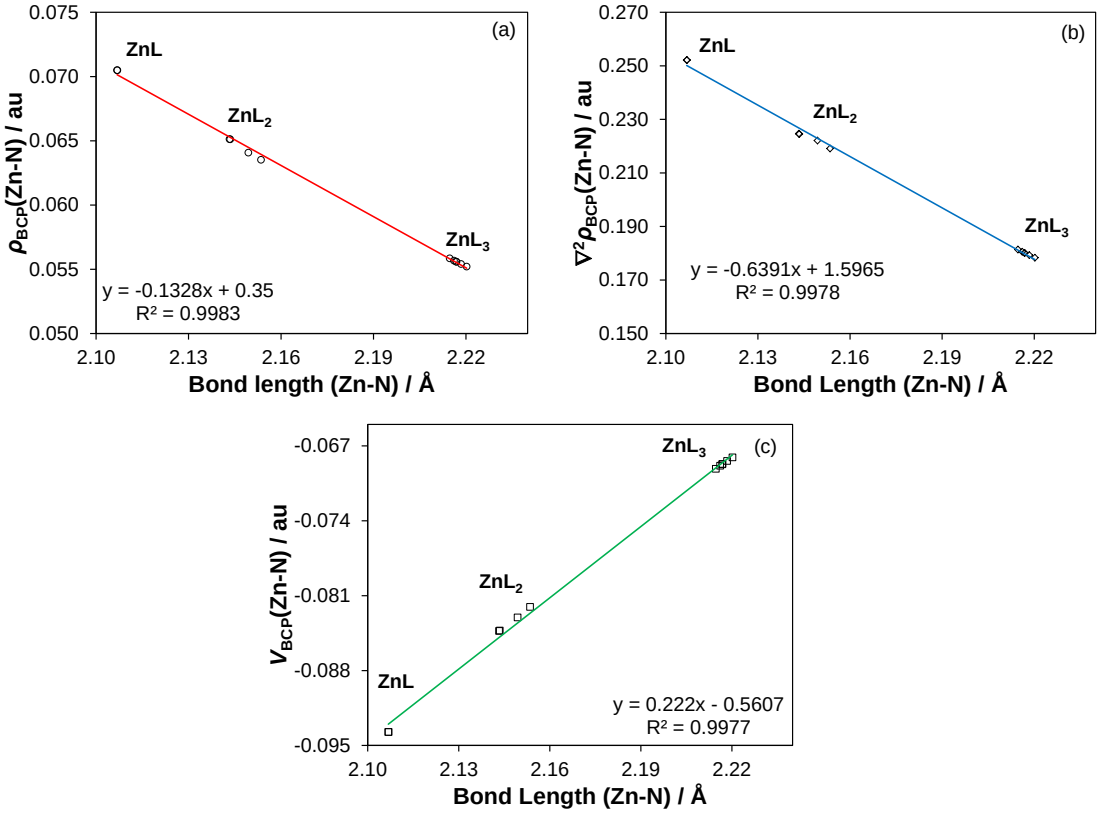

Figure 4.4. Relationships between bond lengths and topological properties at the BCP for Zn–N bonds.

between d(Zn–N) and (i) the electron density, ρ_{BCP}, (ii) the Laplacian of the electron density, $\nabla^2\rho_{BCP}$, and (iii) the potential energy density, V_{BCP}, are observed. Relevant plots for the Lagrangian kinetic energy density, G_{BCP}, the total energy density, H_{BCP}, and the ratio of the

potential energy density and the kinetic energy density, $|V_{BCP}|/G_{BCP}$, are shown in Figure C1 of Appendix C. We have also analysed relevant relationships for the coordination bonds involving water molecules, Zn–O, and they are shown in Figure C2 of Appendix C. All these plots show that ρ_{BCP} and $\nabla^2\rho_{BCP}$ increases while V_{BCP} becomes more negative when d(Zn–L) decreases. This strongly indicates that an increase in crowding in the coordination sphere of the central metal ion results in significant weakening of all coordination bonds; strongest coordination bonds are formed in least crowded ZnL. Also, the admixture of these bonds changes and an increase in covalent character is observed when going from shorter towards longer bonds in ZnL_3.

Intramolecular interactions. Selected topological properties for all intramolecular interactions, as identified by the QTAIM-defined AILs in the ZnL_n complexes, are included in Table 4.3. Since CH•••O interactions exist only in ML and ML_2 and CH•••N interactions only in ML_2 and ML_3, no quantitative relationships can be constructed for them (they would essentially be two-point relationships). However, for both, the CH•••O and CH•••N, interactions; an increase is seen for ρ_{BCP}, $\nabla^2\rho_{BCP}$ and $\left|V_{BCP}\right|$ as the interatomic distance shortens. Also, the properties at BCPs strongly support predominant ionic (closed-shell) character of these intra-molecular hydrogen bonding interactions; G_{BCP}, dominates and the ratio $|V_{BCP}|/G_{BCP} < 1$.

Our theoretical analysis is in full agreement with the topological analysis at BCP obtained from experimental data which was performed by (i) Flaig at al.[63] (this involved weak and strong inter- and intramolecular H-bonds in aminoacids) and (ii) Espinosa at al.[64] (they investigated the X–H•••O interactions in over 83 structures). This clearly indicates that the QTAIM-defined fundamental properties at BCPs exhibit the same universal relationship with d(A–B), regardless if theoretical (here coordination Zn–L and Zn–O as well as intramolecular CH•••O and CH•••N hydrogen bonds) or experimental data are used.

Table 4.3. Topological data at the BCP for all intramolecular interactions in Zn^{II} complexes with 2,2´-bipyridyl (L) optimized at X3LYP[a]

Complex	Atoms	$\rho(r)$	$\nabla^2\rho(r)$	$V(r)$	$G(r)$	$H(r)$	$\lvert V(r)\rvert/G(r)$
ZnL	CH8–O1	0.00862	0.03082	-0.00546	0.00658	0.00112	0.82974
	CH24–O3	0.00862	0.03082	-0.00546	0.00658	0.00112	0.82973
	Average	*0.00862*	*0.03082*	*-0.00546*	*0.00658*	*0.00112*	*0.82973*
	CH14–H18C	0.01142	0.04390	-0.00652	0.00875	0.00222	0.745684
ZnL_2	CH42–O5	0.00981	0.03577	-0.00630	0.00762	0.00132	0.82630
	CH24–O6	0.00993	0.03606	-0.00636	0.00769	0.00133	0.82744
	Average	*0.00987*	*0.03592*	*-0.00633*	*0.00765*	*0.00133*	*0.82687*
	CH26–N2	0.00599	0.02016	-0.00341	0.00422	0.00081	0.80718
	CH8–N4	0.00590	0.01986	-0.00336	0.00416	0.00080	0.80669
	Average	*0.00595*	*0.02001*	*-0.00338*	*0.00419*	*0.00081*	*0.80693*
	CH16–H18C	0.01180	0.04517	-0.00674	0.00902	0.00227	0.74776
	CH36–H32C	0.01170	0.04483	-0.00668	0.00895	0.00226	0.74727
	Average	*0.01175*	*0.04500*	*-0.00671*	*0.00898*	*0.00227*	*0.74751*
ZnL_3	CH20–N55	0.00775	0.02510	-0.00429	0.00528	0.00100	0.81156
	CH54–N56	0.00770	0.02498	-0.00425	0.00525	0.00100	0.80950
	CH38–N57	0.00753	0.02444	-0.00417	0.00514	0.00097	0.81123
	CH18–N58	0.00750	0.02433	-0.00414	0.00511	0.00097	0.81048
	CH2–N59	0.00752	0.02436	-0.00415	0.00512	0.00097	0.81048
	CH36–N60	0.00773	0.02505	-0.00426	0.00526	0.00100	0.81000
	Average	*0.00763*	*0.02471*	*-0.00421*	*0.00519*	*0.00099*	*0.81024*
	CH12–H8C	0.01222	0.04661	-0.00699	0.00932	0.00233	0.75014
	CH30–H26C	0.01234	0.04704	-0.00707	0.00941	0.00235	0.75064
	CH48–H44C	0.01230	0.04688	-0.00704	0.00938	0.00234	0.75049
	Average	*0.01230*	*0.04688*	*-0.00704*	*0.00938*	*0.00234*	*0.75049*

[a] $\rho(r)$, $\nabla^2\rho(r)$, $V(r)$, $G(r)$, and $H(r)$ - all in atomic units.

When atoms A and B are closer, (i) larger electron densities are accumulated within the interatomic bonding region, (ii) $\nabla^2\rho_{BCP}$ and G_{BCP} increase, while (iii) V_{BCP} decreases (becomes more negative). It is very important to stress that, besides the same trends in these topological properties, the positive value of $\nabla^2\rho_{BCP}$ is observed for all of these interactions. QTAIM interpretation of the positive value of $\nabla^2\rho_{BCP}$ (typical for a *closed-shell* interaction) means that the electron density at the BCP is concentrated to the respective atomic basins rather than being contracted towards and along the interatomic surface. An example of the latter case, where $\nabla^2\rho_{BCP} < 0$, is the covalent bond of the C_2–$C_{2'}$ junction.

We now focus on the topological description of the CH•••HC interactions - see Table 4.3 and Figure 4.5. The following trends as a function of interatomic distances are observed, proceeding

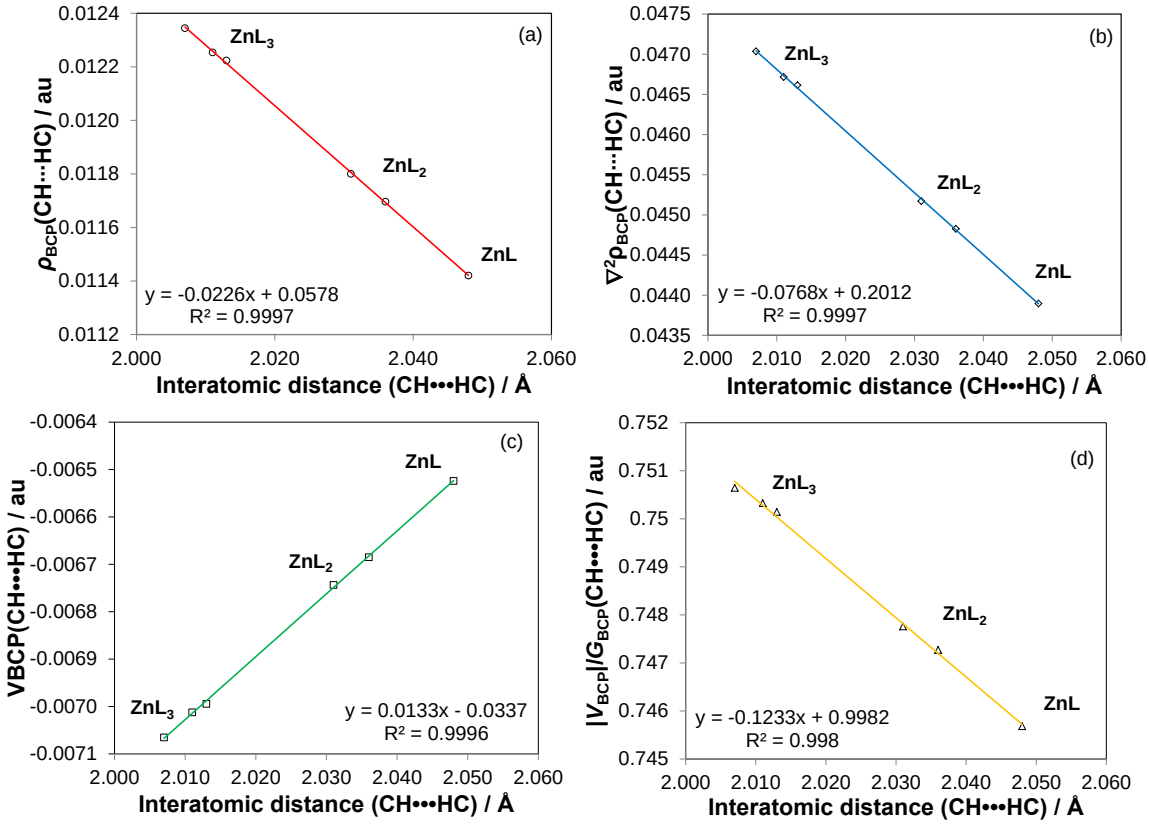

Figure 4.5. Relationships between indicated topological properties at the BCP and d(CH•••HC) in ZnL_n.

from ML to ML_3: (i) an increase in ρ_{BCP}, (ii) an increase in $\nabla^2\rho_{BCP}$ and (iii) V_{BCP} becomes more negative. These are the same trends that are observed for the CH•••O and CH•••N intramolecular interactions as well as the Zn–N and Zn–O coordination bonds. In addition, $\nabla^2\rho_{BCP}$ is positive at the BCPs, hence the CH•••HC interaction can also be termed as a closed-shell interaction.

We conclude this section by stating that the electron density distribution along the AIL of the CH•••HC interaction, as well as the change in the energy densities at BCPs upon additional ligand coordination, is qualitatively identical to those observed for all other, recognized closed-shell bonding interactions. Moreover, as opposed to the coordination bonds, the largest ρ_{BCP} for all intramolecular interactions (CH•••O, CH•••N, CH•••HC) is observed in ML_3 which suggests that they are strongest in the most crowded complex.

IQA Energy Decomposition Analysis. One must realise that the use of the atomic virial theorem in QTAIM somewhat restricts the analysis of molecules in that (i) strictly speaking, only equilibrium structures can be analysed (otherwise $2T + V = 0$ does not hold) and (ii) although QTAIM can be seen as energy decomposition technique, it is restricted to the one-body (atomic) partition of the total energy of a molecule, where atoms have a transferrable kinetic energy T_A which fulfils an atomic virial theorem. Our QTAIM analysis shows trends in the electron distribution between atoms connected by an AIL, a QTAIM-defined bond path indicating the presence of a privileged quantum-mechanical exchange channel[29] which are always of a stabilizing nature. However, a 'classical' interpretation of chemical interaction is concerned with several different energy contributions to the overall interatomic interaction; the analysis of these energy contributions is often used to interpret the physical nature of the interatomic interactions and its local contribution (either stabilising or not) to the overall energy of a molecule. Even though trends of the same nature are observed for all atoms regarded as bonded *as well as* for CH•••HC interactions (they certainly show the interatomic electron density distributed in a stabilizing manner) the net interaction energy between these H-atoms can still be overall repulsive when different energy decomposition analysis are utilised.[41–42,44–45,65–66]

One might, in principle, look for a suitable reference molecule(s) to study physical properties (such as net charges, energies, or delocalisation index, etc.) of 'the same' atoms

either involved or not involved in an interaction of interest (such as CH•••HC). Unfortunately, such a procedure is necessarily arbitrary, often ambiguous and hence prone to misinterpretation because of the difficulty (if not impossibility) in finding a chemically 'identical' reference atom, as is the case here. Therefore, we decided to use the computationally expensive but highly useful IQA approach to determine the interaction energies between atoms as well as understand the origin of each interaction. One might recall that IQA defines the interaction between two atoms as a competing contribution made by classical components (interaction energies between electrons and nuclei as well as Coulombic interaction between electrons of atom A and B) conveniently combined as $V_{\mathrm{cl}}^{\mathrm{AB}}$, and quantum-mechanical contribution, as $V_{\mathrm{XC}}^{\mathrm{AB}}$. Since the IQA scheme is not suitable for DFT wavefunctions,[29,65,67] we re-optimized our molecules at the HF level. As a result, (i) reported bond lengths in Table 4.4 are slightly different when compared with the DFT values shown in Table 4.1, and (ii) the quantum-mechanical energy term $V_{\mathrm{XC}}^{\mathrm{AB}}$ computed at the HF level does not have the correlation term, hence it is reported as $V_{\mathrm{X}}^{\mathrm{AB}}$. We must stress here that our interest is primarily in the general nature and physical properties of the interatomic interactions (are they stabilizing and which energy terms dominate?) and they are appropriately qualitatively described at the HF level, even with modest basis sets.[29,65,67]

We will analyse primarily the IQA results for ML_2, since all intramolecular interactions, CH•••O, CH•••N and CH•••HC, are present only in this complex. The interaction energy, $E_{\mathrm{int}}^{\mathrm{AB}} = V_{\mathrm{cl}}^{\mathrm{AB}} + V_{\mathrm{X}}^{\mathrm{AB}}$, for (i) all relevant intramolecular interactions, (ii) coordination Zn–N and Zn–O bonds, (iii) the covalent C–C bond, and (iv) the intramolecularly nonbonded N-atoms of the ligand (the latter one was done for comparison with other interactions of interest in this work; recall that $E_{\mathrm{int}}^{\mathrm{AB}}$ can be calculated for any two atoms in a molecule) are shown in Table 4.4 (a full set of data for all ZnL_n complexes is provided in Table C4 of Appendix C).

When the relative values of $E_{\mathrm{int}}^{\mathrm{AB}}$ are considered, we found that the coordination bonds are characterised by the largest (by far) $|E_{\mathrm{int}}^{\mathrm{AB}}|$ values. For the Zn–N and Zn–O coordination bonds, $E_{\mathrm{int}}^{\mathrm{AB}}$ is about –390 and –300 kcal mol^{-1}, respectively, followed by C–C interaction which is about 100 kcal mol^{-1} smaller when compared with Zn–O. This is somewhat an

unexpected result and it fully justifies further studies (involving more metal complexes) to explore and understand that better – one must remember, however, that the IQA-defined interaction energy must not be confused with the bond-dissociation energy. The energies of all intramolecular interactions are negative, clearly indicating their local energy stabilizing contribution with the following trend $|E_{\text{int}}^{\text{CH•••O}}| > |E_{\text{int}}^{\text{CH•••N}}| >> |E_{\text{int}}^{\text{CH•••HC}}|$ which appears to corroborate with a general notion when CH•••O and CH•••N are concerned (due to the difference in electronegativity, the latter interaction is expected to be weaker). Importantly, the IQA analysis does predict the interaction between CH•••HC to be of stabilizing nature as a value of –2.74 kcal·mol^{-1} for a weak interaction is not trivial. For comparison, the interaction energy between N--N of the bipyridyl ligand found from IQA is +285.1 kcal·mol^{-1} and thus recovers our classical notion that these atoms are strongly repulsive within this molecule.

To understand the nature of the interactions of interest better, we look next at the energy partitioning terms within IQA for each relevant interaction in ML_2. Our focus is on two interaction energy components (see Eq 8) which describe the physical nature of an interaction, namely whether they might be seen as predominantly of electrostatic, $|V_{\text{cl}}^{\text{AB}}| > |V_{\text{X}}^{\text{AB}}|$, or quantum mechanical exchange origin; the latter case can be seen as a process of delocalization of electrons between atoms involved (classically could be interpreted as a covalent component of a bonding interaction[68]). It is seen in Table 4.4 that all non-covalent bonds and intramolecular interactions which show AILs can be characterised as of a strong ionic nature except CH•••HC. For instance, in case of Zn–OH_2, the $V_{\text{cl}}^{\text{Zn-O}}$ term makes over 12 times larger stabilizing contribution than $V_{\text{X}}^{\text{Zn-O}}$; this is closely followed by Zn–N where the ratio of the classical and electron exchange terms approaches 10 with the latter being quite significant, $V_{\text{X}}^{\text{Zn-N}}$ about –40 kcal·mol^{-1}. The CH•••O and CH•••N interactions show a chemical nature similar to the Zn–N and Zn–O bonds

Table 4.4. Decomposition of two-bodied interaction energies within the IQA framework for all relevant interactions in ZnL_2 complexes with 2,2´-bipyridyl (L).

Atoms	**d(A–B)**	V_{ne}^{AB}	V_{en}^{AB}	V_{nn}^{AB}	V_{C}^{AB}	V_{cl}^{AB}	V_{XC}^{AB} **[a]**	V_{Int}^{AB}	V_{XC}^{AB}/E_{Int}^{AB}
	Å	*au*	*au*	*au*	*au*	*kcal·mol^{-1}*	*kcal·mol^{-1}*	*kcal·mol^{-1}*	
CH···HC	*2.05*	-0.2488	-0.2488	0.2581	0.239	-0.23	-2.51	-2.74	0.916
CH···O	*2.502*	-1.7656	-1.7656	1.6917	1.8195	-12.47	-3.26	-15.73	0.207
CH···N	*2.879*	-1.3988	-1.3988	1.2866	1.4953	-9.91	-1.64	-11.56	0.142
C-C	*1.497*	-11.4030	-11.4030	12.7264	10.233	96.27	-193.41	*-97.15*	1.991
Zn-N1	2.183	-55.1408	-55.1408	50.9086	58.8099	-353.41	-36.73	-390.14	0.094
Zn-N2	2.182	-55.1524	-55.1524	50.9243	58.8145	-355.12	-36.76	-391.88	0.094
Zn-O6	2.236	-59.7008	-59.7008	56.7947	62.1597	-280.51	-22.97	-303.48	0.076
N1-N2	2.676	-11.8153	-11.8153	9.6902	14.4061	292.25	-7.15	285.1	-0.025

[a] Note that only exchange energy is used to calculate full V_{XC}^{AB} term because of the Hartree-Fock approximation.

in that the main stabilizing contribution to E_{int}^{AB} comes mainly from V_{cl}^{AB} with the V_{cl}^{AB}/V_{X}^{AB} ratio approaching 6 and 4 for CH•••N and CH•••O, respectively. We note with interest that the $V_{cl}^{CH•••HC}$ term is very small and negative (the overall IQA-defined electrostatic CH•••HC interaction is not repulsive!) and, most surprisingly, it becomes more negative with an increase in crowding around the central metal ion; it varies from negligible –0.02 to significant –0.52 kcal mol^{-1} in ZnL and ZnL_3, respectively. It means that both terms, V_{cl}^{AB} and V_{X}^{AB}, locally contribute in stabilizing fashion towards the overall molecular energy of these complexes contradicting the classical notion of highly strained H-clashes. In case of CH•••HC, the ratio V_{cl}^{AB}/V_{X}^{AB} of ~0.1 is very different when compared with other intramolecular interactions. Clearly, the chemical nature of these close contacts cannot be seen as of ionic nature as it is almost entirely dominated by the exchange term, $V_{X}^{CH•••HC}$ = –2.51 kcal·mol^{-1} as compared with electrostatic contribution, $V_{cl}^{CH•••HC}$ = –0.23 kcal·mol^{-1} (both values for ML_2).

For comparison, let us now analyse the IQA data generated for a typical covalent bond between C-atoms forming a bridge between pyridyl rings and an interaction between non-bonded N-atoms of the ligand 2,2'-bipyridyl. As one would anticipated, the interaction energy between 2,2′-carbon atoms contains a large repulsive electrostatic term (96.27 kcal·mol^{-1}) which is compensated by much large stabilization due to 'sharing' of electrons, V_{X}^{AB} = –193.41 kcal·mol^{-1}. On the other hand, the N--N interaction is characterised almost entirely by extremely large electrostatic repulsion, V_{cl}^{N--N} = 292.25 kcal·mol^{-1} (only –7.15 kcal·mol^{-1} comes from V_{X}^{N--N} due to an overall charge delocalization throughout the interaction) and this correlates very well with the QTAIM analysis where the bond path between these N-atoms is not observed.

Briefly summarizing this section, we note that for the expected closed-shell bonded interactions, Zn–N, Zn–O, CH•••O and CH•••N, E_{int}^{AB} is composed mostly of electrostatic stabilization due to intra-molecular polarization and significant ionic charge-transfer, with a considerably smaller exchange part. IQA thus recovers our classical notions of coordination and hydrogen bonds. The IQA results for the C–C bond, which we know to be entirely covalent, recovers the classical view as well in that a strong electrostatic repulsion is compensated for by an even greater stabilization due to spin-pairing. From

these results, it is plausible to say that the nature of the CH•••HC interaction is more similar to the C–C bond than the other intramolecular hydrogen bonds present in the molecule, because the interaction energy is dominated by the quantum mechanical exchange energy rather than electrostatic attraction.

Let us consider now the last column in Table 4.4, were we placed the V_{XC}^{AB}/E_{int}^{AB} ratio, called further the exchange-interaction ratio, EIR. One must recall that V_{XC}^{AB} is always negative and if the overall interaction energy term is also of stabilizing nature, E_{int}^{AB} < 0, then the V_{XC}^{AB}/E_{int}^{AB} ratio is positive. From that it would follow that the sign of that ratio can be used to identify an interatomic interaction as overall either (i) locally stabilising, for which EIR > 0 (e.g. positive values of EIR is observed here for all intramolecular CH•••O, CH•••N and CH•••HC interactions), or (ii) locally destabilising, hence non-bonding interatomic interaction for which EIR is negative (as we observe here for the N--N interaction). Incidentally, QTAIM-defined bond paths are only observed for interactions where EIR > 0. It would be of great interest and importance to investigate a large set of different intra- and inter-molecular interactions to find out whether the proposed criterion to distinguish bonding from non-bonding two-body interactions (either interatomic or inter-molecular) exactly follows the presence or absence of a bond path.

The analysis of data seen in Table 4.4, in combination with EIR, leads us to another observation. It appears that the variation in the EIR values (only when EIR > 0) might correlate with a classical notion of a strong covalent, or ionic, or intermediate bonding interaction. Our focus now is on the electrostatic term, V_{cl}^{AB}, which can be either repulsive or attractive. It is clear that there are two possible general cases for which EIR remains positive, namely when (i) V_{cl}^{AB} < 0, or (ii) for V_{cl}^{AB} > 0 when $|V_{XC}^{AB}| > V_{cl}^{AB}$. For 0 < EIR << 1 (when $V_{XC}^{AB} >> E_{int}^{AB}$ or $|V_{XC}^{AB}| << |E_{int}^{AB}|$) a bonding interaction is dominated by electrostatic terms (the smaller EIR the larger degree of ionic character is observed) whereas a value well above 1 (when $|V_{XC}^{AB}| >> |E_{int}^{AB}|$) points at a predominantly or fully classical covalent bond. For instance, in the case of the Zn–O and Zn–N bonds as well as CH•••N and CH•••O interactions, where we observe a predominant ionic character (V_{cl}^{AB} significantly dominates the quantum term, V_{XC}^{AB}) the EIR << 1. On the other hand, EIR is almost 2 for the C–C bond, recovering its classical covalent character fully.

Finally, considering the IQA data shown in Table 4.4 (and Table C4 of Appendix C), the CH•••HC interaction can be interpreted as of bonding nature because (i) classical electrostatic contribution is attractive (by definition, V_{XC}^{AB} is always stabilizing), (ii) $E_{int}^{AB} < 0$, and (iii) EIR > 0 in all the ZnL_n complexes. Regarding the chemical nature of the bonding CH•••HC interactions we note that EIR is close to (but larger than) one. Therefore, we conclude that, using the V_{XC}^{AB}/E_{int}^{AB} as an approximate indicator, CH•••HC shows predominantly covalent character in these complexes and hence should not be placed under the umbrella of a 'classical' intramolecular hydrogen bonding interaction, such as CH•••O. This is important observation as this clearly suggests that the QTAIM-based criteria derived by Popelier[69] for hydrogen bonds might not be applicable to the CH•••HC interactions.

NCI Analysis. While QTAIM describes interatomic interactions in terms of well-defined and highly localized interatomic lines and points (bond paths and bond critical points), NCI discovers and quantifies non-covalent interactions from the analysis of ρ(r) distribution in large interatomic volumes. One must stress here that there is an excellent correlation between QTAIM-defined BCP and appearance of a NCI-defined trough. This is because (i) there is no density gradient at the BCP, hence $s(\rho)_{BCP} = 0$, but (ii) in the 3-D space surrounding the BCP the change in $\nabla\rho$ dominates ($s(\rho)$ approaches zero) and (iii) as a result a steep trough is observed on the NCI-plot at ρ values as found at the QTAIM-defined critical point. Importantly, not only is NCI able to recover the features of QTAIM in real space, but NCI is able to describe interatomic interactions also in the absence of density critical points, such as BCP or RCP.

Figure 4.6 shows 3-D isosurfaces for all of the non-covalent interactions in ZnL_2, as identified by troughs in the reduced density gradient within the NCI formulation; a full set of isosurfaces of individual interactions in ZnL_2 is shown in Figure C3 of Appendix C, whereas full sets of isosurfaces in ZnL and ZnL_3 are shown in Figure C4. The colour of isosurfaces in Figure 4.6 depends on the sign of the λ_2 eigenvalue, giving an indication of the nature of the interaction (the colour scheme used, from blue, through green to red, reflects the following range –0.07 au < sign(λ_2) × ρ < 0.03 au and it is implemented consistently throughout). For regions where $\lambda_2 > 0$ (isosurfaces are shown in red) a local depletion of the electron density can be linked with repulsive forces or steric strain regions,

whereas for $\lambda_2 < 0$ (blue colour is used), locally increased electron density exists and this translates to attractive interatomic interaction.[53,70,72]

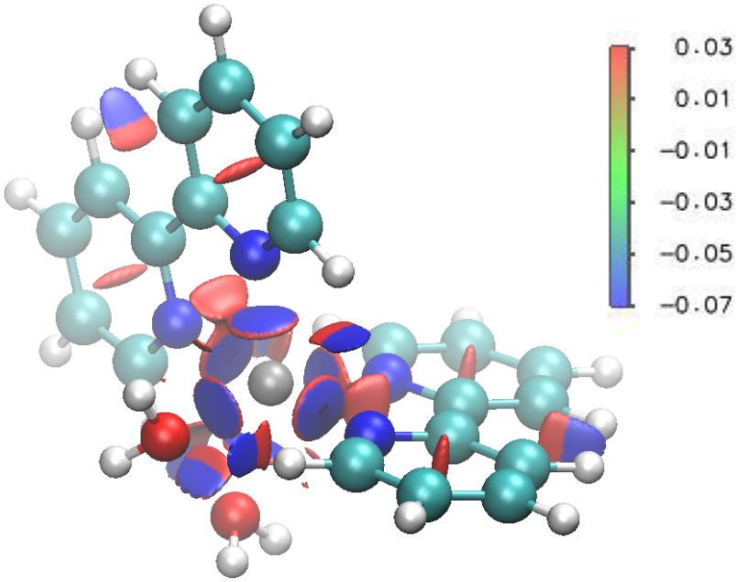

Figure 4.6. NCI isosurfaces of ZnL_2. The surfaces describe the reduced density gradient at an isovalue of 0.5 au. The surfaces are coloured on a blue-green-red scale according to values of sign(λ_2)ρ, ranging from –0.07 to 0.03 au.

Many and very different non-covalent interactions were found by NCI in ZnL_2, some of them not present on the molecular graph (Figure 4.3B). Let us briefly discuss each NCI-defined interaction in more details (purely covalent bonds are above the chosen density cut-off and thus they do not appear in Figure 4.6). The interactions within the coordination Zn–N and Zn–O bonds are shown as large, round discs, surrounded by a ring of depletion. We interpret this as a strong bonding interaction located between the two atoms; the placement of the blue discs follows the QTAIM-defined BCP on a bond path on a molecular graph. However, the large diameter of the blue discs clearly indicates that these bonding interactions do occupy a large space between the central metal ion and an electron-donor atom, either N or O. This, possibly, is nothing more than what one would expect (just a 3-D representation of coordination bonds, quite different when compared with AIL), but the appearance of the red ring surrounding the blue disc must carry additional and possibly significant information.

Similar phenomenon has been recently noted during the study of intermolecular H-bonds formed between two water molecules. This red ring, surrounding the space occupied by the classical hydrogen bond between two water molecules, was significant

only at inter-molecular distances, d(HO–H•••OH_2), shorter than that of the minimum energy on the potential-energy surface.[73] Formation of the red ring has been interpreted as steric repulsion caused by steric crowding which becomes more pronounced with shortening intermolecular distances and eventually resulting in an overall positive interaction potential energy despite the central blue disc still being present. Regarding our coordination bonds, a similar scenario applies and it clearly indicates that the coordination sphere around the central metal ion is strained but with attractive (stabilising) interactions still dominating (otherwise this complex would not form).

All the intra-molecular interactions, CH•••O, CH•••N and CH•••HC, show very characteristic isosurfaces composed of two adjacent, blue and red, 3-D regions. The attractive region (blue) is always located exactly between two interacting atoms, whereas the repulsive (red) region is always located well inside the ring of atoms (this ring is the result of a polyatomic interaction). To understand significance of this NCI-defined interaction better, one might use the IRC[74] path for electrocyclization of butadiene with ELF/NCI snapshots of reactants, transition state, and products described elsewhere.[70] A single stabilizing interaction was initially present when two terminal carbon atoms started to come close to each other (no steric strain or repulsive force was identified between these two C-atoms). When a transitional stage was reached, the NCI analysis showed the two-colour isosurface (similar to what we observe for our intramolecular interactions) at the centre of the ring-to-be. This blue-red isosurface bifurcated along the reaction coordinate into the C−C bond interaction (blue) and the red isosurface (called a ring tension[70]) was placed in the centre of the ring, where a ring critical point must be present.

One should stress that the presence of a ring critical point as well as classical steric repulsions will result in red isosurfaces in the NCI analysis because in both cases a local depletion of electron density takes place. Looking at the intramolecular interaction isosurfaces in Figure 4.6, it is obvious that the centres of the blue and red colours coincide with the BCP and RCP on the molecular graph. One can interpret the presence of a single and two-colour isosurface as a result of these two density critical points (BCP and RCP) being close to each other.

The NCI analysis not only recovered non-covalent interactions found from QTAIM, but also revealed the presence of O--O and O--N interactions as well as an interaction between the close N-atoms of the ligand - no AILs are present in any of these interactions. The O--

N and N--N interactions are clearly repulsive, with a single red disc in the interatomic region of each interaction. However, the O--O interaction is presented similarly to CH•••HC, CH•••O and CH•••N interactions (interactions which *do* contain AILs) - an attractive region directly between the atoms, and a repulsive region localized (in this case) towards the metal centre.

A set of selected NCI-plots (RDG against sign(λ_2)ρ) for ZnL_2 is shown in Figure 4.7 (relevant plots for all interactions of all forms of ZnL_n are shown in Figures C5-C7). It is clearly seen that each kind of diatomic interaction (coordination bond or a classical stabilising intramolecular interaction) as well as polyatomic interaction (such as regions around ring critical points) has a specific NCI signature. The NCI plots of e.g. (i) the Zn–N and Zn–O bonds show a single, large and well-developed trough for which RDG $\rightarrow$ 0 and sign(λ_2)ρ < 0; (ii) the intramolecular H-bond (e.g.CH•••O) has two, narrow and well-developed troughs placed almost symmetrically around the zero value of the electron density, and (iii) RCP of pyridine has only one characteristic trough in the positive range of sign(λ_2)ρ. The values of ρ where each trough approaches zero of the RDG scale ($s(\rho)$ $\rightarrow$ 0) are known as NCI Interaction Critical Points (ICPs).[70] One can see that not only the shapes of troughs, but also the absolute values of ρ at each ICP vary significantly among those interactions and the largest are observed here for the coordination bonds. Moreover, unlike in QTAIM, critical points exist for all significant intramolecular interactions, regardless of the presence or absence of a BCP or AIL. The values of sign(λ_2)ρ at each ICP, ρ_{ICP}^{AB}, for selected non-covalent interactions in ZnL_2 are shown in Table 4.5 (NCI data for ZnL, ZnL_2 and ZnL_3 are shown in Table C5). The ICPs associated with the concentrating, attractive regions are labelled $(-)\rho_{ICP}^{AB}$, and $(+)\rho_{ICP}^{AB}$ indicate the ICPs associated with the depletive regions.

Focusing on $(-)\rho_{ICP}^{AB}$, Zn–N shows a greater concentration of electron density than Zn–O bonds, with $(-)\rho_{ICP}^{Zn\text{-}N}$ more negative by 0.02387 au than $(-)\rho_{ICP}^{Zn\text{-}O}$; this strongly supports the QTAIM and IQA findings (from analysis of either ρ_{BCP} or E_{int}) that the Zn–N bond is much stronger. The NCI data also shows that (i) all the intramolecular interactions are much weaker when compared with coordination bonds when the relevant values of $(-)\rho_{ICP}^{AB}$ are compared and (ii) the trend $\left|(-)\rho_{ICP}^{CH\bullet\bullet\bullet HC}\right| > \left|(-)\rho_{ICP}^{CH\bullet\bullet\bullet O}\right| > \left|(-)\rho_{ICP}^{CH\bullet\bullet\bullet N}\right|$ which reproduced the one observed in the ρ_{BCP} values from the QTAIM analysis. However, the

NCI plots clearly show for, e.g. the CH•••O or CH•••N interactions, two almost identical troughs (which are characterised by close in absolute values of ρ) of opposite sign. So what is the overall physical nature of this kind of interactions when NCI analysis is concerned? Clearly, interpretation of physical meaning of troughs might not be that obvious.

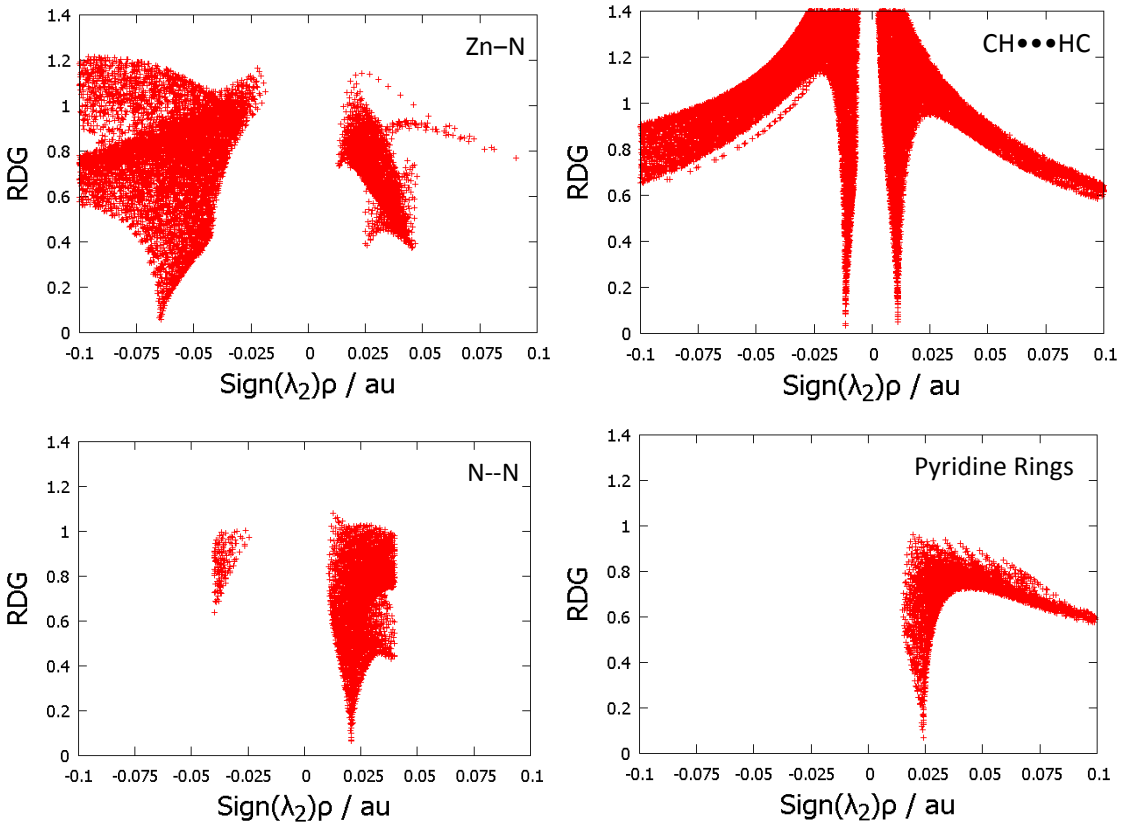

Figure 4.7. NCI-plots for indicated intramolecular interactions in ZnL_2.

Table 4.5. NCI data for all ZnL_2 coordination bonds and intramolecular interactions.

Interaction	$(-)\,\rho_{ICP}^{AB}$ **[a]**	$(+)\,\rho_{ICP}^{AB}$ **[a]**
Zn–N	–0.06449	
Zn–O	–0.04062	
CH•••HC	–0.01155	0.01104
CH•••O	–0.01007	0.00768
CH•••N	–0.00596	0.00580
N--N		0.02082
O--O	–0.01267	0.01298
O--N		0.00959
Pyridine Rings		0.02398

[a] In au.

It is interesting and important to note that the trend in values of density representing troughs in the positive range of sign(λ_2)ρ follows that found at ring critical points of rings formed by these three intramolecular interaction. As a matter of fact, we discovered that the values of ρ at ICPs and RCPs are almost identical: $\rho_{ICP}^{CH\bullet\bullet\bullet HC}$ = 0.01104 and $\rho_{RCP}^{CH\bullet\bullet\bullet HC}$ = 0.001105; $\rho_{ICP}^{CH\bullet\bullet\bullet O}$ = 0.00768 and $\rho_{RCP}^{CH\bullet\bullet\bullet O}$ = 0.00765, and $\rho_{ICP}^{CH\bullet\bullet\bullet N}$ = 0.00580 and $\rho_{RCP}^{CH\bullet\bullet\bullet N}$ = 0.00581, all in ZnL_2. This finding points at previously reported interpretations of RCP regions as either ring-tension,[70] or destabilizing electron "voids".[72] Interpreting the RCP regions as purely destabilizing, however, does not seem to be very convincing because (i) a study[75] showed a good correlation between densities at BCP and RCP and the stronger intramolecular hydrogen bond, as measured by ρ_{BCP}, the larger electron density was observed at the ring critical point of the ring formed by this interaction, (ii) larger values of ρ_{RCP} have been correlated with increased ring aromaticity[76–77], and (iii) since density at ICP can be used as a measure of stabilizing and destabilising contributions to the interaction, then adding e.g. (–) $\rho_{ICP}^{CH\bullet\bullet\bullet N}$ and (+) $\rho_{ICP}^{CH\bullet\bullet\bullet N}$ would result in about zero interaction energy for the CH•••N interactions, but clearly this is not the case. The values of (+) ρ_{ICP} for the various intramolecular interactions showing an AIL are thus related to the polyatomic interaction of the entire ring, and cannot be attributed to steric repulsion for the diatomic intramolecular interactions.

Let us now interpret troughs (placed in the positive range of sign(λ_2)ρ) for other interactions. A much smaller and not that well-developed trough (when compared with the one representing the stabilising contribution) is observed for the coordination bonds. We interpret it as revealing strain caused by the steric crowding around the central metal ion and it corresponds to the red ring around the blue disc on Figure 4.6. A very interesting NCI plot was obtained for the N--N interaction where two troughs, large repulsive and small attractive, are observed; a large red isosurface is observed in Figure 4.6. This overall picture compares surprisingly well with IQA analysis of this interaction where electrostatic repulsion is dominating, $V_{cl}^{N\bullet\bullet\bullet N}$ >> $V_{X}^{N\bullet\bullet\bullet N}$; both analyses consistently showing a repulsive nature for this interaction. A much smaller red disc is observed for the O--N interaction and this correlates well with troughs seen on the NCI plot; clearly, even though much weaker than N--N, the O--N interaction is repulsive. A predominantly repulsive nature of the O--O interaction, which has two comparable troughs, is well presented, particularly in Figure C4, where red discs (with small blue areas) are located between

water molecules coordinated to Zn(II). A very characteristic, single trough is observed for the RCP of a pyridine ring; it is placed, as one would expect, in the positive range of sign(λ_2)ρ.

In summary, The NCI analysis (i) does not provide any evidence of steric strain related to the CH•••HC interaction, (ii) provides additional evidence that the CH•••O, CH•••N and CH•••HC intramolecular interactions are of stabilizing nature, (iii) points at the coordination sphere as a place of significant steric strain, and (iv) does not provide any evidence to support MM-based claim that the ligand is highly strained due to a steric H-clash.

ETS-NOCV-based analysis of deformation densities. ETS-NOCV differs significantly from all three techniques discussed above as it involves molecular and fragment orbitals rather than real space density distributions. A particularly attractive feature of this method is in the visualization of molecular regions from which electrons were removed and regions which gained electrons when fragments were allowed to reproduce the energy minimized final structure of a molecule, in comparison to an "interaction-free" excited state. The examples of dominant NOCVs for Zn–N and Zn–O coordination bonds in ML are shown in Figure 4.8, part a and b, respectively (see also Figure C8 in the SI where a full set of relevant NOCVs for coordination bonds in ZnL_2 and ZnL_3 complexes is shown). Blue and red colours indicate an increase (accumulation) and decrease (donation to a blue region), respectively, of the electron density. It is clearly seen that the electron density is accumulated in the coordination sphere of the central metal ion (within the atomic basin of Zn) while density is depleted mainly from the donor's atomic basin, N5 and N6 of the BPy ligand and O1 of water molecule in case of the Zn–N and Zn–O coordination bonds, respectively. All these NOCVs, for ML in Figure 4.8 as well as for ML_2 and ML_3 in Figure C8, are of the same general shape and can be seen as textbook examples

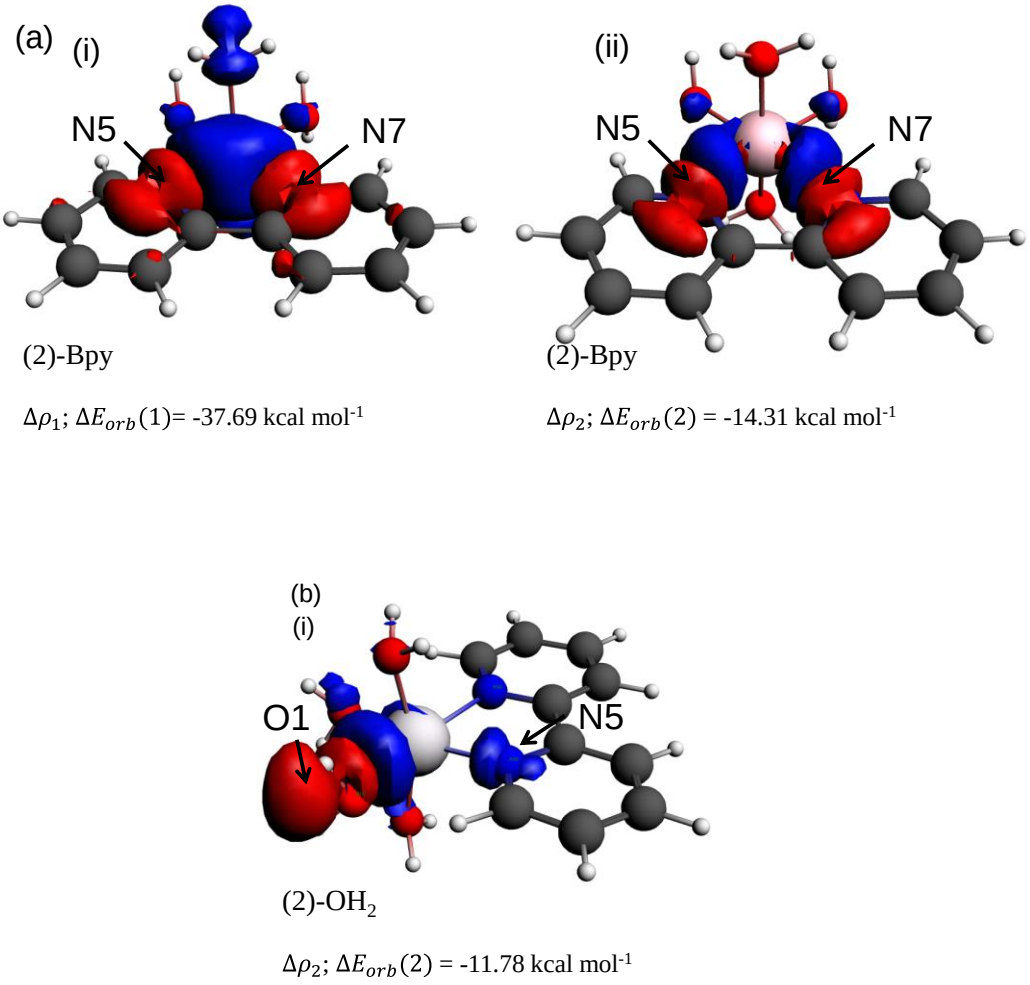

Figure 4.8. Representative NOCVs for (a) Zn–N and (b) Zn–O coordination bonds in ZnL.

of the classical interpretation of coordination bonds, where ligands donate free pair of electrons (electron density) to available d^2sp^3-hybrid orbitals on the central metal ion.

We focus our attention now on the C–C bond forming a junction between the two pyridyl rings; relevant NOCVs in ML are shown in Figure 4.9 (NOCVs for ML_2 and ML_3 are presented in Figure C9 of Appendix C). Two characteristic NOCVs are observed in Figure 4.9 – one NOCV can be ascribed to the traditional σ-orbital (part a) and another NOCV can be seen as representing the π-orbital (part b).

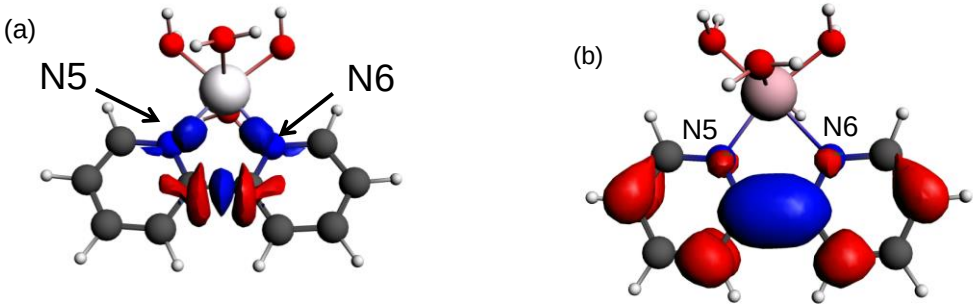

(7)-pyr, α+β

$\Delta\rho_1$; $\Delta E_{orb}(1)$ = -239.547 kcal mol^{-1}

(7)-pyr, α+β

$\Delta\rho_2$; $\Delta E_{orb}(2)$ = -23.98 kcal mol^{-1}

Figure 4.9. Characteristic NOCVs obtained for the C_2–$C_{2'}$ bridge in ZnL.

These NOCVs demonstrate that electron density is accumulated within the region between the bonded atoms (the *bonding* interatomic region) and is depleted either in the regions outside the bond (the *non-bonding* region of the interaction) or in other atoms of the molecule. A predominantly single covalent bond between the two carbon atoms can be deduced from a $\Delta E_{orb}(1)$ value of $\Delta\rho_1$, –239.5 kcal mol^{-1} (a σ-orbital, Figure 4.9a) which is about ten times larger (in absolute value) when compared with $\Delta\rho_2$ representing a π-orbital, Figure 4.9b.

Three very different NOCVs describing intramolecular CH•••O interactions in ML are presented in Figure 4.10 where two characteristic charge density accumulations are clearly observed. The first and dominant NOCV ($\Delta E_{orb}(12)$ = –1.82 kcal mol^{-1}, part a in Fig 10) is related to a polarized electrostatic interaction or complementary intra-atomic-basin type, whereby density is (i) accumulated in the bonding region of the basin of the oxygen atom and (ii) depleted from the hydrogen's atom bonding region.

This type of interaction is consistent with Popelier's QTAIM-based criteria[69] defining a classical H-bond. However, there are also additional NOCVs (with smaller values of ΔE_{orb} = –0.77 and –0.38 kcal mol^{-1}) describing the CH•••O interaction where density accumulates in a channel-like fashion between the bonded atoms. In this case, density is withdrawn from the non-bonding regions of either the O-atom (Figure 4.10b) or the H-atom (Figure 4.10c). We will refer to this type of NOCV as an inter-atomic-basin type because it is localised between two atoms in the bonding region of two atomic basins.

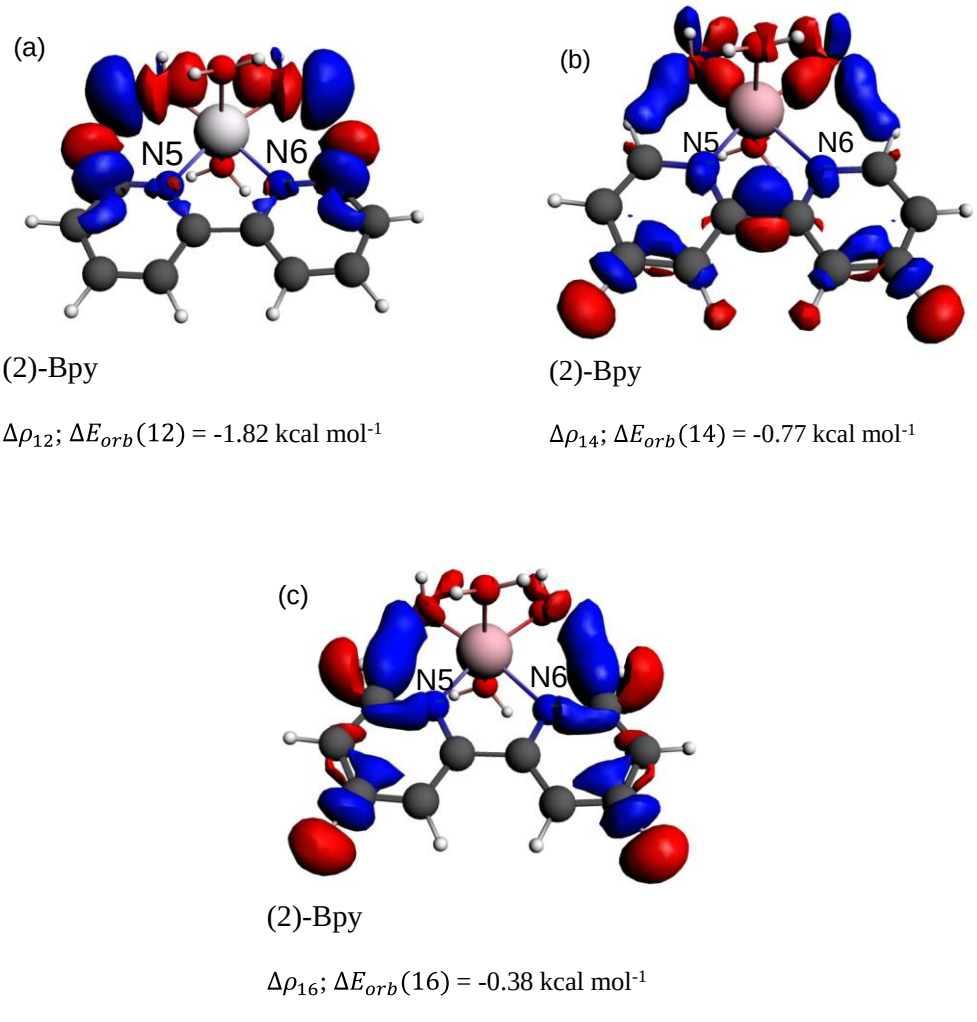

Figure 4.10. NOCV deformation densities for the CH•••O interactions in ZnL. a) Complementary intra-atomic-basin type, b-c) inter-atomic-basin type.

Moreover, it corresponds well with the topological representation of a bonding interaction – the channel-like NOCVs seen in Figures 10b-10c can be compared to the AIL between H and O atoms (a bridge of maximum electron density) and it also corresponds to $V_{\mathrm{X}}^{\mathrm{AB}}$ of IQA analysis. Clearly, the overall picture generated by NOCVs predicts a predominant ionic character of the CH•••O interaction and this correlates well with the IQA analysis very well.

Finally, Figure 4.11 shows most interesting and informative two kinds of NOCVs describing the CH•••HC interaction in ML (full set of intramolecular NOCVs for all ZnL_n complexes is shown in Figure C10 of Appendix C). The first NOCV, $\Delta\rho_{23}$ with $\Delta E_{\mathrm{orb}}(23)$ = –1.8 kcal mol^{-1} in Figure 4.11a, not only shows accumulation of electron density in the bonding region between H-atoms, but also clearly points out at the origin where this

charge comes from - the nonbonding region of atomic basins of the same H-atoms. This can be interpreted as a bonding-type interaction (otherwise an opposite charge deformation would be observed with a depletion between the atoms and accumulation in the non-bonding region of the same H-atoms' atomic basins) and this charge deformation resembles the NOCVs obtained for the CH•••O interaction shown in Figure 4.10 b-c. The second and unique type of NOCV, $\Delta\rho_{21}$ with $\Delta E_{orb}(21) = -2.45$ kcal mol^{-1} in Figure 4.11b, illustrates multi-atomic-basin density accumulation and involves all atoms in the 6-membered ring. Interestingly, the main depletion of the charge appears to be again the non-bonding region of atomic basins of the H-atoms involved in this interaction. These two NOCVs, $\Delta\rho_{23}$ and $\Delta\rho_{21}$, can be compared with the topology of the electron density in the form of AIL in the case of $\Delta\rho_{23}$, while $\Delta\rho_{21}$ compares well with the increased density and gradient ρ paths associated with the formation of a ring critical point on the molecular graph. Moreover, the observed NOCVs strongly indicate a predominant spin-pairing (or covalent) character of the CH•••HC interactions (no evidence is present of any significant electrostatic interaction, such as seen for CH•••O) and this correlates well with the IQA description.

It is clear from the above discussion that NOCVs (i) are always observed between the same atoms for which AILs are generated from the QTAIM analysis, including NOCVs corresponding to the controversial AIL between H-atoms involved in a steric clash and (ii) are distinguishably different providing a very important insight on the nature of the interaction in the ZnLn complexes. Just focusing on intramolecular CH•••HC and CH•••O interactions, it is obvious that they are significantly different. Although both CH•••HC and CH•••O interactions show channel-like interatomic-basin charge accumulations (main contribution found for CH•••HC) the majority of the orbital interaction energy in case of the CH•••O interaction comes from a complementary (or electrostatic) intra-atomic-basin charge rearrangement.

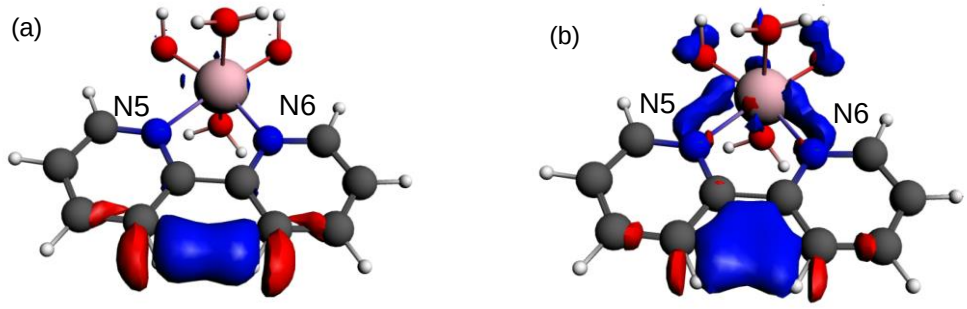

(7)-pyr, α+β

$\Delta\rho_{23}$; $\Delta E_{orb}(23)$ = -1.81 kcal mol^{-1}

(7)-pyr, α+β

$\Delta\rho_{21}$; $\Delta E_{orb}(21)$ = -2.45 kcal mol^{-1}

Figure 4.11. NOCV deformation densities for the CH•••HC interaction in ZnL.

Unfortunately, even though several fragmentation schemes were tested, the deformation density associated with the CH•••N interactions appeared to be too small to generate sufficiently localized NOCVs and we concluded that these interactions in the complexes under investigation are below the resolution of the technique (such an NOCV are shown in Figure C10(b) of Appendix C).

Analysis of ΔE_{orb}. Because the combined ETS-NOCV method allows a partitioning of the total orbital interaction term from ETS, ΔE_{orb}^{T}, in a basis set of NOCVs, we decided to look for trends between the partitioned ΔE_{orb}^{k} and interatomic distances for all coordination bonds and intramolecular interactions. For the following section the superscripts 'T' will refer to the total molecular ΔE_{orb}, 'k' will refer to the energy of a specific NOCV-pair and 'I' will refer to the energy of a combined set of NOCV's describing a single, specific kind of interaction. Relevant data for ETS-NOCVs are collected in Table 4.6 for all coordination bonds and plots of ΔE_{orb}^{I} as a function of the coordination bond lengths are shown in Figure 4.12. The protocol implemented to calculate the average value of ΔE_{orb}^{k} was as follows. When only a single dominant NOCV was found, as shown in Figure 4.8b for the Zn–O coordination bonds in ZnL, then ΔE_{orb}^{I} = ΔE_{orb}^{k} for each individual bond. Because there are four Zn–O bonds in ZnL with corresponding ΔE_{orb}^{k} values of –11.78, –10.88, –1178 and –10.88 kcal mol^{-1}, the average ΔE_{orb}^{k} value of –11.33 was calculated which represents an energy contribution per a single Zn–O coordination bond in ZnL (see Table 4.6). However, for the chelating Zn–N bonds, two separate and similar in nature NOCVs per coordinated ligand were always identified

in all ZnL_n complexes, as shown in Figure 4.8a i-ii for ZnL. The corresponding ΔE_{orb}^{k} values (–37.69 and –14.31 kcal mol^{-1} in ZnL) were averaged and gave ΔE_{orb}^{I} of –26.00 kcal mol^{-1} for a single Zn–N bond formed by a single coordinated ligand. In the case of ZnL_2 and ZnL_3, two and three ΔE_{orb}^{I} values, respectively, were obtained and they were averaged to obtain the energy contribution per a statistical Zn–N bond in a complex. A full set of individual NOCVs, their corresponding isovalues and associated ΔE_{orb}^{k} values is displayed in Table C6.

We discovered that, for both coordination bonds, the stabilizing contribution made by the orbital interaction energy, ΔE_{orb}^{I}, decreases (becomes less negative, hence less stabilising) when going from ML to ML_3. For a single Zn–N bond, ΔE_{orb}^{I} increased by +7.30 kcal·mol^{-1} from –26.00 kcal·mol^{-1} in ZnL to an average value of –18.70 kcal·mol^{-1} in ZnL_3. Significantly weaker Zn–O coordination bonds follow the same trend where ΔE_{orb}^{I} increased by +2.76 kcal·mol^{-1} from an average value of –11.33 kcal·mol^{-1} in ZnL to an average value of –8.75 kcal·mol^{-1} in ZnL_2.

The orbital interaction energy term, ΔE_{orb} from the ETS-NOCV theory, describes the energy changes associated with inter-fragment occupied and virtual orbital mixing as well as intra-fragment density rearrangement. Therefore, when combined with the visual deformation densities shown in Figure 4.8, they can be interpreted as a stabilizing interaction involving occupied orbitals on the ligands (bipyridyl and H_2O) and the unoccupied virtual orbitals on Zn. As our data shows, this stabilization is inversely proportional to the length of the coordination bonds and this corresponds well with trends in the relevant values for ρ_{BCP} (from QTAIM), E_{int} (from IQA) and ρ_{ICP} (from NCI).

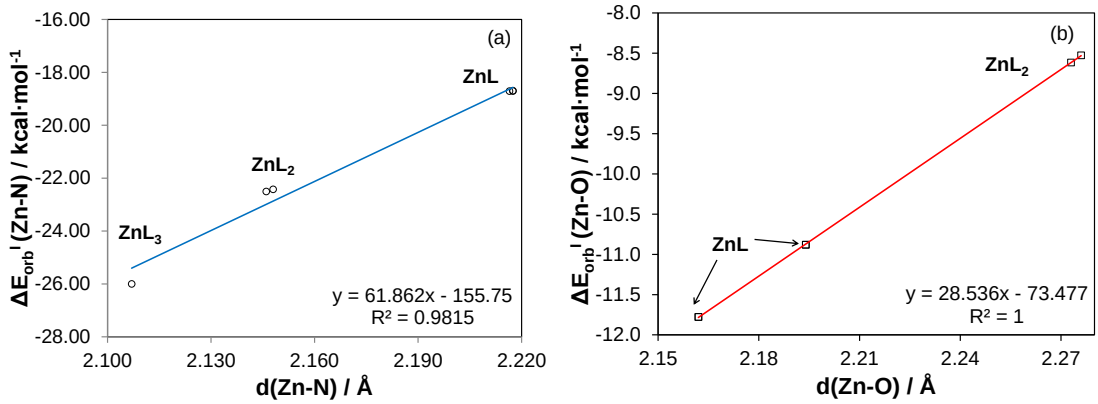

Figure 4.12. Relationships between bond lengths and NOCV orbital interaction energy, ΔE_{orb}^{I}, for a) Zn–N bonds, and b) Zn–O bonds.

Table 4.6. Orbital interaction energies for all Zn–L coordination bonds in Zn^{II} complexes with 2,2´-bipyridyl (L)

Complex	Atoms	Fragmentation Scheme	NOCVs	Averaged ΔE_{orb}^{I} [a]
ZnL	Zn–(N5,N6)	*(2)-Bpy*	1,2	-26.00
	Zn–O1	*(2)-OH_2*	1	-11.78
	Zn–O2	*(2)-OH_2*	1	-10.88
	Zn–O3	*(2)-OH_2*	1	-11.78
	Zn–O4	*(2)-OH_2*	1	-10.88
			Average	*-11.33*
ZnL_2	Zn–(N1,N2)	*(2)-Bpy*	1,2	-22.42
	Zn–(N3,N4)	*(2)-Bpy*	1,2	-22.50
			Average	*-22.46*
	Zn–O5	*(2)-OH_2*	1	-8.62
	Zn–O6	*(2)-OH_2*	1	-8.53
			Average	*-8.57*
ZnL_3	Zn–(N55,N56)	*(2)-Bpy*	1,2	-18.71
	Zn–(N57,N58)	*(2)-Bpy*	1,2	-18.71
	Zn–(N59,N60)	*(2)-Bpy*	1,2	-18.69
			Average	*-18.70*

[a] *Describes a single Zn–L bond. In kcal·mol^{-1}*

Next we analyse ΔE_{orb}^{I} for the CH•••O and CH•••HC intramolecular interactions (the NOCVs describing CH•••N are too delocalized to measure ΔE_{orb}^{I} accurately) and representative set of data obtained for relevant ETS-NOCVs is collected in Table 4.7. It is important to recall that the CH•••O and CH•••HC interactions (i) are characterised by a set of distinctive NOCVs and (ii) not every NOCV shows deformation density changes on every occurrence of a specific interaction in the molecule. For instance, the NOCV Ψ^{26} (shown in Figure C10c iii of Appendix C) describes the energy associated with deformation densities only for *two* CH•••HC interactions, even though three CH•••HC contacts are present in ML_3. Consequently, to generate ΔE_{orb}^{I} describing the orbital energy contribution per a single interaction, the ΔE_{orb}^{26} value was divided by *two*. The full procedure used to generate ΔE_{orb}^{I} for CH•••O and CH•••HC interactions is described in Tables C7 and C8. ΔE_{orb}^{I} for CH•••O bonds becomes more negative by 0.2 kcal·mol^{-1}, from –1.48 kcal·mol^{-1} in ML to –1.68 kcal·mol^{-1} in ML_2, as the d(CH•••O) becomes shorter. The dominant ΔE_{orb}^{k} for this interaction describes the complementary intra-

atomic-basin type, as shown in Figure 4.10a, and is equal to –0.91 kcal·mol^{-1} per bond in ML and –1.11 kcal·mol^{-1} in ML_2. The rest of the contribution to ΔE_{orb}^{I} comes from the channel-like inter-atomic-basin type NOCV shown in Figure 4.8(b-c). Again, following the definition for ΔE_{orb}, we interpreted ΔE_{orb}^{I}(CH•••O) as stabilization resulting from (i) polarizable charge-transfer (from the hydrogen into the oxygen's atomic basin in addition to rearrangements within each basin and functional group) which enhances the electrostatic interaction of an H-bond, and (ii) a covalent-like electron sharing due to the orbital overlap, where density is donated primarily from non-bonding regions into the bonding interatomic region. Importantly, trends observed in E_{orb} obtained for intramolecular interactions (when going from ML to ML_3) follow those generated by the QTAIM, IQA and NCI analyses when ρ_{BCP}, E_{int} and ρ_{ICP} were used, respectively.

Interestingly, the stabilizing orbital energies obtained per a single CH•••HC interaction are about three times larger when compared with the ΔE_{orb}^{I} values obtained per a single CH•••O interaction in ML and ML_2 where these two interactions are present. This correlates very well with the IQA data showing predominant stabilizing contribution coming from the V_{XC}^{AB} term. The ΔE_{orb}^{I}(CH•••HC) values are plotted against the d(CH•••HC) in Figure 4.13 and as for the coordination bonds shown earlier, a good relationship was obtained. The overall increase in the stabilizing contribution coming from ΔE_{orb}^{I}(CH•••HC) is about 3.1 kcal·mol^{-1} per interaction, from –4.27 kcal·mol^{-1} in ML to –7.36 kcal·mol^{-1} in ML_3. This results in very significant total stabilizing contribution made by ΔE_{orb} of about –22 kcal mol^{-1} due to close contacts between clashing H-atoms in ZnL_3. Unlike CH•••O interactions, the NOCVs describing CH•••HC interactions are all of the inter-atomic-basin type. We interpret ΔE_{orb}^{I}(CH•••HC) thus as the stabilization due to density depletion of the orthogonal fragment orbitals in non-bonding regions and density accumulation of the SCF-minimized molecular orbitals inside the bonding interatomic region of this interaction.

Table 4.7. Orbital interaction energies for CH•••O and CH•••HC intramolecular interactions in Zn^{II} complexes with 2,2´-bipyridyl (L)

Complex	Atoms	Fragmentation Scheme	NOCVs	Averaged $\Delta E_{orb}{}^{I}$ [a]	Description
ZnL	H8–O1, H24–O3	*(2)-Bpy (N5,N6)*	12	-0.91	Intra-atomic
			14,16	-0.57	Inter-atomic
			Sum	*-1.48*	
	H14–H18	*(7)-pyr*	21,23	-4.27	Inter-atomic
ZnL_2	H42–O5	*(2)-Bpy (N1,N2)*	15	-1.11	Intra-atomic
			17,18	-0.57	Inter-atomic
			Sum	*-1.68*	
	H24–O6	*(2)-Bpy (N3,N4)*	15	-1.13	Intra-atomic
			17,18	-0.55	Inter-atomic
			Sum	*-1.68*	
	H16–H18, H36–H32	*(7)-pyr*	23,25,26,27	-5.52	Inter-atomic
ZnL_3	H8–H12, H26–H30, H44–H48	*(7)-pyr*	26,27,28,29,30	-7.36	Inter-atomic

[a] *In kcal·mol^{-1}*

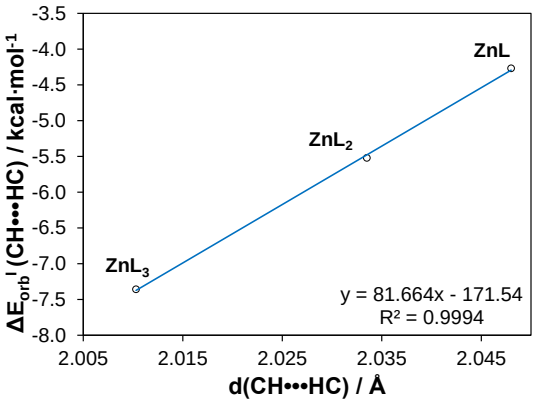

Figure 4.13. Relationship between interatomic distance and NOCV orbital interaction energy for CH•••HC interactions

We conclude, from the analysis of $\Delta E_{orb}{}^{I}$, that stabilizing orbital interactions exist for both coordination bonds as well as the CH•••O and CH•••HC interactions. Like the property-distance relationships from our QTAIM analysis, so does $\Delta E_{orb}{}^{I}$ also correspond with the interaction distance and the orbital stabilization energy in CH•••HC interactions

follows the same general trends that Zn–N, Zn–O and CH•••O do. In addition, trends observed in ETS-NOCV data mimic those obtained from each other method used.

Conclusions

The aim of this work was to investigate the energy components which contribute to the number of interatomic interactions (involving coordination, covalent and intramolecular interactions) with our main focus being on understanding the CH•••HC interactions in the ZnL_n complexes with 2,2′-bipyridyl. To this end we have used four and very different energy partitioning techniques - three of them are based on real space, or topological, methods (QTAIM, IQA and NCI) and the forth one involves molecular and fragment orbitals (ETS-NOCV). Each technique provided us with specific information which, when combined (i) created a consistent description of these interactions and (ii) provided a convenient comparative tool.

The NCI method, which is designed specifically to investigate noncovalent interactions which includes intramolecular steric strain, has not provided any evidence to support the classical notion that the 3,3′-hydrogen atoms are responsible for a highly strained ligand; neither the region between these two H-atoms nor the ligand appear to be strained but instead the NCI plots pointed at the coordination sphere where steric strain was located. Both coordination bonds as well as CH•••O, CH•••N and CH•••HC interactions were found to be of a stabilizing nature. Moreover, NCI plots fully recovered the relative strength of bonding interactions clearly, showing that (i) among coordination bonds, Zn–N is significantly stronger than Zn–O and (ii) the intramolecular interactions are much weaker than coordination bonds.

If the 3,3′-hydrogen atoms were involved in a classically interpreted steric clash, then it should result in significant electrostatic repulsion (a destabilising energy) between these two atoms. The IQA method is designed to recover and quantify, among other energy components, electrostatic contribution towards interatomic interactions, $E_{\mathrm{Int}}^{\mathrm{AB}} = V_{\mathrm{XC}}^{\mathrm{AB}} + V_{\mathrm{cl}}^{\mathrm{AB}}$. Results obtained from IQA fully recovered our classical notions of the chemical character of coordination, as well as covalent, bonds in these complexes (showing a predominantly electrostatic interaction with a measure of electron sharing for the coordination bonds, and a highly repulsive electrostatic interaction but even greater quantum exchange interaction for the covalent bonds). Importantly, with regards to the

main focus of this work, CH•••HC interactions, we showed that (i) the electrostatic energy was always of stabilising nature, $V_{cl}^{AB} < 0$, and (ii) with a decrease in d(CH•••HC), when going from ZnL to ZnL_3, its stabilising contribution increased which we see as another argument opposing the presence of steric repulsion (the same trend in V_{cl}^{AB} was observed for CH•••O and CH•••N intramolecular interactions). The main contribution to the IQA-defined interaction energy was found to be of quantum mechanical nature, $V_{XC}^{AB} >> V_{cl}^{AB}$, which corresponds to a greater covalent character (the CH•••HC interaction is more similar to the C–C covalent bond than to the electrostatic CH•••O and CH•••N interactions and Zn–N and Zn–O coordination bonds). Since the V_{XC}^{AB} term is always stabilising, the overall interaction energy, $E_{Int}^{CH•••HC}$, was always found to be locally stabilising with the largest contribution made in most crowded ZnL_3.

The ETS-NOCV technique qualitatively confirmed the overall nature of the CH•••HC interactions because (i) very well developed NOCVs showing an accumulation of electron density between 3,3′-hydrogen atoms were observed and (ii) NOCVs representing electrostatic interactions (as discovered for the CH•••O interaction, showing its predominant ionic nature and corroborating with IQA analysis) were not present. The accumulation of density in the bonding region of CH•••HC is paired with a density depletion in the non-bonding regions of the interaction in a stabilizing fashion, with ΔE_{Orb}^{I}(CH•••HC) < 0.

Importantly, results obtained from all the techniques employed here were fully consistent. They all have shown the same trends in the energy components with interatomic distances and, considering the CH•••HC interactions as an example, the trends in ρ_{BCP} (from QTAIM), ρ_{ICP} (from NCI), V_{XC}^{AB} and V_{cl}^{AB} (from IQA) and ΔE_{orb} (from ETS-NOCV), when going from ZnL to ZnL_3, demonstrate an increase in the stabilising nature of this interaction. In addition, we found significant correspondence among results obtained from these techniques; as an example, relationships between results obtained from ETS-NOCV and QTAIM for the CH•••HC interactions are shown in in Figure 4.14. Combining the results from these four energy partitioning and interatomic interaction characterising techniques we must conclude that the intramolecular interactions (CH•••HC, CH•••O or CH•••N) in ZnL_n complexes are of locally stabilising nature; all of these interactions show significant spin-pairing which results in a region of concentrated

electron density between the interacting atoms and the formation of a bridge of maximal density - an AIL. The only fundamental difference between these contacts is the larger contribution of electrostatic interactions in CH•••O and CH•••N, making these interactions predominantly of ionic character whereas the CH•••HC interaction can be classified as more covalent.

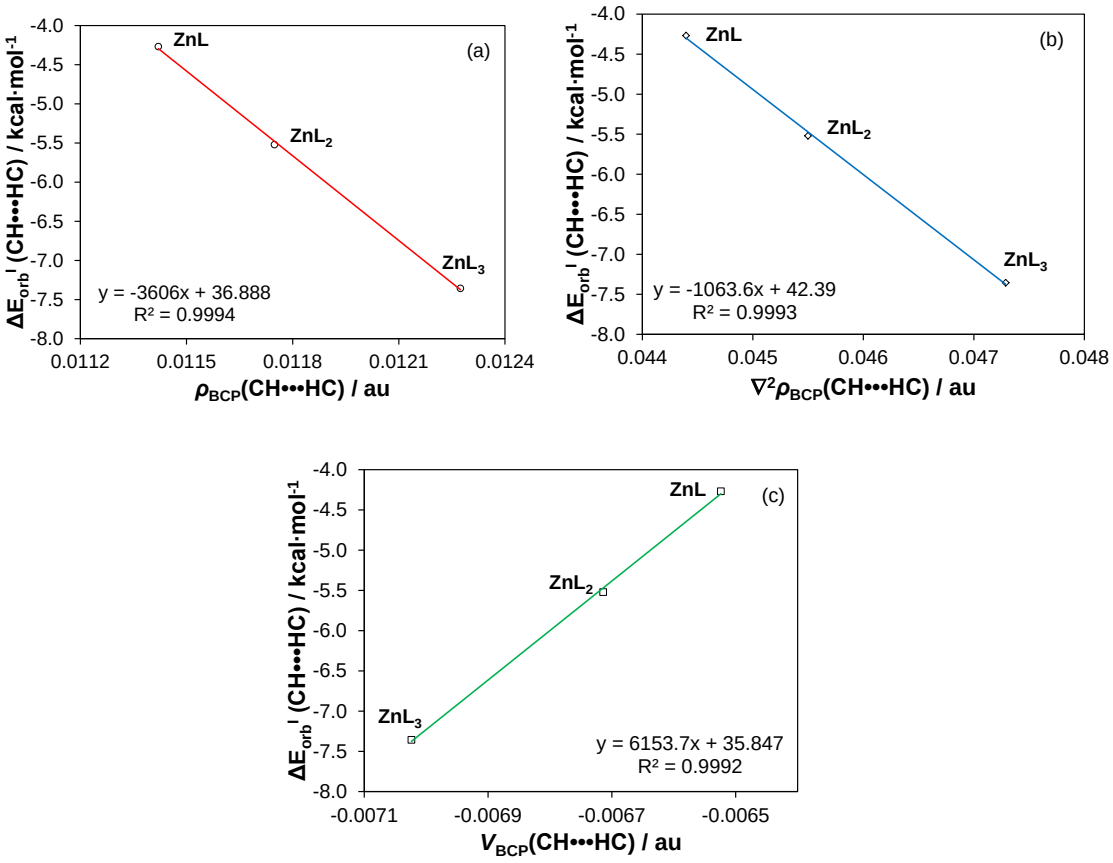

Figure 4.14. Relationship between NOCV orbital interaction energy and topological properties a) ρ_{BCP}, b) $\nabla^2\rho_{BCP}$ and c) V_{BCP} for CH•••HC interactions

Finally, we would like to clarify the difference between the binding and interaction energies, the latter one being a subject of this work. Regarding binding energy, it is defined in IQA as $E_{Bind}^{AB} = \Delta E_{Self}^{A} + \Delta E_{Self}^{B} + E_{Int}^{AB}$, where ΔE_{Self} is the change in self-energy (intra-atomic energy) in relation to a suitable reference frame. In other words, the interaction energy combined with the changes *within* an atomic basin gives a quantity more related to the bond dissociation energy. Calculating ΔE_{Self} is not a problem when the interaction between two atoms in a diatomic molecule is concerned, because the self-energy of a single atom in vacuum can be computed. Regarding atoms in polyatomic molecules, such as the present case, estimation of the change in E_{Self} becomes, in

principle, an impossible task, as an atom which is identical in every physical and chemical manner but without the presence of the specific inter-atomic interaction needs to be found. We have established that, upon changing the ligand 2,2'-bipyridyl from the trans to the cis conformer, practically all atomic energies (either QTAIM-defined kinetic energies or IQA-defined E_{Self}) changed significantly. Although we observe some change in E_{Self} of 3,3'-H atoms when going from *trans* (where they are not involved in the clash) to *cis* conformers of 2,2'-bipyridyl, one is unable to rigorously partition ΔE_{Self}^{H} into $\Delta E_{Self}^{CH\cdots HC}$ and $\Delta E_{Self}^{Trans-to-Cis}$. On the other hand, the interatomic energy can be computed and, in combination with other physical components of this interaction (from the combined insight of multiple techniques), provides an invaluable tool to describe its physical nature. So, if one assumes that a close contact, such as H--H, indeed results in some energy destabilising contribution, call it E_{dest}(H--H), then as we have demonstrated in this work (i) it is not the part of the interaction energy between 3,3'-H atoms and (ii) it does not result in this interatomic region being energetically strained; hence, E_{dest}(H--H) must be hidden either in the self-energies of the H-atoms or is distributed throughout a molecule.

References

[1] NIST Standard Reference Database 46. NIST Critically Selected Stability Constants of Metal Complexes Database; Version 8.0; R. M. Smith, A. E. Martell, Eds.; US Department of Commerce, National Institute of Standards and Technology: Gaithersburg, MD, 2004.

[2] S. T. Howard, *J. Am. Chem. Soc.* **1996**, *118*, 10269–10274

[3] J. Kalenik, Z. Pawełka, *J. Mol. Liq.* **2005**, *121*, 63–68

[4] F. Labat, P. P. Lainé, I. Ciofini, C. Adamo, *Chem. Phys. Lett.* **2006**, *417*, 445–451

[5] C. Blanchet-Boiteux, P. Friant-Michel, A. Marsura, J-B. Regnouf-de-Vains, M. F. Ruiz-López, *J. Mol. Struct.* (THEOCHEM) **2007**, *811*, 169–174.

[6] V. Galasso, G. De Alti, A. Bigotto, *Tetrahedron* **1971**, *27*, 991–997

[7] C. Jaime, J. Font, *J. Mol. Struct.* **1989**, *195*, 103–110.

[8] R. Benedix, P. Birner, F. Birnstock, H. Hening, H-J. Hofmann, *J. Mol. Struct.* **1979**, *51*, 99–105

[9] R. Benedix, P. Birner, H-J. Hening, *J. Mol. Struct.* **1982**, *90*, 65–69

[10] V. Barone, F. Lelj, L. Commisso, N. Russo, C. Caulletti, M. N. Piancastelli, *Chem. Phys.* **1985**, *96*, 435–445.

[11] S. Zahn, W. Reckien, B. Kirchner, H. Staats, J. Matthey, A. Lützen, *Chem. Eur. J.* **2009**, *15*, 2572–2580

[12] I. Alkorta, J. Elguero, C. Roussel, *Comput. Theoret. Chem.* **2011**, *966*, 334–339.

[13] A. H. Göller, U-W. Grummt, *Chem. Phys. Lett.* **2000**, *321*, 399–405

[14] A. H. Göller, U-W. Grummt, *Chem. Phys. Lett.* **2002**, *354*, 233–242.

[15] H. Irving, D. H. Mellor, *J. Chem. Soc.* **1962**, 5222–5237

[16] R. A. Palmer, T. S. Piper, *Inorg. Chem.* **1966**, *5*, 864–878

[17] K. Sone, S. Utsuno, T. Ogura, *J. Inorg. Nucl. Chem.* **1969**, *31*, 117–126

[18] R. Griesser, H. Sigel, *Inorg. Chem.* **1970**, *9*, 1238–1243

[19] R. B. Martin, R. Prados, *J. Inorg. Nucl. Chem.* **1974**, *36*, 1665–1670.

[20] R. D. Hancock, A. E. Martell, *Chem. Rev.* **1989**, *89*, 1875–1914

[21] D. Buist, N. J. Williams, J. H. Reibenspies, R. D. Hancock, *Inorg. Chem.* **2010**, *49*, 5033–5039

[22] G. M. Cockrell, G. Zhang, D. G. VanDerveer, R. P. Thummel, R. D. Hancock, *J. Am. Chem. Soc.* **2008**, *130*, 1420–1430

[23] S. Del Piero, P. Di Bernardo, R. Fedele, A. Melchior, P. Polese, M. Tolazzi, *Eur. J. Inorg. Chem.* **2006**, 3738–3745.

[24] R. D. Hancock, I. V. Nikolayenko, *J. Phys. Chem. A* **2012**, *116*, 8572−8583.

[25] R. F. W. Bader, *in Atoms in Molecules: A Quantum Theory*; Oxford University Press: Oxford, U.K. 1990.

[26] E. A. Zhurova, C. F. Matta, N. Wu, V. V. Zhurov, A. A. Pinkerton, *J. Am. Chem. Soc.* **2006**, *128*, 8849–8861

[27] C. F. Matta, J. Hernández-Trujillo, T. H. Tang, R. F. W. Bader, *Chem. Eur. J.* **2003**, *9*, 1940–1951

[28] R. F. W. Bader, *J. Phys. Chem. A* **2009**, *113*, 10391–10396

[29] A. M. Pendás, E. Francisco, M. A. Blanco, C. Gatti, *Chem. Eur. J.* **2007**, *13*, 9362–9371

[30] F. Cortés-Guzmán, J. Hernández-Trujillo, G. Cuevas, *J. Phys. Chem. A* **2003**, *107*, 9253–9256

[31] J. Echeverría, G. Aullón, D. Danovich, S. Shaik, S. Alvarez, *Nat. Chem.* **2011,** *3*, 323-330

[32] I. Cukrowski, K. K. Govender, *Inorg. Chem.* **2010**, *49*, 6931–6941

[33] I. Cukrowski, C. F. Matta, *Chem. Phys Lett.* **2010**, *499*, 66–69.

[34] K. N. Robertson, O. Knop, T. S. Cameron, *Can. J. Chem.* **2003**, *81*, 727–743

[35] K. N. Robertson, *in Intermolecular Interactions in a Series of Organoammonium Tetraphenyl-borates*; Ph.D. Thesis, Dalhousie University, Halifax, Canada, **2001**

[36] E. A. Zhurova, V. G. Tsirelson, V. V Zhurov, A. I. Stash, A. A. Pinkerton, *Acta Cryst. B* **2006**, *62*, 513–520.

[37] J. Poater, M. Solà, F. M. Bickelhaupt, *Chem. Eur. J.* **2006**, *12*, 2889–2895

[38] J. Poater, M. Solà, F. M. Bickelhaupt, *Chem. Eur. J.* **2006**, *12*, 2902–2905.

[39] R. F. W. Bader, *Chem. Eur. J.* **2006**, *12*, 2896-2901

[40] J. Hernández-Trujillo, C. F. Matta, *Struct. Chem.* **2007**, *18*, 849–857.

[41] T. Ziegler, A. Rauk, *Inorg. Chem.* **1979**, *18*, 1755–1759

[42] T. Ziegler, A. Rauk, *Inorg. Chem.* **1979**, *18*, 1558–1565

[43] T. Ziegler, A. Rauk, *Theor. Chim. Acta* **1977**, *46*, 1-10.

[44] M. Mitoraj, A. Michalak, *J. Mol. Model*. **2007**, *13*, 347-355

[45] M. Mitoraj, A. Michalak, T. Ziegler, *J. Chem. Theory Comput.* **2009**, *5*, 962-975.

[46] I. Cukrowski, K. K. Govender, M. P. Mitoraj, M. Srebro, *J. Phys. Chem. A* **2011**, *115*, 12746–12757.

[47] Cambridge Crystallographic Data Centre, 12 Union Road, Cambridge CB2 1EZ, U.K.

[48] G. te Velde, F. M. Bickelhaupt, S. J. A. van Gisbergen, C. Fonseca Guerra, E. J. Baerends, J. G. Snijders, T. Ziegler, *J. Comp. Chem.* **2001**, *22*, 931

[49] C. Fonseca Guerra, J. G. Snijders, G. te Velde, E. J. Baerends, *Theoretical Chemistry Accounts* **1998**, *99*, 391

[50] E. J. Baerends, T. Ziegler, J. Autschbach, D. Bashford, A. Bérces, F. M. Bickelhaupt, C. Bo, P. M. Boerrigter, L. Cavallo, D. P. Chong, L. Deng, R. M. Dickson, D. E. Ellis, M. van Faassen, L. Fan, T. H. Fischer, C. Fonseca Guerra, A. Ghysels, A. Giammona, S. J. A. van Gisbergen, A. W. Götz, J. A. Groeneveld, O. V. Gritsenko, M. Grüning, S. Gusarov, F. E. Harris, P. van den Hoek, C. R. Jacob, H. Jacobsen, L. Jensen, J. W. Kaminski, G. van Kessel, F. Kootstra, A. Kovalenko, M. V. Krykunov, E. van Lenthe, D. A. McCormack, A. Michalak, M. Mitoraj, J. Neugebauer, V. P. Nicu, L. Noodleman, V. P. Osinga, S. Patchkovskii, P. H. T. Philipsen, D. Post, C. C. Pye, W. Ravenek, J. I. Rodríguez, P. Ros, P. R. T. Schipper, G. Schreckenbach, J. S. Seldenthuis, M. Seth, J. G. Snijders, M. Solà, M. Swart, D. Swerhone, G. te Velde, P. Vernooijs, L. Versluis, L. Visscher, O. Visser, F. Wang, T. A. Wesolowski, E. M. van Wezenbeek, G. Wiesenekker, S. K. Wolff, T. K. Woo, A. L. Yakovlev, ADF2012, SCM, Theoretical Chemistry, Vrije Universiteit, Amsterdam, The Netherlands, http://www.scm.com

[51] Gaussian 09, Revision A.1, M. J. Frisch, G. W. Trucks, H. B. Schlegel, G. E. Scuseria, M. A. Robb, J. R. Cheeseman, G. Scalmani, V. Barone, B. Mennucci, G. A. Petersson, H. Nakatsuji, M. Caricato, X. Li, H. P. Hratchian, A. F. Izmaylov, J. Bloino, G. Zheng, J. L. Sonnenberg, M. Hada, M. Ehara, K. Toyota, R. Fukuda, J. Hasegawa, M. Ishida, T. Nakajima, Y. Honda, O. Kitao, H. Nakai, T. Vreven, J. A. Montgomery, Jr., J. E. Peralta, F. Ogliaro, M. Bearpark, J. J. Heyd, E. Brothers, K. N. Kudin, V. N. Staroverov, R. Kobayashi, J. Normand, K. Raghavachari, A. Rendell, J. C. Burant, S. S. Iyengar, J. Tomasi, M. Cossi, N. Rega, J. M. Millam, M. Klene, J. E. Knox, J. B. Cross, V. Bakken, C. Adamo, J. Jaramillo, R. Gomperts, R. E. Stratmann, O. Yazyev, A. J. Austin, R. Cammi, C. Pomelli, J. W. Ochterski, R. L. Martin, K. Morokuma, V. G. Zakrzewski, G. A. Voth, P. Salvador, J. J. Dannenberg, S. Dapprich, A. D. Daniels, Ö. Farkas, J. B. Foresman, J. V. Ortiz, J. Cioslowski, and D. J. Fox, Gaussian, Inc., Wallingford CT, 2009.

[52] AIMAll (Version 12.08.21), T. A. Keith, TK Gristmill Software, Overland Parks KS, USA, 2012 (aim.tkgristmill.com)

[53] E. R. Johnson, S. Keinan, P. Mori-Sánchez, J. Contreras-García, A. J. Cohen, W. Yang, *J. Am. Chem. Soc.* **2010**, *132*, 6498–6506

[54] W. Humphrey, A. Dalke, K. Schulten, *J. Molec. Graphics*, **1996**, *14.1*, 33-38.

[55] Bader, R. F. W.; Essén, H. *J. Chem. Phys.* **1984**, *80*, 1943–1960.

[56] D. Cramer, E. Kraka, *Angew. Chem. Int. Ed. Engl.* **1984**, *23*, 627–628

[57] D. Cramer, E. Kraka, *Croat. Chem.* Acta **1984**, *57*, 1259–1281.

[58] R. G. A. Bone, R. F. W. Bader, *J. Phys. Chem.* **1996**, *100*, 10892–10911

[59] M. F. Bobrov, G. V. Popova, V. G. Tsirelson, *Russ. J. Phys. Chem.* **2006**, *80*, 584–590

[60] P. Macchi, A. Sironi, *Coord. Chem. Rev.* **2003**, *238-239*, 383–412

[61] E. Espinosa, I. Alkorta, J. Elguero, E. Molins, *J. Chem. Phys.* **2002**, *117*, 5529–5542.

[62] S. Jenkins, I. Morrison, *Chem. Phys. Lett.* **2000**, *317*, 97–102.

[63] R. Flaig, T. Koritsanszky, B. Dittrich, A. Wagner, P. Luger, *J. Am. Chem. Soc*. **2002**, *124*, 3407–3417.

[64] E. Espinosa, E. Molins, C. Lecomte, *Chem. Phys. Lett.* **1998**, *285*, 170–173.

[65] E. Francisco, A. Martín Pendás, M. A. Blanco, *J. Chem. Theory Comput.* **2006**, *2*, 90–102

[66] K. Kitaura, K. Morokuma, *Int. J. Quantum Chem.* **1976**, *10*, 325–340

[67] A. Martín Pendás, M. A. Blanco, E. Francisco, *J. Comput. Chem.* **2007**, *28*, 161–184.

[68] M. A. Blanco, A. Martín Pendás, E. Francisco, *J. Chem. Theory Comput.* **2005**, *1*, 1096–1109.

[69] U. Koch, P. L. A. Popelier, *J. Phys. Chem.* **1995**, *99*, 9747–9754.

[70] N. Gillet, R. Chaudret, J. Contreras-García, W. Yang, B. Silvi, J-P. Piquemal *J. Chem. Theory Comput.* **2012**, *8*, 3993−3997.

[72] A. Otero-de-la-Roza, E. R. Johnson, J. Contreras-García, *Phys. Chem. Chem. Phys.* **2012**, *14*, 12165-12172.

[73] J. Contreras-García, W. Yang, E. R. Johnson, *J Phys Chem A* **2011**, *115*, 12983–12990.

[74] K. Fukui, *Acc. Chem. Res.* **1981**, *14*, 363–368

[75] S. J. Grabowski, *Monatshefte für Chemie*, **2002**, *113*, 1373–1380.

[76] M. Palusiak, T. M. Krygowski, *Chem.–Eur. J.*, **2007**, *13*, 7996-8006.

[77] S. T. Howard, T. M. Krygowski, *Can. J. Chem.*, **1997**, *75*, 1174-1181.

Chapter 5

Bonding Interactions in Ni^{II} Complexes with 2,2′-Bipyridyl

Abstract

Interatomic interactions in the equilibrium structures of the NiL_n complexes (L = 2,2′-bipyridyl) were investigated at the UX3LYP/6-311++G(d,p) level of theory in solvent (PCM/UFF). The DFT-computed structures and their topological properties (from QTAIM) are strongly supported by numerous correlations with experimental formation constants of Ni^{II} with L. QTAIM-based analysis correctly predicted the character and relative strength of the Ni–N and Ni–OH_2 coordination bonds as well as the covalent character of the C–C bonds in L. For both coordination bonds and all intramolecular interactions (CH•••HC, CH•••O and CH•••N), the relationships involving topological properties follow the same trends; with a decrease in the distance between atoms involved (i) ρ_{BCP} and $\nabla^2\rho_{BCP}$ increases, (ii) the local potential energy density V_{BCP} becomes more negative, (iii) the local kinetic energy density G_{BCP} becomes more positive, and (iv) the ratio $|V(r)|/G(r)$ increases, showing that all these interactions are predominantly of an ionic character. The covalent C2–C3 bond of 2,2′-bipyridyl shows the same trends in $\rho(r)$, $V(r)$ and $G(r)$.

Introduction

The ligand 2,2′-bipyridyl (L) is an important representative of α-diimines and it has excellent ability to form complexes, hence its chemistry with tenths of metal ions has been investigated experimentally for years resulting in hundreds of the formation constants reported.[1] Knowledge of the conformational structure of α-diimine ligands and information about the rotational energy barrier are important and useful for a better understanding of the complex formation process and trends in stability of complexes. Hence not surprisingly, these ligands have also been extensively studied computationally[2–14] and for over 40 years it is known that the most stable conformer of 2,2′-bipyridyl has two N-atoms *trans* to each other (s-*trans* conformer).[6–12] Lower stability of the conformer with nitrogens *cis* to each other (s-*cis* conformer) was attributed mainly to the steric hindrance of the 3,3′-hydrogen atoms and destabilizing nitrogen lone pair-lone pair interactions[8–14] in 2,2′-bipyridyl. To act as a chelate, this ligand must, however, attain the s-*cis* conformation resulting in the 3,3′-hydrogen atoms being in the close contact, CH•••HC (Figure 5.1).

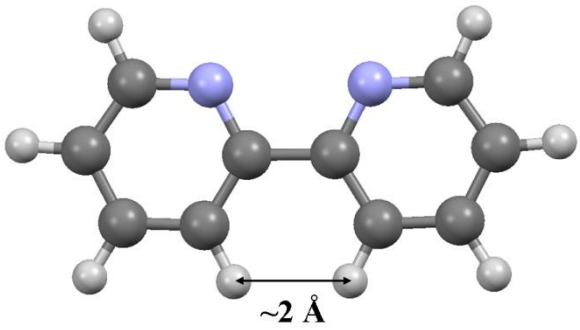

Figure 5.1. Higher energy conformer of the free ligand 2,2′-bipyridyl, as found in metal complexes, with N-atoms *cis* to each other (s-*cis* conformer) showing steric clash between 3,3′-hydrogen atoms.

It is well-known fact that many, if not majority, of metal complexes with this ligand in crystals show nearly-planar structure of 2,2′-bipyridyl with geometric H-clashes present. These H-clashes are assumed to be also present in a solution and were often used to explain trends in experimental formation constants.[15–23] For instance, the unusual trend in the formation constants of Cu^{II} was attributed to steric repulsion between the 3,3′-hydrogens already fifty years ago.[15] More recently, the observed difference of about 1.4 log units for a

set of metal ions with 1,10-phenanthroline and 2,2′-bipyridyl (the latter ligand forms weaker complexes) was attributed to highly strained ligand in the s-*cis* conformer (as it is required for coordination to metal ions) because of the steric hindrance between the hydrogen atoms.[20]

Close contacts between H-atoms are present in many molecules, e.g. in a natural estrogen, Estrone (3-hydroxy-1,3,5-(10)-estratrien-17-one)[24] and became a subject of controversy. This is because several examples of intra- and intermolecular CH•••HC close contacts were interpreted as the H–H bonding interactions, either from the calculated[24–30] or experimental[24,31–33] electron density distributions, using the quantum theory of atoms in molecules (QTAIM)[34] of Bader. The formation of H–H bonds in some molecules was challenged in the literature[35–36] and rebutted.[37–38] Criticism of the QTAIM-based interpretation of bonding interactions between clashing hydrogen atoms is based mainly on the "Pauli or exchange repulsions" (the destabilizing energy contribution acting on the clashing atoms) obtained from the energy decomposition analysis, such as the Extended Transition State (ETS) method[39–41] used in the study of *ortho*-hydrogens in planar biphenyl.[35]

Recently, we have reported[29–30] the QTAIM-based study of Ni^{II} and Zn^{II} complexes with NTPA (nitrilotri-3-propanoic acid) and NTA (nitrilotriacetic acid) which form three 6-membered and 5-membered coordination rings, respectively. Our analysis revealed that (i) the CH•••HC contacts in the Ni^{II} and Zn^{II} complexes with NTPA cannot be used to explain the experimental trend in the formation constants in aqueous medium (NTPA complexes are significantly weaker when compared with NTA) and (ii) there are bonding interactions between H-atoms involved in the CH•••HC contacts. The ETS-NOCV charge and energy decomposition method[42–43] (ETS combined with the Natural Orbitals for Chemical Valence (NOCV) theory) as well as QTAIM were used recently[44] to study H-clashes in the ZnNTPA complex. This first implementation of QTAIM and ETS-NOCV in the study of non-bonding interactions in metal complexes has conclusively demonstrated[44] that the CH•••HC contacts are characterized by (i) the electron flow channel between the H-atoms involved as discovered by the ETS-NOCV analysis (on average, ΔE_{orb} = –1.35 kcal mol^{-1}) and (ii) QTAIM defined a bond path which indicates the presence of a preferred quantum-mechanical exchange channel;[45] hence the presence of bonding interactions between the H-atoms of the CH•••HC

contacts was confirmed by these two and so different methods (theories). However, it is reasonable to assume that close intramolecular contacts between the H-atoms in e.g. the ZnNTPA complex or the 3,3′-hydrogen atoms in metal complexes with 2,2′-bipyridyl might result in significant destabilizing Pauli contribution to the overall local interaction energy. Also, in principle, the ΔE_{Pauli} term (accounting for the repulsive Pauli interaction between occupied orbitals on two fragments in the combined molecule) might be most significant. Clearly, it would be of great interest and paramount importance to gain further insight on the nature of not only the CH•••HC contacts but *all intramolecular interactions* in metal complexes from ETS-NOCV. Unfortunately, there is not yet implementation of the Pauli decomposition into NOCV-like-channels required to obtain information on Pauli contribution and electrostatic term which *act solely between the atoms involved in intramolecular close contacts*. In our opinion, however, the presence of a significant destabilizing energy contribution (if confirmed) does not exclude the presence of a bonding interaction,[44] the electron flow channel or a bond path.

In this work we expand our investigations of the CH•••HC close contacts in metal complexes and focus on the 3,3′-hydrogen atoms of the ligand 2,2′-bipyridyl (L). The topological (from QTAIM) and structural properties (from DFT) found for the CH•••HC intramolecular close contacts are compared with several interatomic interactions which are known to be of a bonding nature. We decided to perform a study where the interactions between 3,3′-hydrogen atoms of L where compared against properties of the Ni–N and Ni–H_2O coordination bonds, CH–N and CH–O intramolecular hydrogen bonds, as well as C–C covalent bonds of 2,2′-bipyridyl. We are of an opinion that the comparison-based conclusions (arrived at by analogy) could be considered here as valid because (i) a single topological analysis of the electron density distribution was performed on the same octahedral complexes, $[NiL(H_2O)_4]^{2+}$, $[NiL_2(H_2O)_2]^{2+}$ and $[NiL_3]^{2+}$ in aqueous medium, where all these interactions are present simultaneously (for simplicity, these complexes will be shown throughout the text as NiL, NiL_2 and NiL_3) and (ii) all analyses were performed on the equilibrium structures where the electron density and 3-D nuclei distributions were such that the Feynman force acting on the nuclei vanished; there are no net repulsive or attractive forces acting on nuclei in these structures.

Some preliminary results from the analysis of atomic energies and atomic net charges, studied in comparative fashion as L is transformed from *s*-trans to the forms the ligand takes as it exists in complexes, are shown in Appendix B. We also explored the changes of atomic energies and charges when the ligand forms the various complexes with Ni^{2+}. In this approach we will attempt to localize the strain caused by the preorganization and confirm whether the destabilization is truly caused by the formation of the CH•••HC interaction, as well as providing additional insight to the nature of other intramolecular interactions present in complexes. These results are termed preliminary, as any study involving the virial-based QTAIM atomic energies is necessarily difficult as the molecular virial ratio needs to be exactly met, and special considerations needs to be taken for structures not at equilibrium. Such considerations are not addressed in the current work, and therefore our analysis of atomic energies is not yet definitive. In the future we also wish to couple QTAIM-atomic energies with the Interacting Quantum Atoms (IQA) defined atomic energies for consistency. Regardless, novel insights are presented in this appendix.

Computational Methods

Molecular modelling was performed with the aid of Gaussian 09, revision B.01, software package.[46] GaussView5.09b[47] was utilized for molecular visualization and construction purposes. Constructed molecules were optimized at the unrestricted X3LYP/6-311++G(d,p) level of theory. The X3LYP functional is an admixture of an extended three-parameter (X3) exchange functional[48–50] coupled with the Lee-Yang-Parr (LYP) electron-correlation functional.[51] Whilst a correlated functional, such as B3LYP, does not describe weak interactions very well because of an inadequate description of electron correlation,[52–54] X3LYP does improve the description of softer interactions, such as intramolecular hydrogen bonds,[48,55–59] whilst describing the structure and electronic properties of molecular systems[48,57–59] in a well-defined manner. Optimization of Ni^{II} complexes was performed with a triple spin multiplicity as only octahedral complexes were of interest here. The structural and electronic properties of each complex were investigated in water as a solvent (ε = 78.39) using the polarizable continuum model (PCM) and universal force field (UFF)

atomic radii (a default solvation model in Gaussian). We performed frequency calculations by determining analytically the second derivatives of the UX3LYP potential energy surfaces with respect to the fixed atomic nuclear coordinates to determine whether each of the minimized structures corresponded to an energy minimum or a saddle point. A tight gradient convergence criterion with ultrafine integration grid was used in all calculations. All reported geometries belong to genuine minimum energy conformations (imaginary frequencies are not present).

The wavefunction files required for the analysis of the topological properties of the electron charge density using the atoms in molecules framework of Bader[34] were generated at the same level of theory (UX3LYP/6-311++G(d,p), PCM/UFF). The topological properties of the electron density, $\rho(r)$, its Laplacian, $\nabla^2\rho(r)$, the local potential energy density, $V(r)$, the local kinetic energy density $G(r)$, and the total energy densities, $H(r)$ were evaluated at all the bond critical points (BCPs) and ring critical points (RCPs) using the AIMAll[60] program using very high basin quadrature with the Proaim integration method. We used QTAIM because (i) it is based on fundamental laws of physics and chemistry (Feynman, Ehrenfest, and virial theorems of quantum mechanics apply), (ii) no prior assumptions were made in the development of this theory, (iii) there are numerous examples where, from the properties of the charge density gradient vector field, the concepts of atoms, bonds, and structures were always fully reproduced, (iv) ρ(r) is a fundamental property of atoms and molecules in all phases, (v) for a single configuration of the nuclei, theoretically calculated ρ(r) represents the time-independent distribution of ρ(r) throughout 3-D space and, importantly, (vi) ρ(r) can also be determined experimentally.

Results and Discussions

Structural Properties of the NiL_n Complexes. The energy-optimized solvent structures of the NiL, NiL_2, and NiL_3 complexes of Ni^{II} with 2,2′-bipyridyl are shown in Figure 5.2 (Cartesian coordinates are provided in Tables E1–E3, Appendix E). Selected structural data for all the coordination bonds and intramolecular contacts are presented in Table 5.1. A large increase in the Ni–N bonds lengths, BL(Ni–N), from 2.059 to 2.128 Å, and a decrease in the

N-Ni-N bite angle (BA) from 80 to 77.5° is observed when going from NiL to NiL_3. At the same time, BA and BL(Ni–N) are virtually of the same value within a particular complex, e.g. BL(Ni–N) in NiL_2 and NiL_3 are 2.091 ± 0.002 and 2.128 ± 0.001 Å, respectively. We found an excellent linear relationship between these two structural properties, BL(Ni–N) and BA (Figure E1 of Appendix E) and the observed trend can be attributed to an increase in crowding of the atoms around the central metal ion. The distance between clashing H-atoms, d(CH•••HC), decreased significantly from 2.098 Å in NiL to 2.064 Å in most crowded NiL_3 and variation in d(CH•••HC) correlates well with BA and BL(Ni–N) – see Figures E2-E3, Appendix E. Importantly, a large increase in the atom crowding has not shown a significant impact on the geometry of the coordinated L molecules and near-planar structures are observed as measured by the absolute values of the N-C-C-N dihedral angle, DA. For instance, we found DA(N-C-C-N) of 1.6° and 4.8° in NiL and NiL_3, respectively. Considering H-atoms which form the CH•••HC close contacts, DA are always below 1°, e.g. DA(H50-C49-C44-C35) = 0.51° in NiL_3.

There are also other intramolecular close contacts, namely (i) CH•••O involving H_2O and 2,2′-bipyridyl with an average distance d_{Avg}(CH•••O) = 2.489 and 2.426 Å in NiL and NiL_2, respectively, and (ii) CH•••N between coordinated 2,2′-bipyridyl molecules with d_{Avg}(CH•••N) = 2.690(1) and 2.630(3) Å in NiL_2 and NiL_3, respectively (Table 5.1). In total, we found 3, 6 and 9 contacts in the NiL, NiL_2 and NiL_3 complexes, respectively, and when going from NiL to NiL_3, the distances between the atoms involved decreased by about 0.04, 0.06 and 0.06 Å for CH•••HC, CH•••O and CH•••N, respectively.

Most significant structural changes observed in the ligand molecules, as e.g. $\delta 2$ = BA(NiL_3) – BA(NiL), are shown in Figure 5.3. Two changes, $\delta 1$ = 0.069 Å due to elongation of BL(Ni–N) (an increase by ~3.37 %) and $\delta 2$ = –3.54° due to narrowing of the bite angles (a decrease by ~4.42 %) brought the geometry around the central metal ion in NiL_3 closer to the minimum strain BL(M–N) of 2.5 Å and BA of 69° predicted from MM.[21,61] This is an important but unexpected observation as it suggests that least strained L might be in most crowded NiL_3. The covalent bonds of the ligand remained virtually unchanged

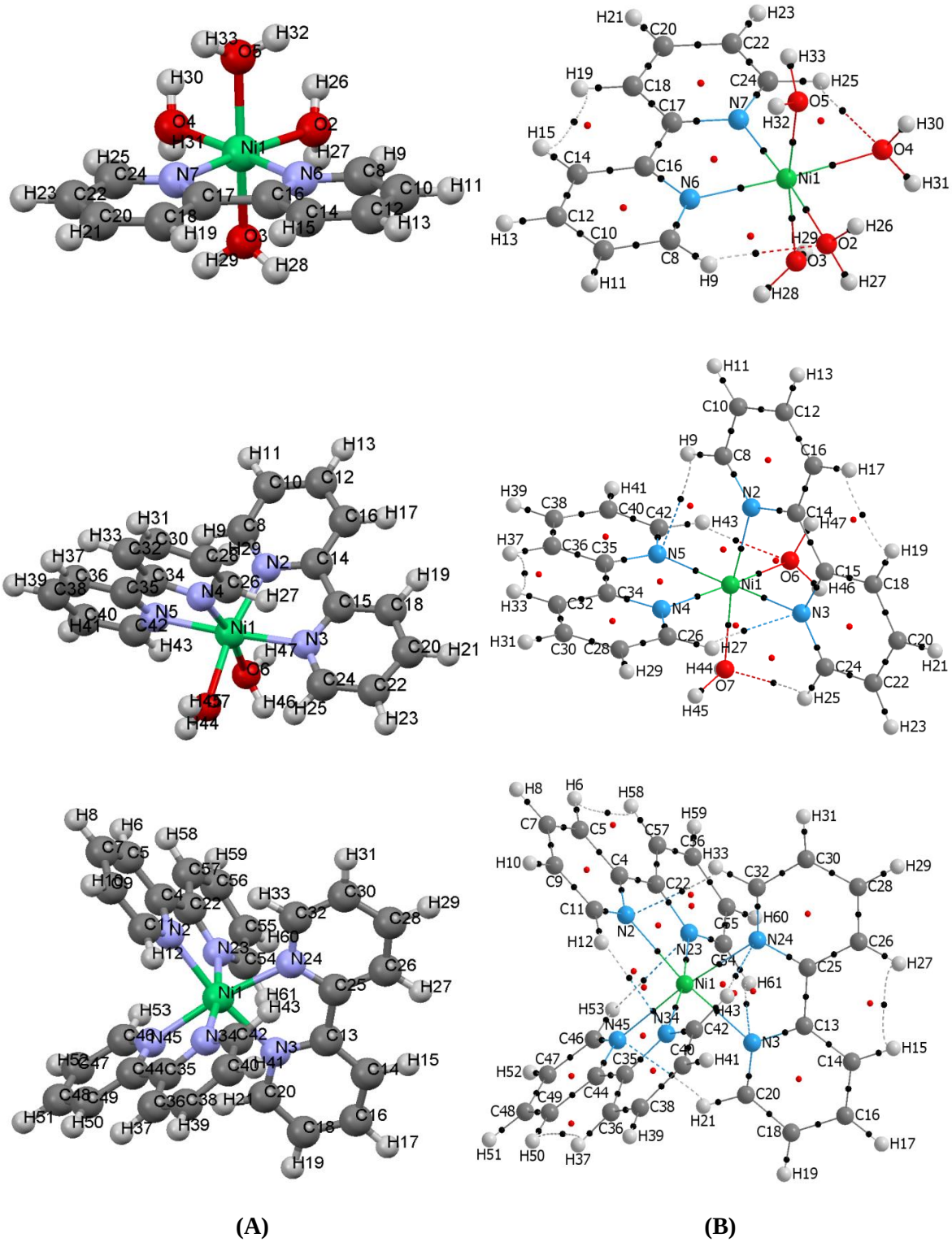

Figure 5.2. (A) – Ball-and-stick representation of the energy-optimized solvent structures of the Ni^{II} complexes (NiL, NiL_2 and NiL_3, L = 2,2′-bipyridyl) discussed in this work. (B) – Molecular graphs of these complexes.

Table 5.1. Selected structural data of the Ni^{II} complexes with 2,2′-bipyridyl (L).[a]

Complex	Bond length (Å)		Bite angle (deg)		Torsion (deg)		Close contacts (Å)	
NiL	Ni–O2	2.117	N6-Ni-N7	80.05	N6-C16-C17-N7	–1.60	C**H15•••H19**C	2.098
	Ni–O3	2.128			**H15**-C14-C16-C17	–0.27	CH9•••O2	2.489
	Ni–O4	2.117			**H19**–C18–C17–C16	–0.27	CH25•••O4	2.489
	Ni–O5	2.127						
	average:	*2.122*						
	std dev:	*0.006*						
	Ni–N6	2.059						
	Ni–N7	2.059						
NiL_2	Ni–N2	2.092	N2-Ni-N3	78.85	N2-C14-C15-N3	–2.22	C**H17•••H19**C	2.075
	Ni–N3	2.090	N4-Ni-N5	78.87	**H17**-C16-C14-C15	–0.47	C**H33•••H37**C	2.075
	Ni–N4	2.092			**H19**-C18-C15-C14	0.24	CH43•••O6	2.426
	Ni–N5	2.089			N4-C34-C35-N5	–2.21	CH25•••O7	2.426
	average:	*2.091*			**H33**-C32-C34-C35	–0.46	CH27•••N3	2.691
	std dev:	*0.002*			**H37**-C36-C35-C34	0.24	CH9•••N5	2.689
	Ni–O6	2.174						
	Ni–O7	2.174						
NiL_3	Ni–N2	2.129	N2-Ni-N23	77.50	N2-C4-C22-N23	4.42	C**H15•••H27**C	2.064
	Ni–N23	2.128	N3-Ni-N24	77.53	**H6**-C5-C4-C22	0.39	C**H6•••H58**C	2.061
	Ni–N3	2.128	N34-Ni-N45	77.50	**H58**-C57-C22-C4	0.41	C**H37•••H50**C	2.063
	Ni–N24	2.128			N3-C13-C25-N24	4.80	CH33•••N2	2.624
	Ni–N34	2.129			**H15**-C14-C13-C25	0.49	CH61•••N3	2.632
	Ni–N45	2.128			**H27**-C26-C25-C13	0.50	CH53•••N23	2.632
	average:	*2.128*			N34-C35-C44-N45	4.76	CH43•••N24	2.629
	std dev:	*0.001*			**H37**-C36-C35-C44	0.38	CH12•••N34	2.627
					H50-C49-C44-C35	0.51	CH21•••N45	2.634

[a] H-atoms involved in steric clashes are printed in bold.

(typically, variation in BL(C–C) or BL(C–H) is on the fourth or fifth decimal place) except BL(C2–C3) which became longer, $\delta 5$ = 0.0023 Å. The distance between two pyridyl rings, BL(C2–C2′), remained almost unchanged ($\delta 4$ = 0.00087 Å) but the separation between the N-donor atoms increased, $\delta 3$ = 0.0165 Å. Unexpectedly, two distances which are located in the region of steric hindrance became significantly shorter, namely d(H3•••H3′) and d(C3•••C3′) for which $\delta 7$ = –0.036 Å and $\delta 6$ = –0.0209 Å, respectively. It is then puzzling why, since quite significant structural changes took place in L, the two pyridyl rings have not twisted

along the C2–C2′ bond to avoid the clash or the separation between pyridyl rings, BL(C2–C2′), has not increased significantly, e.g. by about 0.01 Å, as it was observed between phenyl fragments in biphenyl?[35]

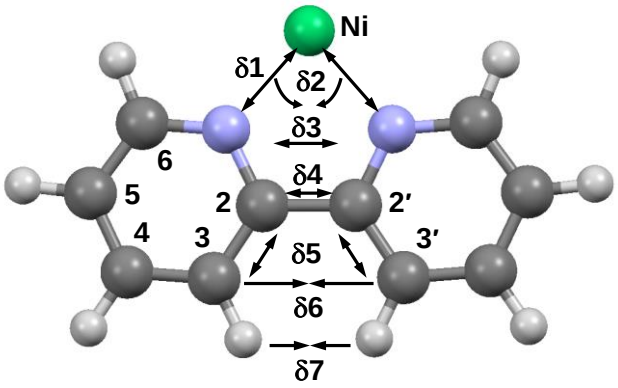

Figure 5.3. Schematic representation of structural changes observed in the ligand molecule involved in the complexes with Ni^{II}.

QTAIM-based Topological Analysis of the Coordination Bonds. It is generally accepted that the accumulation of electronic charge between a pair of nuclei is a necessary condition for atoms to be chemically bonded and from quantum chemistry it follows that this accumulation of charge is also a sufficient condition at which the forces acting on the nuclei are balanced when a molecule attains minimum energy equilibrium geometry. The QTAIM theory demonstrates that the presence of an atomic interaction line (AIL) in such equilibrium geometry satisfies both the necessary and sufficient conditions for identifying bonding interactions of any kind.[34] The line of maximum charge density linking two nuclei is called a bond path and the fundamental properties of bonding interactions can be obtained from the analysis of the topological properties of electron density at a bond critical point; a bond path and its bond critical point are inseparable in QTAIM when a bonding interaction takes place between two nuclei. Also, it has been reported that the QTAIM-defined bond path indicates the presence of a preferred quantum-mechanical exchange channel (a direct electron-exchange channel between atoms) and the inter-atomic exchange-correlation energy always stabilizes the local interaction.[45] For any assembly of atoms which are known to be a molecule, the network of bond paths linking pairs of neighbouring nuclei is generated by QTAIM, called a molecular graph, which isolates the dominating and characteristic for each molecule pairwise interactions, regardless if a molecule is at the thermodynamic equilibrium or not.[34] It is seen

in Figure 5.2 that the molecular graphs of the NiL, NiL_2, and NiL_3 reproduced all covalent and coordination bonds well as displayed by the bond paths with requisite bond critical points.

The nature and strength of bonding interactions between atoms are of central significance in chemistry hence, not surprising, the topological properties at bond critical points are often related to classical interpretation of chemical bonds. For a predominantly covalent interaction $\rho(r) > 0.1$ a.u. and $\nabla^2\rho(r) < 0$ at the BCP.[62] In the case of a "closed shell" (ionic) interaction $\rho(r)$ is usually small (e.g. for a classical H-bond $\rho(r)$ is ~10^{-2} a.u.[28]) whilst $\nabla^2\rho(r) > 0$. At the boundary between the two regions, i.e. at $\nabla^2\rho(r) \sim 0$, the binding is an admixture of these two effects. The sign and magnitude of the total energy density at a BCP, $H(r) = G(r) + V(r)$, has also been used to characterize the nature of the bonding.[63–64] For a covalent interaction, the local electron potential energy density $V(r)$ dominates and $H(r) < 0$, whereas for a predominantly ionic interaction, the local electron kinetic energy density $G(r)$ dominates and $H(r) > 0$.[65–67] Another useful description is the ratio $|V(r)|/G(r)$;[68–69] $|V(r)|/G(r) < 1$ is characteristic of an ionic interaction, $|V(r)|/G(r) > 2$ is diagnostic of a covalent interaction, and $1 < |V(r)|/G(r) < 2$ is indicative of interactions of intermediate character. It is seen in Table 5.2 that for the metal-ligand coordination bonds (Ni–N and Ni–OH_2) ρ_{BCP} is small (0.047 a.u. $< \rho(r) <$ 0.077 a.u.) and $\nabla^2\rho_{BCP} > 0$ (0.25 a.u. $< \nabla^2\rho(r) <$ 0.35 a.u.) indicating a "closed shell" character of the coordination bonds. However, since $H(r) < 0$ and near zero and $1< |V(r)|/G(r) < 1.1$, these coordination bonds can be seen as an admixture of predominantly ionic with some covalent character.

***Ni–N Coordination Bonds*:** Relationships between the Ni–N bond length (in the NiL, NiL_2 and NiL_3 complexes) and topological properties at BCPs are shown in Figure 5.4 and Figure E4, Appendix E. A decrease in ρ_{BCP}(Ni–N) and $\nabla^2\rho_{BCP}$(Ni–N), Figures 5.4(a-b), with an increase in BL(Ni–N) indicates that the strength of this bond decreases in the order NiL > NiL_2 > NiL_3.

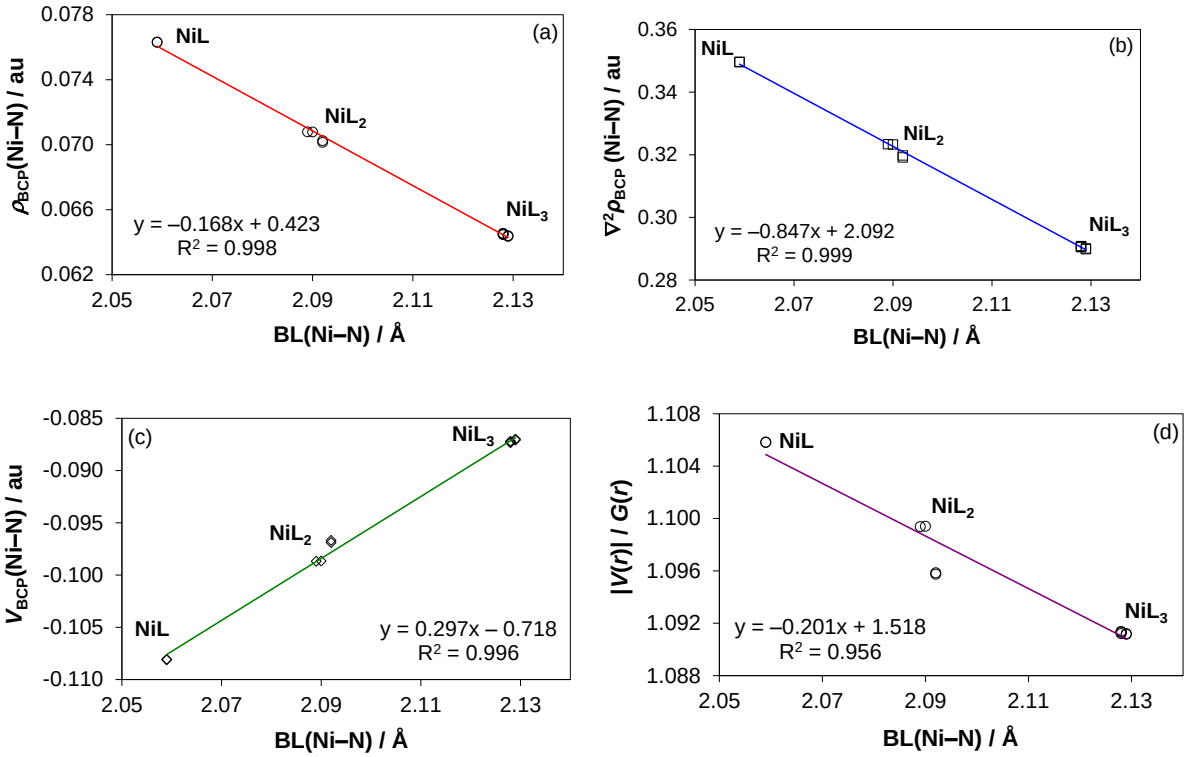

Figure 5.4. Relationships between BL(Ni–N) (in the NiL, NiL_2 and NiL_3 complexes) and the indicated topological properties at BCPs.

Also, the covalent component of this coordination bond decreases in the same order when more ligand molecules are coordinated because (i) V_{BCP}(Ni–N) and H_{BCP}(Ni–N) become less negative, Figure 5.4(c) and Figure C4(b), respectively, and (ii) the $|V(r)|/G(r)$ ratio decreases from 1.106 a.u. in NiL to 1.091 a.u. in NiL_3, Figure 5.4(d). The decrease in the intermediate character of the Ni–N coordination bond (it becomes more ionic) can easily be understood from and correlates very well with a significant increase in this bond length, from 2.059 in NiL to 2.128 Å in NiL_3. In general, the topological data at the BCPs of the Ni–N coordination bonds demonstrate all the characteristic properties and trends of a classical bonding interaction.

Ni–OH₂ Coordination Bonds: Water molecules act as an additional ligand completing the octahedral structures of the Ni^{II} complexes. The Ni–OH_2 bonds are longer when compared with BL(Ni–N), on average, by 0.06 and 0.08 Å in NiL and NiL_2, respectively. Also, a significant smaller electron density at BCPs is observed (on average, ρ_{BCP}(Ni–OH_2) is 0.053

and 0.047 a.u. whereas ρ_{BCP}(Ni–N) is 0.076 and 0.070 a.u. in NiL and NiL_2, respectively). The topological properties indicate that the Ni–OH_2 bonds contribute appreciably to the overall stability of the complexes, but they are weaker than the Ni–N bonds. This explains well the experimental observation that the ligand 2,2′-bipyridyl easily competes for Ni^{II} with water molecules, hence the Ni^{II} complexes with this ligand are formed spontaneously. Based on $|V(r)|/G(r)$, the Ni–OH_2 bonds show smaller degree of covalency when compared with stronger Ni–N bonds.

We also explored the topological properties at BCPs associated with the coordinated water molecules. It is seen in Figures E5(a-d) of Appendix E that the relationships between BL(Ni–OH_2) and ρ_{BCP}(Ni–OH_2), $\nabla^2\rho_{BCP}$(Ni–OH_2), V_{BCP}(Ni–OH_2), and G_{BCP}(Ni–OH_2) follow the same trends as found for the Ni–N coordination bond.

Validation of Computed Structures and Topological Data: The experimental complex formation constants carry, although indirectly, all the information about structural and topological properties of complexes formed in aqueous medium. Since the overall complex formation constants, as log β_n, are known[1] (log β_1 = 7.04, log β_2 = 13.86 and log β_3 = 20.16) we decided to examine whether the properties of the DFT-generated NiL, NiL_2 and NiL_3 structures correlate well with available experimental data. Regarding the topological properties, we found nearly perfect a linear relationship between the log β_n and ρ_{BCP}(Ni–N) values – Figure 5.5(a) – and it can be explained using the computed BL(Ni–N) values. The Ni–N bonds in NiL have the largest ρ_{BCP}(Ni–N) among all Ni–N bonds in the NiL_n complexes. On average, four longer Ni–N bonds in NiL_2 are weaker than two Ni–N bonds in NiL ($\rho_{BCP}(Ni–N)_{NiL} > \rho_{BCP}(Ni–N)_{NiL_2}$); hence log $\beta_2 < 2 \times$ log β_1 and, following the same reasoning, log $\beta_3 < 3 \times$ log β_1. Also the relationship between log β_n and $\nabla^2\rho_{BCP}$(Ni–N), Figure E6 of Appendix E,) follows the same trend. It was suggested recently[29] that a variation in the electron density at a ring critical point of a structural chelating ring might be linked with strength of a complex. Indeed, ρ_{RCP} *vs.* log β_n in Figure 5.5(b) and $\nabla^2\rho_{RCP}$ *vs.* log β_n in Figure E6 of Appendix E, confirm this suggestion and, at the same time, support the computed topological properties; similar trends exist for $V(r)$, $G(r)$ and $H(r)$ at the BCPs of the

Table 5.2. Topological data for the coordination bonds and chelating rings in the Ni^{II} complexes with 2,2′-bipyridyl (L)[a]

Complex	Bond						Ring		
	atoms	$\rho(r)$	$\nabla^2\rho(r)$	$V(r)$	$G(r)$	$H(r)$	$\lvert V(r)\rvert/G(r)$	Atoms	$\rho(r)$	$\nabla^2\rho(r)$
NiL	Ni–N6	0.07632	0.34968	–0.10811	0.09777	–0.01035	1.10584	Ni-N6-C16-C17-N7	0.02335	0.13704
	Ni–N7	0.07629	0.34953	–0.10806	0.09772	–0.01034	1.10581			
	average:	*0.07631*	*0.3496*	*–0.10809*	*0.09774*	*–0.01034*	*1.10582*			
	Ni–O2	0.05337	0.30595	–0.07614	0.07631	0.00017	0.99772			
	Ni–O3	0.0518	0.29397	–0.07276	0.07313	0.00036	0.99502			
	Ni–O4	0.05337	0.30593	–0.07614	0.07631	0.00017	0.99774			
	Ni–O5	0.05182	0.29411	–0.07280	0.07316	0.00037	0.995			
	average:	*0.05259*	*0.29999*	*–0.07446*	*0.07473*	*0.00027*	*0.99637*			
NiL_2	Ni–N2	0.07014	0.31913	–0.09668	0.08823	–0.00845	1.09574	Ni-N2-C14-C15-N3	0.02267	0.13069
	Ni–N3	0.07078	0.32327	–0.09866	0.08974	–0.00892	1.09941	Ni-N4-C34-C35-N5	0.02267	0.13072
	Ni–N4	0.07025	0.31975	–0.09689	0.08841	–0.00847	1.09585	*average:*	*0.02267*	*0.1307*
	Ni–N5	0.07079	0.32337	–0.09868	0.08976	–0.00892	1.09937			
	average:	*0.07049*	*0.32138*	*–0.09773*	*0.08904*	*–0.00869*	*1.09759*			
	Ni–O6	0.04662	0.25216	–0.06381	0.06343	–0.00039	1.00609			
	Ni–O7	0.04667	0.2525	–0.06389	0.06351	–0.00038	1.006			
	average:	*0.04664*	*0.25233*	*–0.06385*	*0.06347*	*–0.00038*	*1.00605*			
NiL_3	Ni–N2	0.0644	0.29008	–0.08707	0.0798	–0.00728	1.0912	Ni-N2-C4-C22-N23	0.02191	0.12382
	Ni–N23	0.06455	0.29084	–0.08733	0.08002	–0.00731	1.09137	Ni-N3-C13-C25-N24	0.0219	0.12372
	Ni–N3	0.0645	0.29059	–0.08725	0.07995	–0.00730	1.09132	Ni-N34-C35-C44-N45	0.0219	0.12375
	Ni–N24	0.06446	0.29048	–0.08720	0.07991	–0.00729	1.0912	*average:*	*0.0219*	*0.12376*
	Ni–N34	0.06436	0.28983	–0.08699	0.07972	–0.00727	1.09116			
	Ni–N45	0.06452	0.29072	–0.08729	0.07998	–0.00730	1.09133			
	average:	*0.06446*	*0.29042*	*–0.08719*	*0.0799*	*–0.00729*	*1.09126*			

[a] $\rho(r)$, $\nabla^2\rho(r)$, $V(r)$, $G(r)$, and $H(r)$ - all in atomic units.

Ni–N bonds. Also structural properties, such as distances between clashing H-atoms, d(CH•••HC), or N-atoms of the pyridyl rings, d(N•••N), as well as the lengths of the covalent C2–C3 and C2–C2′ bonds in 2,2′-bipyridyl correlate with log β values well – Figures 5.5(c-d).

We are of an opinion that all these relationships together with the trends found for the coordination Ni–N (Figures 5.4(a-d)) and Ni–OH_2 (Figures E4(a-d), Appendix E) bonds support the energy-optimized solvent structures of the NiL, NiL_2 and NiL_3 complexes and their topological data.

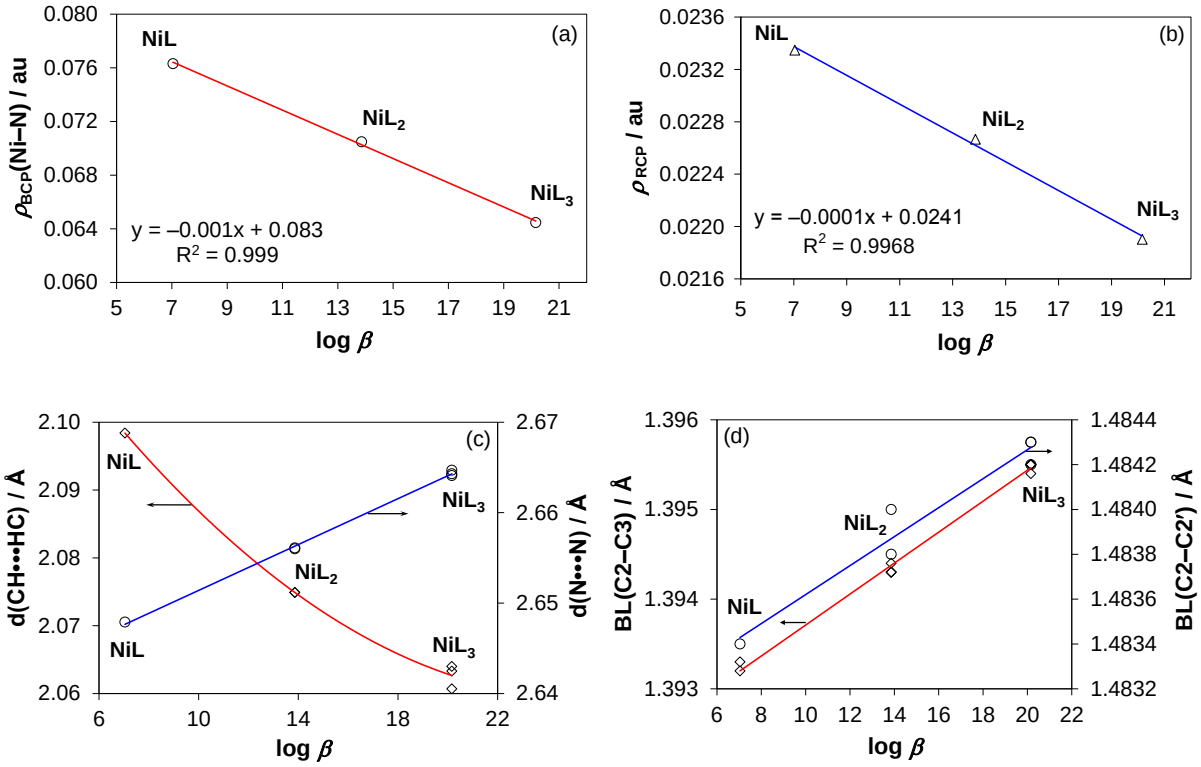

Figure 5.5. Strong correlations between experimental overall formation constants, as log β, of the NiL, NiL_2 and NiL_3 complexes (L = 2,2′-bipyridyl) and (a) - the electron density at the BCPs of the Ni–N coordination bonds, (b) - the electron density at the RCP of the structural chelating rings, (c) - distances between clashing H-atoms, d(CH•••HC), and N-atoms of 2,2′-bipyridyl, d(N•••N), (d) - BL(C2–C3) as well as BL(C2–C2′) of 2,2′-bipyridyl.

QTAIM-based Topological Analysis of Intramolecular Close Contacts. There are several intramolecular close contacts of different kind present in the Ni(II) complexes and to facilitate the discussion that follows we introduced the following terms: (i) structural bonds and structural chelating rings (we refer to those seen in the ball-and-stick representation of the

complexes in Figure 5.2) and (ii) non-structural bonds and non-structural either chelating or non-chelating rings which resulted from the intramolecular interactions characterized by the bond path with requisite BCP (they are seen on molecular graphs in Figure 5.2).

CH•••N Intramolecular Contacts: There are two CH•••N contacts in NiL_2 (CH27•••N3 and CH9•••N5) and six in NiL_3 (CH33•••N2, CH61•••N3, CH53•••N23, CH43•••N24, CH12•••N34, and CH21···N45). Since all these contacts have a bond path (Figure 5.2) we were able to analyse the trends in the topological properties at the BCPs by following the same approach as implemented for the Ni–N and Ni–OH_2 coordination bonds. Even though the values of ρ_{BCP}, $\nabla^2\rho_{BCP}$, V_{BCP}, and G_{BCP} of the CH•••N interactions are about an order of magnitude smaller when compared with those found for the coordination bonds (Table 5.2), the trends shown in Figures E7(a-d) of Appendix E are exactly the same as found for the Ni–N and Ni–OH_2 bonds. This is not entirely surprising because there is no controversy when the character of this kind of interaction, either intra- or intermolecular, is considered;[70–74] they are classified as a hydrogen bonding interaction, or a CH–N hydrogen bond which adds to the overall stability of a molecule.

The CH–N bonds appear to be stronger in the most crowded NiL_3 complex when measured by the larger electron density at BCPs (0.00745 and 0.00825 a.u. in NiL_2 and NiL_3, respectively) and the Laplacian at these BCPs (0.0256 and 0.0279 a.u. in NiL_2 and NiL_3, respectively) - Table 5.3. This correlates well with the bond lengths, $BL(CH–N)_{NiL_2} > BL(CH–N)_{NiL_3}$. The CH–N bonds show predominantly an ionic character: $G(r)$ dominates, the small and positive value of the total energy density H(r) is observed (0.0010 and 0.0011 a.u. for NiL_2 and NiL_3, respectively) and $|V(r)|/G(r) < 1$.

CH•••O Intramolecular Contacts: They involve the coordinated water molecules and are present in NiL and NiL_2. We could not fully analyse the trends in the topological properties of the CH•••O interactions because distances d(CH•••O), either in NiL or in NiL_2, are exactly the same and this would result in two-point relationships. However, since the trends in the topological properties appear to be very much the same as found for the both coordination and intramolecular CH–N hydrogen bonds, then without a doubt, all the above confirms the bonding nature of this interaction.[75–81] The intramolecular CH–O hydrogen bonds show here

a strong predominance of an ionic character with the ratio $|V(r)|/G(r) = 0.835$ (well below 1) and using the reported relationship,[82] $E_{Stab}(CH–O) = ½V_{BCP}(CH–O)$, we estimated the local energy stabilizing contributions made in NiL and NiL_2 as –1.97 and –2.19 kcal mol^{-1}, respectively.

CH•••HC Intramolecular Contacts: It is now well accepted that all the interactions discussed above, when identified in molecules, are of bonding nature. In other words, they contribute to the overall decrease of the total electronic energy of a molecule. We would like to point out that, regardless whether relatively strong coordination bonds (Ni–N and $Ni–OH_2$) or weak bonding interactions (intramolecular CH–N and CH–O hydrogen bonds) are considered, (i) they all are characterized by the presence of the QTAIM-defined a bond path with the requisite BCP and (ii) the trends in the fundamental properties at their BCPs are the same.

As one can see in Figure 5.2, there are QTAIM-defined bond paths with the BCPs between H-atoms involved in the CH•••HC contacts. From Figures 5.6(a-d) and Figure E8 it follows that with a decrease in the distance between the H-atoms involved (i) ρ_{BCP} and $\nabla^2\rho_{BCP}$ increase, (ii) V_{BCP} becomes more negative, (iii) G_{BCP} becomes more positive, and (iv) the ratio $|V(r)|/G(r)$ increases following the trends found above for all bonding interactions, including the coordination bonds. Let us consider the following observations: (i) the QTAIM-based analysis of, e.g. the ρ_{BCP} values, correctly predicted formation of much stronger Ni–N coordination bonds when compared with the $Ni–OH_2$ coordination bonds (otherwise the Ni^{II} complexes with L would not form), (ii) formation of intramolecular CH–O and CH–N hydrogen bonds was identified and verified, (iii) the H-atoms in the CH•••HC contacts are linked, as found for all bonding interactions, with a bond path, and (iv) the analysis of data shown in Table 5.3 shows $\rho_{BCP}(CH•••HC) \geq \rho_{BCP}(CH–O) >> \rho_{BCP}(CH–N)$ and $\nabla^2\rho_{BCP}(CH•••HC) > \nabla^2\rho_{BCP}(CH–O) >> \nabla^2\rho_{BCP}(CH–N)$.

So what is the difference between the CH•••HC and all other bonding interactions? Clearly, when using QTAIM-defined fundamental topological properties, there appears to be none. This leads us to the conclusion that the CH•••HC contacts not only should be seen as the QTAIM-defined H–H bonding interaction but it might be strongest among all intramolecular

interactions when ρ_{BCP} and $\nabla^2\rho_{BCP}$ are accounted for (i.e., in terms of electron concentration in the bonding region, which does not necessarily include inter-basin electrostatic effects). Moreover, its strength, hence also local energy stabilizing contribution to the overall stability of a complex, might increase when going from least crowded NiL to most crowded NiL_3 because ρ_{BCP}(CH•••HC) in NiL_3 is largest.

There is another argument one might consider in the support of the above. Formation of a complex with a polydentate ligand always results in coordination bonds and structural chelating rings. With an increase in strength of a complex, stronger coordination bonds and chelating rings are formed as measured by ρ_{BCP} and $\nabla^2\rho_{BCP}$ as well as ρ_{RCP} and $\nabla^2\rho_{RCP}$. From Table 5.3 it is seen that not only ρ_{BCP} and $\nabla^2\rho_{BCP}$ of the CH•••HC contacts are the largest but also rings formed by these contacts are characterized by the largest electron density among all non-structural rings, ρ_{RCP}(CH•••HC) >> ρ_{RCP}(CH–O) > ρ_{RCP}(CH–N) and similar trend is observed for the Laplacian at the RCPs.

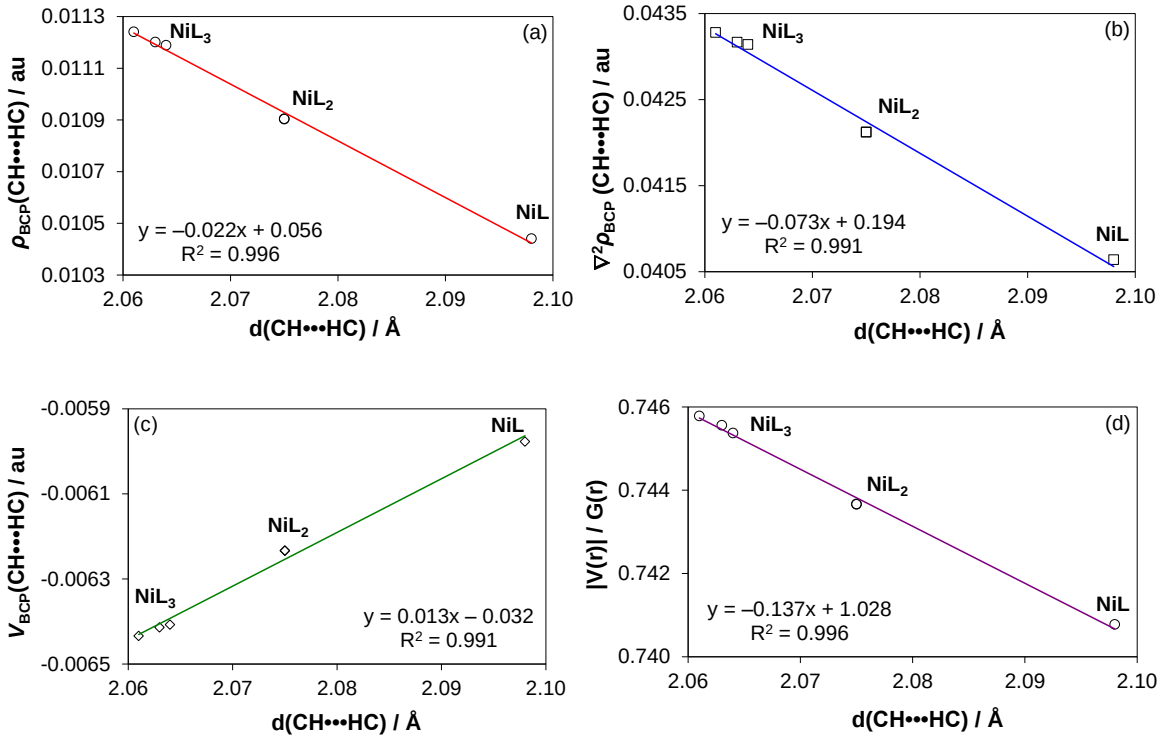

Figure 5.6. Relationships between d(CH•••HC) in NiL_n and indicated topological properties at BCPs.

Table 5.3. Topological data for the intramolecular interactions and non-structural rings in the NiL_n complexes with 2,2′-bipyridyl (L)[a]

Complex	Bond							Ring		
	Atoms	$\rho(r)$	$\nabla^2\rho(r)$	$V(r)$	$G(r)$	$H(r)$	$\lvert V(r)\rvert/G(r)$	Atoms	$\rho(r)$	$\nabla^2\rho(r)$
NiL	CH15–H19C	0.01044	0.04064	–0.00598	0.00807	0.00209	0.74078	C14-**H15-H19**-C18-C17-C16	0.01014	0.05036
	CH9–O2	0.00980	0.03506	–0.00627	0.00752	0.00124	0.83445	Ni-**O2-H9**-C8-N6	0.00820	0.03805
	CH25–O4	0.00980	0.03505	–0.00627	0.00752	0.00124	0.83442	Ni-**O4-H25**-C24-N7	0.00820	0.03804
NiL_2	CH17–H19C	0.01090	0.04212	–0.00623	0.00838	0.00215	0.74366	C14-C15-C18-**H19-H17**-C16	0.01049	0.05284
	CH33–H37C	0.01090	0.04212	–0.00623	0.00838	0.00215	0.74367	C32-**H33-H37**-C36-C35-C34	0.01049	0.05284
	CH43–O6	0.01088	0.03897	–0.00698	0.00836	0.00138	0.83467	Ni-N5-C42-**H43-O6**	0.00846	0.03949
	CH25–O7	0.01088	0.03896	–0.00698	0.00836	0.00138	0.83470	Ni-N3-C24-**H25-O7**	0.00846	0.03948
	CH27–N3	0.00744	0.02556	–0.00439	0.00539	0.00100	0.81438	Ni-**N3-H27**-C26-N4	0.00726	0.02875
	CH9–N5	0.00747	0.02563	–0.00440	0.00540	0.00100	0.81449	Ni-N2-C8-**H9-N5**	0.00728	0.02885
NiL_3	CH15–H27C	0.01119	0.04314	–0.00641	0.00860	0.00219	0.74537	C13-C14-**H15-H27**-C26-C25	0.01073	0.05418
	CH6–H58C	0.01124	0.04328	–0.00643	0.00863	0.00219	0.74578	C4-C5-**H6-H58**-C57-C22	0.01076	0.05445
	CH37–H50C	0.01120	0.04317	–0.00641	0.00860	0.00219	0.74556	C35-C36-**H37-H50**-C49-C44	0.01074	0.05423
	average:	*0.01121*	*0.04320*	*–0.00642*	*0.00861*	*0.00219*	*0.74557*	average:	*0.01074*	*0.05429*
	CH33–N2	0.00834	0.02817	–0.00484	0.00594	0.00110	0.81485	Ni-**N2-H33**-C32-N24	0.00774	0.03176
	CH61–N3	0.00822	0.02780	–0.00477	0.00586	0.00109	0.81440	Ni-**N3-H61**-C54-N23	0.00767	0.03138
	CH53–N23	0.00822	0.02781	–0.00478	0.00586	0.00109	0.81432	Ni-**N23-H53**-C46-N45	0.00767	0.03140
	CH43–N24	0.00827	0.02794	–0.00480	0.00589	0.00109	0.81465	Ni-**N24-H43**-C42-N34	0.00770	0.03154
	CH12–N34	0.00829	0.02803	–0.00482	0.00591	0.00110	0.81474	Ni-N2-C11-**H12-N34**	0.00771	0.03162
	CH21–N45	0.00818	0.02768	–0.00475	0.00584	0.00108	0.81429	Ni-N3-C20-**H21-N45**	0.00764	0.03126
	average:	*0.00825*	*0.02790*	*–0.00479*	*0.00588*	*0.00109*	*0.81454*	average:	*0.00769*	*0.03149*

[a] $\rho(r)$, $\nabla^2\rho(r)$, $V(r)$, $G(r)$, and H(r) - all in atomic units. Atoms involved in the interactions are printed in bold.

QTAIM-based Topological Analysis of the C2–C3 bonds. We explored the topological properties of the coordination and intramolecular bonding interactions above and it was of importance to compare the trends found with those obtained for typical covalent bonds in 2,2′-bipyridyl using the same theory and methodology. Our attention is now on the C2–C3 bond of the pyridyl rings because its length varied the most. As one can see in Figures 5.7(a-d) and Figures E9(a-b), all the topological properties clearly confirm the strong classical covalent character of this bond, because (i) ρ_{BCP} >> 0.1 a.u. (~0.31 a.u.), (ii) $\nabla^2\rho_{BCP}$ << 0 (~ –0.875 a.u.), (iii) the local potential energy density (~ –0.420 a.u.) dominates the local kinetic energy density significantly (~ 0.101 a.u.), (iv) the total energy density $H(r)$ << 0 (~ –0.32 a.u.) and (v) $|V(r)|/G(r)$ >> 2 (~ 4.163). Importantly, the trends between BL(C2–C3) and ρ_{BCP}(C2–C3), V_{BCP}(C2–C3) and G_{BCP}(C2–C3) are again the same as observed for both coordination and all intramolecular bonding interactions analysed above. Moreover, the opposite trends in $\nabla^2\rho_{BCP}$ and $|V(r)|/G(r)$ seen in Figure 5.7 correctly describe the variation in the covalent character where with a decrease in BL(C2–C3) the Laplacian becomes more negative

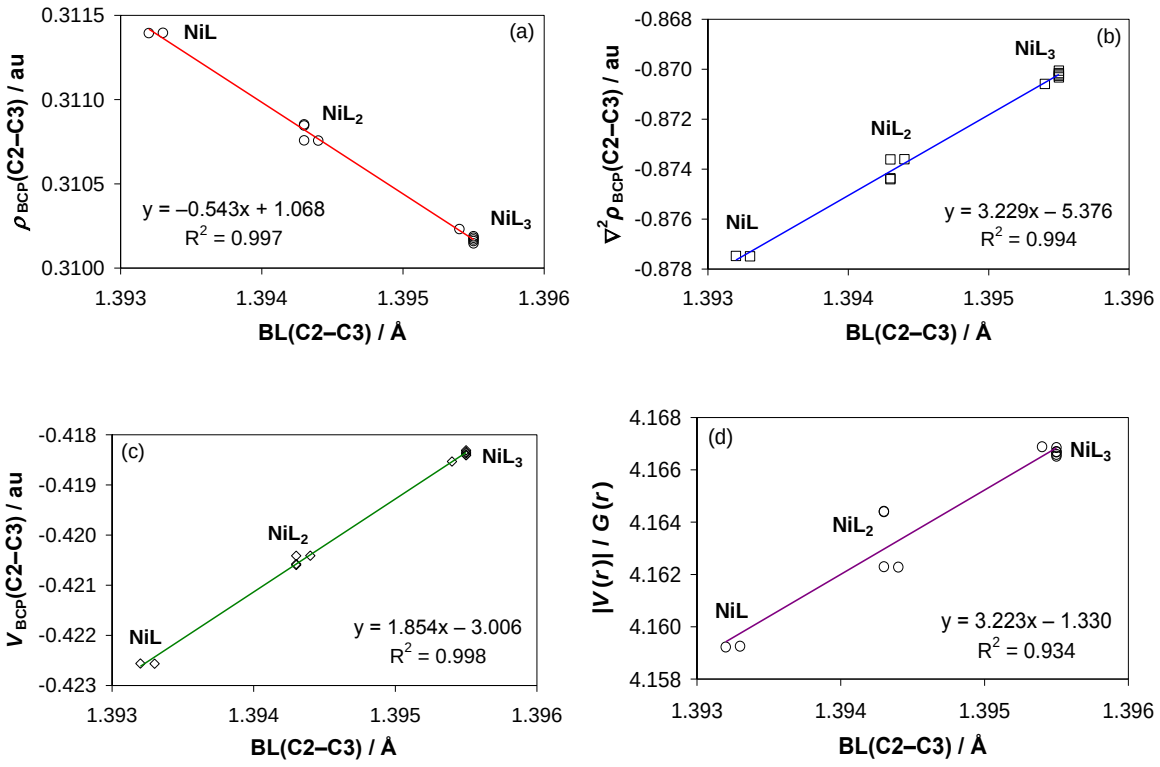

Figure 5.7. Relationships between BL(C2–C3) of 2,2′-bipyridyl in NiL_n and the indicated topological properties at the BCPs of this covalent bond.

and the $|V(r)|/G(r)$ ratio increases. Clearly, without a single failure, the topological analysis correctly predicted the presence of all inter-atomic interactions which are known to be of a bonding nature in these complexes.

It was also gratifying to note that good relationships exist between the log β_n values and the topological properties at the BCPs of the C2–C3 bonds in NiL_n – two examples are shown in Figure 5.8 – and they further support the computed topological properties of the DFT-generated structures.

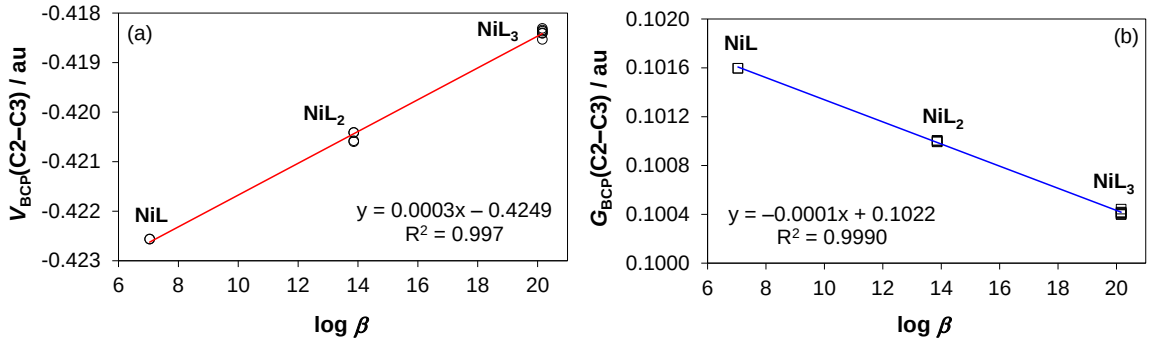

Figure 5.8. Strong correlations between experimental log β_n of NiL_n (L = 2,2′-bipyridyl) and the indicated topological properties at the BCPs of the C2–C3 covalent bond.

Conclusions

An extensive comparative analyses of the topological properties (the electron density $\rho(r)$, the Laplacian $\nabla^2\rho(r)$, the local electron potential energy density $V(r)$ and the local electron kinetic energy density $G(r)$ obtained from QTAIM of Bader) at the BCPs of (i) the coordination Ni–N and Ni–OH_2 bonds, (ii) the covalent C2–C3 bond in 2,2′-bipyridyl (L), and (iii) intramolecular interactions (CH•••N, CH•••O and CH•••HC) were conducted on the energy-minimized NiL, NiL_2 and NiL_3 complexes (at the UX3LYP/6-311++G(d,p) level of theory in water as a solvent, PCM/UFF) with our main focus being on the 3,3′-hydrogen atoms of 2,2′-bipyridyl.

To judge credibility of the DFT-generated structures of the NiL_n complexes, the experimental overall complex formation constants, as log β_n, of NiL, NiL_2 and NiL_3 were used. Numerous relationships between the log β_n values and either the topological

properties or structural data of (i) the coordination and covalent bonds, and (ii) all intramolecular interaction were analysed. In each case well-defined trends were found and since the topological data originated from the structures where all these interactions are present and only well-defined points in space (BCPs and RCPs) of the electron density distributions in NiL_n were selected to generate these trends, we consider the DFT-computed structures as reliable and representative.

The analysis of structural data revealed that, when going from least crowded NiL to most crowded NiL_3: (i) BL(Ni–N) increases, (ii) the bite angle N–Ni–N decreases, (iii) *all intramolecular contacts become shorter*, including CH•••HC, and (iv) the distance between N-atoms of 2,2′-bipyridyl increases, but surprisingly (v) d(C3•••C3′) of 2,2′-bipyridyl becomes shorter, (vi) the distance between the pyridyl rings remains virtually unchanged, (vii) the coordinated 2,2′-bipyridyl molecules stay near-planar with dihedral angles involving the 3,3′-hydrogen atoms of 2,2′-bipyridyl well below 1°, and (viii) the pyridyl rings do not twist along the C2–C2′ bond of 2,2′-bipyridyl to avoid the steric clash.

Regarding topological properties, whether coordination bonds or intramolecular interactions were analysed, all examined relationships followed the same trends and on decrease of the distance between atoms involved (i) ρ_{BCP} and $\nabla^2\rho_{BCP}$ increases, (ii) the local potential energy density V_{BCP} becomes more negative, (iii) the local kinetic energy density G_{BCP} becomes more positive, and (iv) the ratio $|V(r)|/G(r)$ increases, showing that all these interactions are predominantly of an ionic character, including the coordination bonds. Also, we have showed that the trends in $\rho(r)$, $V(r)$ and $G(r)$ of the coordination and intramolecular bonds follow those found for the covalent C2–C3 bond of 2,2′-bipyridyl. Strength of all intramolecular interactions, as measured by $\rho(r)$, increases according to $\rho_{BCP}(NiL) < \rho_{BCP}(NiL_2) < \rho_{BCP}(NiL_3)$ whereas opposite trend is observed for the coordination bonds which are weakest in NiL_3.

We have showed that the intramolecular CH•••HC contacts in NiL_3 are characterized by the topological properties which imitate those found in either classical coordination, covalent or intramolecular hydrogen bonds present in these complexes. From the comparative analyses of the topological properties we have concluded that the CH•••HC intramolecular interaction must also have a bonding component. We are of the opinion that the presence of the QTAIM-defined bonding interaction, such as H–H bonding interaction between H-atoms of the intramolecular CH•••HC close contact, does not

exclude a possibility of significant energy destabilizing contributions, such as the ΔE_{Pauli} term which accounts for the repulsive Pauli interaction between occupied orbitals on two fragments in the combined molecule. To gain a direct and full insight on the nature of *all intramolecular interactions* would require information on Pauli contribution and electrostatic terms which *act solely between the atoms involved in intramolecular close contacts*, but to the best of our knowledge this is not available yet.

References

[1] NIST Standard Reference Database 46. NIST Critically Selected Stability Constants of Metal Complexes Database; Version 8.0; R. M. Smith, A. E. Martell, Eds.; US Department of Commerce, National Institute of Standards and Technology: Gaithersburg, MD, 2004.

[2] S. T. Howard, *J. Am. Chem. Soc.* **1996**, *118*, 10269–10274.

[3] J. Kalenik, Z. Pawełka, *J. Mol. Liq.* **2005**, *121*, 63–68.

[4] F. Labat, P. P. Lainé, I. Ciofini, C. Adamo, *Chem. Phys. Lett.* **2006**, *417*, 445–451.

[5] C. Blanchet-Boiteux, P. Friant-Michel, A. Marsura, J-B. Regnouf-de-Vains, M. F. Ruiz-López, *J. Mol. Struct.* (THEOCHEM) **2007**, *811*, 169–174.

[6] V. Galasso, G. De Alti, A. Bigotto, *Tetrahedron* **1971**, *27*, 991–997.

[7] C. Jaime, J. Font, *J. Mol. Struct.* **1989**, *195*, 103–110.

[8] R. Benedix, P. Birner, F. Birnstock, H. Hening, H-J. Hofmann, *J. Mol. Struct*. **1979**, *51*, 99–105.

[9] R. Benedix, P. Birner, H-J. Hening, *J. Mol. Struct.* **1982**, *90*, 65–69.

[10] V. Barone, F. Lelj, L. Commisso, N. Russo, C. Caulletti, M. N. Piancastelli, *Chem. Phys.* **1985**, *96*, 435–445.

[11] S. Zahn, W. Reckien, B. Kirchner, H. Staats, J. Matthey, A. Lützen, *Chem. Eur. J.* **2009**, *15*, 2572–2580.

[12] I. Alkorta, J. Elguero, C. Roussel, *Comput. Theoret. Chem.* **2011**, *966*, 334–339.

[13] A. H. Göller, U-W. Grummt, *Chem. Phys. Lett.* **2000**, *321*, 399–405.

[14] A. H. Göller, U-W. Grummt, *Chem. Phys. Lett.* **2002**, *354*, 233–242.

[15] H. Irving, D. H. Mellor, *J. Chem. Soc*. **1962**, 5222–5237.

[16] R. A. Palmer, T. S. Piper, *Inorg. Chem.* **1966**, *5*, 864–878.

[17] K. Sone, S. Utsuno, T. Ogura, *J. Inorg. Nucl. Chem.* **1969**, *31*, 117–126

[18] R. Griesser, H. Sigel, *Inorg. Chem.* **1970**, *9*, 1238–1243.

[19] R. B. Martin, R. Prados, *J. Inorg. Nucl. Chem*. **1974**, *36*, 1665–1670.

[20] R. D. Hancock, A. E. Martell, *Chem. Rev.* **1989**, *89*, 1875–1914.

[21] D. Buist, N. J. Williams, J. H. Reibenspies, R. D. Hancock, *Inorg. Chem.* **2010**, *49*, 5033–5039.

[22] G. M. Cockrell, G. Zhang, D. G. VanDerveer, R. P. Thummel, R. D. Hancock, *J. Am. Chem. Soc*. **2008**, *130*, 1420–1430.

[23] S. Del Piero, P. Di Bernardo, R. Fedele, A. Melchior, P. Polese, M. Tolazzi, *Eur. J. Inorg. Chem.* **2006**, 3738–3745.

[24] E. A. Zhurova, C. F. Matta, N. Wu, V. V. Zhurov, A. A. Pinkerton, *J. Am. Chem. Soc.* **2006**, *128*, 8849–8861.

[25] C. F. Matta, J. Hernández-Trujillo, T. H. Tang, R. F. W. Bader, *Chem. Eur. J.* **2003**, *9*, 1940–1951.

[26] R. F. W. Bader, *J. Phys. Chem. A* **2009**, *113*, 10391–10396.

[27] A. M. Pendás, E. Francisco, M. A. Blanco, C. Gatti, *Chem. Eur. J.* **2007**, *13*, 9362–9371.

[28] F. Cortés-Guzmán, J. Hernández-Trujillo, G. Cuevas, *J. Phys. Chem. A* **2003**, *107*, 9253–9256.

[29] I. Cukrowski, K. K. Govender, *Inorg. Chem.* **2010**, *49*, 6931–6941.

[30] I. Cukrowski, C. F. Matta, *Chem. Phys Lett.* **2010**, *499*, 66–69.

[31] K. N. Robertson, O. Knop, T. S. Cameron, *Can. J. Chem.* **2003**, *81*, 727–743.

[32] K. N. Robertson, *in Intermolecular Interactions in a Series of Organoammonium Tetraphenyl-borates*; Ph.D. Thesis, Dalhousie University, Halifax, Canada, **2001.**

[33] E. A. Zhurova, V. G. Tsirelson, V. V Zhurov, A. I. Stash, A. A. Pinkerton, *Acta Cryst. B* **2006**, *62*, 513–520.

[34] R. F. W. Bader, *in Atoms in Molecules: A Quantum Theory*; Oxford University Press: Oxford, U.K. 1990.

[35] J. Poater, M. Solà, F. M. Bickelhaupt, *Chem. Eur. J.* **2006**, *12*, 2889–2895.

[36] J. Poater, M. Solà, F. M. Bickelhaupt, *Chem. Eur. J.* **2006**, *12*, 2902–2905.

[37] R. F. W. Bader, *Chem. Eur. J.* **2006**, *12*, 2896-2901.

[38] J. Hernández-Trujillo, C. F. Matta, *Struct. Chem.* **2007**, *18*, 849–857.

[39] T. Ziegler, A. Rauk, *Inorg. Chem.* **1979**, *18*, 1755–1759.

[40] T. Ziegler, A. Rauk, *Inorg. Chem.* **1979**, *18*, 1558–1565.

[41] T. Ziegler, A. Rauk, *Theor. Chim. Acta* **1977**, *46*, 1-10.

[42] M. Mitoraj, A. Michalak, *J. Mol. Model*. **2007**, *13*, 347–355.

[43] M. Mitoraj, A. Michalak, T. Ziegler, *J. Chem. Theory Comput.* **2009**, *5*, 962-975.

[44] I. Cukrowski, K. K. Govender, M. P. Mitoraj, M. Srebro, *J. Phys. Chem. A* **2011**, *115*, 12746–12757.

[45] A. M. Pendás, E. Francisco, M. A. Blanco, C. Gatti, *Chem. Eur. J.* **2007**, *13*, 9362–9371.

[46] Gaussian 09, Revision B. 01, M. J. Frisch, G. W. Trucks, H. B. Schlegel, G. E. Scuseria, M. A. Robb, J. R. Cheeseman, G. Scalmani, V. Barone, B. Mennucci, G. A. Petersson, H. Nakatsuji, M. Caricato, X. Li, H. P. Hratchian, A. F. Izmaylov, J. Bloino, G. Zheng, J. L. Sonnenberg, M. Hada, M. Ehara, K. Toyota, R. Fukuda, J.

Hasegawa, M. Ishida, T. Nakajima, Y. Honda, O. Kitao, H. Nakai, T. Vreven, J. A. Montgomery, Jr., J. E. Peralta, F. Ogliaro, M. Bearpark, J. J. Heyd, E. Brothers, K. N. Kudin, V. N. Staroverov, R. Kobayashi, J. Normand, K. Raghavachari, A. Rendell, J. C. Burant, S. S. Iyengar, J. Tomasi, M. Cossi, N. Rega, J. M. Millam, M. Klene, J. E. Knox, J. B. Cross, V. Bakken, C. Adamo, J. Jaramillo, R. Gomperts, R. E. Stratmann, O. Yazyev, A. J. Austin, R. Cammi, C. Pomelli, J. W. Ochterski, R. L. Martin, K. Morokuma, V. G. Zakrzewski, G. A. Voth, P. Salvador, J. J. Dannenberg, S. Dapprich, A. D. Daniels, Ö. Farkas, J. B. Foresman, J. V. Ortiz, J. Cioslowski, D. J. Fox, Gaussian, Inc., Wallingford CT, **2010**.

[47] GaussView, Version 5.09b, R. Dennington, T. Keith, J. Millam, *Semichem Inc.*; Shawnee Mission, KS, **2009**.

[48] X. Xu, W. A. Goddard, *Proc. Natl. Acad. Sci. U.S.A.* **2004**, *101*, 2673–2677.

[49] X. Xu, W. A. Goddard, *J. Phys. Chem. A* **2004**, *108*, 2305–2313.

[50] X. Xu, Q. Zhang, R. P. Muller, W. A. Goddard, *J. Chem. Phys.* **2005**, *122*, 014105.

[51] C. Lee, W. Yang, R. G. Parr, *Phys. Rev.* B **1988**, *37*, 785–789.

[52] N. Díaz, D. Suárez, K. M. Merz, *Chem. Phys. Lett.* **2000**, *326*, 288–292.

[53] T. van Mourik, R. J. Gdanitz, *J. Chem. Phys.* **2002**, *116*, 9620–9623.

[54] M. O. Sinnokrot, C. D. Sherrill, *J. Phys Chem.* A **2006**, *110*, 10656–10668.

[55] J. P. Perdew, K. Burke, M. Ernzerhof, *Phys. Rev. Lett.* **1996**, *77*, 3865–3868.

[56] I. Hyla-Kryspin, G. Haufe, S. Grimme, *Chem. Eur. J.* **2004**, *10*, 3411–3422.

[57] B. Hammer, L. B. Hansen, J. K. Nørskov, *Phys. Rev.* B **1999**, *59*, 7413–7421.

[58] Y. Zhang, W. Yang, *Phys. Rev. Lett.* **1998**, *80*, 890–890.

[59] S. N. Maximoff, J. E. Peralta, V. Barone, G. E. Scuseria, *J. Chem. Theory Comput.* **2005**, *1*, 541–545.

[60] AIMAll (Version 11.04.03), Todd A. Keith, **2011** (http://aim.tkgristmill.com).

[61] R. D. Hancock, *Acc. Chem. Res.* **1990**, *23*, 253-257.

[62] R. F. W. Bader, H. Essén, *J. Chem. Phys.* **1984**, *80*, 1943–1960.

[63] D. Cramer, E. Kraka, *Angew. Chem. Int. Ed. Engl.* **1984**, *23*, 627–628.

[64] D. Cramer, E. Kraka, *Croat. Chem.* Acta **1984**, *57*, 1259–1281.

[65] R. G. A. Bone, R. F. W. Bader, *J. Phys. Chem.* **1996**, *100*, 10892–10911.

[66] M. F. Bobrov, G. V. Popova, V. G. Tsirelson, *Russ. J. Phys. Chem.* **2006**, *80*, 584-590.

[67] P. Macchi, A. Sironi, *Coord. Chem. Rev.* **2003**, *238-239*, 383-412.

[68] E. Espinosa, I. Alkorta, J. Elguero, E. Molins, *J. Chem. Phys.* **2002**, *117*, 5529-5542.

[69] S. Jenkins, I. Morrison, *Chem. Phys. Lett.* **2000**, *317*, 97-102.

[70] M. Kubicki, T. Borowiak, G. Dutkiewicz, M. Souhassou, C. Jelsch, C. Lecomte, *J. Phys. Chem. B* **2002,** *106*, 3706–3714.

[71] S. Wojtulewski, S. J. Grabowski, *Chem. Phys. Lett.* **2003**, *378*, 388–394.

[72] S. Wojtulewski, S. J. Grabowski, *Chem. Phys.* **2005**, *309*, 183–188.

[73] M. Domagała, S. J. Grabowski, *J. Phys. Chem. A* **2005**, *109*, 5683–5688.

[74] P. R. Mallinson, G. T. Smith, C. C. Wilson, E. Grech, K. Wozniak, *J. Am. Chem. Soc.* **2003**, *125*, 4259-4270.

[75] U. Koch, P. L. A. Popelier, *J. Phys. Chem.* **1995**, *99*, 9747–9754.

[76] S. J. Grabowski, *J. Mol. Struct.* **2001**, *562*, 137–143.

[77] Y. P. Yurenko, R. O. Zhurakivsky, S. P. Samijlenko, M. Ghomi, D. M. Hovorun, *Chem. Phys. Lett.* **2007**, *447*, 140–146.

[78] Y. P. Yurenko, R. O. Zhurakivsky, M. Ghomi, S. P. Samijlenko, D. M. Hovorun, *J. Phys. Chem. B* **2007**, *111*, 6263-6271.

[79] P. Munshi, T. N. Guru Row, *J. Phys. Chem. A* **2005**, *109*, 659-672.

[80] O. V. Shishkin, G. V. Palamarchuk, L. Gorb, J. Leszczynski, *J. Phys. Chem. B* **2006**, *110*, 4413–4422.

[81] R. Parthasarathi, S. S. Raman, V. Subramanian, T. Ramasami, *J. Phys. Chem. A* **2007**, *111*, 7141-7148.

[82] E. Espinosa, E. Molins, C. Lecomte, *Chem. Phys. Lett.* **1998**, *285*, 170–173.

Chapter 6

Conclusions

This work has studied theoretically the intramolecular interactions present in 2,2′-Bipyridine (BPy) and aqueous complexes of BPy with Zn^{II} and Ni^{II}, with specific focus on the nature of the interaction between supposedly clashing hydrogen atoms in the 3,3′-positions of BPy. The study was conducted using four different theoretical tools and methods - the Quantum Theory of Atoms in Molecules (QTAIM), the Interacting Quantum Atoms (IQA) energy decomposition scheme, the Non-Covalent Interactions (NCI) method and the Extended Transition State coupled with Natural Orbitals for Chemical Valence (ETS-NOCV) energy decomposition scheme.

It was found that the CH•••HC interaction in BPy can be labelled as a bonding interaction as opposed to a steric clash, based on the following conclusions: i) an atomic interaction line - a bridge of maximal density and density concentration - is present in all classical bonds as well as the CH•••HC interaction, ii) charge density is accumulated within the H-atoms as the CH•••HC interaction forms, iii) the IQA-defined interaction energy between 3,3′-H-atoms is always attractive, iv) NCI shows a region of density concentration in the bonding region of these atoms, v) ETS-NOCV revealed accumulation of density in the bonding region of the CH•••HC interaction in a stabilizing fashion, vi) the net Pauli-NOCV deformation density revealed that orbital mixing accumulates more density in the bonding region than enforcing the Pauli Exclusion Principle removes, vii) the CH•••HC interaction shows the exact same geometrical and topological trends as a function of the interaction distance as all other classical (known) bonds, including M–L coordination bonds, covalent bonds and hydrogen bonds and viii) the CH•••HC interaction shows no similarities to an accepted and truly repulsive interaction (i.e. the N--N lone-pair-lone-pair repulsion present in all forms of *s*-cis BPy). We also made some important observations regarding the *nature* and electronic mechanisms of the CH•••HC interaction: i) the interaction is privileged - electrons in the interacting H atoms will rather delocalize within the other H atomic basin than among other atoms in the ring, ii) the interaction is unstrained electrostatically, iii) the interaction is quantum mechanical in origin, iv) the interaction is a typical closed-shell interaction and shows the same trends as other closed-shell interactions and v) the nature of the interaction is identical in the free ligand as it is in complexes. Finally, some observations regarding preliminary results based on atomic energy analysis (IQA and QTAIM-defined) can be made regarding the local or molecular stabilization/destabilization incurred by formation of the CH•••HC interaction: i) the interaction is locally stabilizing, by stabilizing C and H atoms involved and ii) the

interaction (together with the very repulsive N--N interaction) destabilizes C2–C3 and C2–C2′ bonds in *s*-cis conformer when it is not involved in a complex. The extent of C–C destabilization due to CH•••HC is unknown, and it is possible that only the N--N interaction is responsible for the C–C destabilization.

We also studied other intramolecular interactions - the N--N and CH•••N interactions in free BPy, and CH–O and CH–N hydrogen bonds in ZnL_n and NiL_n complexes with BPy. It was found that the N--N interaction is highly repulsive, and from preliminary atomic energy analysis in NiL_n complexes, accounts for all of the strain during the preorganization of BPy from *s*-trans to the form necessary for complexation. The nature of the strain in N--N is both electrostatic (very large repulsive electrostatic interaction energies were observed) and electronic (depletion of electron density in the inter-nuclear region was observed). The CH•••N interaction in the *s*-trans form of BPy was found to be a truly electrostatic interaction - although a quantum mechanical component is seen (resulting in electron concentration in the bonding region), it was concluded that this exchange is marginal and can be seen as similar to the exchange of non-interacting atoms based on studies of the exchange of neighbouring and competing interactions, as well as the concentration and depletion of critical points within the interaction. No atomic interaction line is seen for the CH•••N interaction, but electrostatic charge deformations (including an accumulation of electrons on the N atom and a withdrawal of electrons on the H atom, as well as NOCVs reflecting electrostatic behaviour) were observed. Finally, CH–N and CH–O bonds in ZnL_n and NiL_n complexes were shown to be of an ionic nature, as expected. These bonds show atomic interaction lines as well as very significant electron-flow channels from ETS-NOCV analysis. In comparison, no atomic interaction lines are seen for the CH•••N interactions in free BPy.

Finally, a few novel contributions were made to the field of theoretical chemistry. In Chapter 3, we introduced for the first time (to our knowledge) the net Pauli-Orbital and Pauli-NOCV deformation densities, as a qualitative measure of the dominant charge-transfer effect in the ETS-scheme. Specifically, this method showed that the Pauli deformation (resulting from enforcing the Pauli Exclusion Principle *via* orthogonalization of fragment promolecular orbitals) is dominant in electronically strained interactions, such as the N--N interaction, but recessive to orbital mixing in bonding interactions such as a covalent C–C bond or the CH•••HC interaction. We also introduced the Privileged Exchange Index (PEI) - an NCI-based diagnostic, which predicts the presence of a bond

path perfectly. Interpretation of the PEI in conjunction with the interpretation of bond paths as privileged exchange channels[1] allowed us to improve on the current interpretation of a bond path, in that we suggest a bond path signal a non-marginal covalent component of any interaction, independent of the electrostatic or overall interaction energies. In Chapter 4, we introduced the Energy Interaction Ratio (EIR), a single number which can classify interactions based on their repulsive/attractive natures as well as whether the interaction is electrostatic, intermediate or quantum-mechanical in origin. We also suggest the use of 1D maps of the electron density along a specific vector intersecting the interaction between atoms. This method, which we implemented new code for, might prove useful in the understanding of 3D topological properties, the appearance of atomic interaction lines and NCI-defined regions. Finally, this work represents the first collaboration of QTIAM, IQA, NCI and ETS-NOCV, and the coherent picture that these methods produces are truly remarkable.

Comparison with biphenyl.

The question on the nature of CH•••HC interactions generated a large body of work throughout the previous decade. Most of the previous studies were focussed on biphenyl or similar molecules, but the chemical environment of H-atoms in bipyridyl is to some extent similar to those in biphenyl. Therefore, it is interesting to compare the results presented in this work with the results of previous studies on biphenyl. Although no direct comparison of geometrical, atomic or topological property changes is possible, some qualitative similarities can be observed.

Both biphenyl and bipyridyl exhibit a local maximum in the potential energy surface for the conformer with a close contact between the H-atoms in the 3,3′ positions, and a local minimum at $\phi(1) = 46.8°$ for biphenyl (RHF/6-311++G(d,p)/gas)[6] and $\phi(1) = 37°$ for bipyridyl (RHF/6-311++G(d,p)/PCM-UFF, Section 3.1). An atomic interaction line is observed for both molecules for $\Phi(1) = 0°$. Matta *et al*[6] did an atom-by-atom comparison of QTAIM-defined atomic energies in biphenyl (RHF/6-311++G(d,p)/gas) and showed that the only two atoms which are significantly destabilized (by +22 kcal mol^{-1} each) in $\Phi(1) = 0°$ compared to $\Phi(1) = 46.8°$ are the junction carbons forming the C–C bond between the two phenyl rings. The atoms which are significantly stabilized (by –8.2 kcal mol^{-1} each) in biphenyl are the H-atoms involved in the CH•••HC interaction. We observed similar destabilizations (+15.01 kcal mol^{-1} each) for the C11 and C12 atoms and

stabilizations (–5.16 kcal mol^{-1} each) for H13 and H20 in bipyridyl (Figures A3 and A1, Appendix A). Interestingly, we also observed stabilizations for C3 and C10 - the carbon atoms involved in the CH•••HC interaction - of –1.19 kcal mol^{-1} each, in comparison with a destabilization of +0.5 kcal mol^{-1} for similar atoms in biphenyl. However, we also reported a *stabilization* of N-atoms in *s*-cis, showing the importance of other effects (such as conjugation, solvent, and intramolecular interactions) affecting the system.

Matta *et al*[6] also showed the stabilizing effects of the formation of a zero-flux surface, and calculated the contribution to the CH•••HC to be V_s(H|H) = –20.6 kcal mol^{-1}, compared to V_s(H|H) = –22.76 kcal mol^{-1} in bipyridyl (Figure A4, Appendix A; values converted from au to kcal mol^{-1}). Interestingly, Matta *et al* reported a destabilization of the interatomic surface for the C–H bond of about V_s(C|H) = +1.25 kcal mol^{-1} per C–H bond, compared to a stabilization seen for BPy, V_s(C|H) = –6.72 kcal mol^{-1}.

Finally, the topological properties for the CH•••HC interaction (measured at the BCP of the AIL) are very similar for both systems. ρ_{BCP}(CH•••HC) = 0.0103 au in biphenyl and 0.0123 au in BPy; $\nabla^2\rho_{BCP}$(CH•••HC) = 0.056 au in biphenyl and 0.050 au in BPy; V_{BCP}(CH•••HC) = –0.009 au in biphenyl and –0.008 au in BPy.

Therefore, qualitatively and from a QTAIM viewpoint, the CH•••HC in BPy is very similar to the CH•••HC in biphenyl. However, the *primary* arguments of Matta *et al* are based on the atomic stabilization in terms of QTAIM-defined atomic energies, and the existence (as well as interpretation and meaning) of an atomic interaction line. The inconsistencies between QTAIM- and IQA-defined atomic energies are very apparent from the results in Appendix A, and the interpretation and physical meaning of an atomic interaction line is far from clear. However, the results from this work have shed some additional light on the CH•••HC interaction in BPy, which is *possibly* applicable to the interactions in biphenyl as well.

Future Studies.

Whilst this study investigated the properties and charge distributions of the interactions *between* atoms, the effect of these interactions on the atoms themselves might be profoundly different in nature. Specifically, the formation of an attractive interaction usually results in a destabilization of the internal energy of the atoms involved as the atoms will experience increased pressure - as a result of the decrease of atomic volume that

interacting atoms must undergo, and as a result of increased electronic delocalization (which leads to increased density in each atom). However, it has never been shown (according to our knowledge) whether the presence of an attractive interaction can lead to an even greater atomic destabilization.

The remaining term of the IQA decomposition scheme, E_{Self}^{IQA}, can be used to study the changes in the internal energy of atoms. To discover the change in E_{Self}^{IQA} related to the formation of an intramolecular interaction is a non-trivial task, as a suitable and chemically identical reference state or atom is needed. The formation of an interatomic interaction is then stabilizing the atoms or fragments involved if the change in E_{Self}^{IQA} is smaller than the absolute interaction energy. Changes in E_{Self}^{IQA} have also been linked to the Pauli repulsion term in EDA-based schemes, ΔE_{Pauli}. Our results, based on the net deformation density (Chapter 3), suggest that only the N--N interaction in BPy is possibly locally destabilizing, whereas the CH•••HC and CH•••N interactions are locally stabilizing. However, further investigation is needed to relate the net deformation densities to binding energies.

If an interaction is locally stabilizing to the atoms and fragments involved, it is still possible that the interaction is the cause of a *molecular* destabilization. In other words, the strain caused by the interaction is localized elsewhere in the molecule - either because of geometric strain or electron transfer related to the formation of the interaction. Applying the techniques used in this paper we can study the changes in other interactions - such as the C2–C2′ junction bond in BPy - and evaluate the possibility of non-localized strain as a result of the formation of intramolecular interactions. While such studies will not change the nature of the interactions of interest, it will help to understand the potential energy surface and various geometric observations described in Chapter 3.

Our conclusions also naturally predict the possibility of a repulsive interaction that show no electronic strain - just as the CH•••N interaction in free BPy is attractive because of electrostatics but essentially non-bonding quantum mechanically, so is there the possibility of a privileged but repulsive interaction. We have recently discovered such interactions in the protonated forms of BPy - CH--$^{+}$HN and NH^{+}--$^{+}$HN interactions which show repulsive interaction energies but in the presence of AILs. These interactions will contribute to the classification of the CH•••HC interaction as a bonding interaction as well as show the full spectrum and interpretation of an AIL.

Our calculations neglected electron correlation completely (HF calculations, including all IQA calculations) and otherwise treated electron correlation only approximately (all DFT calculations). While it has been shown before[1] that all of the methods used give reasonable results at lower (HF and DFT) levels, and the qualitative results will not change significantly, it might still be informative to study the effects of correlation on the interactions in BPy. In addition, Van der Waal forces (specifically dispersive effects) have usually been used to explain weak bonding observed for homopolar interactions. While very recent studies[2] seem to suggest that CH•••HC interactions in most alkane dimers are in fact not driven by dispersion, it is still necessary to consider whether the CH•••HC, CH•••N, CH–O and CH–N interactions will change significantly if dispersion effects are added.

In terms of developments in the field of theoretical chemistry, this study identifies a few areas of future research. Firstly, the ETS-NOCV method is not well defined for molecules with fragments with unpaired electrons, such as the Ni(BPy) system. Studying and developing appropriate protocol for applying ETS-NOCV on such systems will expand the method's usefulness. In addition, the NOCV method for partitioning ΔE_{Orb} has greatly extended the ETS scheme. However, the same has not yet been developed for partitioning the other terms of ETS - ΔE_{Pauli} and ΔE_{Elstat}. Paritioning of ΔE_{Pauli} will be very useful in particular, as it can greatly aid interpretation of all the interactions. The indicators suggested in this work - PEI and EIR - should be tested on many more interactions and systems to prove their validity and possible applications. Lastly, Appendix A suggested a great discrepancy in QTAIM-defined and IQA-defined atomic energies. Further research in this field is critically needed, as atomic energy analysis can provide a lot of insight into any chemical problem.

Finally, the question of the chemical bond and its relation to bonding interactions and its definition in terms of intramolecular bonding should be addressed. The concept of a chemical bond is philosophical in nature, and it is the field of conceptual and fundamental chemistry that this question should be asked. However, every theorem, interpretation and experimental observation leads to increased understanding of the chemical bond, and it is therefore of critical importance that we keep applying the scientific method to the question of chemical bonding. This statement is made with regards to the central theme of this study - the CH•••HC interaction - as the debate surrounding the controversial nature of this

interaction seems to be inciting increasingly unscientific and subjective comments from some of the correspondents involved, including appeals to tradition and appeals to utility[3], bad physics and bad grammar[4,5]. Rather, the debate regarding the CH•••HC interaction - regardless of the eventual conclusion - should serve as a scientific focal point for the most important question in the study of chemistry - "What is the chemical bond?".

References

[1] A. M. Pendás, E. Francisco, M. A. Blanco, C. Gatti, *Chem. Eur. J.* **2007**, *13*, 9362–9371

[2] D. Danovich, S. Shaik, F. Neese, J. Echeverría, G. Aullón, S. Alvarez, *J. Chem. Theory Comp.*, **2013**, *9*, 1977–1991

[3] R. D. Hancock, I. V. Nikolayenko, *J. Phys. Chem. A* **2012**, *116*, 8572−8583

[4] S. Grimme, C. Mück-Lichtenfield, G. Erker, G. Kehr, H. Wang, H. Beckers, H. Willner, *Angew. Chem. Int. Ed.*, **2009**, *48*, 2592–2595

[5] R. F. W. Bader, *J. Phys. Chem. A.*, **2009**, *113*, 10391–10396

[6] J. Hernández-Trujillo, C. F. Matta, *Struct. Chem.*, **2007**, *18*, 849–857

Appendix A

Preliminary atomic energy results for 2,2′-Bipyridyl

The results and discussions of Chapter 3 are mainly focussed on the static interaction between two atoms. However, the induced effects resulting from the formation of the interaction on the atoms and fragments involved, as well as the molecule as a whole, are still unexplored. Studies of this kind usually need a perfect reference frame - one which is identical to the molecule of interest but without the presence of the intramolecular bond being studied. Such a state is usually not available, and therefore interpretation carries a necessary degree of ambiguity. Nevertheless, in this appendix we will briefly present preliminary studies towards understanding the local (atomic) and global (molecular) effects caused by the formation of intramolecular interactions in BPy.

First, we will consider a virial-based atomic energy approach from QTAIM; then, we will consider the atomic energies as defined by IQA, as well as look at the changes in interaction energies throughout the rest of the molecule.

QTAIM Atomic Energies. Figure A1 shows the hydrogen atomic energy changes relative to the perpendicular conformer ($\Phi(1) = 90°$). Clearly, **H13** (and **H20**) are the only hydrogen atoms that changes significantly in energy. We therefore assume that the effects of conjugation (which partially leads to the rotation barrier at $\Phi = 90°$[1–3]) plays an insignificant role in the atomic energies of hydrogens, and that the changes in E(**H13**) is the result of the formation of the CH•••N and CH•••HC interactions. E(**H13**) increases +3.24 kcal·mol^{-1} from $\Phi(1) = 90°$ to *s*-trans, when it is involved in the CH•••N interaction. This observation is in line with the observations regarding the atomic net charge (**H13** loses electrons when it is involved in the CH•••N interaction, Chapter 3) as well as Popelier and Koch's criteria for hydrogen bonding[4] - the hydrogen atom is destabilized. When **H13** is involved in the CH•••HC interaction, however, E(**H13**) becomes more negative by a very significant –7.30 kcal·mol^{-1} from $\Phi = 90°$ to *s*-cis. In the QTAIM picture, **H13** and **H20** are thus destabilized when it is involved in the CH•••N interaction, but provides a combined local stabilization of –14.60 kcal·mol^{-1} when the CH•••HC interaction is formed.

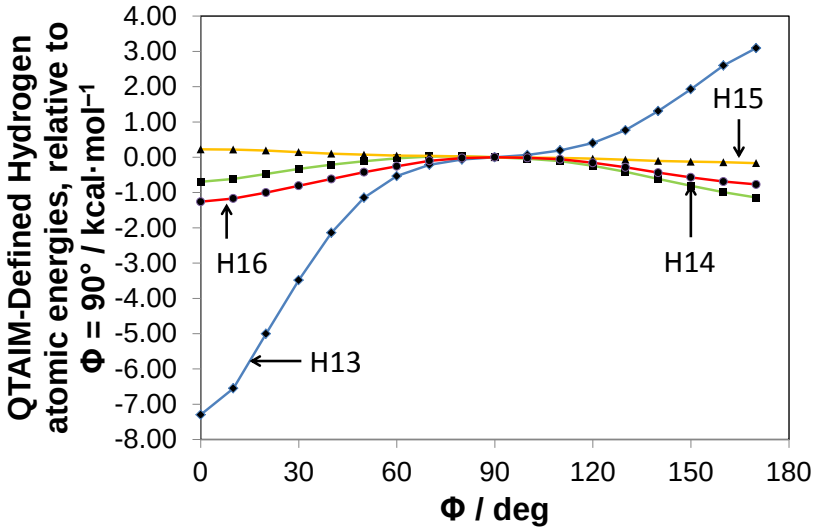

Figure A1. QTAIM-defined atomic energies of H-atoms in BPy, relative to Φ(1) = 90°. **H13** is the blue line, H14 the green line, H15 the yellow line and H16 the red line.

Next, we consider the atomic energies of N1 and N2, shown in Figure A2. N1 appears to be quite destabilized in Φ(1) = 90°, which unfortunately makes it difficult to gauge the effect of the formation of intramolecular interactions on N-atoms in *s*-cis and *s*-trans. The destabilization of N1 (and C3 - see below) at Φ(1) = 90° is related to conjugative effects - these atoms, being bonded to the junction carbons, are destabilized the most because of the loss of conjugation[1–3]. However, E(N1) in *s*-cis is +4.55 kcal·mol^{-1} higher in energy than in *s*-trans, proof of either the stabilization of N1 in the CH•••N interaction or destabilization of N1 because of the N--N interaction (since conjugation effect in *s*-cis and *s*-trans must be very similar). The additional QTAIM-defined energy components in Figure A2 show that the reason for the destabilized N1 in *s*-cis relative to *s*-trans is mainly because of a lesser surface potential energy – the bonds to N1 (C12–N1 and C6–N1) are weaker in *s*-cis than they are in *s*-trans, an effect most likely related to the loss of electrons in N1 in *s*-cis.

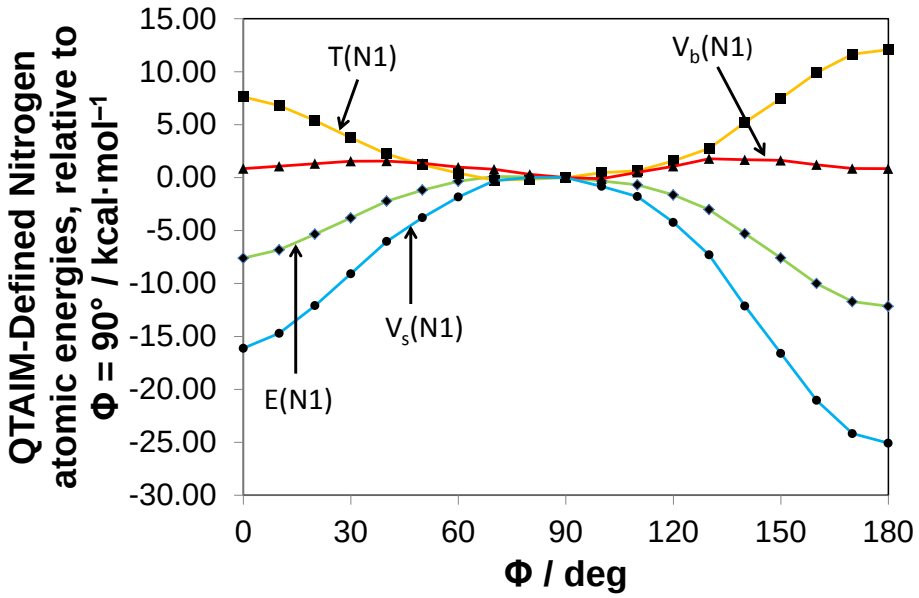

Figure A2 - QTAIM-defined nitrogen atomic energies, relative to Φ(1) = 90°. The green line gives the overall atomic energy, the blue line the atomic surface potential energy, the red line the atomic basin potential energy, and the yellow line the atomic kinetic energy.

Figure A3 shows the atomic energy changes related to the carbon atoms in the molecule, relative to Φ(1) = 90°. C3 and C5, the carbon bonded to **H13** and the carbon meta to C3 and N1, respectively, show a similar pattern to N1 - destabilized in Φ(1) = 90° because of a loss of conjugation. C4, the carbon bonded to C3 and C5, remains relatively unchanged. C6, the carbon bonded to C5 and N1, is stabilized in Φ(1) = 90° - possibly due to its position next to the destabilized N1 and C5 atoms. Finally, C12 (the junction carbon) is at its lowest in Φ(1) = 90°, and destabilized in both *s*-cis and *s*-trans. However, E(C12) in *s*-cis is +12.61 kcal·mol^{-1} higher than E(C12) in *s*-trans - an observation which can only be attributed to the presence of CH•••HC and N--N interactions in *s*-cis and the resultant lengthening of the C11–C12 bond.

Table A1 shows the QTAIM atomic energies and net charges in *s*-cis relative to *s*-trans. The increased molecular electronic energy of *s*-cis relative to *s*-trans is +4.06 kcal·mol^{-1}; the sum of the atomic energy changes +11.48 kcal·mol^{-1}, a difference which can be attributed to inexact wavefunctions and integration errors. However, it is clear from Table A1 that the largest changes in atomic energies are those seen for the nitrogen atoms, the junction carbon atoms, and the hydrogen atoms involved in intramolecular interactions. Specifically, N1, N2, C11 and C12 are the main cause of destabilization in *s*-cis, whereas

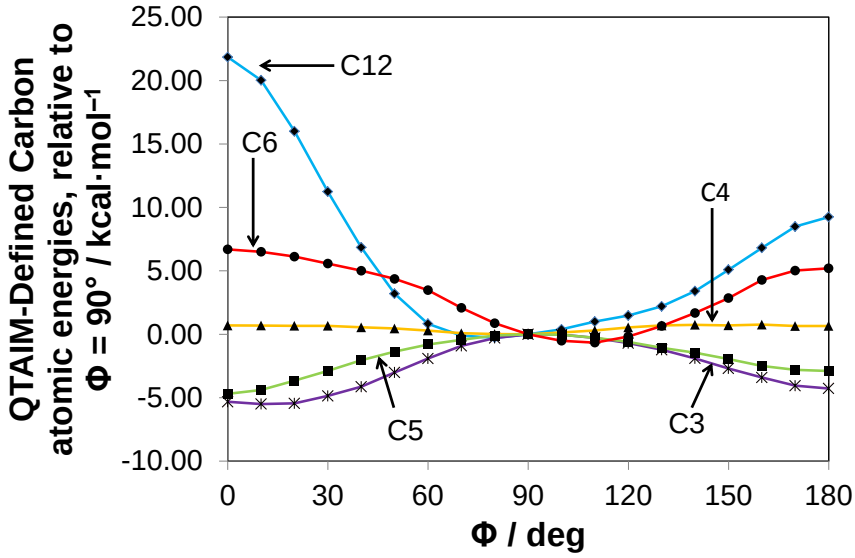

Figure A3. QTAIM-defined carbon atomic energies relative to Φ(1) = 90°. The blue line are for E(C12), the purple line E(C3), the yellow line E(C4), the green line E(C5) and the red line E(C6).

H13 and **H20** is the main cause of stabilization. In the QTAIM picture, the presence of N--N and (possibly) CH•••HC interactions causes destabilizations elsewhere in the molecule, most notably in the C11 and C12 atoms (unfortunately, it is impossible to calculate the relative destabilization either N--N or CH•••HC causes to the C11–C12 bond). Since the IQA-defined interaction energy for the N--N interaction is much greater than the interaction energy for the CH•••HC interaction ($|E_{Int}^{N--N}| \gg |E_{Int}^{CH\cdots HC}|$), it is probable that the N--N interaction is almost solely responsible for the destabilization in the C11–C12 bond, and importantly, the main reason for the increased energy of *s*-cis when compared to *s*-trans. It is difficult to say what the effect of the CH•••N interaction is on the interacting atoms, as E(N1) is a problem case due to its severe destabilization in Φ(1) = 90°. The CH•••HC interaction, however, is a locally stabilizing interaction as the involved atoms are stabilized significantly.

Lastly, it is informative to study the changes in the surface potentials of different interactions, $V_s(A\|B)$, as an indication of the changes in the QTAIM-defined interaction virials. Figure A4 shows the combined surface virials for the interactions which form the C12,C3,H13,H20,C10,C11 H-H ring in *s*-cis, relative to Φ(1) = 90°. Remarkably, when the CH•••HC interaction forms, there is an immediate strengthening of the C3–**H13** interactomic surface and a weakening of the C3–C12 and C12–C11 surfaces. The

Table A1. QTAIM atomic energies of *s*-cis, relative to *s*-trans

	Δq(A) *e*	**ΔE(A)** kcal·mol^{-1}
N1	0.01627	4.55
C12	0.01038	12.61
C3	-0.00768	-1.05
C4	0.00569	0.04
C5	0.00032	-1.81
C6	0.00621	1.50
Sum	*0.01492*	*11.30*
H13	-0.03152	-10.53
H14	0.00218	0.50
H15	0.00136	0.39
H16	-0.00130	-0.46
Sum	*-0.02928*	*-10.10*
Total Atomic Energies		*11.48*
Molecular Energy		*4.06*

destabilization of C12 in *s*-cis can now be better understood as well - the presence of the CH•••HC interaction draws charge from the C12–C11 and C3–C12 bonds (and consequently, C12 is destabilized), weakening these interactions and strengthening the C3–**H13** bond and **H13•••H20** interaction. This observation corroborates with geometrical observations, discussed in Chapter 3: d(C12–C11) and d(C3–C12) increased in *s*-cis whilst d(C3–**H13**) and d(**H13•••H20)** decreased.

IQA Atomic Energies. Figure A5 shows the changes in IQA-defined atomic energy, decomposed into self- and interaction energies, for **H13** relative to Φ(1) = 90°. The total interaction energy of **H13** with all other atoms, E_{Inter}^{IQA}(**H13**), becomes more negative in both *s*-cis and *s*-trans and reflects the presence of CH•••HC and CH•••N intramolecular interactions, respectively. E_{Inter}^{IQA} in *s*-cis is lower than in *s*-trans by –1.40 kcal·mol^{-1}. Correspondingly, as **H13** is involved in intramolecular interactions, the intra-atomic self

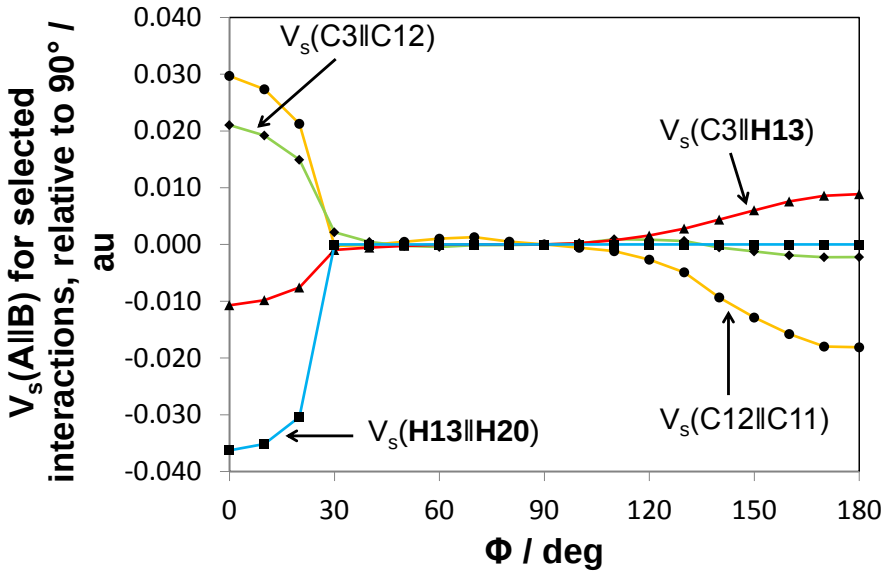

Figure A4 QTAIM-defined changes in the surface virial, V_s(A‖B), relative to Φ(1) = 90°. The blue line show the **H13**,**H20** interaction, the red line the C3,**H13** bond, the green line the C3,C12 bond and the yellow line the C12,C11 bond.

energy, E_{Self}^{IQA}(**H13**), increases by almost the same value (+2.33 and +2.81 kcal·mol^{-1} in *s*-cis and *s*-trans, respectively, relative to Φ(1) = 90°) as a result of the deformation caused upon interaction. Combining E_{Inter}^{IQA}(**H13**) and E_{Self}^{IQA}(**H13**) gives E_{Total}^{IQA}(**H13**) and we see that **H13** (and **H20**) is overall destabilized by +2.19 kcal·mol^{-1} in *s*-trans and +0.30 kcal·mol^{-1} in *s*-cis, relative to Φ(1) = 90°. For *s*-trans, the destabilization is in line with our QTAIM findings, as well as Koch and Popelier's criteria for H-bonds[4]. However, the destabilization of **H13** in *s*-cis is directly opposed to QTAIM-defined atomic energies, which showed that **H13** is significantly stabilized in *s*-cis. That said, the changes in atomic energies cannot be attributed to only the formation of the CH•••HC interaction, and it is possible that changes in other bonds (such as the C3–H13 bond) as well as conjugation effects can cause additional deformation (leading to an increased E_{Self}^{IQA} term) in **H13**. In addition, IQA atomic energy analysis of **H13** reveals that there truly is no steric repulsion between these atoms - an increase of +0.30 kcal·mol^{-1} per H-atom is not significant at all and cannot be used to explain a molecular energy increase of +4.06 kcal·mol^{-1}. The differences between IQA and QTAIM atomic energies will be discussed later.

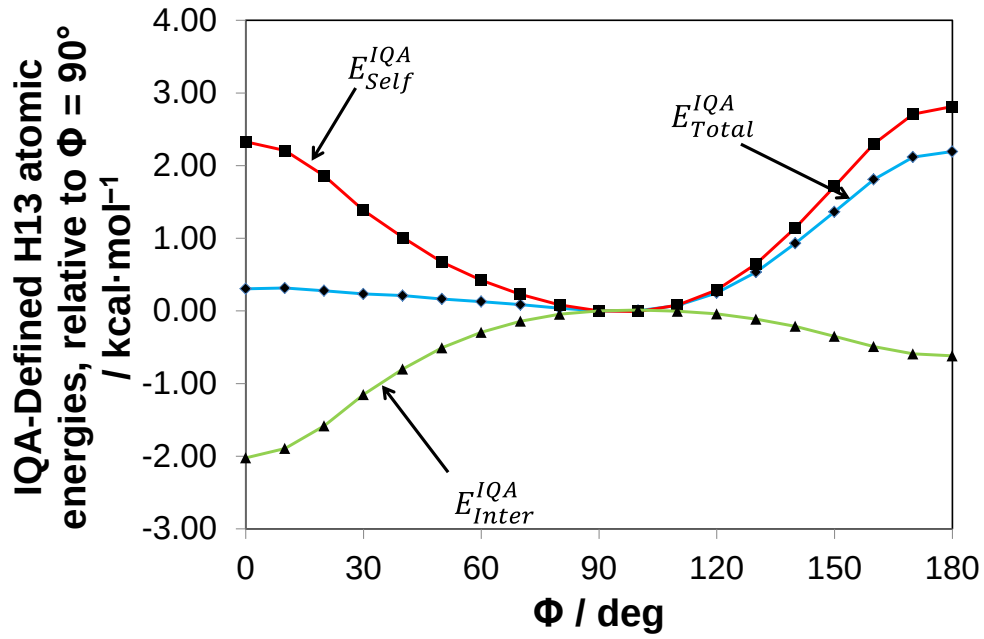

Figure A5, IQA decomposed atomic energies of **H13**, relative to Φ(1) = 90°. The blue line gives the total IQA atomic energy, the green line the total interaction energy of **H13** with all other atoms, and the red line the intra-atomic self energy.

Next we look at the IQA-defined atomic energies of N1, shown in Figure A6. E^{IQA}_{Inter}(N1) increases by +4.47 kcal·mol^{-1} in *s*-cis (when it is involved in the N--N interaction) and becomes more negative by –12.00 kcal·mol^{-1} in *s*-trans (when it is involved in the CH•••N interaction). E^{IQA}_{Self}(N1), on the other hand, shows a slight increase of +2.58 kcal·mol^{-1} in *s*-cis and a large increase of +8.21 kcal·mol^{-1} is *s*-trans. The total IQA-defined atomic energy, E^{IQA}_{Total}(N1), shows a very intuitive picture where N1 is destabilized by +7.05 kcal·mol^{-1} in *s*-cis and is stabilized by –3.79 kcal·mol^{-1} in *s*-trans, corresponding with the highly repulsive N--N interaction in *s*-cis and the formation of the attractive CH•••N interaction in *s*-trans. However, since all the covalent bonds of each ring (including those involving N1) will change significantly because of conjugation, the IQA energy changes given by Figure A6 cannot be attributed solely to the N--N and CH•••N interactions.

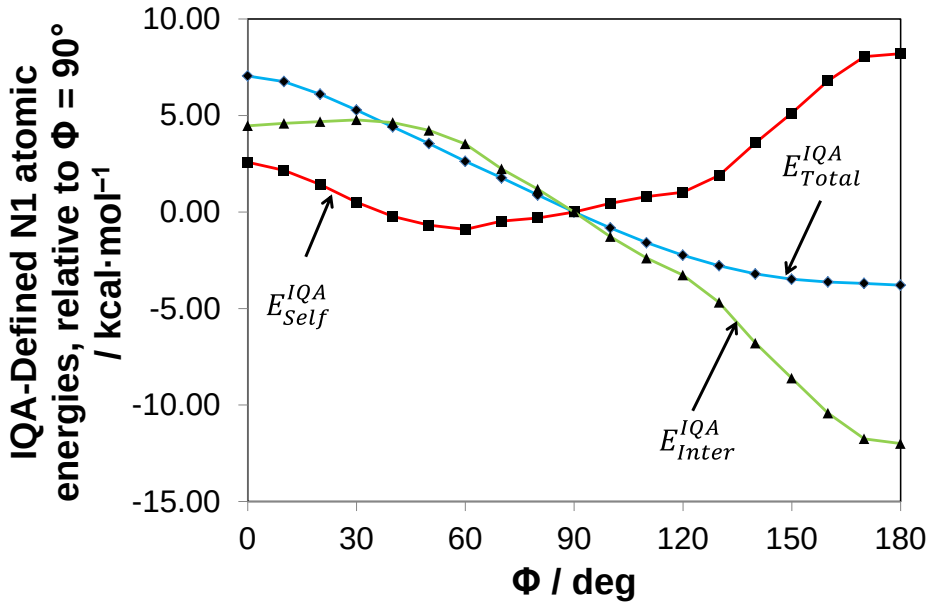

Figure A6. N1 IQA energy changes, relative to Φ(1) = 90°. The blue line gives the total IQA atomic energy for N1, the green line the total interaction energy of N1 with all other atoms, and the red line the intra-atomic self-energy.

Finally, Figure A7 shows the total IQA atomic energy changes for C12, C3 and C6 (due to expensive IQA calculations, C4 and C5 were only calculated for selected conformers; however, the IQA-defined energies for these atoms changed marginally). The largest change occurs in C12, but unlike the QTAIM-defined energies, C12 is significantly destabilized in Φ(1) = 90°, and is slightly more stable in *s*-cis than in *s*-trans (by –1.27 kcal·mol^{-1}). Figure A8 shows the IQA decomposition for C12 alone and indicates that E^{IQA}_{Self}(C12) is the dominant contribution to the changes in IQA-atomic energy, causing a stabilization of C12 in *s*-cis and *s*-trans. Interestingly, E^{IQA}_{Inter}(C12) is the highest in *s*-trans (+4.54 kcal·mol^{-1}) and second-highest in *s*-cis (+1.29 kcal·mol^{-1}).

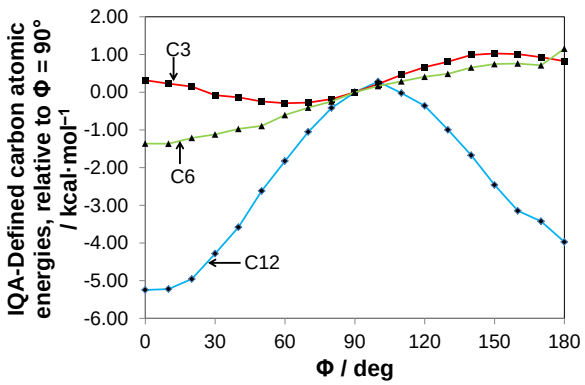

Figure A7. IQA total atomic energy changes relative to Φ(1) = 90°. The blue line show the IQA energy for C12, the red line C3 and the green line C6.

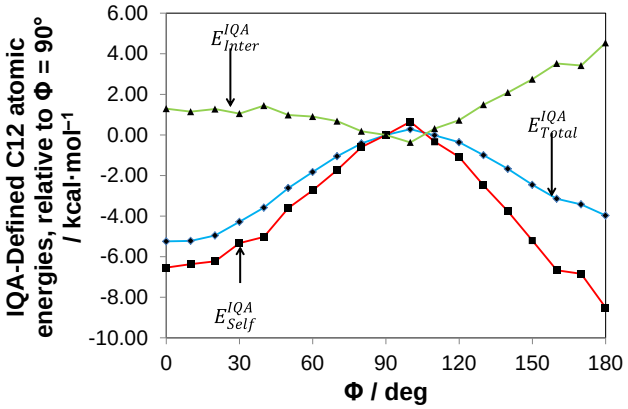

Figure A8. Decomposition of the IQA total atomic energy for C12, relative to Φ(1) = 90°. The blue line gives the total IQA atomic energy, the green line show the total interaction energy of C12 with all other atoms, and the red line show the intra-atomic self-energy.

IQA-defined atomic energies of all atoms in *s*-cis relative to s-trans are given in Table A2. In the IQA picture, the increased energy of *s*-cis is because of the increased interaction energy of N1 (because of the N--N interaction), despite stabilizations in C12, C6 and **H13** (in comparison to the destabilized **H13** in *s*-trans).

Table A2. IQA-defined atomic energies in *s*-cis, relative to *s*-trans

	ΔE_{Total}^{IQA} kcal·mol^{-1}	ΔE_{Self}^{IQA} kcal·mol^{-1}	ΔE_{Inter}^{IQA} kcal·mol^{-1}
N1	10.84	-5.63	16.47
C12	-1.27	1.97	-3.25
C3	-0.51	0.85	-1.36
C4	0.57	0.48	0.09
C5	0.10	0.07	0.03
C6	-2.52	1.09	-3.60
Sum	-3.63	4.46	-8.09
H13	-1.89	-0.48	-1.40
H14	*0.24*	*0.06*	0.18
H15	0.06	-0.04	0.10
H16	-0.12	0.01	-0.13
Sum	-1.70	-0.46	-1.25
Total Atomic Energies	11.01	-3.25	14.26
Molecular Energy	*4.06*		

Lastly, Figure A9 shows the changes in the diatomic interaction energy, E_{Int}^{AB}, for the bonds and interactions forming the C12, C3, **H13**, **H20**, C10 and C11 ring in *s*-cis, relative to Φ = 90° (in analogy to Figure A4 showing the QTAIM-defined V_s(A‖B)). As the **H13•••H20** interaction forms, a slight strengthening of the C3–**H13** bond (–0.34 kcal·mol^{-1}) and a slight weakening of the C3–C12 (+0.11 kcal·mol^{-1}) and C12–C11 (+0.47 kcal·mol^{-1}) bonds are observed. There is a dramatic strengthening of the C12–C11 bond in *s*-trans (–12.27 kcal·mol^{-1}), corroborating with the decrease in d(C12–C11). These results are qualitatively similar to the interactions described by the QTAIM-defined surface virials, in that the CH•••HC interaction causes a stabilization of the C3–C12 bond and a destabilization of the C3–C12 and C12–C11 bonds.

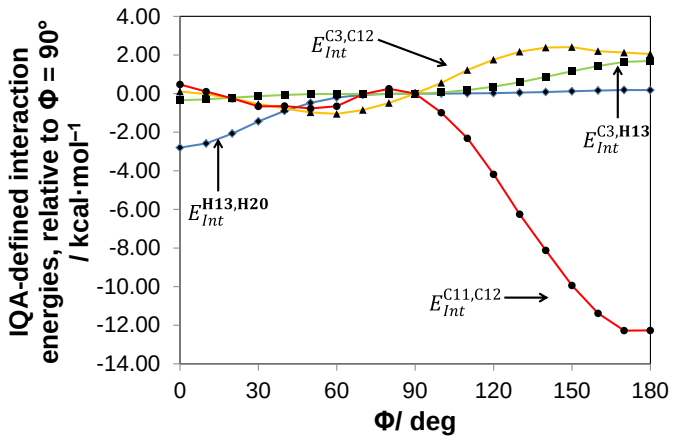

Figure A9. IQA interaction energy changes for the atoms forming the intramolecular CH•••HC ring, relative to Φ(1) = 90°. The blue line show the interaction energy for the **H13•••H20** interaction, the green line for the C3–**H13** bond, the yellow line for the C3–C12 and the red line for the junction C11–C12 bond.

QTAIM and IQA Comparison. Clearly, the results from QTAIM-defined and IQA-defined atomic energy analyses differ significantly: whereas QTAIM suggests that the origin of the increased energy of *s*-cis is mainly because of destabilization of the junction C12 and C11 atoms, IQA suggests that it is because of destabilized N atoms (due to formation of the N--N repulsion). That said, Figures A4 and A9, related to the potential of the interatomic surface virials (QTAIM) and the interaction energy (IQA), respectively, correlate better - the C11–C12 bond is destabilized and the **H13•••H20** interaction is stabilized in *s*-cis relative to *s*-trans in both theories as well as corroborating with the geometrical observation of an increase in d(C11–C12) in *s*-cis.

To explain the different results from atomic energy analyses, we must first point out the fundamental difference between the two theories. Whereas IQA calculates the interactions of each particle (protons and electrons) with each other, QTAIM assumes satisfaction of the virial ratio ($\frac{|V(\boldsymbol{r})|}{T(\boldsymbol{r})} = 2$) and calculates the atomic energy based on the exact kinetic energy alone[5]. More importantly, calculations of QTAIM atomic energies assume the *atomic* virial ratio ($\frac{|V(\Omega)|}{T(\Omega)} = 2$). Since the atomic virial ratio is usually not met exactly in most calculated wavefunctions, IQA seems at first to be a more fundamental and exact approach. However, the atomic virial theorem is a recognized quantum mechanical observable[6–9] and rooted in the physics of an open system - it *should* be met in a real, physical system. Therefore, comparing QTAIM and IQA atomic energies and evaluating the atomic virial ratio and its relative change for each atom can give an indication of where the wavefunction is describing atoms in an inadequate fashion, similar to the approach used by Shaik *et al* in the development of charge-shift bonding mechanics[10–12].

The average molecular virial ratio for BPy over the range of $0° \leq \Phi(1) \leq 180°$ is 2.00034, with a standard deviation of 0.00001, which is of adequate accuracy[5]. The average atomic virial ratio, including standard deviations and spreads, for each atom of one pyridine ring is given in Table A3. In general, the hydrogen and nitrogen atoms show average atomic virials smaller than 2, whereas the carbon atoms show an average atomic virial slightly larger than 2. However, only **H13** (and **H20**) show standard deviations on the third decimal - on average an order of magnitude larger than the standard deviations for all other atoms. The change in atomic virial ratio for the hydrogen atoms is shown in Figure A10. Even though H14, H15 and H16 show different average virial ratios, the changes in the atomic virial ratios of these atoms are similar and significantly small, meaning that the relative changes in atomic energies are reliable. However, **H13** shows a significant decrease in the atomic virial ratio as the CH•••HC interaction is formed; from 1.9233 in $\Phi(1) = 90°$ to 1.9052 in *s*-cis. A lowered atomic virial ratio indicates that the absolute value of the atomic potential energy is too small relative to the kinetic energy. The relative IQA-defined atomic energies for **H13** in *s*-cis in comparison to $\Phi(1) = 90°$ or *s*-trans are thus underestimated, either because of an overestimated kinetic energy or underestimated potential energy, and in reality would be closer to the QTAIM-defined atomic energies.

Table A3. Atomic Virial ratios

Atom	Average Virial Ratio	Standard Deviation	Spread
N1	1.9875	0.0001	0.0004
C3	2.0016	0.0001	0.0002
C4	2.0012	0.0000	0.0001
C5	2.0016	0.0001	0.0002
C6	2.0113	0.0001	0.0004
C12	2.0101	0.0004	0.0012
Average	*2.0051*	*0.0001*	*0.0004*
H13	1.9202	0.0063	0.0202
H14	1.9254	0.0009	0.0019
H15	1.9259	0.0003	0.0008
H16	1.9114	0.0009	0.0022
Average	*1.9207*	*0.0021*	*0.0063*

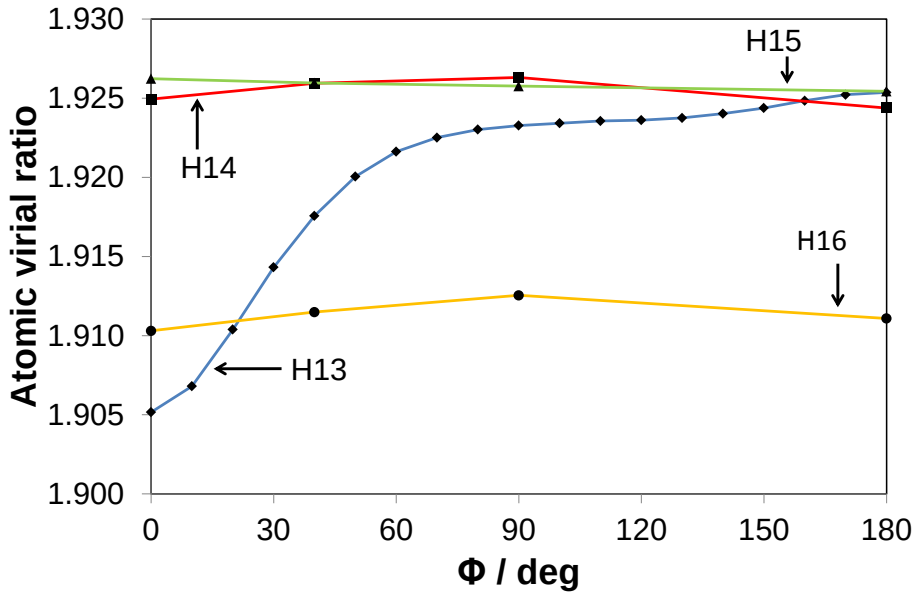

Figure A10. Atomic Virial Ratios from IQA calculations. Blue show the atomic virial ratio for **H13**, red for H14, green for H15 and the yellow line for H16.

The reasons, as well as possible solutions for the large deviation in atomic virial ratio as the CH•••HC interaction is formed is of critical importance to understanding this type of interaction and should be studied more extensively in the future. For the scope of this work, it is enough to say that **H13** and **H20** will be more stabilized in *s*-cis than what IQA atomic energy analysis is suggesting. Since the change in IQA-defined atomic energy for

H13 is +0.30 kcal·mol^{-1} in *s*-cis relative to Φ(1) = 90°, we can safely state that the actual change in atomic energy of **H13** and **H20** is somewhere between +0.30 and –7.30 kcal·mol^{-1}. The nature of the CH•••HC interaction is therefore very likely locally stabilizing to the atoms (and possibly fragments) involved.

In summary, correlating QTAIM and IQA energetic results leads to the observation that the decreased stability of *s*-cis relative to *s*-trans is due to destabilizations in the C11–C12 bond as well as the N1 and N2 atoms (because of formation of the N--N interaction). In addition, the stabilizing influence of the CH•••N interaction in *s*-trans is lost in *s*-cis. However, the CH•••HC interaction formed by **H13** and **H20** in *s*-cis is locally stabilizing, causing C3, **H13**, **H20** and C10 atoms to be stabilized (as well as the C3–**H13** and C10–**H20** bonds and the **H13•••H20** interaction to be strengthened). There is evidence though that the formation of an interatomic surface between **H13** and **H20** causes a destabilization in the atomic surface of C11–C12, contributing to the lengthening of d(C11–C12) in *s*-cis.

References

[1] S. T. Howard, *J. Am. Chem. Soc.*, **1996**, *118*, 10269–10274

[2] L. Oresmaa, M. Haukka, P. Vainiotale, T. A. Pakkanen, *J. Org. Chem.*, **2002**, *67*, 8216–8219

[3] S. Zahn, W. Reckien, B. Kirchner, H. Staats, J. Matthey, A. Lützen, *Chem. Eur. J.*, **2009**, *15*, 2572–2580

[4] U. Koch, P. L. A. Popelier, *J. Phys. Chem.*, **1995**, *99*, 9747–9754

[5] R. F. W. Bader, *in Atoms in Molecules: A Quantum Theory*; Oxford University Press: Oxford, U.K. 1990.

[6] R. F. W. Bader, "*The Lagrangian Approach to Chemisty"* in The Quantum Theory of Atoms in Molecules: From Solid State to DNA and Drug Design, Wiley-VCH, Weinheim, 2007

[7] R. F. W. Bader, *J. Mol. Struct: Theochem*, **2010**, *943*, 2–18

[8] R. F. W. Bader, *J. Phys. Chem. A.*, **2007**, *111*, 7966–7972

[9] S. Srebrenik, R. F. W. Bader, *J. Chem. Phys.*, **1975**, *63*, 3945

[10] S. Shaik, D. Danovich, W. Wu, P. C. Hiberty, *Nat. Chem.*, **2009**, *1*, 443–449

[11] S. Shaik, D. Danovich, B. silvi, D. L. Lauvergnat, P. C. Hiberty, *Chem.–Eur. J.*, **2005**, *11*, 6358–6371

[12] S. Shaik, P. Maitre, G. Sini, P. C. Hiberty, *J. Am. Chem. Soc.*, **1992**, *114*, 7861–7866

Appendix B.

Supplementary Information for Chapter 3

Table B1. Cartesian coordinates for 2,2′-Bipyridine with DA(N1,C12,C11,N2) = 0° (*s*-Cis)

Standard orientation					
Center Number	**Atomic Number**	**Atomic Type**	**Coordinates (Angstroms)**		
			X	**Y**	**Z**
1	7	0	-1.365	-1.182	0.044
2	7	0	1.365	-1.182	-0.044
3	6	0	-1.488	1.206	-0.039
4	6	0	-2.877	1.154	-0.041
5	6	0	-3.506	-0.085	0.004
6	6	0	-2.699	-1.220	0.042
7	6	0	2.699	-1.220	-0.042
8	6	0	3.506	-0.085	-0.004
9	6	0	2.877	1.154	0.041
10	6	0	1.488	1.206	0.039
11	6	0	0.750	0.014	-0.024
12	6	0	-0.750	0.014	0.024
13	1	0	-0.998	2.169	-0.083
14	1	0	-3.456	2.070	-0.082
15	1	0	-4.586	-0.176	0.002
16	1	0	-3.148	-2.209	0.069
17	1	0	3.148	-2.209	-0.069
18	1	0	4.586	-0.176	-0.002
19	1	0	3.456	2.070	0.082
20	1	0	0.998	2.169	0.083

Thermochemical data: (au)

```
Zero-point correction=                           0.167733
Sum of electronic and zero-point Energies=       -492.189737
Sum of electronic and thermal Energies=          -492.182451
Sum of electronic and thermal Enthalpies=        -492.181506
Sum of electronic and thermal Free Energies=     -492.221865
```

Table B2. Cartesian coordinates for 2,2′-Bipyridine with DA(N1,C12,C11,N2) = 40°

Standard orientation					
Center	**Atomic**	**Atomic**	**Coordinates (Angstroms)**		
Number	**Number**	**Type**	**X**	**Y**	**Z**
1	7	0	-1.400	-1.170	0.280
2	7	0	1.400	-1.170	-0.280
3	6	0	-1.462	1.146	-0.294
4	6	0	-2.852	1.136	-0.269
5	6	0	-3.514	-0.052	0.023
6	6	0	-2.735	-1.172	0.300
7	6	0	2.735	-1.172	-0.300
8	6	0	3.514	-0.052	-0.023
9	6	0	2.852	1.136	0.269
10	6	0	1.462	1.146	0.294
11	6	0	0.748	-0.044	0.070
12	6	0	-0.748	-0.044	-0.070
13	1	0	-0.950	2.077	-0.494
14	1	0	-3.406	2.047	-0.464
15	1	0	-4.595	-0.109	0.060
16	1	0	-3.207	-2.118	0.559
17	1	0	3.207	-2.118	-0.559
18	1	0	4.595	-0.109	-0.060
19	1	0	3.406	2.047	0.464
20	1	0	0.950	2.077	0.494

Thermochemical data: (au)

```
Zero-point correction=                           0.167879
Sum of electronic and zero-point Energies=       -492.192106
Sum of electronic and thermal Energies=          -492.183996
Sum of electronic and thermal Enthalpies=        -492.183051
Sum of electronic and thermal Free Energies=     -492.225654
```

Table B3. Cartesian coordinates for 2,2′-Bipyridine with DA(N1,C12,C11,N2) = 90°

Standard orientation					
Center Number	Atomic Number	Atomic Type	Coordinates (Angstroms) X	Y	Z
1	7	0	-0.512	1.541	-1.120
2	7	0	0.512	-1.541	-1.120
3	6	0	0.569	1.357	0.947
4	6	0	0.541	2.740	1.113
5	6	0	-0.001	3.531	0.113
6	6	0	-0.541	2.866	-0.976
7	6	0	0.541	-2.866	-0.976
8	6	0	0.001	-3.531	0.113
9	6	0	-0.541	-2.740	1.113
10	6	0	-0.569	-1.357	0.947
11	6	0	-0.175	-0.731	-0.263
12	6	0	0.175	0.731	-0.263
13	1	0	0.928	0.757	1.775
14	1	0	0.910	3.182	2.034
15	1	0	-0.062	4.610	0.196
16	1	0	-1.048	3.424	-1.767
17	1	0	1.048	-3.424	-1.767
18	1	0	0.062	-4.610	0.196
19	1	0	-0.910	-3.182	2.034
20	1	0	-0.928	-0.757	1.775

Thermochemical data: (au)

```
Zero-point correction=                           0.167583
Sum of electronic and zero-point Energies=       -492.190186
Sum of electronic and thermal Energies=          -492.182815
Sum of electronic and thermal Enthalpies=        -492.181871
Sum of electronic and thermal Free Energies=     -492.222611
```

Table B4. Cartesian coordinates for 2,2′-Bipyridine with DA(N1,C12,C11,N2) = 180° (*s*-trans)

Standard orientation					
Center Number	**Atomic Number**	**Atomic Type**	**Coordinates (Angstroms)**		
			X	**Y**	**Z**
1	7	0	-1.690	-1.073	0.800
2	7	0	1.690	-1.073	-0.800
3	6	0	-1.099	0.230	-0.756
4	6	0	-2.320	0.922	-0.715
5	6	0	-3.312	0.501	0.113
6	6	0	-2.890	-0.499	0.917
7	6	0	2.890	-0.499	-0.917
8	6	0	3.312	0.501	-0.113
9	6	0	2.320	0.922	0.715
10	6	0	1.099	0.230	0.756
11	6	0	0.717	-1.073	0.226
12	6	0	-0.717	-1.073	-0.226
13	1	0	-0.328	0.745	-1.324
14	1	0	-2.441	1.838	-1.294
15	1	0	-4.276	0.993	0.231
16	1	0	-3.518	-0.841	1.755
17	1	0	3.518	-0.841	-1.755
18	1	0	4.276	0.993	-0.231
19	1	0	2.441	1.838	1.294
20	1	0	0.328	0.745	1.324

Thermochemical data: (au)

```
Zero-point correction=                           0.167918
Sum of electronic and zero-point Energies=       -492.196025
Sum of electronic and thermal Energies=          -492.187886
Sum of electronic and thermal Enthalpies=        -492.186942
Sum of electronic and thermal Free Energies=     -492.230357
```

Table B5. QTAIM-defined atomic volumes (at 0.0004 au isodensity surface), relative to DA(N1,C12,C11,N2) = 90°.

Φ(1)	N1	C3	C4	C5	C6	C12	H13	H14	H15	H16
0	-8.49	-1.24	-0.07	0.47	-0.32	7.75	-7.01	-0.08	-0.03	0.25
10	-8.05	-1.49	0.06	0.43	-0.41	7.44	-6.79	-0.09	0.00	0.33
20	-7.17	-1.95	0.05	0.33	-0.33	6.71	-5.90	0.03	-0.05	0.34
30	-6.17	-1.95	0.14	0.25	-0.34	5.68	-4.81	0.01	0.02	0.21
40	-4.96	-2.14	0.05	0.36	-0.36	4.78	-3.54	-0.10	0.05	0.28
50	-3.69	-2.06	0.19	0.38	-0.07	3.52	-2.22	0.01	-0.01	0.15
60	-2.36	-1.55	0.17	0.30	-0.22	2.32	-1.26	-0.17	-0.07	0.18
70	-1.15	-0.78	0.04	0.12	-0.18	1.15	-0.41	-0.13	0.03	0.10
80	-0.22	-0.10	0.05	0.13	-0.08	0.26	-0.03	-0.04	0.05	0.23
90	*0.00*	*0.00*	*0.00*	*0.00*	*0.00*	*0.00*	*0.00*	*0.00*	*0.00*	*0.00*
100	-0.42	-0.28	0.12	-0.08	0.10	0.33	-0.07	0.03	-0.02	0.10
110	-1.39	-0.90	0.11	-0.01	0.12	1.23	-0.63	-0.14	-0.09	0.02
120	-2.81	-1.32	0.28	0.08	0.18	2.25	-1.40	-0.07	-0.05	0.11
130	-4.49	-1.57	0.28	0.27	0.25	3.34	-2.44	0.17	-0.05	0.24
140	-6.17	-1.71	0.33	0.35	0.12	4.49	-3.72	0.13	0.13	0.12
150	-7.67	-1.67	0.32	0.57	-0.01	5.52	-5.02	0.16	0.06	0.18
160	-8.89	-1.30	0.60	0.36	0.03	6.49	-6.06	0.20	0.01	0.23
170	-9.66	-1.23	0.44	0.37	-0.07	7.02	-6.86	0.25	0.12	0.30
180	-9.95	-1.13	0.59	0.32	-0.22	7.53	-7.10	0.14	0.18	0.42

All volumes in au.

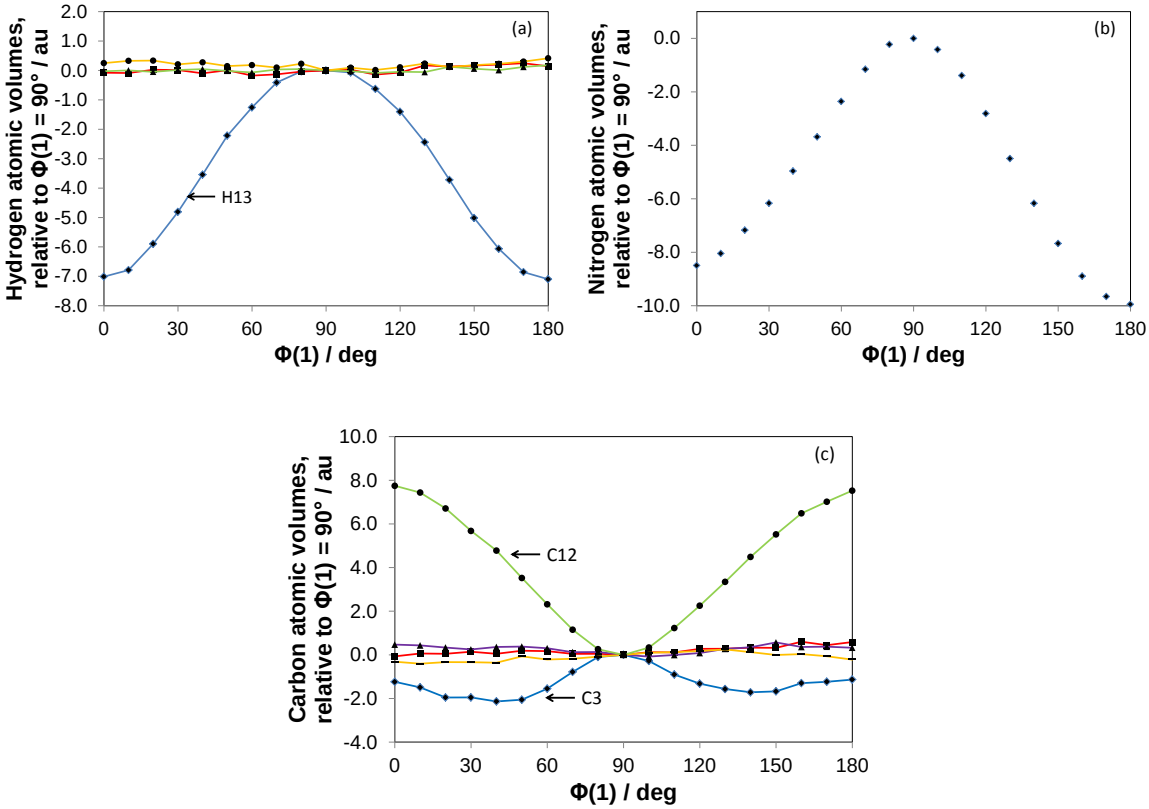

Figure B1. QTAIM-defined atomic volumes of a) hydrogen atoms, b) nitrogen atom, and c) carbon atoms.

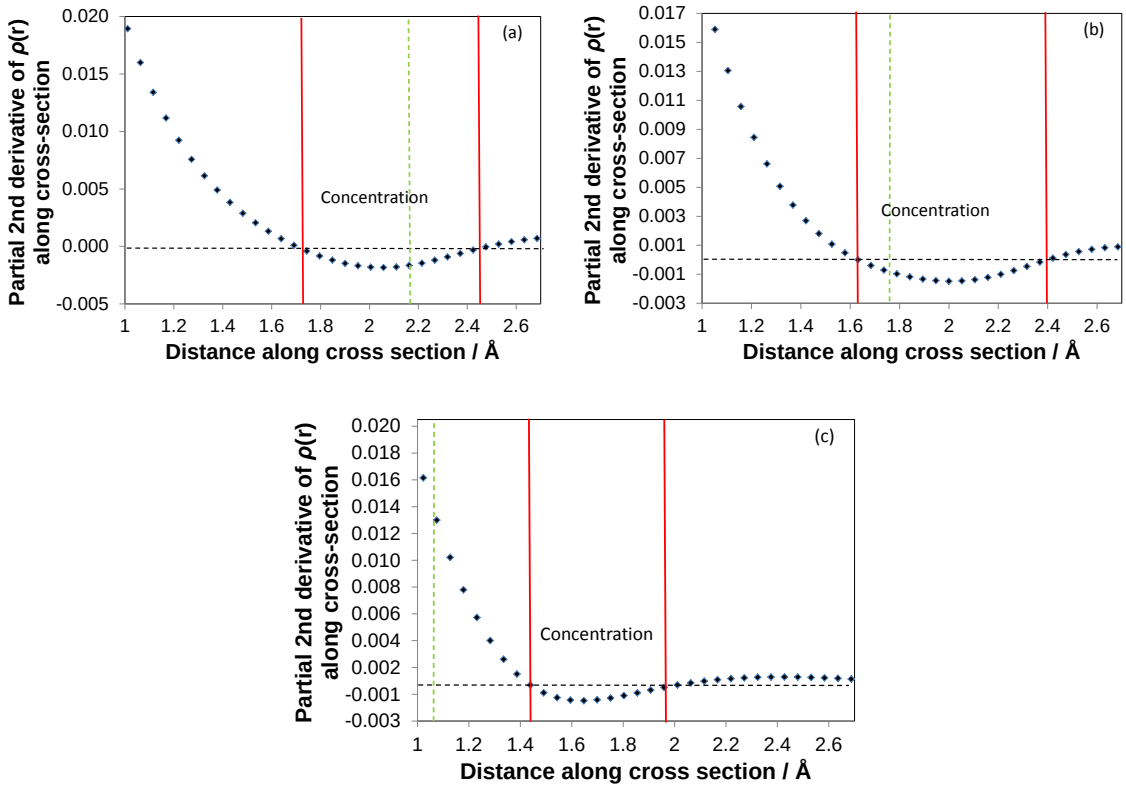

Figure B2. Partial 2nd derivatives of $\rho(\mathbf{r})$ along the vector given by λ_2 for a) the CH•••HC interaction, b) the CH•••N interaction and c) the N--N interaction. The distance on the vector where the geometric interaction line crosses is indicated by the green line for each graph.

Appendix C.

Supplementary Information for Chapter 4

Table C1. Cartesian coordinates for the $[ZnL(H_2O)_4]^{2+}$ complex (L = 2,2′-bipyridyl)

Standard orientation					
Center	Atomic	Atomic	Coordinates (Angstroms)		
Number	Number	Type	X	Y	Z
1	8	0	-2.7284	-1.5638	0.0093
2	8	0	-1.6885	-0.0051	2.1465
3	8	0	-2.7285	1.5636	-0.0093
4	8	0	-1.6885	0.0049	-2.1464
5	7	0	0.3884	-1.3413	0.039
6	7	0	0.3883	1.3414	-0.039
7	6	0	0.3029	-2.6759	0.0598
8	1	0	-0.6945	-3.0912	0.0732
9	6	0	1.4249	-3.4886	0.06
10	1	0	1.3138	-4.5629	0.0785
11	6	0	2.6754	-2.8858	0.0345
12	1	0	3.5753	-3.485	0.0317
13	6	0	2.7642	-1.5004	0.0089
14	1	0	3.7317	-1.0238	-0.0136
15	6	0	1.5961	-0.7435	0.0132
16	6	0	1.596	0.7436	-0.0133
17	6	0	2.7641	1.5005	-0.009
18	1	0	3.7316	1.0241	0.0135
19	6	0	2.6752	2.886	-0.0345
20	1	0	3.5751	3.4852	-0.0318
21	6	0	1.4247	3.4887	-0.0601
22	1	0	1.3135	4.563	-0.0785
23	6	0	0.3027	2.6759	-0.0598
24	1	0	-0.6947	3.0912	-0.0732
25	1	0	-3.417	-1.5173	-0.6684
26	1	0	-3.2011	-1.6273	0.8513
27	1	0	-1.1748	-0.6202	2.6883
28	1	0	-1.6211	0.8442	2.6055
29	1	0	-3.2013	1.627	-0.8512
30	1	0	-3.4171	1.5171	0.6685
31	1	0	-1.6211	-0.8443	-2.6055
32	1	0	-1.1749	0.6201	-2.6883
33	30	0	-1.2358	0	0

Molecular Electronic Energy: -2580.08621989 au

Table C2. Cartesian Coordinates for the $[ZnL_2(H_2O)_2]^{2+}$ Complex (L = 2,2′-Bipyridyl)

Standard orientation

Center Number	Atomic Number	Atomic Type	Coordinates (Angstroms)		
			X	Y	Z
1	7	0	-0.9093	-1.4706	0.5552
2	7	0	-2.0434	0.6451	-0.6517
3	7	0	0.9088	1.4651	0.5628
4	7	0	2.0436	-0.6407	-0.6593
5	8	0	-0.3424	-1.3276	-2.5354
6	8	0	0.3439	1.355	-2.5237
7	6	0	-0.285	-2.5157	1.1073
8	1	0	0.7599	-2.6377	0.8613
9	6	0	-0.9261	-3.4072	1.9527
10	1	0	-0.3817	-4.2396	2.3744
11	6	0	-2.269	-3.1959	2.2345
12	1	0	-2.8072	-3.8671	2.8893
13	6	0	-2.2143	-1.2608	0.8155
14	6	0	-2.8409	-0.0877	0.1502
15	6	0	-2.9211	-2.1132	1.6604
16	1	0	-3.9654	-1.9433	1.8701
17	6	0	-4.1818	0.2486	0.3246
18	1	0	-4.8198	-0.3378	0.9669
19	6	0	-4.6986	1.3527	-0.3379
20	1	0	-5.7369	1.6247	-0.2088
21	6	0	-3.8693	2.0965	-1.167
22	1	0	-4.2312	2.961	-1.7042
23	6	0	-2.5465	1.7041	-1.2967
24	1	0	-1.864	2.2428	-1.9378
25	6	0	0.2839	2.5082	1.1173
26	1	0	-0.7651	2.6212	0.8841
27	6	0	0.9272	3.4059	1.9545
28	1	0	0.3802	4.233	2.3832
29	6	0	2.276	3.2081	2.2169
30	1	0	2.8168	3.8855	2.8631
31	6	0	2.9293	2.1277	1.6393
32	1	0	3.9786	1.9701	1.833
33	6	0	2.2175	1.2633	0.8103
34	6	0	2.8401	0.0847	0.1507
35	6	0	4.175	-0.2659	0.3413
36	1	0	4.8095	0.3105	0.9961
37	6	0	4.6891	-1.3722	-0.3205
38	1	0	5.723	-1.6552	-0.1798
39	6	0	3.8625	-2.1046	-1.1623
40	1	0	4.2226	-2.9693	-1.7002

Standard orientation					
Center	**Atomic**	**Atomic**	**Coordinates (Angstroms)**		
Number	**Number**	**Type**	**X**	**Y**	**Z**
41	6	0	2.5438	-1.702	-1.3025
42	1	0	1.8624	-2.2349	-1.9494
43	1	0	0.8967	0.9448	-3.2033
44	1	0	0.7707	2.2023	-2.3389
45	1	0	-0.9049	-0.9088	-3.2012
46	1	0	-0.7694	-2.1755	-2.3531
47	30	0	0.0004	0.0032	-0.7246

Molecular Electronic Energy: -2922.51597175 au

Table C3. Cartesian Coordinates for the $[ZnL_3]^{2+}$ Complex (L = 2,2′-Bipyridyl)

Standard orientation					
Center	Atomic	Atomic	Coordinates (Angstroms)		
Number	Number	Type	X	Y	Z
1	6	0	-1.40207	-1.64497	-2.33947
2	1	0	-0.39724	-1.62114	-2.73541
3	6	0	-2.42222	-2.27121	-3.03819
4	1	0	-2.21734	-2.73989	-3.99007
5	6	0	-3.69338	-2.27697	-2.48014
6	1	0	-4.51849	-2.75479	-2.98993
7	6	0	-3.89454	-1.66278	-1.25246
8	1	0	-4.87781	-1.66428	-0.80905
9	6	0	-2.81906	-1.05154	-0.60734
10	6	0	-2.95952	-0.37681	0.710249
11	6	0	-4.17183	-0.32453	1.39812
12	1	0	-5.06176	-0.77453	0.986819
13	6	0	-4.23066	0.31464	2.627853
14	1	0	-5.16431	0.360527	3.171296
15	6	0	-3.07963	0.894651	3.144157
16	1	0	-3.07781	1.404577	4.096791
17	6	0	-1.91225	0.807	2.402173
18	1	0	-0.99498	1.248219	2.763739
19	6	0	-0.86565	2.030244	-2.28001
20	1	0	-1.36787	1.149496	-2.6528
21	6	0	-0.93963	3.231065	-2.96817
22	1	0	-1.5017	3.293103	-3.88887
23	6	0	-0.2784	4.331741	-2.44055
24	1	0	-0.31036	5.288729	-2.94304
25	6	0	0.430065	4.190194	-1.25656
26	1	0	0.946718	5.039648	-0.8381
27	6	0	0.460971	2.949593	-0.62021
28	6	0	1.194113	2.727119	0.653853
29	6	0	1.891358	3.746505	1.301616
30	1	0	1.920885	4.743891	0.89178
31	6	0	2.551241	3.472203	2.490483
32	1	0	3.092982	4.25468	3.003863
33	6	0	2.501186	2.185478	3.009732
34	1	0	2.993657	1.926745	3.936106
35	6	0	1.787485	1.22439	2.311351
36	1	0	1.72113	0.21159	2.680461
37	6	0	2.05581	-0.28349	-2.40092
38	1	0	1.51013	0.578379	-2.75671
39	6	0	3.102706	-0.81283	-3.13952

Standard orientation					
Center	Atomic	Atomic	Coordinates (Angstroms)		
Number	Number	Type	X	Y	Z
40	1	0	3.380656	-0.36527	-4.08315
41	6	0	3.771961	-1.9179	-2.63137
42	1	0	4.59577	-2.36187	-3.17296
43	6	0	3.370347	-2.45041	-1.41509
44	1	0	3.883763	-3.30914	-1.01212
45	6	0	2.306459	-1.86518	-0.72861
46	6	0	1.825637	-2.37935	0.581266
47	6	0	2.42708	-3.46	1.226953
48	1	0	3.270635	-3.96839	0.786649
49	6	0	1.932769	-3.88466	2.451444
50	1	0	2.394144	-4.7179	2.963319
51	6	0	0.843748	-3.226	3.005812
52	1	0	0.422911	-3.52346	3.955391
53	6	0	0.295274	-2.16298	2.305248
54	1	0	-0.55345	-1.62316	2.698674
55	7	0	-1.59023	-1.04891	-1.15745
56	7	0	-1.84802	0.186083	1.219808
57	7	0	-0.18437	1.887761	-1.13838
58	7	0	1.149949	1.482749	1.165096
59	7	0	1.664059	-0.79285	-1.22817
60	7	0	0.771816	-1.74474	1.127776
61	30	0	-0.0103	-0.00619	-0.00379

Molecular Electronic Energy: -3264.94124288

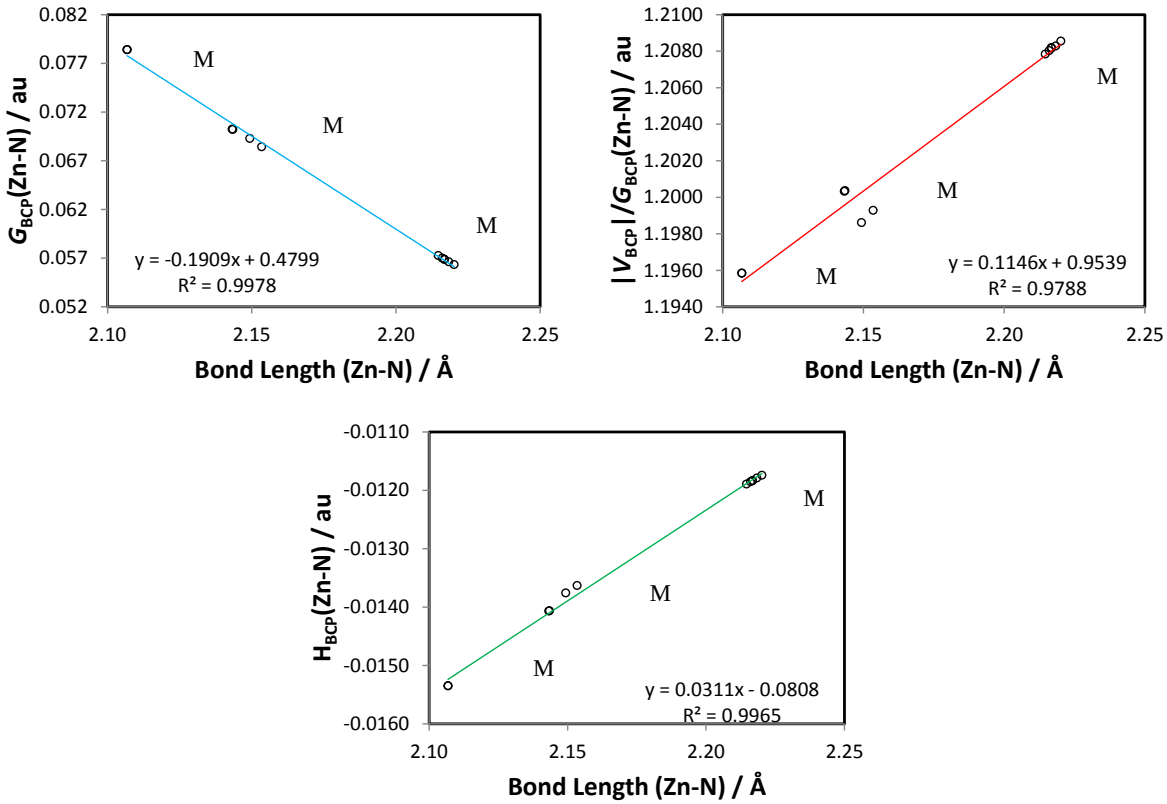

Figure C1. Additional relationships between bond lengths and topological properties at the BCP for Zn–N bonds.

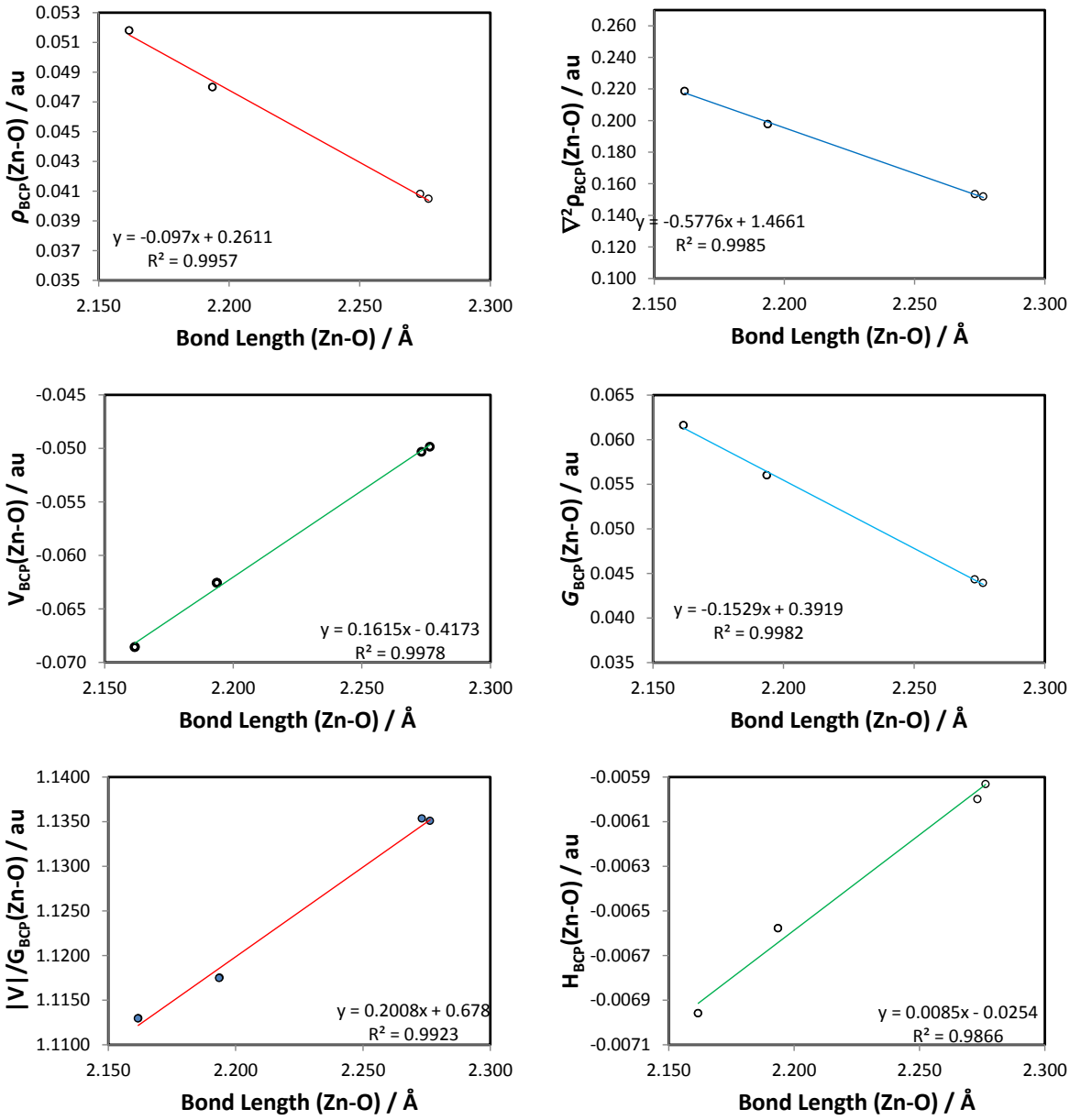

Figure C2 Relationships between bond lengths and topological properties at the BCP for Zn–O bonds.

Table C4. Decomposition of two-bodied interaction energies within the IQA framework for all relevant bonds in Zn^{II} complexes with 2,2´-bipyridyl

Complex	**Atoms**	**d(A–B)** Å	V_{ne}^{AB} *au*	V_{en}^{AB} *au*	V_{nn}^{AB} *au*	V_{C}^{AB} *au*	E_{cl}^{AB} *kcal·mol^{-1}*	E_{XC}^{AB} *kcal·mol^{-1}*	E_{Int}^{AB} *kcal·mol^{-1}*	E_{XC}^{AB}/E_{Int}^{AB} *kcal·mol^{-1}*
ZnL	*CH···HC*	*2.06*	-0.2472	-0.2472	0.2569	0.2375	-0.02	-2.48	-2.5	0.993
	CH···O	*2.6*	-1.7008	-1.7008	1.6285	1.7542	-11.86	-2.64	-14.5	0.182
	C-C	*1.497*	-11.4042	-11.4042	12.7218	10.2391	95.69	-193.43	-97.74	1.979
	Zn-N5	*2.145*	-56.0668	-56.0668	51.8045	59.7401	-369.65	-40.14	-409.79	0.098
	Zn-N6	*2.145*	-56.0670	-56.0670	51.8046	59.7402	-369.65	-40.14	-409.79	0.098
	Zn-O1	*2.157*	-61.8194	-61.8194	58.8847	64.2786	-298.43	-28.04	-326.47	0.086
	N5-N6	*2.673*	-11.8316	-11.8316	9.7005	14.4307	293.69	-7.03	286.67	–0.025
ZnL_2	*CH···HC*	*2.05*	-0.2488	-0.2488	0.2581	0.239	-0.23	-2.51	-2.74	0.916
	CH···O	*2.502*	-1.7656	-1.7656	1.6917	1.8195	-12.47	-3.26	-15.73	0.207
	CH···N	*2.879*	-1.3988	-1.3988	1.2866	1.4953	-9.91	-1.64	-11.56	0.142
	C-C	*1.497*	-11.4030	-11.4030	12.7264	10.233	96.27	-193.41	*-97.15*	1.991
	Zn-N1	2.183	-55.1408	-55.1408	50.9086	58.8099	-353.41	-36.73	-390.14	0.094
	Zn-N2	2.182	-55.1524	-55.1524	50.9243	58.8145	-355.12	-36.76	-391.88	0.094
	Zn-O6	2.236	-59.7008	-59.7008	56.7947	62.1597	-280.51	-22.97	-303.48	0.076
	N1-N2	2.676	-11.8153	-11.8153	9.6902	14.4061	292.25	-7.15	285.1	-0.025
ZnL_3	*CH···HC*	2.073	-0.2463	-0.2463	0.2553	0.2364	-0.52	-2.36	-2.88	0.821
	CH···N	2.746	-1.4669	-1.4669	*0.2553*	*0.2364*	-11.71	-2.26	-13.97	0.162
	C-C	1.496	-11.4046	-11.4046	0.5106	0.4729	96.79	-193.41	-96.62	2.002
	Zn-N2	2.229	-54.0400	-54.0400	49.8607	57.6798	-338.51	-32.93	-371.44	0.089
	Zn-N23	2.228	-54.0550	-54.0550	49.8744	57.6956	-338.79	-32.89	-371.68	0.088
	N2-N23	2.690	-11.7953	-11.7953	9.6755	14.3793	291.34	-7.24	284.11	-0.025

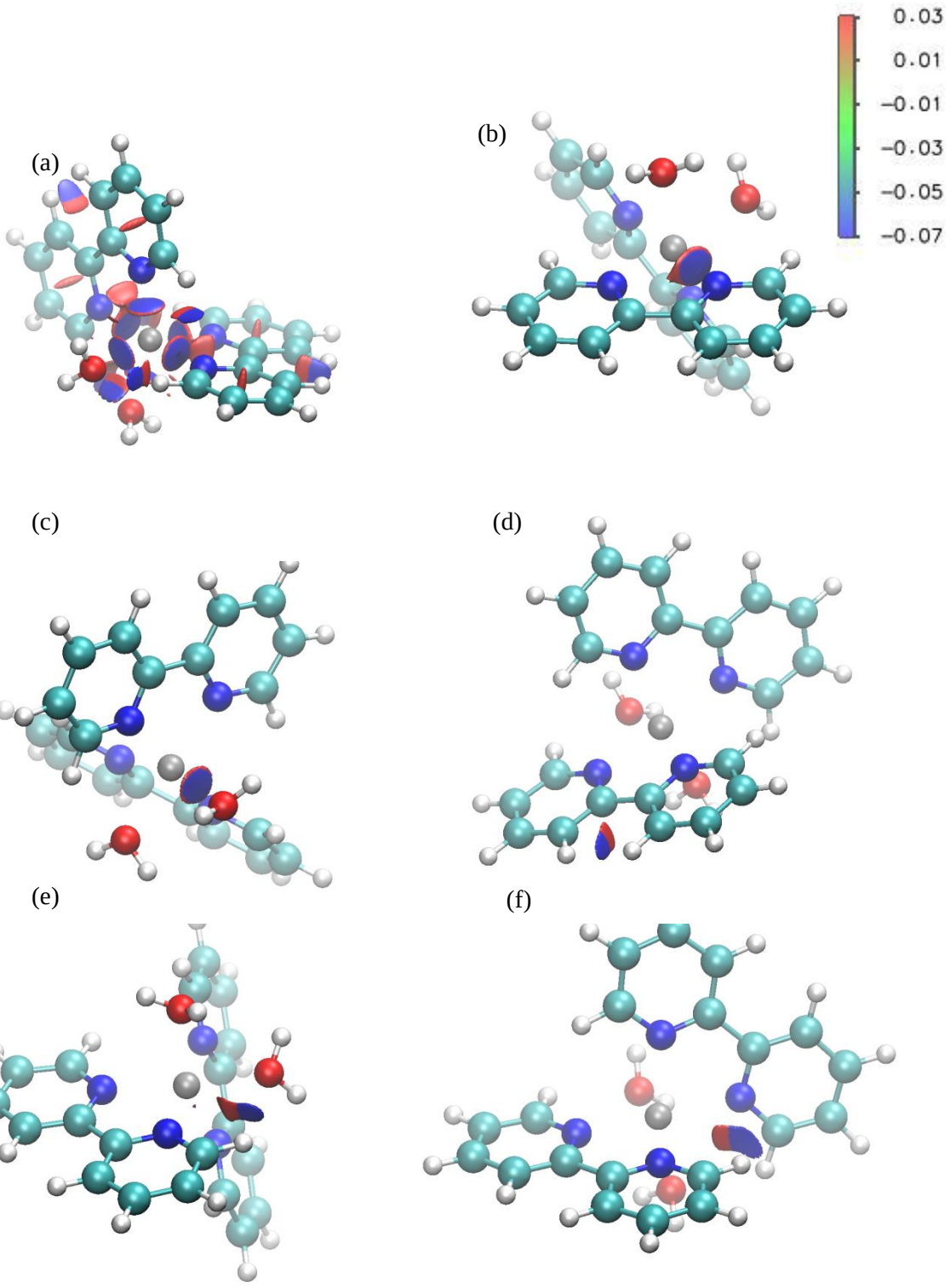

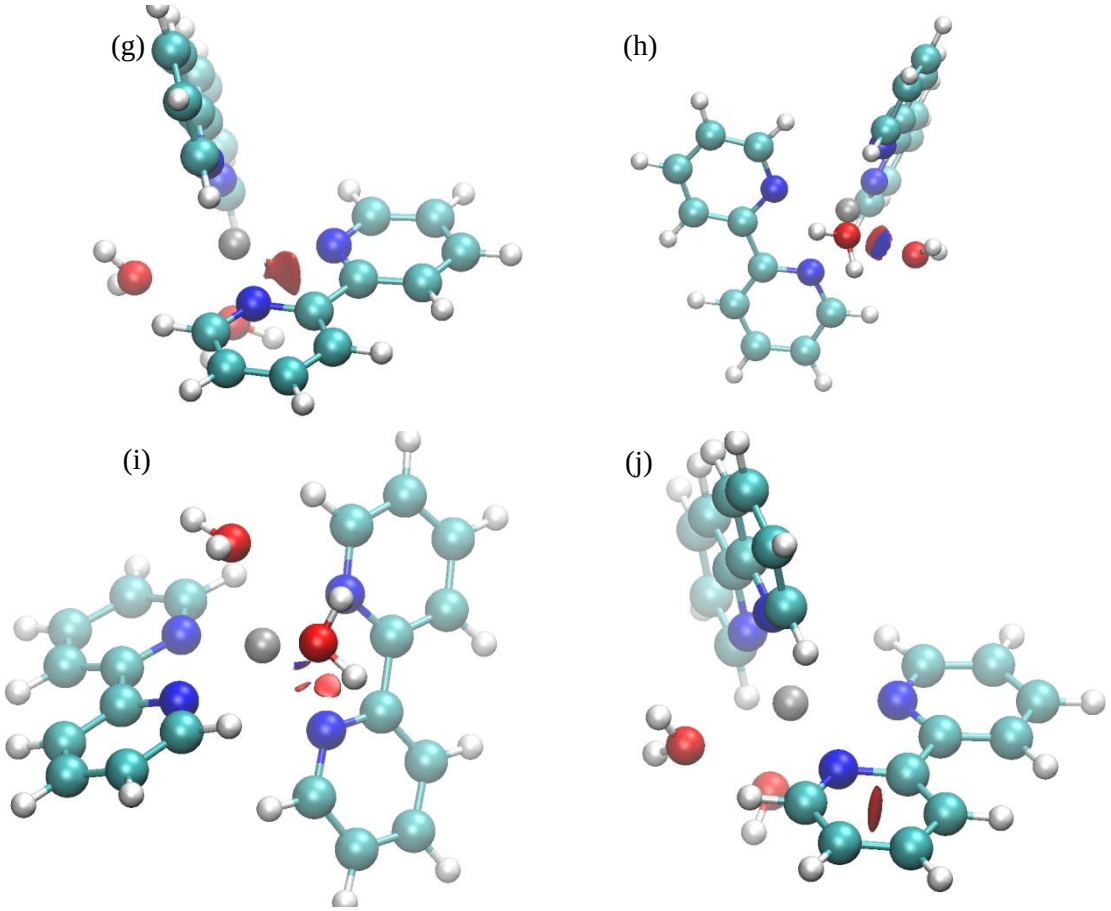

Figure C3. NCI isosurfaces for all the interactions in ZnL_2. (a) All interactions. (b) Zn–N. (c) Zn–O. (d) CH•••HC. (e) CH•••O. (f) CH•••N. (g) N--N. (h) O--O. (i) O--N. (j) Pyridine Ring. The surfaces indicate the reduced density gradient at an isovalue of 0.5 au. The colour scheme used, from blue, through green to red, reflects the following range –0.07 au < sign(λ_2) × ρ < 0.03 au.

(a)

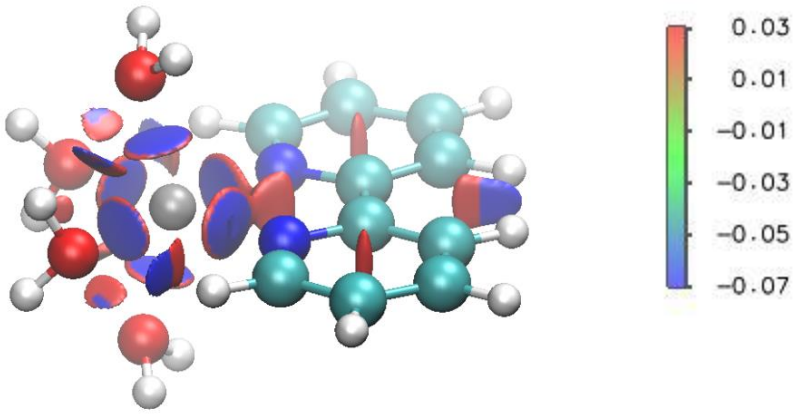

(b)

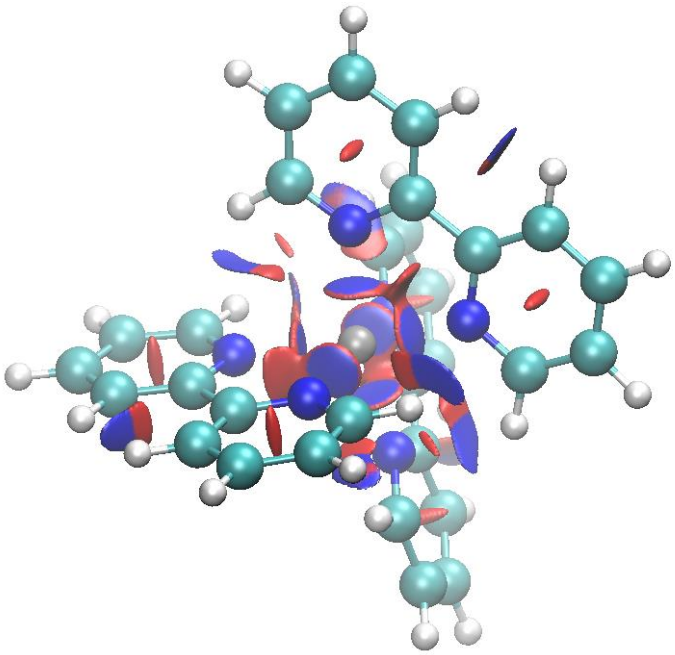

Figure C4. NCI isosurfaces for (a) ZnL and (b) ZnL_3. The surfaces indicate the reduced density gradient at an isovalue of 0.5 au. The colour scheme used, from blue, through green to red, reflects the following range –0.07 au < sign(λ_2) × ρ < 0.03 au.

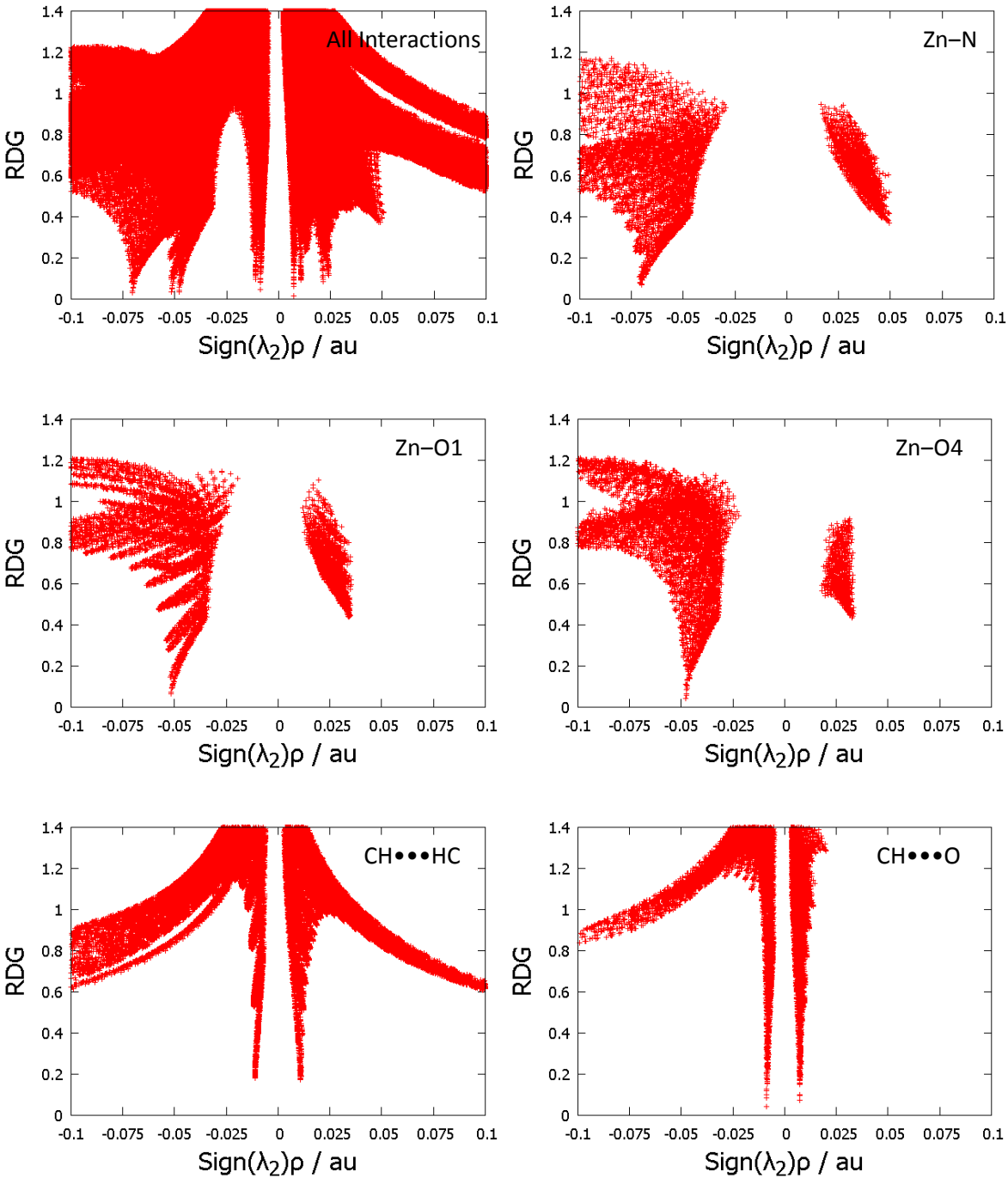

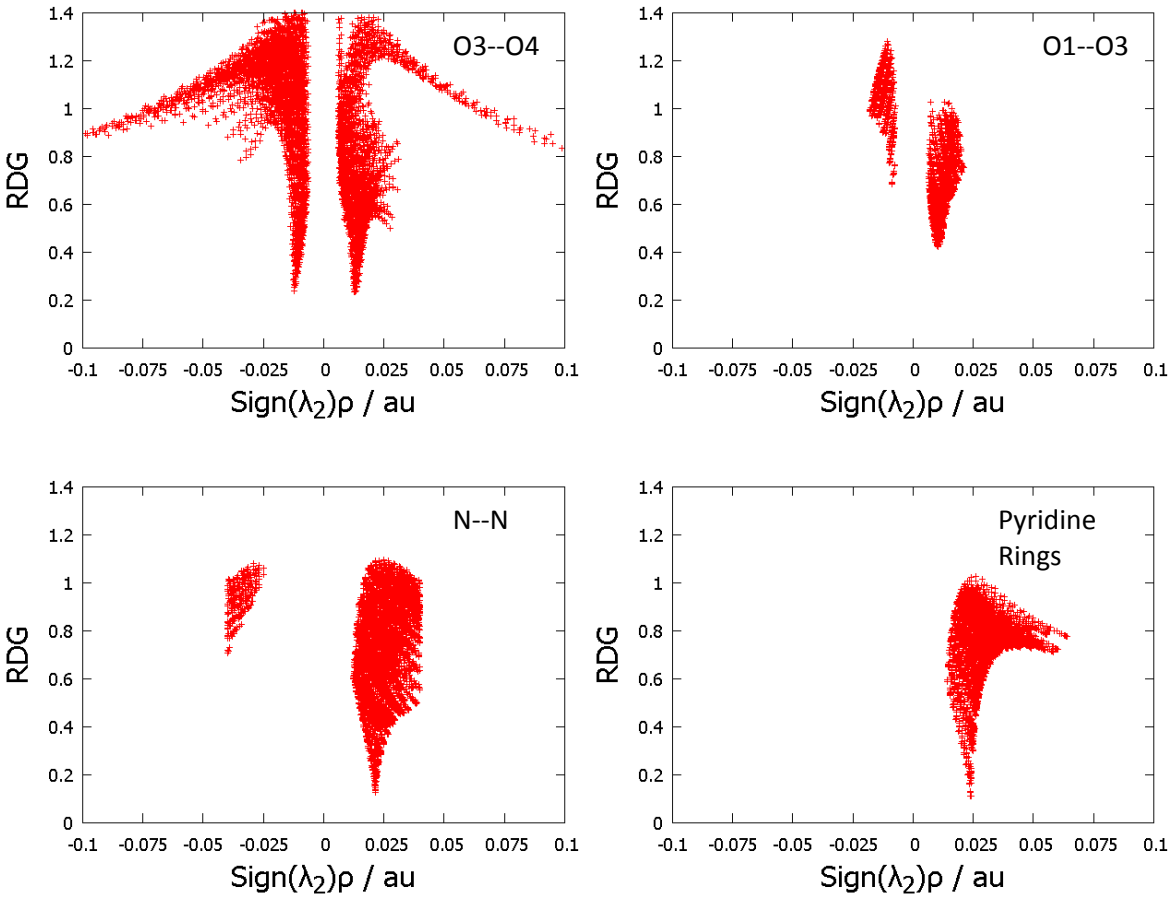

Figure C5. NCI-Plots for interactions in ZnL.

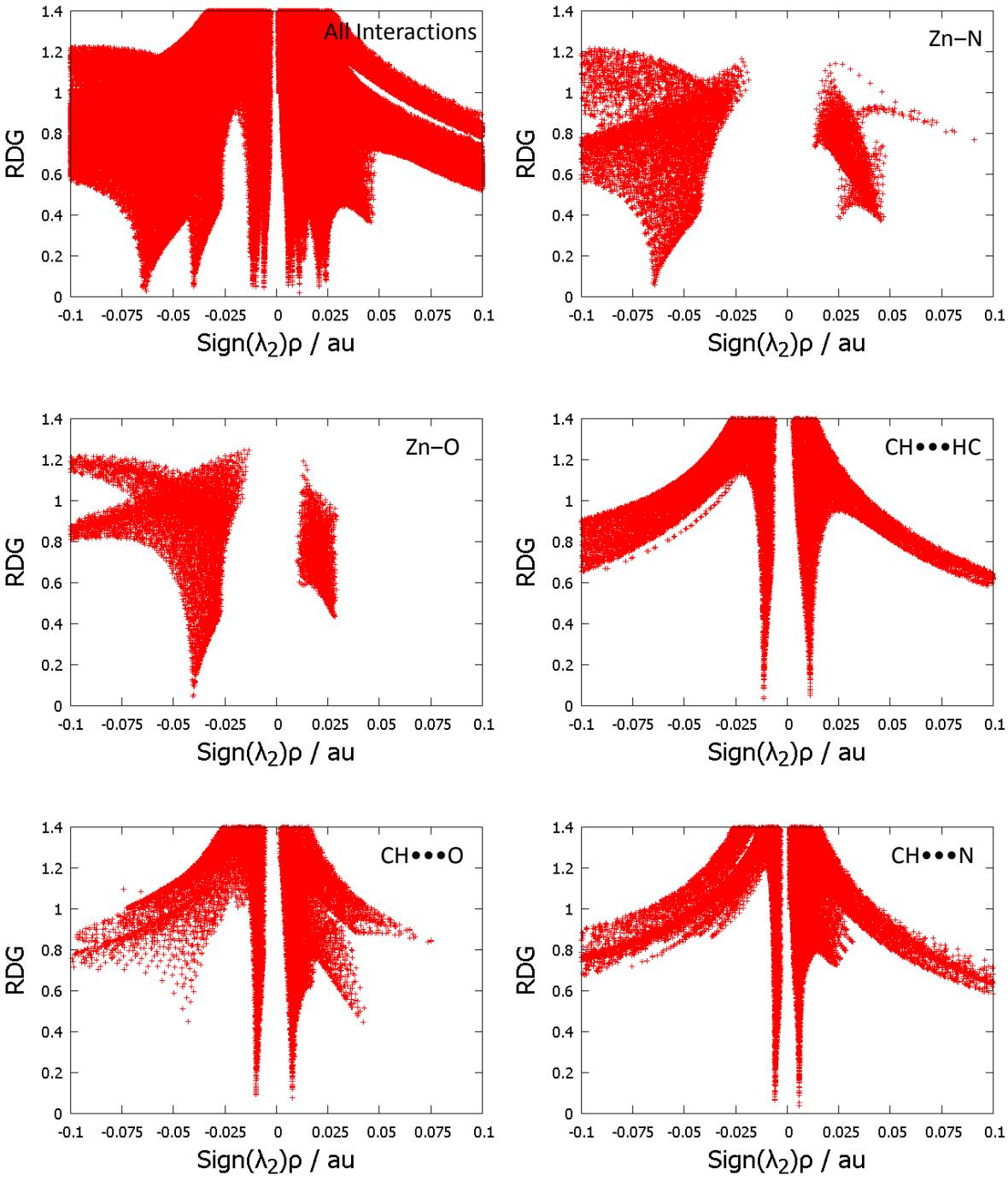

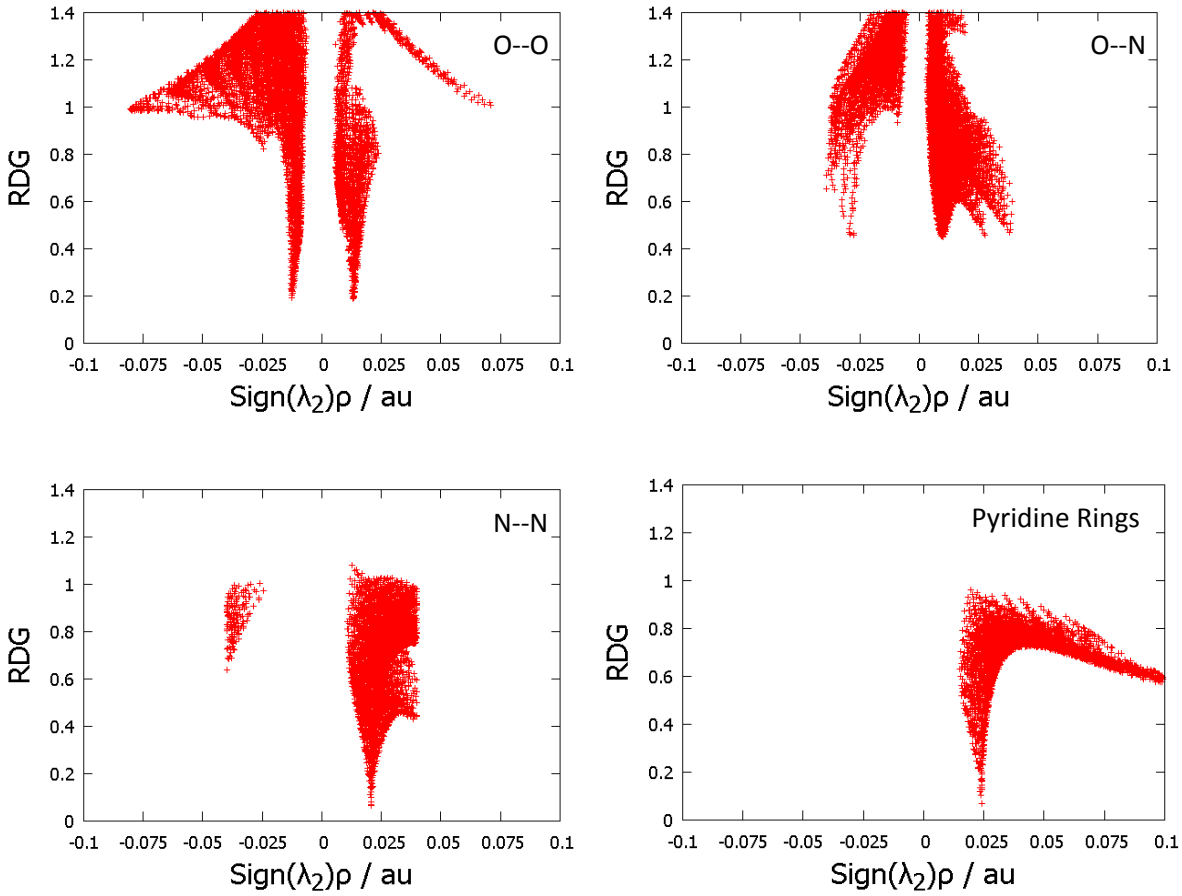

Figure C6. NCIPlots for all interactions in ZnL_2.

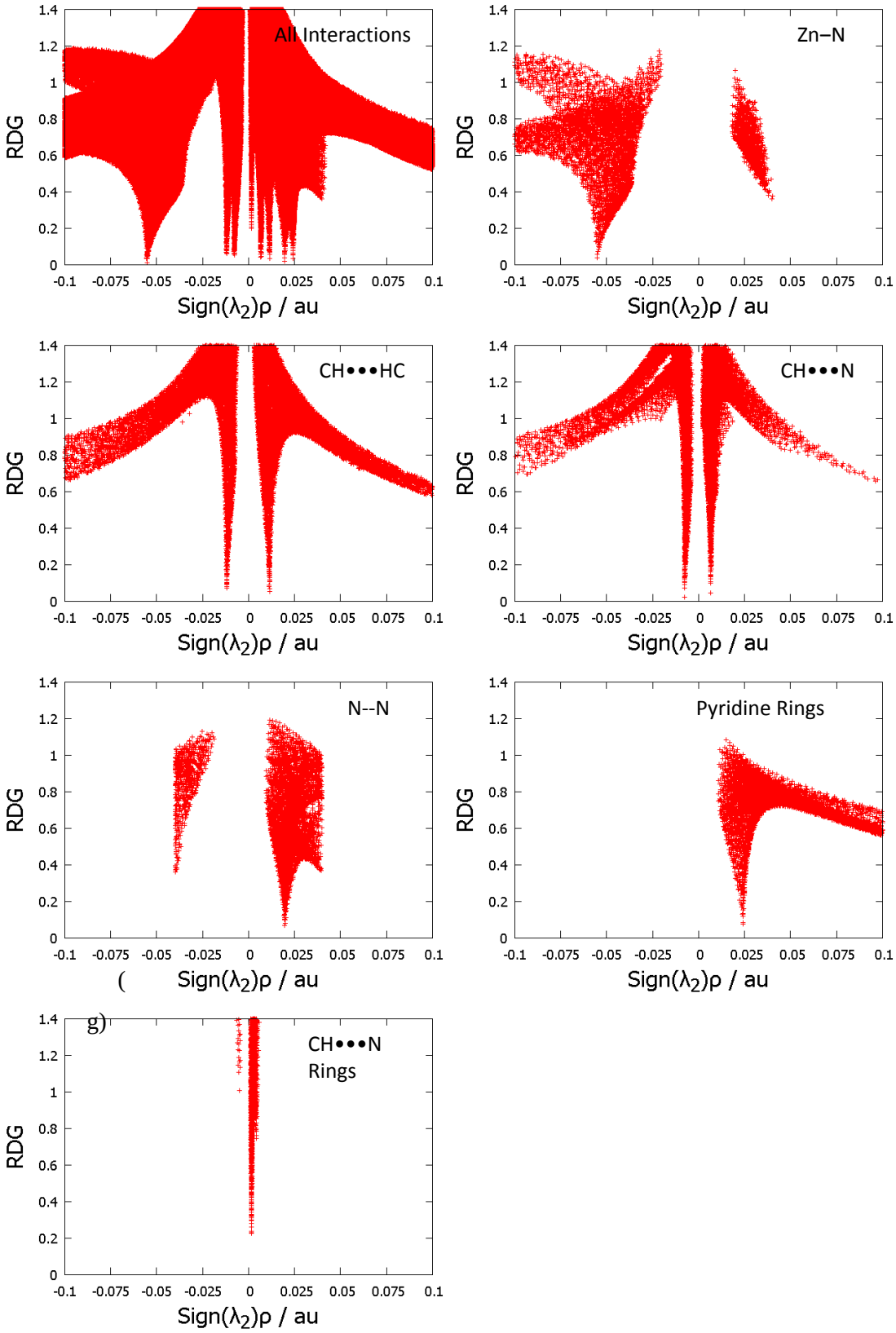

(g)

Figure C7. NCI-Plots for interactions in ZnL_3. .

Table C5. NCI-plot data for ZnL, ZnL_2 and ZnL_3

Complex	Interaction	(–)-ρ_{ICP}(A,B)	(+)-ρ_{ICP}(A,B)
ZnL	Zn–N	-0.07030	
	Zn–O1	-0.05162	
	Zn–O4	-0.04786	
	CH•••HC	-0.01126	0.01084
	CH•••O	-0.00869	0.00736
	N--N		0.02152
	O3--O4	-0.01231	0.01271
	O1--O3		0.01047
	Pyridine Rings		0.02395
ZnL_2	Zn–N	-0.06449	
	Zn–O	-0.04062	
	CH•••HC	-0.01155	0.01104
	CH•••O	-0.01007	0.00768
	CH•••N	-0.00596	0.00580
	N--N		0.02082
	O--O	-0.01267	0.01298
	O--N		0.00959
	Pyridine Rings		0.02398
ZnL_3	Zn–N	-0.05520	
	CH•••HC	-0.01199	0.01134
	CH•••N	-0.00763	0.00663
	N--N		0.01983
	Pyridine Rings		0.02406
	CH•••N Rings		0.00154

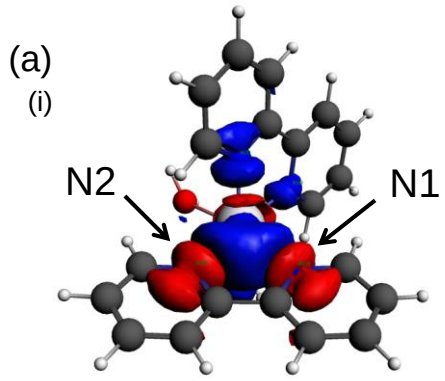

(2)-Bpy

$\Delta\rho_1$; $\Delta E_{orb}(1)$ = -33.23 kcal mol^{-1}

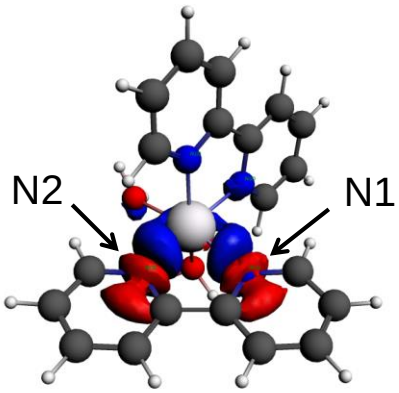

(2)-Bpy

$\Delta\rho_2$; $\Delta E_{orb}(2)$ = -11.61 kcal mol^{-1}

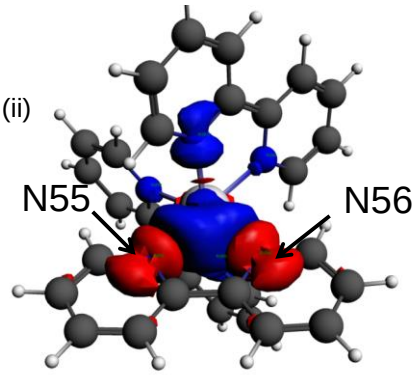

(2)-Bpy

$\Delta\rho_1$; $\Delta E_{orb}(1)$ = -28.62 kcal mol^{-1}

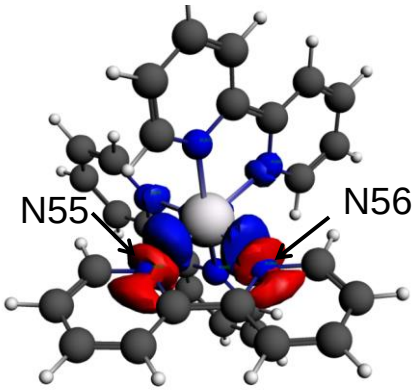

(2)-Bpy

$\Delta\rho_2$; $\Delta E_{orb}(2)$ = -8.80 kcal mol^{-1}

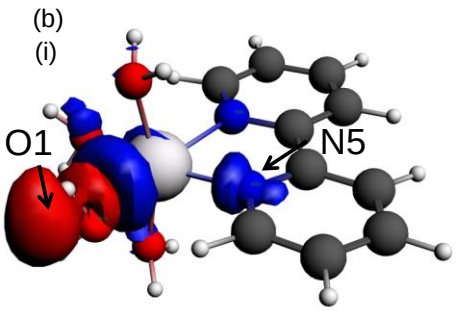

(2)-OH_2

$\Delta\rho_2$; $\Delta E_{orb}(2)$ = -11.78 kcal mol^{-1}

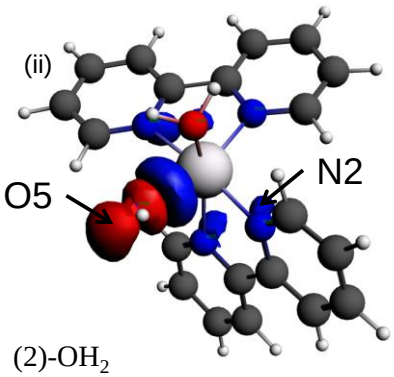

(2)-OH_2

$\Delta\rho_1$; $\Delta E_{orb}(1)$ = -8.62 kcal mol^{-1}

Figure C8. NOCVs for (a) Zn–N bonds in (i) ZnL_2 and (ii) ZnL_3, and (b) Zn–O bonds in (i) ZnL and (ii) ZnL_2.

(i)

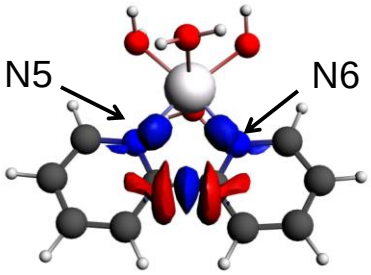

(7)-pyr, α+β

$\Delta\rho_1$; $\Delta E_{orb}(1)$ = -239.547 kcal mol^{-1}

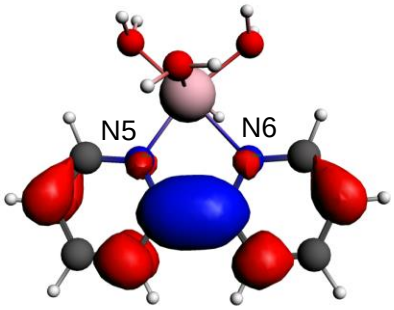

(7)-pyr, α+β

$\Delta\rho_2$; $\Delta E_{orb}(2)$ = -23.98 kcal mol^{-1}

(ii)

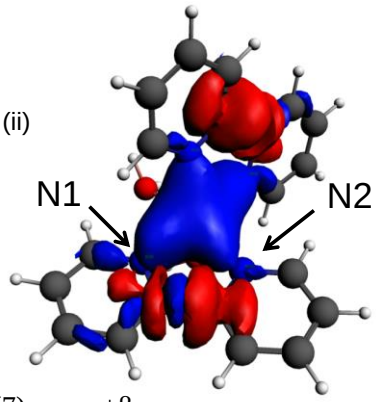

(7)-pyr, α+β

$\Delta\rho_1$; $\Delta E_{orb}(1)$ = -241.14 kcal mol^{-1}

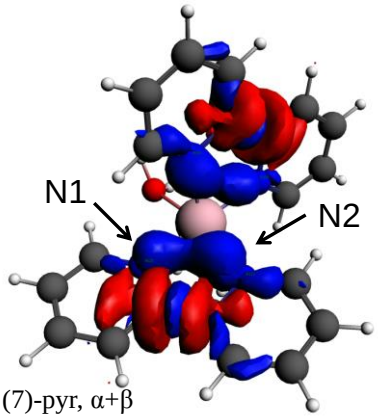

(7)-pyr, α+β

$\Delta\rho_2$; $\Delta E_{orb}(2)$ = -231.46 kcal mol^{-1}

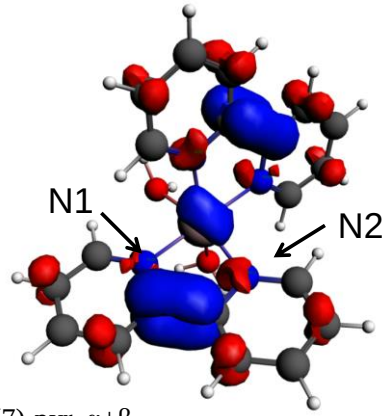

(7)-pyr, α+β

$\Delta\rho_3$; $\Delta E_{orb}(3)$ = -27.22 kcal mol^{-1}

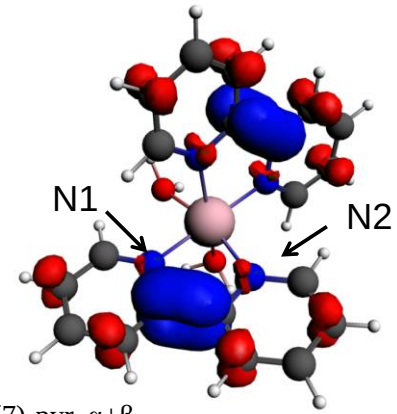

(7)-pyr, α+β

$\Delta\rho_4$; $\Delta E_{orb}(4)$ = -23.24 kcal mol^{-1}

(iii)

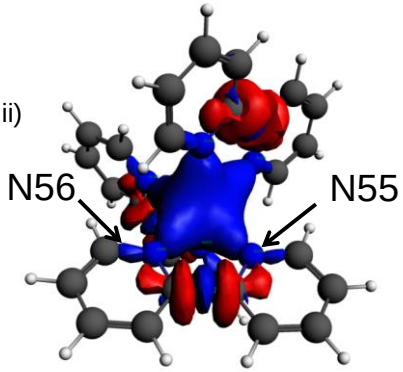

(7)-pyr, α+β

$\Delta\rho_1$; $\Delta E_{orb}(1)$ = -241.54 kcal mol^{-1}

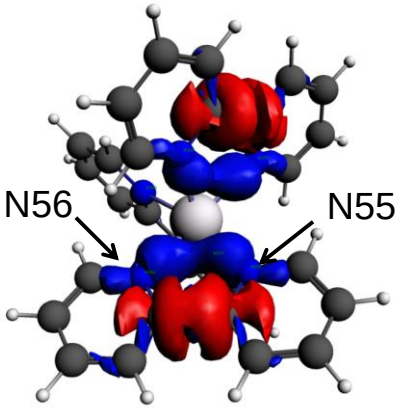

(7)-pyr, α+β

$\Delta\rho_2$; $\Delta E_{orb}(2)$ = -228.60 kcal mol^{-1}

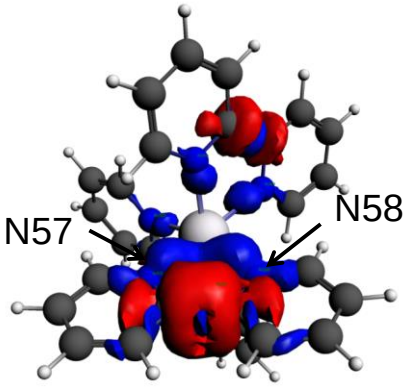

(7)-pyr, α+β

$\Delta\rho_3$; $\Delta E_{orb}(3)$ = -228.57 kcal mol^{-1}

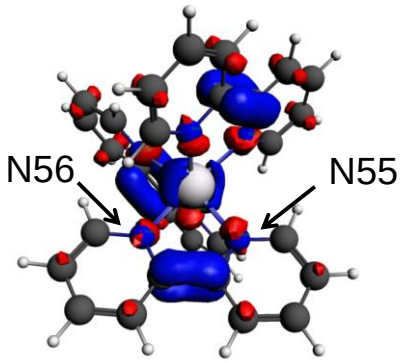

(7)-pyr, α+β

$\Delta\rho_4$; $\Delta E_{orb}(4)$ = -28.75 kcal mol^{-1}

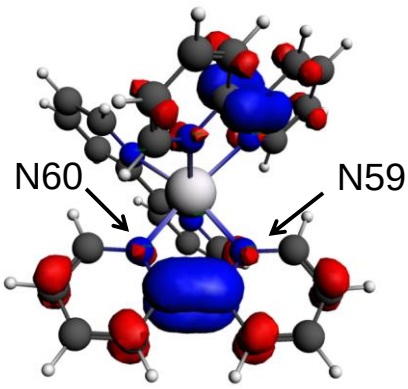

(7)-pyr, α+β

$\Delta\rho_5$; $\Delta E_{orb}(5)$ = -22.79 kcal mol^{-1}

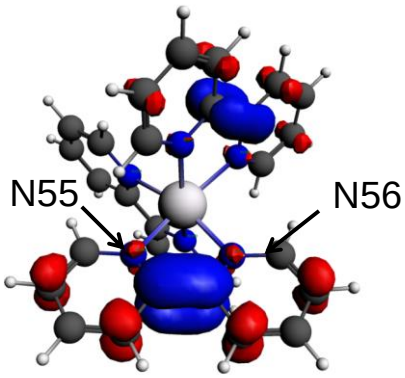

(7)-pyr, α+β

$\Delta\rho_6$; $\Delta E_{orb}(6)$ = -21.19 kcal mol^{-1}

Figure C9. NOCV deformation densities for C–C bonds in (i) ZnL, (ii) ZnL_2 and (iii) ZnL_3

(a)

(i)

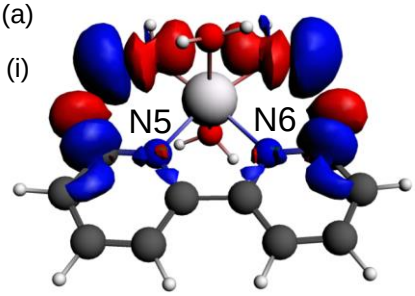

(2)-Bpy

$\Delta\rho_{12}$; $\Delta E_{orb}(12)$ = -1.82 kcal mol^{-1}

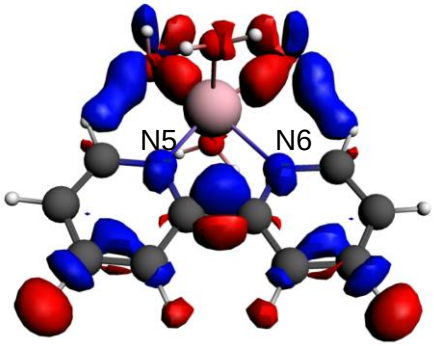

(2)-Bpy

$\Delta\rho_{14}$; $\Delta E_{orb}(14)$ = -0.77 kcal mol^{-1}

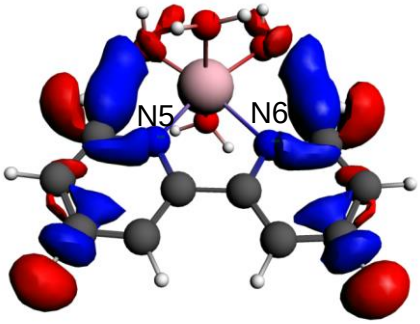

(2)-Bpy

$\Delta\rho_{16}$; $\Delta E_{orb}(16)$ = -0.38 kcal mol^{-1}

(ii)

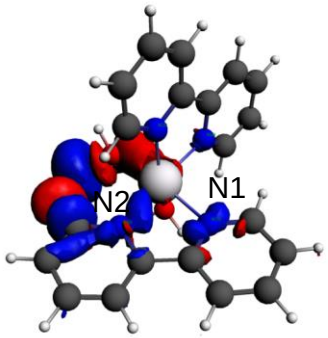

(2)-Bpy

$\Delta\rho_{15}$; $\Delta E_{orb}(15)$ = -1.11 kcal mol^{-1}

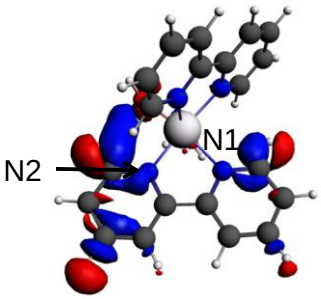

(2)-Bpy

$\Delta\rho_{18}$; $\Delta E_{orb}(18)$ = -0.28 kcal mol^{-1}

(b)

(i)

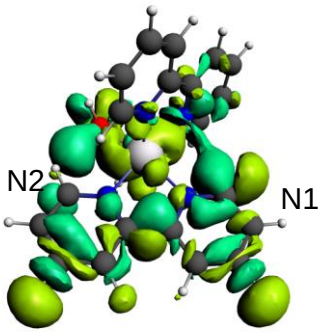

(2)-Bpy

$\Delta\rho_{17}$; $\Delta E_{orb}(17)$ = -0.58 kcal mol^{-1}

(c)

(i)

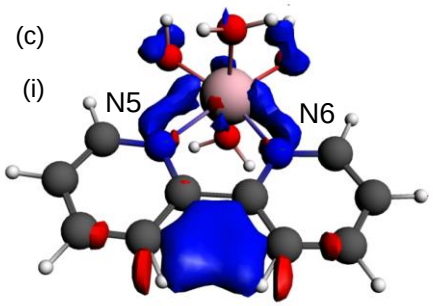

(7)-pyr, α+β

$\Delta\rho_{21}$; $\Delta E_{orb}(21)$ = -2.45 kcal mol^{-1}

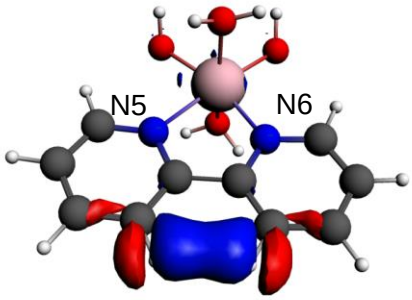

(7)-pyr, α+β

$\Delta\rho_{23}$; $\Delta E_{orb}(23)$ = -1.81 kcal mol^{-1}

(ii)

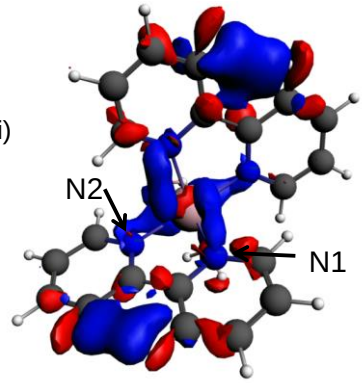

(7)-pyr, α+β

$\Delta\rho_{23}$; $\Delta E_{orb}(23)$ = -2.42 kcal mol^{-1}

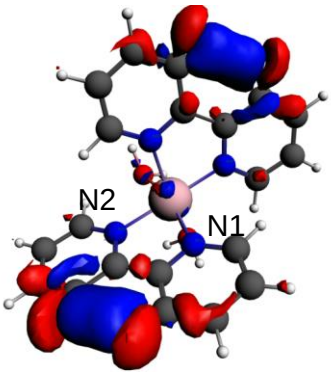

(7)-pyr, α+β

$\Delta\rho_{25}$; $\Delta E_{orb}(25)$ = -1.43 kcal mol^{-1}

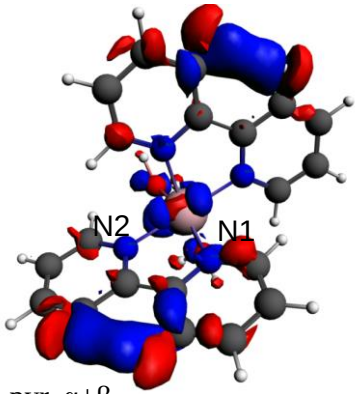

(7)-pyr, α+β

$\Delta\rho_{26}$; $\Delta E_{orb}(26)$ = -1.71 kcal mol^{-1}

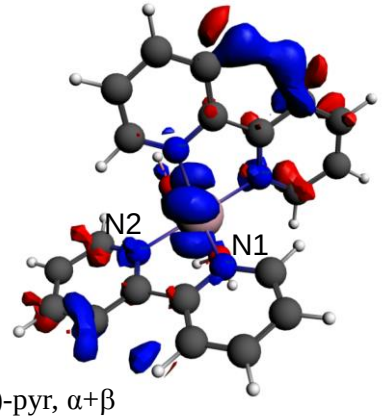

(7)-pyr, α+β

$\Delta\rho_{27}$; $\Delta E_{orb}(27)$ = -2.74 kcal mol^{-1}

(iii)

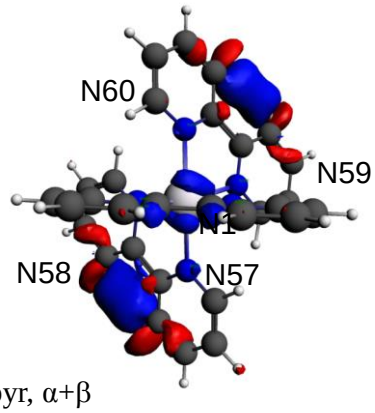

(7)-pyr, α+β

$\Delta\rho_{26}$; $\Delta E_{orb}(26)$ = -2.04 kcal mol^{-1}

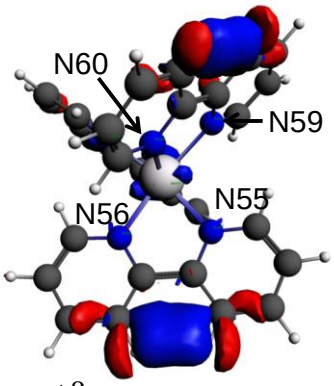

(7)-pyr, α+β

$\Delta\rho_{27}$; $\Delta E_{orb}(27)$ = -2.04 kcal mol^{-1}

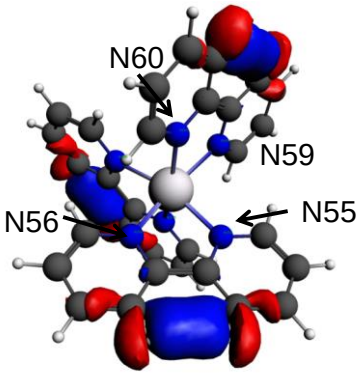

(7)-pyr, α+β

$\Delta\rho_{28}$; $\Delta E_{orb}(28)$ = -1.31 kcal mol^{-1}

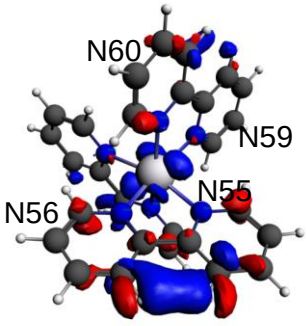

(7)-pyr, α+β

$\Delta\rho_{29}$; $\Delta E_{orb}(29)$ = -2.42 kcal mol^{-1}

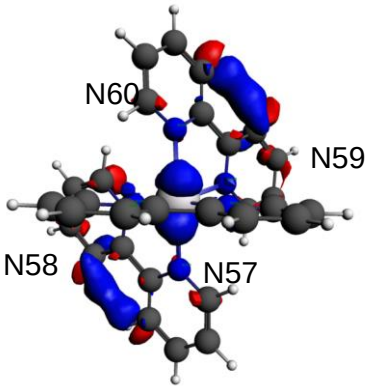

(7)-pyr, α+β

$\Delta\rho_{30}$; $\Delta E_{orb}(30)$ = -2.60 kcal mol^{-1}

Figure C10. NOCV deformation densities for (a) CH•••O interactions in (i) ZnL and (ii) ZnL_2, (b) CH•••N interactions for ZnL_2, and (c) CH•••HC interactions for (i) ZnL, (ii) ZnL_2 and (iii) ZnL_3

Table C6. NOCVs describing all interactions in all ZnBPy complexes

Complex	Structural Bonds					Intramolecular interactions				
	Bond	**Scheme**	***k***	**|Eigenvalue|** *(au)*	**ΔE_{orb}^{k}** *(kcal·mol^{-1})*	**Interaction**	**Scheme**	***k***	**|Eigenvalue|** *(au)*	**ΔE_{orb}^{k}** *(kcal·mol^{-1})*
ZnL	Zn–N	(2)-BPy	1	0.43715	-37.69	CH•••HC	(7)-Pyr	21	0.06034	-2.45
			2	0.23906	-14.31			23	0.05304	-1.81
	Zn–O1	(2)-OH_2	1	0.26448	-11.78	CH•••O	(2)-BPy	12	0.06581	-1.82
	Zn–O2	(2)-OH_2	1	0.26261	-10.88			14	0.04664	-0.77
	Zn–O3	(2)-OH_2	1	0.26408	-11.78			16	0.04114	-0.38
	Zn–O4	(2)-OH_2	1	0.26296	-10.88					
	C–C	(7)-Pyr	1	1.10324	-239.55					
			2	0.38952	-23.98					
ZnL_2	Zn–N1/N2	(2)-BPy	1	0.44706	-33.23	CH•••HC	(7)-Pyr	23	0.05881	-2.42
			2	0.23805	-11.61			25	0.05533	-1.43
	Zn–N3/N4	(2)-BPy	1	0.44758	-33.37			26	0.05307	-1.71
			2	0.23803	-11.64			27	0.05101	-2.74
	Zn–O5	(2)-OH_2	1	0.23801	-8.62	CH•••O (N1/N2)	(2)-BPy	15	0.05571	-1.11
	Zn–O6	(2)-OH_2	1	0.237	-8.53			18	0.0419	-0.28
	C–C	(7)-Pyr	1	1.10164	-241.14	CH•••O (N3/N4)	(2)-BPy	15	0.05595	-1.13
			2	1.0962	-231.46			18	0.04209	-0.26
			3	0.38961	-27.22					
			4	0.38654	-23.24	CH•••N (N1/N2)	(2)-BPy	17	0.04667	-0.58
						CH•••N (N3/N4)	(2)-BPy	17	0.04664	-0.58

Complex	Structural Bonds					Intramolecular interactions				
	Bond	**Scheme**	***k***	**|Eigenvalue|** *(au)*	**ΔE_{orb}^{k}** *(kcal·mol^{-1})*	**Interaction**	**Scheme**	***k***	**|Eigenvalue|** *(au)*	**ΔE_{orb}^{k}** *(kcal·mol^{-1})*
ZnL_3	Zn–N55/N56	(2)-BPy	1	0.42853	-28.62	CH•••HC	(7)-Pyr	26	0.05804	-2.04
			2	0.21834	-8.80			27	0.05793	-2.04
	Zn–N57/N58	(2)-BPy	1	-0.42898	-28.64			28	0.05604	-1.31
			2	-0.21828	-8.77			29	0.05427	-2.42
	Zn–N59/N60	(2)-BPy	1	0.42872	-28.62			30	0.05397	-2.60
			2	0.21819	-8.76					
	C–C	(7)-Pyr	1	1.10	-241.54					
			2	1.09	-228.60					
			3	1.09	-228.57					
			4	0.38	-28.75					
			5	0.38	-22.79					
			6	0.38	-21.19					

Table C7. Calculating ΔE_{orb}^{I} for CH•••HC interactions

	NOCV Pair	**ΔE_{orb}^{k}** *(kcal mol^{-1})*	**# Bonds**	**Averaged (ΔE_{orb}^{k}/#Bonds)**
ZnL	21	-2.45	1	-2.45
	23	-1.81	1	-1.81
	sum	*-4.27*		*-4.27*
ZnL_2	23	-2.42	2	-1.21
	25	-1.43	2	-0.72
	26	-1.71	2	-0.86
	27	-2.74	1	-2.74
	sum	*-8.30*		*-5.52*
ZnL_3	26A	-1.02	*2*	-0.51
	27A	-1.02	*2*	-0.51
	28A	-0.65	*3*	-0.22
	29A	-1.22	*1*	-1.22
	30A	-1.29	*2*	-0.65
	26B	-1.02	*1*	-1.02
	27B	-1.02	*2*	-0.51
	28B	-0.65	*3*	-0.22
	29B	-1.20	*1*	-1.20
	30B	-1.30	*1*	-1.30
	sum	*-10.41*		*-7.36*

Table C8. Calculating ΔE_{orb}^{I} for CH•••O interactions

	NOCV Pair	**ΔE_{orb}^{k}** *(kcal mol^{-1})*	**# Bonds**	**Averaged (ΔE_{orb}^{k}/#Bonds)**
ZnL	12	-1.82	2	-0.91
	14	-0.77	2	-0.38
	16	-0.38	2	-0.19
	sum	*-2.96*		*-1.48*
ZnL_2	15	-1.11	1	-1.11
N1-N2	17	-0.58	2	-0.29
	18	-0.28	1	-0.28
	sum	*-1.97*		*-1.68*
ZnL_2	15	-1.13	1	-1.13
N3-N4	17	-0.58	2	-0.29
	18	-0.26	1	-0.26
	sum	*-1.97*		*-1.68*

Appendix D.

Preorganization of 2,2′-Bipyridine for complex-formation with Ni^{II}.

In order to coordinate to a metal in a bidentate fashion, L must twist around the junction C2–C2′ bond from the lowest energy *s*-trans to a higher energy conformer with 1,1′ nitrogens cis towards each other. As was mentioned already, the N--N and CH•••HC interactions formed in this way were used to explain trends in formation constants as it was believed that these interactions are destabilizing[1–5]. In this section we will compare the ligand *as it exists in Ni-complexes* with the lowest energy *s*-trans conformer, in order to elucidate whether the N--N or CH•••HC interactions are responsible for the destabilization due to preorganization. In addition, the changes in atomic properties when going from the preorganized L(*as in complex)* to ML_n will be studied to further elucidate the changes the ligand must undergo (including formation of CH•••O and CH•••N interactions) when forming complexes with Ni^{II}.

In this section, QTAIM-defined atomic energies and charges will be used in a comparative basis. The atomic energies, as defined by the virial theorem for a subsystem bounded by zero-flux surfaces in the electron density, can be used to estimate the relative stabilization or destabilization of a bound atom in comparison to a free atom. For an atom involved in an intramolecular or intermolecular bond, it is possible to estimate the atomic stabilization due to formation of the bond by comparing the atomic energies of an atom involved in the bond with a non-bonded reference atom, identical or similar to the bonded atom. In order to correctly and accurately estimate the atomic stabilization or destabilization it is a necessary and critical condition that the reference atom is in a very similar chemical environment as the bonded atom. This condition unfortunately is not always easily met and the task of finding a suitable reference atom becomes a formidable one. For instance, different hydrogens on each ring of the *s*-trans conformer of L have considerably different atomic energies and cannot be used as reference atoms to each other unless very careful considerations are taken. Therefore, we will restrict our analysis to comparing atoms in the same position on L with each other, i.e. comparing H4 (as indicated in Figure 5.3). in *s*-trans with H4 in L*(As in Complex, NiL)* with H13 or H21 in NiL (as indicated in Figure 5.2).

L(*As in Complex)* Atomic Properties. The strain energy of the ligand, calculated as the difference between a single point calculation of each form of L(*as in complex)* and the molecular energy of the lowest energy conformer of L, *s*-trans, is shown in Table D1. The ligand is the most strained in NiL with a strain energy of +5.51 $kcal \cdot mol^{-1}$ higher than the free

energy of *s*-trans. The strain energy is 0.44 kcal·mol^{-1} lower in NiL_3 with a free energy difference of 5.07 kcal·mol^{-1}.

Table D1. Strain energies of L, as it exists in aqueous complexes with Ni^{II}.

	Average Strain Energy	
	E(ZPVE) kcal·mol^{-1}	**$G_{(aq)}$** kcal·mol^{-1}
NiL	4.87	5.51
NiL_2	4.61	5.26
NiL_3	4.40	5.07

The change in atomic energies of L(*as in complex*) relative to equivalent atoms in the *s*-trans conformer of L is given in Table D2. The only atoms significantly destabilized when L(*trans*) rearranges to L(*as in complex*) are the nitrogen atoms, by +20.99 kcal·mol^{-1} in L(*in NiL*) and +21.81 kcal·mol^{-1} in L(*in NiL_3*). All other atoms are stabilized or do not change significantly. This result is expected when it is realized that the nitrogen atoms are necessarily close to each other in order to bind in a bidentate fashion to Ni. All other atoms follow the same general trend as that seen L(*cis*) relative to L(*trans*), with the exception of C2, the carbon atom involved in the bridging C–C bond between pyridyl rings. In L(*cis*), the C–C bond lengthens from its equilibrium value of 1.492 Å in L(*trans*) to 1.500 Å. However, in $Ni(BPy)^{2+}$ complexes the C–C bond length remains relatively constant at 1.484 Å and consequently C2 is stabilized relative to C2 in L(*trans*). In addition, **H3** and **H3′** are stabilized by an average of –8 kcal·mol^{-1} each, which is comparable with **H3** in L(*cis*). This observation is discussed later in this Appendix. Lastly, it must be pointed out that all other changes in the atomic energies of hydrogens are within the range of –1 kcal·mol^{-1}.

The change in atomic charges, $q(\Omega)$, of L(*As in complex*) relative to L(*trans*) is shown in Table D3. The largest changes in $q(\Omega)$ are again seen for N and **H3** atoms. The net charge of N atoms increases significantly from those in L(*trans*), becoming increasingly positive and thus losing electrons. $q(\Omega)$ decreases significantly in C2 in the pre-organized ligands, as well as in H3, showing that these atoms have an increased electron population relative to L(*trans*). The net charges of all the other atoms change insignificantly in the 3rd decimal place or

Table D2 Atomic energies of L(*as in complex*) relative to L(*trans*)

	Ring 1 (*kcal mol^{-1}*)										
	N1	C6	C5	C4	C3	C2	**H6**	H5	H4	**H3**	**Sum**
L in NiL: N6 (CH—O)	20.99	-2.35	-3.34	1.94	0.21	-5.07	-0.52	-1.30	-0.03	-7.97	2.57
L in NiL$_2$: N2 (CH—N)	21.88	-2.89	-3.86	1.23	-0.02	-4.47	-0.99	-1.21	0.03	-8.21	1.50
L in NiL$_2$: N4 (CH—N)	21.87	-2.98	-3.90	1.21	-0.06	-4.37	-1.00	-1.19	0.03	-8.22	1.38
L in NiL$_3$: N2 (CH—N)	21.55	-3.34	-3.39	1.21	0.10	-3.49	-1.25	-1.06	0.13	-8.32	2.14
L in NiL$_3$: N3 (CH—N)	22.11	-3.33	-3.47	0.99	0.00	-3.47	-1.14	-1.02	0.10	-8.29	2.49
L in NiL$_3$: N34 (CH—N)	21.81	-3.33	-3.42	1.08	0.09	-3.45	-1.22	-1.04	0.09	-8.30	2.31
L(cis)	3.92	-0.52	-2.26	-1.32	0.50	10.19	-0.37	0.33	0.39	-8.88	1.98

	Ring2 (*kcal mol^{-1}*)										
	N1′	C6′	C5′	C4′	C3′	C2′	**H6′**	H5′	H4′	**H3′**	**Sum**
L in NiL: N7 (CH—O)	20.94	-2.35	-3.31	1.88	0.15	-5.00	-0.52	-1.32	-0.05	-7.99	2.43
L in NiL$_2$: N3 (CH—O)	22.73	-3.16	-3.13	1.54	-0.02	-4.55	-0.82	-1.18	0.07	-8.23	3.25
L in NiL$_2$: N5 (CH—O)	22.74	-3.19	-3.18	1.55	0.00	-4.42	-0.81	-1.19	0.10	-8.23	3.37
L in NiL$_3$: N23 (CH—N)	22.00	-3.29	-3.43	1.05	0.02	-3.50	-1.17	-1.06	0.08	-8.29	2.40
L in NiL$_3$: N24 (CH—N)	21.92	-3.52	-3.52	1.07	0.03	-3.50	-1.25	-1.02	0.12	-8.29	2.05
L in NiL$_3$: N45 (CH—N)	22.01	-3.43	-3.56	1.03	0.09	-3.47	-1.23	-1.07	0.11	-8.27	2.22
L(cis)	3.92	-0.52	-2.26	-1.32	0.50	10.19	-0.37	0.33	0.39	-8.88	1.98

Table D3. Atomic net charges, q(A), relative to L(*trans*)

	Ring 1 (*au*)										
	N1	C6	C5	C4	C3	C2	**H6**	H5	H4	**H3**	**Sum**
L in NiL: N6 (CH—O)	0.03688	-0.00364	0.00223	0.00403	0.00101	-0.01463	0.00178	-0.00303	0.00144	-0.02619	-0.00011
L in NiL$_2$: N2 (CH—N)	0.03683	-0.00256	0.00184	0.00389	0.00062	-0.01397	0.00043	-0.00271	0.00153	-0.02632	-0.00042
L in NiL$_2$: N4 (CH—N)	0.03674	-0.00274	0.00186	0.00391	0.00064	-0.01374	0.00045	-0.00273	0.00152	-0.02634	-0.00042
L in NiL$_3$: N2 (CH—N)	0.03575	-0.00358	0.00187	0.00388	0.00030	-0.01182	-0.00008	-0.00231	0.00176	-0.02617	-0.00041
L in NiL$_3$: N3 (CH—N)	0.03621	-0.00381	0.00185	0.00389	0.00032	-0.01228	0.00009	-0.00231	0.00170	-0.02611	-0.00044
L in NiL$_3$: N34 (CH—N)	0.03599	-0.00367	0.00184	0.00390	0.00030	-0.01201	-0.00001	-0.00231	0.00170	-0.02611	-0.00038
L(cis)	0.01535	0.00378	0.00072	0.00291	-0.00272	0.00357	-0.00119	0.00113	0.00203	-0.02590	-0.00032

	Ring2 (*au*)										
	N1′	C6′	C5′	C4′	C3′	C2′	**H6′**	H5′	H4′	**H3′**	**Sum**
L in NiL: N7 (CH—O)	0.03681	-0.00369	0.00222	0.00408	0.00104	-0.01453	0.00177	-0.00304	0.00140	-0.02623	-0.00016
L in NiL$_2$: N3 (CH—O)	0.03811	-0.00526	0.00212	0.00416	0.00075	-0.01383	0.00119	-0.00270	0.00169	-0.02630	-0.00007
L in NiL$_2$: N5 (CH—O)	0.03806	-0.00538	0.00216	0.00412	0.00075	-0.01369	0.00122	-0.00273	0.00171	-0.02629	-0.00006
L in NiL$_3$: N23 (CH—N)	0.03608	-0.00389	0.00188	0.00390	0.00027	-0.01194	0.00006	-0.00235	0.00168	-0.02614	-0.00046
L in NiL$_3$: N24 (CH—N)	0.03612	-0.00377	0.00190	0.00389	0.00032	-0.01210	-0.00005	-0.00229	0.00175	-0.02613	-0.00038
L in NiL$_3$: N45 (CH—N)	0.03614	-0.00377	0.00191	0.00388	0.00028	-0.01213	-0.00001	-0.00236	0.00171	-0.02609	-0.00044
L(cis)	0.01535	0.00379	0.00072	0.00291	-0.00272	0.00357	-0.00119	0.00113	0.00203	-0.02590	-0.00032

lower. Atomic charges therefore follow the atomic energies - where an outflow of electrons is seen (i.e. for N1), the atom is destabilized, and where an inflow of electrons is seen (i.e. for C2 or **H3**) the corresponding atoms are stabilized.

It is thus clear that the strain caused by preorganization of L before complexation is entirely localized to the N atoms, and can be rationalized by the formation of a repulsive N--N (lone-pair-lone-pair) interaction - a hypothesis supported by the outflow of atomic electron density. On the other hand, the supposedly clashing hydrogens, 3,3′-H atoms, are in fact significantly stabilized when the CH•••HC interaction is formed, accompanied by an inflow of electron density. Very interesting is the comparison of L(*cis*) to L(*As in Complex*). In the atomic energy analysis of L(*cis*) relative to L(*trans*), the strain is mostly localized to the 2,2′-carbon atoms - an energy difference of +10.92 kcal·mol^{-1} is seen. However, as we have just shown, these atoms are stabilized in L(*As in complex)*, and the strain is shifted to the N-atoms - C2 is stabilized by –5.07 kcal·mol^{-1} in L(*As in NiL*) relative to L(*trans*). The changes in the atomic energies of 3,3′-hydrogens remain relatively similar - –7.97 kcal·mol^{-1} in L(*in ML*) and –8.88 kcal·mol^{-1} in L(*cis*). Clearly, 3,3′-H atoms cannot be used to explain the strain in the preorganization of L.

Next we investigate the changes in atomic energies and charges when L(*As in complex*) coordinates to Ni to form the various NiL_n structures Table D4 shows the changes in atomic energies of ligand atoms in Ni complexes, relative to the same atoms in equivalent L(*As in complex*) structures. It is very important to note that every atom increases tremendously in energy. The carbon atoms of each BPy molecule are destabilized the most, with an average increase in carbon atomic energy of +56.84 kcal·mol^{-1} in NiL, +48.96 kcal·mol^{-1} in NiL_2, and +42.73 kcal·mol^{-1} in NiL_3. The nitrogen atoms show a much smaller change due to the formation of Ni–N bonds - an average increase of +10.68 kcal·mol^{-1} in NiL, +3.37 kcal·mol^{-1} in NiL_2 and an average decrease of –1.10 kcal·mol^{-1} in NiL_3. It is interesting to observe that the largest destabilizations in N-atoms occur in NiL, where the Ni–N bonds are the strongest, correlating qualitatively with the partly electrostatic nature of the Ni–N coordination bond. It also indicates that the ligand is the most strained in NiL. Hydrogen atoms follow the same general trend, with the largest destabilizations

Table D4. Comparison of ΔE(A) in complexes relative to L(*As in Complex*)

	Ring 1 *(kcal mol^{-1})*										
	N1	C6	C5	C4	C3	C2	**H6**	H5	H4	**H3**	**Sum**
ML (CH—O)	10.64	49.90	62.98	54.89	61.92	54.53	**13.92**	8.46	7.32	8.37	332.94
ML2: N2 (CH—N)	4.76	44.57	54.93	47.21	53.45	47.12	**8.96**	7.89	6.76	7.73	283.37
ML2: N4 (CH—N)	4.69	44.66	54.98	47.24	53.49	47.03	**8.99**	7.88	6.76	7.74	283.47
ML3: N2 (CH—N)	-1.21	37.71	47.88	40.89	46.43	40.52	8.00	7.16	6.10	6.94	240.42
ML3: N3 (CH—N)	-1.03	37.81	47.88	40.97	46.53	40.60	8.06	7.11	6.13	7.00	241.06
ML3: N34 (CH—N)	-0.93	37.74	47.86	40.97	46.47	40.45	7.97	7.14	6.16	6.97	240.78

	Ring2 *(kcal mol^{-1})*										
	N1′	C6′	C5′	C4′	C3′	C2′	**H6′**	H5′	H4′	**H3′**	**Sum**
ML (CH—O)	10.72	49.86	62.92	54.94	61.98	54.49	**13.93**	8.48	7.35	8.40	333.08
ML2: N3 (CH—O)	2.01	41.40	54.04	46.96	53.31	46.52	**12.82**	7.66	6.63	7.65	279.00
ML2: N5 (CH—O)	2.01	41.47	54.09	46.95	53.30	46.39	**12.81**	7.67	6.60	7.66	278.94
ML3: N23 (CH—N)	-1.15	37.80	47.92	40.97	46.45	40.48	8.05	7.16	6.16	6.96	240.81
ML3: N24 (CH—N)	-1.27	37.86	47.93	40.98	46.52	40.63	7.92	7.11	6.12	6.95	240.74
ML3: N45 (CH—N)	-1.03	37.82	47.94	40.96	46.49	40.56	8.06	7.15	6.11	6.94	241.01

Table D5. Atomic net charges $\Delta q(\Omega)$ in complexes relative to L(*As in Complex*)

	Ring 1 *(au)*									
	N1	C6	C5	C4	C3	C2	**H6**	H5	H4	**H3**
ML: N6 (CH—O)	-0.06664	0.00046	0.03349	0.02355	0.03150	0.00745	**0.05464**	0.03052	0.02602	0.02903
ML2: N2 (CH—N)	-0.06013	0.00418	0.03293	0.02257	0.02955	0.00689	**0.03518**	0.02861	0.02421	0.02688
ML2: N4 (CH—N)	-0.06005	0.00437	0.03292	0.02256	0.02955	0.00666	**0.03521**	0.02864	0.02423	0.02691
ML3: N2 (CH—N)	-0.05704	0.00242	0.03002	0.02077	0.02707	0.00499	0.03292	0.02621	0.02200	0.02429
ML3: N3 (CH—N)	-0.05693	0.00245	0.02999	0.02072	0.02700	0.00539	0.03301	0.02616	0.02208	0.02441
ML3: N34 (CH—N)	-0.05693	0.00241	0.03003	0.02080	0.02705	0.00475	0.03279	0.02622	0.02214	0.02429

	Ring2 *(au)*									
	N1′	C6′	C5′	C4′	C3′	C2′	**H6′**	H5′	H4′	**H3′**
ML: N7 (CH—O)	-0.06660	0.00056	0.03360	0.02357	0.03145	0.00711	**0.05466**	0.03053	0.02605	0.02907
ML2: N3 (CH—O)	-0.06579	-0.00101	0.03081	0.02182	0.02899	0.00577	**0.05249**	0.02788	0.02375	0.02659
ML2: N5 (CH—O)	-0.06571	-0.00084	0.03078	0.02187	0.02900	0.00545	**0.05246**	0.02792	0.02374	0.02659
ML3: N23 (CH—N)	-0.05693	0.00262	0.02999	0.02081	0.02710	0.00510	0.03302	0.02622	0.02213	0.02432
ML3: N24 (CH—N)	-0.05716	0.00248	0.02998	0.02077	0.02716	0.00510	0.03266	0.02614	0.02208	0.02438
ML3: N45 (CH—N)	-0.05687	0.00265	0.02994	0.02073	0.02697	0.00524	0.03303	0.02619	0.02204	0.02428

in NiL (average of +9.53 kcal·mol^{-1}), followed by NiL_2 (average of +8.26 kcal·mol^{-1}) and NiL_3 (average of +7.06 kcal·mol^{-1}). Atomic net charges show an average outflow of electrons for carbon and hydrogen atoms of all forms of NiL_n and an average inflow of electrons for nitrogen atoms.

Looking at the changes in hydrogen atomic energies and charges, a few interesting observations can be made: Firstly, the average atomic energies and charges of H3, one of the hydrogens involved in the CH•••HC interaction, do not show any significant differences when compared to H4 or H5, the hydrogens not involved in any interactions. This observation indicates that, qualitatively, the CH•••HC interaction does not change significantly when L coordinates to Ni^{2+}, and that the only significantly different changes in these atoms occurs when the CH•••HC interaction is formed - going from L(*trans*) to L(*As in complex*). Secondly, H6 and H6′ show significant changes compared to H4 or H5, specifically when these atoms are involved in the CH•••O interaction (NiL and the N3 and N5 pyridine rings of NiL_2). Table D6 compares the atomic energies of these atoms to the average atomic energies of the remaining H-atoms on each ring (3,3′-H, 4,4′-H and 5,5′-H), and Table D7 compares the atomic net charges. When H6 is involved in the CH•••O interaction, H6 is destabilized by +13.93 kcal·mol^{-1} in NiL (an increase of +5.87 larger than other H-atoms) and +12.82 kcal·mol^{-1} in N3 and N5 rings of NiL_2 (an increase of +5.51 larger than other H-atoms). On the other hand, when H6 is involved in the CH•••N interaction, H6 is destabilized by +8.98 kcal·mol^{-1} in N2 and N4 rings of NiL_2 (an increase of +1.52 larger than other H-atoms) and +8.01 kcal·mol^{-1} in NiL_3 (an increase of +1.27 larger than other H-atoms). This observation clearly shows the destabilization due to formation of the partly electrostatic H-bonds, in line with Koch and Popelier's criteria for hydrogen bonding[6] and reflects the greater strength of the CH•••O interaction than the CH•••N interaction. The changes in atomic net charges reflect this observation - on average, H6 when involved in the CH•••O interaction shows a much greater outflow of electrons than H6 when involved in the CH•••N interaction.

Table D6. Comparison of the increase in E(H6) and E(H6′) and the average increase of the remaining E(H)

	Ring 1 *(kcal mol^{-1})*			**Ring 2** *(kcal mol^{-1})*		
	E(H6)	Average E(H')[a]	*Difference*	**E(H′)**	Average E(H')[a]	*Difference*
ML	13.92	8.05	*5.87*	13.93	8.08	*5.86*
ML2: N2-N3	8.96	7.46	*1.50*	12.82	7.31	*5.51*
ML2: N4-N5	8.99	7.46	*1.53*	12.81	7.31	*5.50*
ML3: N2-N23	8.00	6.73	*1.26*	8.05	6.76	*1.29*
ML3: N3-N24	8.06	6.75	*1.31*	7.92	6.73	*1.20*
ML3: N34-N45	7.97	6.76	*1.22*	8.06	6.74	*1.32*

[a] E(H') refers to the average of E(H3), E(H4) and E(H5) of each ring.

Table D7. Comparison of the net charge increase *q*(H6) and q(H6′)) and the average increase of the remaining *q*(H)

	Ring 1 *(au)*			**Ring 2** *(au)*		
	***q*(H6)**	Average *q*(H')[a]	*Difference*	***q*(H6′)**	Average *q*(H')[a]	*Difference*
ML	0.05464	0.02852	*0.02612*	0.05466	0.02855	*0.02611*
ML2: N2-N3	0.03518	0.02657	*0.00861*	0.05249	0.02607	*0.02641*
ML2: N4-N5	0.03521	0.02659	*0.00862*	0.05246	0.02608	*0.02637*
ML3: N2-N23	0.03292	0.02417	*0.00875*	0.03302	0.02422	*0.00880*
ML3: N3-N24	0.03301	0.02422	*0.00880*	0.03266	0.02420	*0.00846*
ML3: N34-N45	0.03279	0.02422	*0.00858*	0.03303	0.02417	*0.00886*

[a] *q*(H') refers to the average of *q*(H3), *q*(H4) and *q*(H5) of each ring.

In conclusion, the preliminary results of this appendix have shown that preorganization of L from the lowest energy L(*trans*) to the ligands as they exist in a complex, L(*As in complex*), causes i) significant strain in the N-atoms and repulsive N--N interaction, signified by large increases in the atomic energies of N-atoms and an outflow of electrons from these atoms and ii) significant stabilization of the 3,3′-H-atoms when the CH•••HC interaction is formed, signified by large decreases in the atomic energies of 3,3′-H-atoms and an inflow of electrons to these atoms. Our results thus confirm the notion that the lone-pair-lone-pair repulsion between N atoms is a cause of the preorganization strain that L must undergo, but rejects the classical suggestions that 3,3′-H-atoms are involved in a destabilizing "steric clash". In addition, it is clear that L(*cis*) cannot be used as an analogue to study the preorganization of L as the junction C2–C2′ bond is destabilized in L(*cis*) (signified by a lengthening of d(C2–C2′) and consequent destabilization in the atomic energies of these atoms) whereas the same bond is stabilized in L(*As in complex*) conformers.

We have also shown here the nature of the relatively destabilized 6,6′-H-atoms when these atoms are involved in the CH•••O and CH•••N interactions, in line with the notion that these interactions are true H-bonds. In the context of these results, it is clear that the nature of the CH•••HC interaction does not change when L(*As in complex)* coordinates to Ni^{2+}.

References

[1] F. Labat, P. P. Lainé, I. Ciofini, C. Adamo, *Chem. Phys. Lett.* **2006**, *417*, 445–451.

[2] C. Blanchet-Boiteux, P. Friant-Michel, A. Marsura, J-B. Regnouf-de-Vains, M. F. Ruiz-López, *J. Mol. Struct*. (THEOCHEM) **2007**, *811*, 169–174.

[3] V. Galasso, G. De Alti, A. Bigotto, *Tetrahedron* **1971**, *27*, 991–997.

[4] C. Jaime, J. Font, *J. Mol. Struct.* **1989**, *195*, 103–110.

[5] R. Benedix, P. Birner, F. Birnstock, H. Hening, H-J. Hofmann, *J. Mol. Struct*. **1979**, *51*, 99–105.

[6] U. Koch, P. L. A. Popelier, *J. Phys. Chem.* **1995**, *99*, 9747–9754.

Appendix E.

Supplementary Information for Chapter 5

Table E1. Cartesian coordinates for the $[NiL(H_2O)_4]^{2+}$ complex (L = 2,2′-bipyridyl)

Standard orientation					
Centre number	Atomic number	Atomic type	Coordinates (Angstroms)		
			X	Y	Z
1	28	0	–0.003314	–1.252948	0.000307
2	8	0	–1.517880	–2.731207	–0.058713
3	8	0	–0.000015	–1.482281	–2.114907
4	8	0	1.503789	–2.738940	0.056994
5	8	0	–0.006821	–1.483489	2.115245
6	7	0	–1.323074	0.326928	–0.012787
7	7	0	1.324714	0.320178	0.013298
8	6	0	–2.657678	0.227958	–0.010665
9	1	0	–3.059188	–0.776982	–0.022206
10	6	0	–3.483011	1.344886	0.005236
11	1	0	–4.557464	1.221891	0.004813
12	6	0	–2.893164	2.603215	0.023748
13	1	0	–3.502351	3.498108	0.039405
14	6	0	–1.506525	2.706649	0.023453
15	1	0	–1.039031	3.680266	0.042281
16	6	0	–0.737791	1.544822	0.002297
17	6	0	0.745628	1.541021	–0.002216
18	6	0	1.520260	2.698915	–0.023770
19	1	0	1.057657	3.674877	–0.042992
20	6	0	2.906348	2.588468	–0.023932
21	1	0	3.520093	3.480243	–0.039839
22	6	0	3.489795	1.327168	–0.004948
23	1	0	4.563608	1.198740	–0.004355
24	6	0	2.658811	0.214465	0.011243
25	1	0	3.055230	–0.792501	0.023104
26	1	0	–1.567200	–3.378760	0.656274
27	1	0	–1.547564	–3.235897	–0.882199
28	1	0	–0.678330	–1.004362	–2.609925
29	1	0	0.826350	–1.336583	–2.593856
30	1	0	1.530987	–3.245034	0.879713
31	1	0	1.548847	–3.385754	–0.658964
32	1	0	–0.832390	–1.335248	2.594763
33	1	0	0.673437	–1.008255	2.610199

Thermochemical data for the $[NiL(H_2O)_4]^{2+}$ complex:

Zero-point correction:	0.261841 a.u.
Sum of electronic and zero-point Energies:	–2308.802435 a.u.
Sum of electronic and thermal Energies:	–2308.781103 a.u.
Sum of electronic and thermal Enthalpies:	–2308.780159 a.u.
Sum of electronic and thermal Free Energies:	–2308.852275 a.u.

Table E2. Cartesian coordinates for the $[NiL_2(H_2O)_2]^{2+}$ complex (L = 2,2′-bipyridyl)

Standard orientation					
Centre number	Atomic number	Atomic type	Coordinates (Angstroms)		
			X	Y	Z
1	28	0	0.000204	–0.001231	–0.827426
2	7	0	0.732547	1.357739	0.585123
3	7	0	2.020223	–0.532281	–0.765399
4	7	0	–0.733458	–1.358370	0.585218
5	7	0	–2.019215	0.532014	–0.766891
6	8	0	0.394978	1.410777	–2.432754
7	8	0	–0.392756	–1.413225	–2.432667
8	6	0	0.007110	2.276246	1.233240
9	1	0	–1.040099	2.338975	0.967845
10	6	0	0.551306	3.115571	2.196419
11	1	0	–0.074289	3.845213	2.692408
12	6	0	1.902147	2.987572	2.496703
13	1	0	2.364970	3.620221	3.243577
14	6	0	2.047274	1.227922	0.867188
15	6	0	2.772214	0.189559	0.093764
16	6	0	2.659013	2.033914	1.826624
17	1	0	3.709372	1.924688	2.053776
18	6	0	4.141429	–0.041929	0.219308
19	1	0	4.741005	0.538567	0.905026
20	6	0	4.737490	–1.030728	–0.554432
21	1	0	5.799819	–1.220741	–0.466729
22	6	0	3.955853	–1.763974	–1.439220
23	1	0	4.379913	–2.539364	–2.062768
24	6	0	2.598410	–1.479821	–1.514050
25	1	0	1.945179	–2.014298	–2.191037
26	6	0	–0.008933	–2.277061	1.234108
27	1	0	1.038327	–2.340661	0.969134
28	6	0	–0.554159	–3.115435	2.197514
29	1	0	0.070679	–3.845248	2.694204
30	6	0	–1.905050	–2.986296	2.497130
31	1	0	–2.368650	–3.618222	3.244132
32	6	0	–2.660939	–2.032440	1.826238
33	1	0	–3.711323	–1.922349	2.052851
34	6	0	–2.048203	–1.227372	0.866663
35	6	0	–2.772035	–0.188735	0.092523
36	6	0	–4.141034	0.044118	0.217772
37	1	0	–4.741271	–0.535447	0.903701
38	6	0	–4.736049	1.033106	–0.556549
39	1	0	–5.798207	1.224172	–0.469074
40	6	0	–3.953606	1.765140	–1.441614
41	1	0	–4.376838	2.540613	–2.065620

Standard orientation					
Centre number	Atomic number	Atomic type	Coordinates (Angstroms)		
			X	Y	Z
42	6	0	–2.596415	1.479658	–1.516131
43	1	0	–1.942645	2.013137	–2.193402
44	1	0	–0.911470	–1.111184	–3.189359
45	1	0	–0.784573	–2.255549	–2.168233
46	1	0	0.916576	1.110049	–3.187978
47	1	0	0.784429	2.253686	–2.166711
41	1	0	–4.376838	2.540613	–2.065620
42	6	0	–2.596415	1.479658	–1.516131
43	1	0	–1.942645	2.013137	–2.193402

Thermochemical data for the $[NiL_2(H_2O)_2]^{2+}$ complex:

Zero-point correction:	0.371741 a.u.
Sum of electronic and zero-point Energies:	–2651.126692 a.u.
Sum of electronic and thermal Energies:	–2651.101114 a.u.
Sum of electronic and thermal Enthalpies:	–2651.100170 a.u.
Sum of electronic and thermal Free Energies:	–2651.182573 a.u.

Table E3. Cartesian coordinates for the $[NiL_3]^{2+}$ complex (L = 2,2′-bipyridyl)

Standard orientation					
Centre number	Atomic number	Atomic type	Coordinates (Angstroms)		
			X	Y	Z
1	28	0	0.001042	0.000887	–0.003744
2	7	0	–0.400680	–1.782703	1.086340
3	7	0	0.074631	1.829887	–1.088786
4	6	0	–1.394313	–2.550218	0.590538
5	6	0	–1.713541	–3.779298	1.169089
6	1	0	–2.504283	–4.393306	0.763592
7	6	0	–0.998501	–4.216686	2.277066
8	1	0	–1.235942	–5.168472	2.735451
9	6	0	0.020570	–3.418500	2.782967
10	1	0	0.602792	–3.717888	3.643998
11	6	0	0.285441	–2.209609	2.152799
12	1	0	1.070329	–1.557199	2.511821
13	6	0	–0.683373	2.828369	–0.587642
14	6	0	–0.667320	4.101860	–1.157974
15	1	0	–1.267715	4.900710	–0.747883
16	6	0	0.138186	4.342457	–2.264020
17	1	0	0.159975	5.326183	–2.715914
18	6	0	0.911396	3.307515	–2.776346
19	1	0	1.551967	3.449029	–3.636362
20	6	0	0.849322	2.067690	–2.153733
21	1	0	1.434740	1.233907	–2.518373
22	6	0	–2.106226	–2.003945	–0.591723
23	7	0	–1.618678	–0.848324	–1.090995
24	7	0	–1.343517	1.237417	1.088049
25	6	0	–1.515523	2.480903	0.591402
26	6	0	–2.427949	3.366945	1.165670
27	1	0	–2.569864	4.357170	0.758375
28	6	0	–3.166098	2.963028	2.271183
29	1	0	–3.877732	3.640692	2.725874
30	6	0	–2.979129	1.682833	2.778727
31	1	0	–3.531076	1.325733	3.637669
32	6	0	–2.058329	0.853399	2.152063
33	1	0	–1.882374	–0.151736	2.511769
34	7	0	1.746353	0.543948	1.087593
35	6	0	2.908038	0.067268	0.591743
36	6	0	4.132380	0.409410	1.167240
37	1	0	5.059882	0.033127	0.761171
38	6	0	4.153756	1.250813	2.272582
39	1	0	5.096993	1.524628	2.728321
40	6	0	2.952971	1.733721	2.778911
41	1	0	2.921752	2.390590	3.637702

Standard orientation					
Centre number	Atomic number	Atomic type	Coordinates (Angstroms)		
			X	Y	Z
42	6	0	1.773243	1.354820	2.151717
43	1	0	0.815838	1.708018	2.511235
44	6	0	2.790677	–0.825107	–0.588556
45	7	0	1.546756	–0.977212	–1.090668
46	6	0	1.363544	–1.764663	–2.156998
47	6	0	2.404303	–2.440688	–2.780230
48	6	0	3.687411	–2.293589	–2.267056
49	6	0	3.883816	–1.478193	–1.159470
50	1	0	4.875878	–1.361277	–0.748488
51	1	0	4.526886	–2.806484	–2.719396
52	1	0	2.204562	–3.064197	–3.641233
53	1	0	0.348925	–1.851050	–2.522610
54	6	0	–2.208191	–0.296158	–2.157963
55	6	0	–3.310328	–0.862673	–2.784997
56	6	0	–3.820792	–2.050694	–2.275574
57	6	0	–3.213800	–2.627800	–1.167171
58	1	0	–3.605405	–3.548265	–0.759466
59	1	0	–4.681021	–2.524597	–2.731448
60	1	0	–3.750225	–0.378515	–3.646438
61	1	0	–1.777971	0.628014	–2.520720

Thermochemical data for the $[NiL_3]^{2+}$ complex:

Zero-point correction:	0.481768 a.u.
Sum of electronic and zero-point Energies:	–2993.447314 a.u.
Sum of electronic and thermal Energies:	–2993.417475 a.u.
Sum of electronic and thermal Enthalpies:	–2993.416531 a.u.
Sum of electronic and thermal Free Energies:	–2993.510266 a.u.

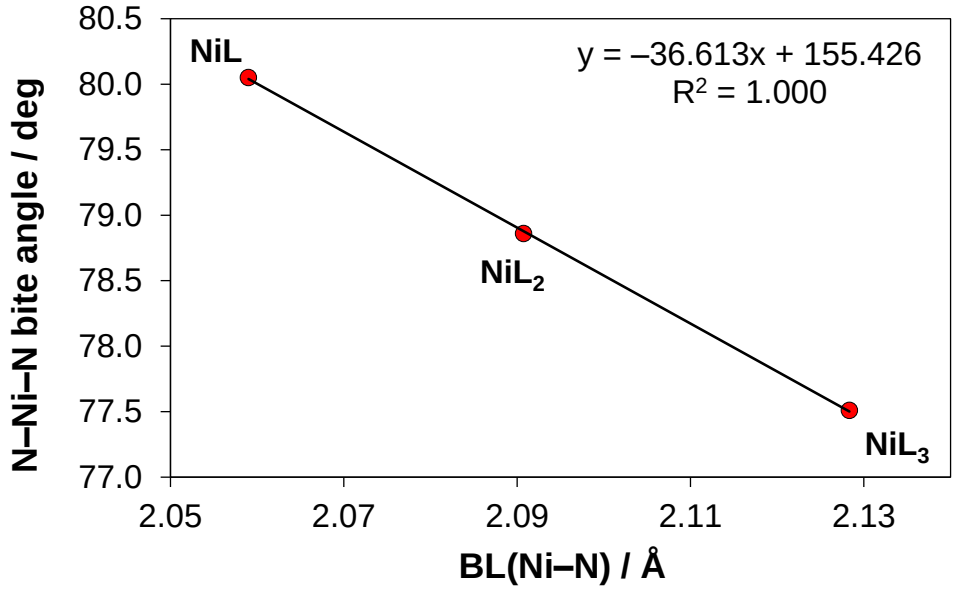

Figure E1. Relationship between the Ni–N bond length and N–Ni–N bite angle in the energy-optimized in solvent Ni^{II} complexes with 2,2′-bipyridyl (L).

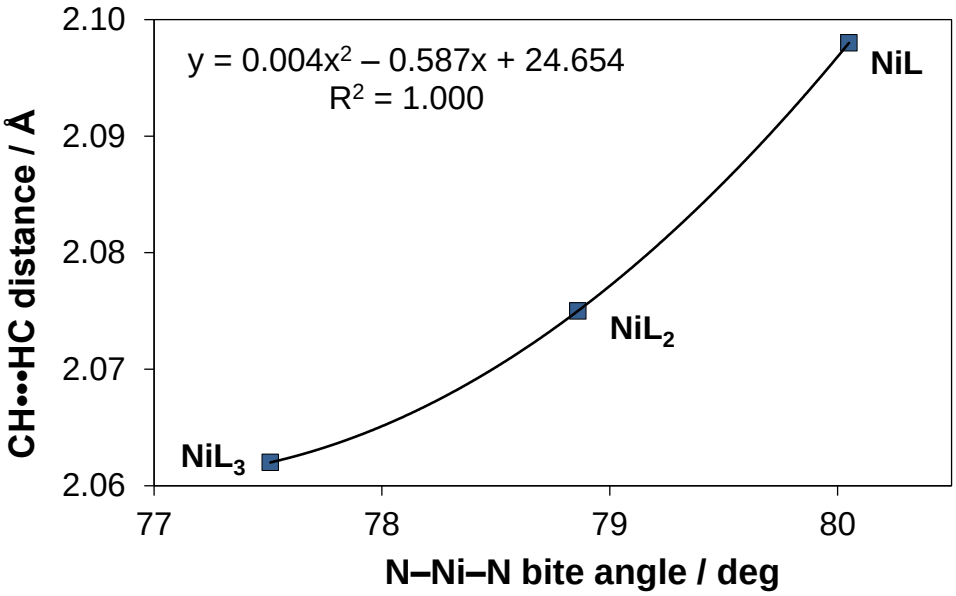

Figure E2. Relationship between the N–Ni–N bite angle and the CH•••HC distance in the energy-optimized in solvent Ni^{II} complexes with 2,2′-bipyridyl (L).

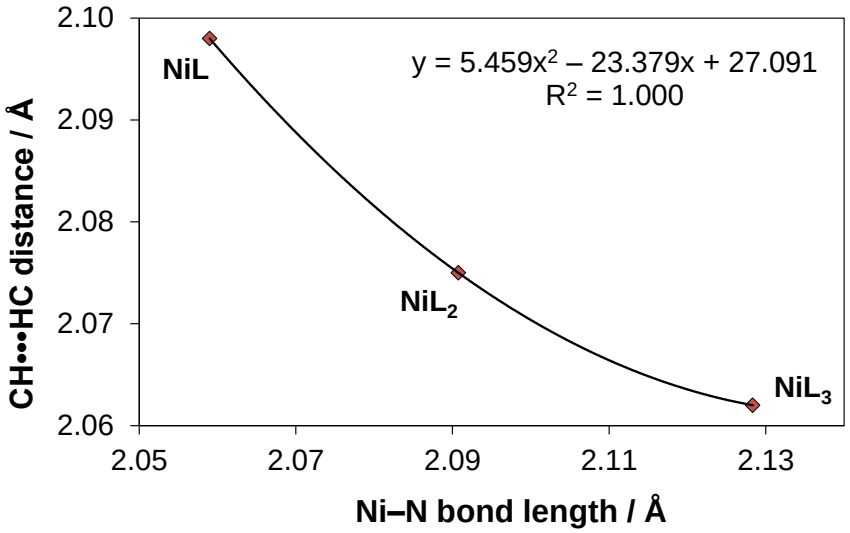

Figure E3. Relationship between the Ni–N bond length and d(CH•••HC) in the energy-optimized in solvent Ni^{II} complexes with 2,2′-bipyridyl (L).

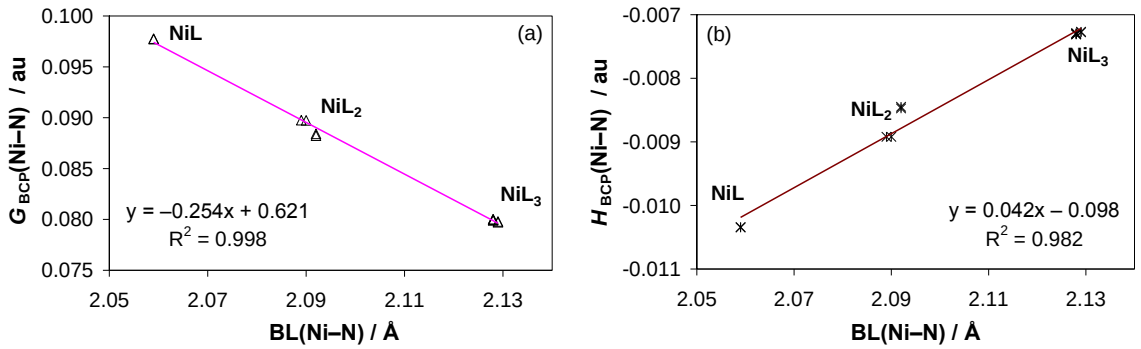

Figure E4. Relationships between BL(Ni–N) (in the NiL, NiL_2 and NiL_3 complexes) and topological properties: (a) - local kinetic energy density $G(r)$, (b) – total energy density $H(r)$, at the BCPs of these coordination bonds.

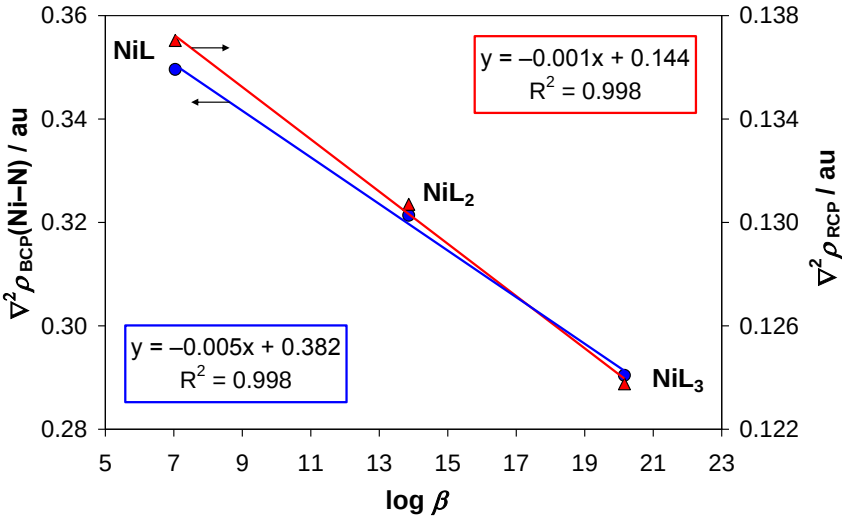

Figure E6. Strong relationships between the experimental overall formation constants of the NiL, NiL_2 and NiL_3 complexes, log β_n (L = 2,2′-bipyridyl) and the Laplacian at: circles - the Ni–N coordination bond critical points, triangles – the chelating ring critical points.

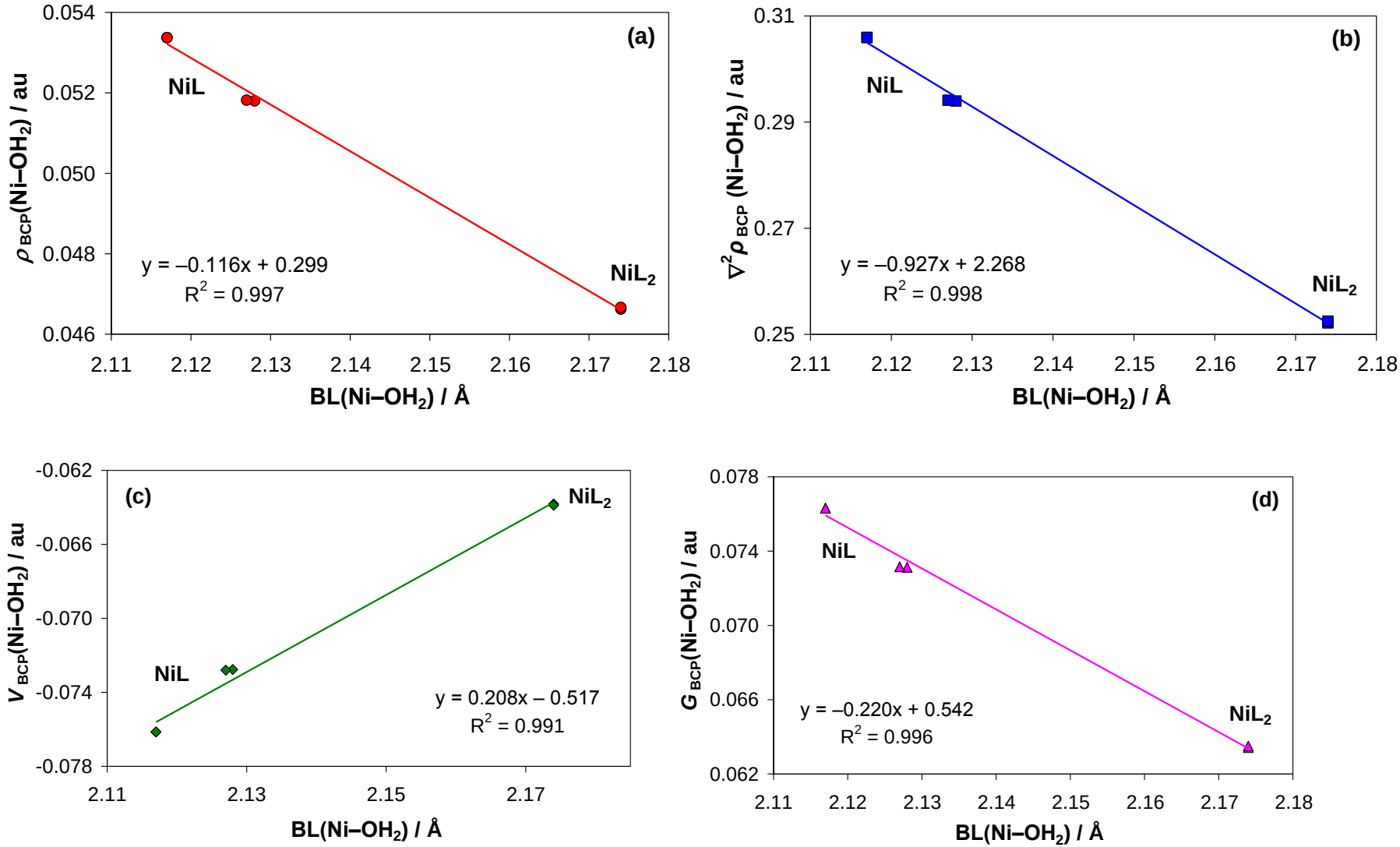

Figure E5. Relationships between the coordination bond length, BL(Ni–OH_2), (in NiL and NiL_2, L = 2,2′-bipyridyl) and the topological properties: (a) ρ_{BCP}(Ni–OH_2); (b) $\nabla^2\rho_{BCP}$(Ni–OH_2); (c) V_{BCP}(Ni–OH_2) and (d) G_{BCP}(Ni–OH_2).

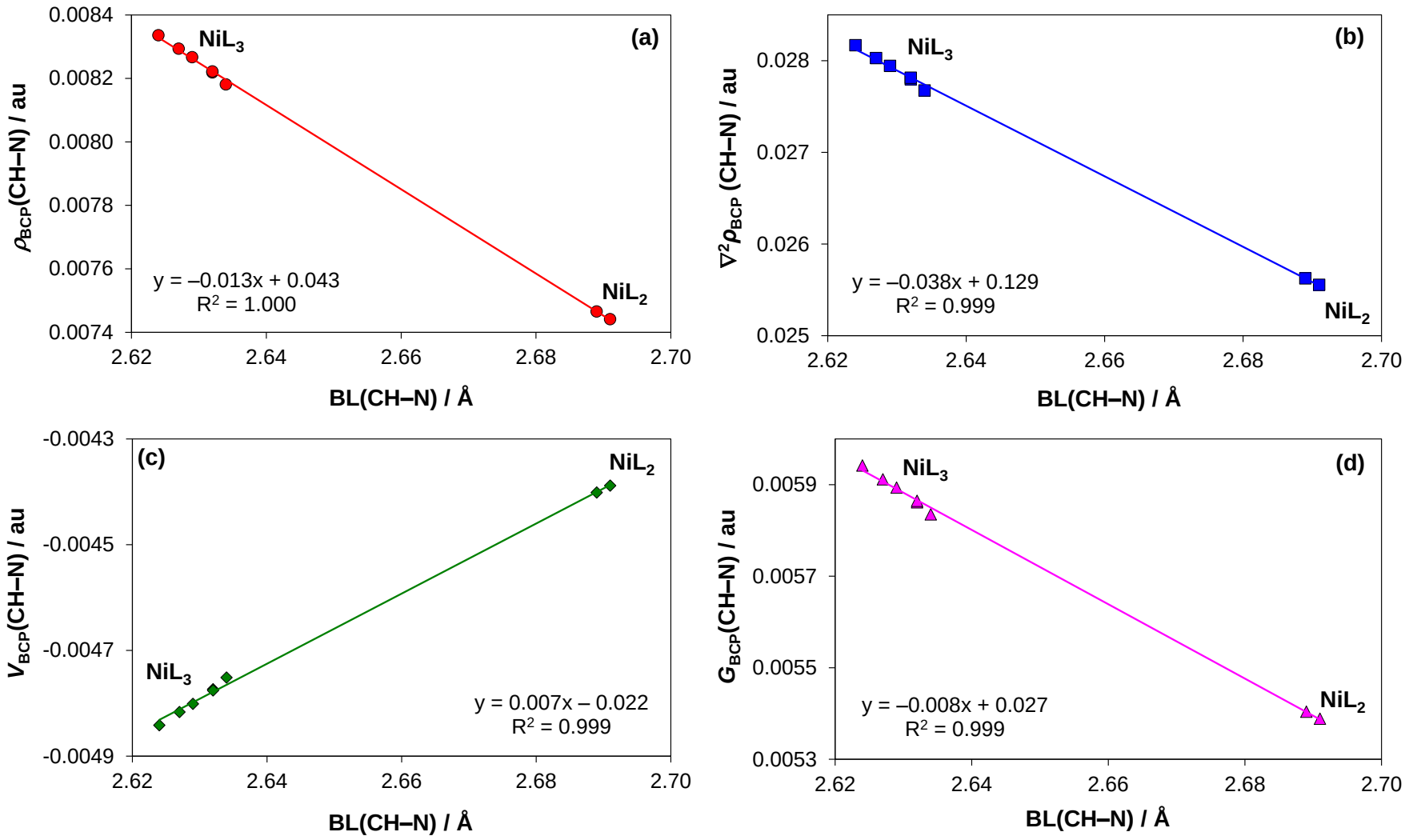

Figure E7. Relationships between the intramolecular bond length, BL(CH–N) (in the NiL_2 and NiL_3 complexes with 2,2′–bipyridyl) and the topological properties: (a) ρ_{BCP}(CH–N), (b) $\nabla^2\rho_{BCP}$(CH–N), (c) V_{BCP}(CH–N) and (d) G_{BCP}(CH–N).

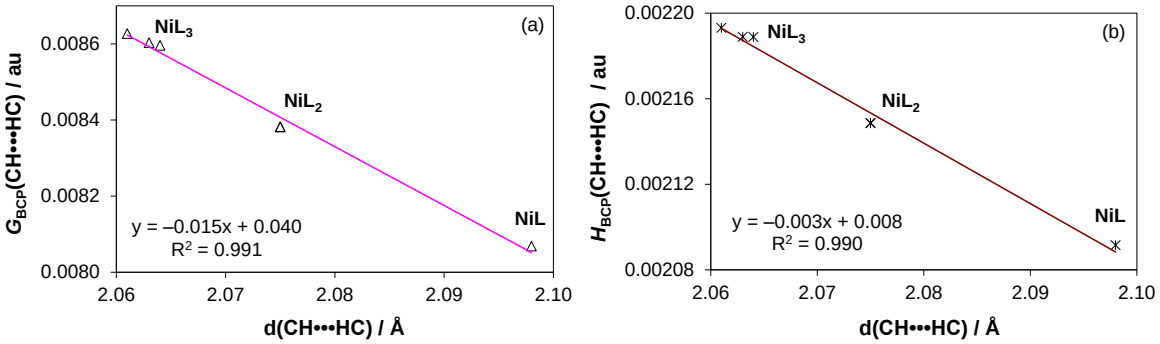

Figure E8. Relationships between d(CH•••HC) in the NiL, NiL_2 and NiL_3 complexes and indicated topological properties at the BCPs.

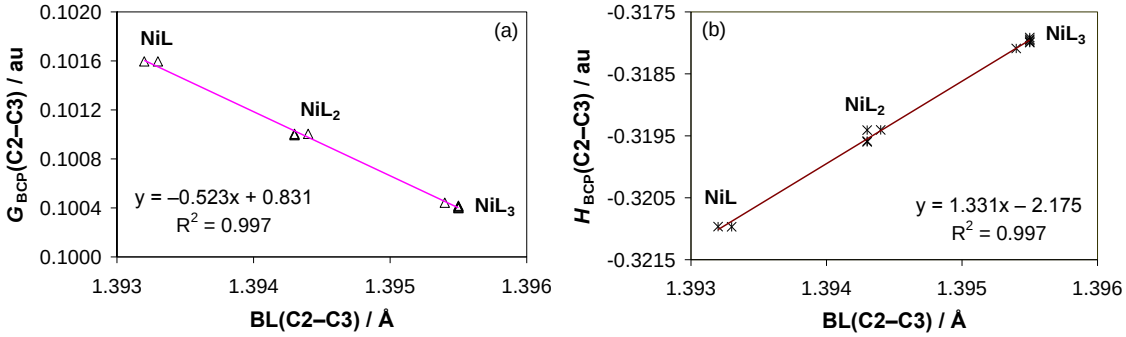

Figure E9. Relationships between BL(C2–C3) of a pyridyl rings and the indicated topological properties at the BCPs of these bonds in the NiL, NiL_2 and NiL_3 complexes.

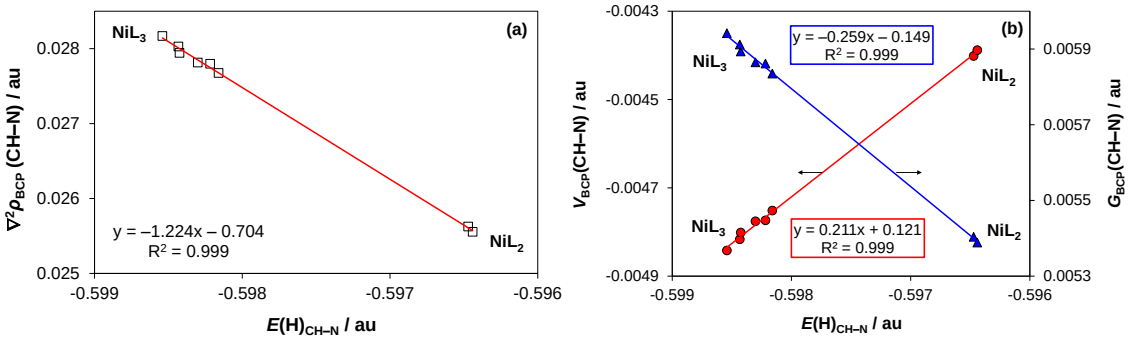

Figure E10. Relationships between the atomic energy of H–atoms involved in the CH–N bonds in the Ni^{II} complexes with 2,2′–bipyridyl (L) and: (a) – the Laplacian $\nabla^2\rho_{BCP}$(CH–N), (b) V_{BCP}(CH–N) (circles) and G_{BCP}(CH–N) (triangles).

Table E4. Atomic energies, $E(\Omega)$, of H- and N-atoms involved (in bold) and not involved in the CH–N bonds in the Ni^{II} complexes with 2,2′-bipyridyl (L).

Complex	Atom	$E(\Omega)$ (a.u.)	Atom	$E(\Omega)$ (a.u.)	$\delta E(\Omega)$[a]
NiL_2	**H9**	–0.5964710	H11	–0.5898039	–4.18
	H27	–0.5964408	H29	–0.5897993	
	average:	*–0.5964559*	*average:*	*–0.5898016*	
			H11	–0.5898039	–3.87
			H29	–0.5897993	
			H13	–0.5907922	
			H31	–0.5907891	
			average:	*–0.5902961*	
			std dev:	*0.00057*	
			H11	–0.5898039	–3.79
			H13	–0.5907922	
			H21	–0.5909404	
			H23	–0.5901210	
			H29	–0.5897993	
			H31	–0.5907891	
			H39	–0.5909368	
			H41	–0.5901175	
			average:	–0.5904125	
			std dev:	0.0005	
	N3	–55.3278705	N2	–55.3248230	–1.87
	N5	–55.3278404	N4	–55.3249433	
	average:	*–55.3278554*	*average:*	*–55.3248832*	
NiL_3	**H12**	–0.5984324	H10	–0.5907232	–4.77
	H61	–0.5982175	H60	–0.5907332	
	H53	–0.5983012	H52	–0.5907587	
	H43	–0.5984251	H41	–0.5907291	
	H33	–0.5985409	H31	–0.5907606	
	H21	–0.5981602	H19	–0.5907511	
	average:	*–0.5983462*	*average:*	*–0.5907427*	
	std dev:	*0.00014*	*std dev:*	*0.00002*	

[a] $\delta E(\Omega) = E_{Avg}$(in-contact) – E_{Avg}(contact-free) in kcal mol^{-1}.

Table E5. Atomic energies, *E*(H), of H-atoms involved (in bold) and not involved in the CH•••HC contacts in the Ni^{II} complexes with 2,2′–Bipyridyl (L).

Complex	Atom	*E*(H) (a.u.)	Atom	*E*(H) (a.u.)	δ*E*(H)[a]
NiL	**H15**	–0.5959819	H13	–0.5899865	–3.76
	H19	–0.5959718	H21	–0.5899834	
	average:	*–0.5959769*	*average:*	*–0.5899849*	
			H13	–0.5899865	–4.06
			H11	–0.5890307	
			H21	–0.5899834	
			H23	–0.5890340	
			average:	*–0.5895086*	
			std dev:	*0.00055*	
NiL_2	**H17**	–0.5974008	H13	–0.5907922	–4.15
	H19	–0.5975544	H21	–0.5909404	
	average:	*–0.5974776*	*average:*	*–0.5908663*	
			H13	–0.5907922	–4.43
			H21	–0.5909404	
			H23	–0.5901210	
			H11	–0.5898039	
			average:	*–0.5904144*	
			std dev:	*0.00054*	
	H33	–0.5973986	H31	–0.5907891	–4.15
	H37	–0.5975514	H39	–0.5909368	
	average:	*–0.5974750*	*average:*	*–0.5908629*	
			H31	–0.5907891	–4.43
			H39	–0.5909368	
			H41	–0.5901175	
			H29	–0.5897993	
			average:	*–0.5904107*	
			std dev:	*0.00054*	
NiL_3	**H15**	–0.5986877	H17	–0.5916886	–4.43
	H27	–0.5987764	H29	–0.5916641	
	average:	*–0.5987320*	*average:*	*–0.5916763*	
	H6	–0.5988317	H8	–0.5916961	–4.46
	H58	–0.5987608	H59	–0.5916671	
	average:	*–0.5987963*	*average:*	*–0.5916816*	
	H37	–0.5987615	H39	–0.5916692	–4.44
	H50	–0.5987505	H51	–0.5916969	
	average:	*–0.5987560*	*average:*	*–0.5916830*	

[a] $\delta E(H) = E_{Avg}$(in-contact) – E_{Avg}(contact-free) in kcal mol^{-1}.

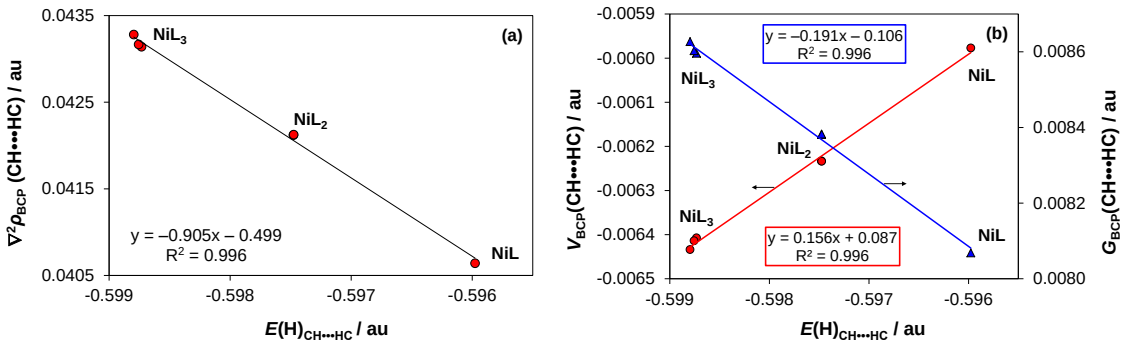

Figure E11. Relationships between the atomic energy of H–atoms involved in the CH•••HC contacts in the Ni^{II} complexes with 2,2′–bipyridyl (L) and: (a) - $\nabla^2\rho_{BCP}$(CH•••HC), (b) - V_{BCP}(CH•••HC) (circles) and G_{BCP}(CH•••HC) (triangles).